

**SYNTHESIS, CHARACTERIZATION AND SOME  
PROPERTIES OF NEW SOLUBLE TRIARYLAMINE-BASED  
AROMATIC POLYAMIDES**

**THESIS SUBMITTED IN FULFILMENT OF THE  
REQUIREMENTS FOR THE DEGREE OF DOCTOR OF  
PHILOSOPHY**

**AZHAR KAMIL RASHID**

**DEPARTMENT OF CHEMISTRY  
FACULTY OF SCIENCE  
UNIVERSITY OF MALAYA  
KUALA LUMPUR**

**2014**

**UNIVERSITY OF MALAYA**  
**ORIGINAL LITERARY WORK DECLARATION**

Name of Candidate: **AZHAR KAMIL RASHID** (Passport No: G1966902)

Registration / Matric No. : **SHC100010**

Name of Degree: **Doctor of philosophy**

Title of Project Paper / Research Report / Dissertation / Thesis ("This Work"):

**SYNTHESIS, CHARACTERIZATION AND SOME PROPERTIES OF NEW SOLUBLE TRIARYLAMINE-BASED AROMATIC POLYAMIDES.**

Field of Study: **Polymer Science**

I do solemnly and sincerely declare that:

- (1) I am the sole author / writer of this work
- (2) This work is original
- (3) Any use of any work in which copyright exists was done by way of fair dealing and for permitted purpose and any excerpt or extract from, or reference to or reproduction of any copyright work has been disclosed expressly and sufficiently and the title of the work and its authorship have been acknowledged in this work.
- (4) I do not have any actual knowledge nor ought I reasonably to know that the making of this work constitutes an infringement of any copyright work.
- (5) I hereby assign all and every right in the copyright to this work to the University of Malaya ("UM"), who henceforth shall be the owner of the copyright in this work and that any reproduction or use in any form or by any means whatsoever is prohibited without the written consent of UM have been first had and obtained
- (6) I am fully aware that if in the course of making this work I have infringed any copyright whether intentionally or otherwise, I may be subject to legal action or any other action as may be determined by UM.

Candidate's Signature

Date:

Subscribed and solemnly declared before,

Witness's Signature

Date:

Name:

Designation:

## ABSTRACT

Six new triphenylamine-containing aromatic diacid monomers, 4,4'-dicarboxy-4"-isopropyltriphenylamine, **Ma**, 4,4'-dicarboxy-2'4"-dimethyltriphenylamine **Mb**, 4,4'-dicarboxy-4"-ethyltriphenylamine, **Mc**, 4,4'-dicarboxy-4"-phenoxy triphenylamine, **Md**, 4,4'-dicarboxy-4"--(N-pyrrolyl)triphenylamine **Me**, 4,4',4'',4'''-(1,4-phenylene bis(azanetriyl)) tetrabenzoic acid, **Mf**, were successfully synthesized via the aromatic nucleophilic fluoro displacement reaction of 4-fluorobenzonitrile with aniline-derivatives using sodium hydride as the base, followed by alkaline hydrolysis of the dinitrile intermediates (**Ia**, **Ib**, **Ic**, **Id**, **Ie**, **If**). A series of poly(amine-amide)s were prepared by the direct phosphorylation polycondensation from the newly synthesized diacid monomers with various aromatic diamines. FTIR,  $^1\text{H}$  and  $^{13}\text{C}$  NMR spectroscopic techniques were used to identify the chemical structures of the dicyano intermediate, the carboxylic acid monomer and the resultant poly(amine-amide)s containing the triphenylamine moieties. These aromatic poly(amine-amide)s were found to be readily soluble in a variety of organic solvents and could afford strong and tough films via solution casting. They exhibited excellent thermal stability with 10% weight loss temperatures in the range of (401.2 - 577.4) °C as recorded by TGA and high glass transition temperatures between 234.5 - 292.6°C. In dilute N-methyl pyrrolidone (NMP) solution, these polymers exhibited a medium to strong UV-Vis absorption bands at the range 305 - 363 nm and photoluminescence in the blue region at 429 ~ 488 nm. Cyclic voltammetry of the poly(amine-amide)s films cast onto an ITO-coated glass substrate in dry acetonitrile ( $\text{CH}_3\text{CN}$ ) containing 0.1 M of tetrabutylammonium perchlorate ( $\text{Bu}_4\text{AlNH}_4\text{ClO}_4$ ) as an electrolyte exhibited one oxidation half-wave redox couples ( $E_{1/2}$ ) at 1.13 - 1.27 V vs Ag/AgCl, and revealed electrochromic characteristics with a color change from pale yellow to blue at applied potentials switched between 0.0 and 1.6 V at scan rate 0.1 V. The obtained values of the HUMO and LUMO energy levels

of the currently synthesized transporting materials were in the range of 5.52 - 5.66 eV and 2.44 - 2.62 eV respectively with band gap of values of 3.04 - 3.15 eV.

## ABSTRAK

Enam monomer baharu trifenilamina yang mengandungi diasid aromatik, 4,4'-dikarboksi-4"-isopropiltrifenilamina, **Ma**, 4,4'-dikarboksi-2'4"-dimetiltrifenilamina **Mb**, 4,4'-dikarboksi-4"-etiltrifenilamina **Mc**, 4,4'-dikarboksi-4"-fenoksi-trifenilamina, **Md**, 4,4'-dikarboksi-4"-(N-pirrolil)trifenilamina, **Me**, 4,4,4",4"-(1,4-fenilena bis (azanetriyl )) asid tetrabenzoik, **Mf**, telah berjaya disintesis melalui tindak balas penyesaran nukleofilik fluoro aromatik 4-fluorobenzonitril dengan derivatif anilina menggunakan natrium hidrida sebagai bes, diikuti dengan hidrolisis beralkali bagi perantaraan dinitril (**Ia**, **Ib**, **Ic**, **Id**, **Ie**, **If**). Satu siri poli(amina–amida) telah disediakan melalui polikondensasi pemfosforilan langsung daripada monomer diasid baharu yang telah disintesis dengan pelbagai diamina aromatik. Teknik spektroskopi FTIR,  $^1\text{H}$  dan  $^{13}\text{C}$  NMR telah digunakan untuk mengenal pasti struktur kimia bagi perantara disiano, monomer asid karboksilik dan poli(amina-amida) yang mengandungi moiety trifenilamina. Poli(amine-amida) aromatik ini didapati mudah larut dalam pelbagai pelarut organik dan mampu memberi tipisan yang kuat dan kukuh melalui acu-bentuk larutan. Polimer ini mempamerkan kestabilan terma yang baik dengan suhu 10% kehilangan berat melebihi 401.2 - 577.4 °C seperti dicatatkan oleh TGA dan suhu kaca peralihan yang tinggi antara 234.5 - 292.6°C. Dalam larutan cair N-metil pirrolidon (NMP), polimer ini mempamerkan jalur penyerapan UV-Vis yang sederhana ke kuat pada julat 305 - 363 nm dan fotoluminescens di kawasan biru pada 423 ~ 488 nm. Voltammetri kitaran bagi tipisan poli(amina-amida) yang di'acu-bentuk" pada substrat kaca saduran-ITO dalam asetonitril kering yang mengandungi 0.1 M tetrabutylammonium perklorat (TBAP) sebagai elektrolit mempamerkan pengoksidaan separuh-gelombang pasangan redoks ( $E_{1/2}$ ) pada 1.13 – 1.27 V vs Ag/AgCl, dan menunjukkan ciri-ciri elektrokromik dengan perubahan warna dari kuning pucat kepada biru di keupayaan gunaan ditukarganti antara 0.0 dan 1.6 V pada kadar imbasan 0.1 V.

Nilai yang diperoleh bagi aras tenaga HUMO dan LUMO untuk bahan pengangkutan yang disintesis ini ialah dalam lingkungan 5.52 - 5.66 eV dan 2.44 - 2.62 eV masing-masing dengan ruang jalur bernilai 3.04 - 3.15 eV.

## **ACKNOWLEDGEMENTS**

First, I would like to thank Allah for giving me the ability and strength, thus allowing me to complete this study.

I would like to express my sincere gratitude to my main supervisor, Professor Dr. Rosiyah Yahya and co-supervisor, Dr. Phang Sook Wai for help, support, good advice and patience along the period of research and writing.

I would like to acknowledge the financial academic and technical support of the University of Malaya especially for the research grants PS382-2010B.

Special thanks to the University of Baghdad for giving me the opportunity to do this research and for the financial support.

I also would like to thank all my friends, group members and my PhD colleagues in the Department of Chemistry for the real brotherhood and friendship that they showed me along the period of PhD study especially to Mr. Raied Mustafa Shakir, Mr. Zulkifli Bin Abu Hassan and Mr. Ahmad Danial Azzahari for their cooperation and help.

My appreciation to the NMR and thermal staff, Miss. Norzalida Zakaria, Mr Fateh Ngaliman and Mr. Nordin Mohamad for their greater assistance to handle the instruments.

Special love and respect without limits to my wife whose effort every kinds of impossibilities for the success of this work.

Great thanks to my parents, brothers and sisters who have given me their unequivocal support throughout, as always, for which my mere expression of thanks likewise does not suffice.

## TABLE OF CONTENTS

ABSTRACT.....	ii
ABSTRAK.....	iv
ACKNOWLEDGMENTS.....	vi
TABLE OF CONTENTS.....	vii
LIST OF FIGURES.....	xi
LIST OF TABLES.....	xiv
LIST OF ABBREVIATIONS AND SYMBOLS.....	xv
LIST OF APPENDICES.....	xviii
CHAPTER 1: INTRODUCTION.....	1
1.1. Introduction.....	1
1.2. Research Objective.....	2
1.3. Thesis Outline .....	2
CHAPTER 2: BACKGROUND AND LITERATURE REVIEW .....	4
2.1. Aromatic Polyamides .....	4
2.1.1. Aromatic Polyamide Synthesis .....	4
2.1.1.1. Low -Temperature Solution Method.....	4
2.1.1.2. High-Temperature Solution Method.....	5
2.1.1.3. Alternative Polymerization Methods .....	6
2.1.2. Types of the Aromatic Polyamides .....	7
2.1.2.1. Optically Active Polyamides .....	7
2.1.2.2. Luminescent and Electrochromic Polyamides .....	9
2.1.3. Improvement of Optical Properties of Polyamides.....	10
2.1.3.1. Polyamides with Fluorinated and Chlorinated Substituents .....	100



2.1.3.2. Polyamides with Bulky Pendant Groups .....	11
2.1.3.3. Polyamides with Segmented Blocks .....	12
2.1.3.4. Unclassified Polyamide Structures .....	12
2.1.4. Behavior of Polyamides in PLEDs .....	13
2.1.5. Aromatic Poly(amine-amide)s in light emitting devices .....	14
2.1.6. Commercial aromatic polyamides.....	14
CHAPTER 3: POLY ORGANIC LIGHT EMITTING DIODES (POLEDs).....	18
3.1. Use of Poly Organic light Emitting Diodes (POLEDs) .....	20
3.2. POLEDs Structure.....	20
3.2.1. Electron-Injector Electrode (EIE) (cathode) .....	21
3.2.2. Hole Blocking/Exciton Blocking Materials (HBMs/EBMs) .....	22
3.2.3. Electron-Transport Materials/Layer (ETMs/ETL).....	23
3.2.4. Emissive Materials (EMs).....	25
3.2.5. Hole Transport Materials (HTMs) .....	26
3.3. Energy Band Diagrams of OLEDs Operation.....	29
3.4. Operation-base of POLEDs .....	30
3.5. Energy Transfer in OLEDs .....	31
3.6. Fabrication of OLEDs .....	33
3.6.1. Substrate Preparation .....	33
3.6.2. Device Fabrication .....	34
3.7. Advantages of Organic Light-Emitting Devices.....	35
3.8. Applications of Organic Light-Emitting Devices .....	36

3.8.1. Flat Panel Display .....	36
3.8.2. Solid-State-Lighting .....	38
3.9. Electronic Transitions of OLEDs .....	39
3.9.1. Luminescence of OLEDs .....	39
3.9.2. Fluorescence and Phosphorescence .....	39
CHAPTER 4 : EXPERIMENTAL .....	41
4.1. Materials .....	41
4.2. Characterization methods and instruments .....	41
4.2.1. Fourier Transform Infrared Analysis (FTIR) .....	41
4.2.2. UV-vis Absorption and Photoluminescence (PL) spectra .....	41
4.2.3. Nuclear Magnetic Resonance ( $^1\text{H}$ -NMR and $^{13}\text{C}$ -NMR) .....	42
4.2.4. Differential Scanning Calorimetry (DSC) .....	42
4.2.5. Thermogravimetry Analysis (TGA) .....	43
4.2.6. Electrochemical Properties .....	44
4.3. Synthesis of monomers ( <b>Ma-Mf</b> ) .....	44
4.3.1. General synthesis of intermediates ( <b>Ia-Ig</b> ): .....	45
4.3.1.1. Synthesis of 4,4'-dicyano-4''-isopropyltriphenylamine ( <b>Ia</b> ) .....	45
4.3.1.2. Synthesis of 4,4'-dicyano-4''-2,4-dimethylaniline ( <b>Ib</b> ) .....	46
4.3.1.3. Synthesis of 4,4'-dicyano-4''-2-ethylaniline ( <b>Ic</b> ) .....	46
4.3.1.4. Synthesis of 4,4'-dicyano-4''-phenoxytriphenylamine ( <b>Id</b> ) .....	46
4.3.1.5. Synthesis of 4,4'-dicyano-4''-(1H-pyrrol-1-yl)triphenylamine ( <b>Ie</b> ) .....	47
4.3.1.6. Synthesis of 4,4',4'',4'''-(1,4-phenylenebis(azanetriyl))tetrabenzonitrile ( <b>If</b> ) .....	47

4.3.2. General synthesis of monomers ( <b>Ma-Mf</b> ) .....	48
4.3.2.1. Synthesis of 4,4'-dicarboxy-4''-isopropyltriphenylamine ( <b>Ma</b> ) .....	48
4.3.2.2. Synthesis of 4,4'-dicarboxy-4''-2,4-dimethyltriphenylamine ( <b>Mb</b> ).....	49
4.3.2.3. Synthesis of 4,4'-dicarboxy-4''- 2-ethyltriphenylamine ( <b>Mc</b> ) .....	49
4.3.2.4. Synthesis of 4, 4'-dicarboxy-4''-phenoxytriphenylamine ( <b>Md</b> ) .....	49
4.3.2.5. Synthesis of 4,4'-dicarboxy-4''-(1H-pyrrol-1-yl)triphenylamine ( <b>Me</b> ) .....	50
4.3.2.6. Synthesis of 4,4',4'',4'''-(1,4-phenylenebis(azanetriyl))tetrabenzonic acid ( <b>Mf</b> )..	50
4.3.3. General synthesis of polyamides.....	51
4.3.3.1. Synthesis of Poly(amine amide) ( <b>Pa1</b> ) .....	51
4.3.3.2. Synthesis of Poly(amine amide) ( <b>Pb1</b> ) .....	52
4.3.3.3. Synthesis of Poly(amine amide) ( <b>Pc1</b> ).....	52
4.3.3.4. Synthesis of Poly(amine amide) ( <b>Pd1</b> ) .....	53
4.3.3.5. Synthesis of Poly(amine amide) ( <b>Pe1</b> ).....	53
4.3.3.6. Synthesis of Poly(amine amide) ( <b>Pf1</b> ) .....	53
4.3.3.7. Synthesis of Poly(amine amide) ( <b>Pa2</b> ) .....	54
4.3.3.8. Synthesis of Poly(amine amide) ( <b>Pb2</b> ) .....	54
4.3.3.9. Synthesis of Poly(amine amide) ( <b>Pc2</b> ).....	54
4.3.3.10. Synthesis of Poly(amine amide) ( <b>Pd2</b> ) .....	55
4.3.3.11. Synthesis of Poly(amine amide) ( <b>Pe2</b> ).....	55
4.3.3.12. Synthesis of Poly(amine amide) ( <b>Pf2</b> ) .....	56
CHAPTER 5: RESULTS AND DISCUSSION.....	57
5.1. Monomer synthesis .....	57

5.2. Characterization of the synthesized monomers.....	611
5.2.1. FTIR spectra of synthesized monomers.....	61
5.2.2. NMR spectrum of synthesized monomers .....	63
5.3. Poly(amine-amide)s synthesis.....	67
5.3.1. FTIR spectra of synthesized poly(amine-amide)s.....	69
5.3.2. C NMR spectra of the synthesized poly(amine-amide)s.....	71
5.4. Solubility.....	80
5.5. Thermal properties .....	81
5.6. Optical properties .....	87
5.7. Electrochemical Properties .....	92
CHAPTER 6: CONCLUSION AND SUGGESTIONS FOR FUTURE WORK .....	97
6.1: Conclusion .....	97
6.2. Suggestion for future work .....	99
REFERENCES.....	100
LIST OF PUBLICATIONS.....	110
APPENDICES .....	111

## LIST OF FIGURES

<b>Figure 2-1:</b> Reaction of diacid dichloride with diamine .....	5
<b>Figure 2-2:</b> Reaction of diacid with diamine.....	6
<b>Figure 2-3:</b> Reaction of diacid with diisocyanate.....	6
<b>Figure 2-4:</b> Palladium-catalyzed carbonylation-polycondensation reaction.....	7
<b>Figure 2-5:</b> Synthesis of pendant polyisophthalamides.....	8

<b>Figure 2-6:</b> Structures of polyisophthalamides having a pendant L-alanine.....	9
<b>Figure 2-7:</b> Halogenated polyamides .....	11
<b>Figure 2-8:</b> Improvement of optical properties of PLEDs using bulky groups.....	12
<b>Figure 2-9:</b> Unclassified polyamide structures.....	13
<b>Figure 2-10:</b> Structures of (PPPT) and (PMPI).....	16
<b>Figure 3-1:</b> Historical and predicted power efficiencies for various light sources .....	20
<b>Figure 3-2:</b> General structure of POLED .....	21
<b>Figure 3-3:</b> Chemical structures some hole blockers/exciton blocking materials.....	23
<b>Figure 3-4:</b> Some common electron-transport materials (ETM <sub>s</sub> ) .....	24
<b>Figure 3-5:</b> Energy level relationships and energy transfers in a host-guest system: (a) Favorable HOMO-LUMO level alignment (b) Poor energy transfer G→T1H) (c)Efficient energy transfer (T1G→S0) in phosphorescent host-guest systems.....	25
<b>Figure 3-6:</b> Some commonly known compounds as a host-guest system.....	26
<b>Figure 3-7:</b> Chemical structure of some HTMs... ..	27
<b>Figure 3-8:</b> Some starburst hole transporting materials.....	28
<b>Figure 3-9:</b> Schematic energy band diagrams about OLEDs operation. For simplicity, single organic layer is assumed between two electrodes; (a) before the electrical contact, (b) after the electrical contact, (c) with the applied voltage bias through both electrodes, charge carriers are ready to be injected at V=V <sub>bi</sub> , and (d) charge carriers are finally injected into the organic layer at V>V <sub>bi</sub> , forming excitons and emitting the light.....	29
<b>Figure 3-10:</b> The energy diagram of a double heterostructure device. Holes (red circles) and electron (blue circles) are injected from their respective electrodes into the HOMO and LUMO of the organic molecules. The holes and electrons migrate along the interface, forming an exciton at that interface and radiative decaying through the emission of a photon.....	32
<b>Figure 3-11:</b> Energy diagram of an OLED with HTL, EML (containing host (orange) and dopant (green) energy levels) and ETL .....	32
<b>Figure 3-12:</b> Dexter energy transfer from host to dopant.....	34
<b>Figure 3-13:</b> Förster energy transfer from host to dopant .....	35
<b>Figure 3-14:</b> One of the first examples of a roll-to-roll PLED on plastic.....	36
<b>Figure 3-15:</b> Schematic illustration of organic thin film growth processes; (a) a vacuum thermal evaporation (VTE) and (b) a spin-coating methods.....	35

<b>Figure 3-16:</b> Examples of flexible OLEDs applications, (a) Flexible OLEDs by Universal display corporation, (b) Flexible OLEDs on garments.....	36
<b>Figure 3-17:</b> Various OLEDs display applications: (a) 11" OLED display, (Sony, XEL-1), (b) 4" active-matrix OLED display (Samsung Mobile Display, SMD), (c) 31" OLED TV (SMD, prototype), (d) 3-D TV based on a LCD display (SMD).....	37
<b>Figure 3-18:</b> Various OLEDs lighting applications .....	38
<b>Figure 3-19:</b> Vectorial representations of an electron's spin magnetic moment, an UP and a DOWN orientation along an arbitrary Z axis.....	400
<b>Figure 3-20:</b> Vectorial representation of the three triplet states (a, b and c) with magnetic quantum number $M_s = (1, 0 \text{ and } -1)$ and a singlet state (d), with up and down spin vectors represented by $(\alpha)$ and $(\beta)$ respectively.....	400
<b>Figure 4-1:</b> (a) Synthesis of intermediates ( <b>Ia-Ij</b> ) (b) synthesized intermediates ( <b>Ia-Ij</b> ) .....	45
<b>Figure 4-2:</b> (a) Synthesis of monomers ( <b>Ma -Mf</b> ), (b) synthesized monomers ( <b>Ma-Mf</b> ) .....	Er
<b>ror! Bookmark not defined.</b>	
<b>Figure 4-3:</b> Synthetic route of the polyamides .....	51
<b>Figure 5-1:</b> Synthesis routes of (a) intermediate <b>Ia</b> and (b) its monomer ( <b>Ma</b> ).....	57
<b>Figure 5-2:</b> Reaction Mechanism of (a) the aromatic nucleophilic fluoro-displacement reaction and (b) the hydrolysis of nitrile intermediate to the carboxylic compound.....	59
<b>Figure 5-3:</b> FT-IR spectra of compound ( <b>Ma</b> ) .....	61
<b>Figure 5-4:</b> NMR spectrum of compound <b>Ia</b> and its molecular structure (a) $^1\text{H}$ and .....	63
<b>Figure 5-5:</b> NMR spectrum of compound ( <b>Ma</b> ) and its molecular structure (a) $^1\text{H}$ .....	64
<b>Figure 5-6:</b> Synthesis routes of poly(amine-amide)s ( <b>Pa1</b> ), ( <b>Pa2</b> ) .....	68
<b>Figure 5-7:</b> NMR-spectrum of poly(amine amide) ( <b>Pa1</b> ) in DMSO-d <sub>6</sub> (a) $^1\text{H}$ and (b) $^{13}\text{C}$ .....	69
<b>Figure 5-8:</b> NMR-spectra of synthesized poly(amine amide) ( <b>Pa2</b> ) in DMSO-d <sub>6</sub> ; (a) $^1\text{H}$ and (b) $^{13}\text{C}$ .....	72
<b>Figure 5-9:</b> NMR-spectra of synthesized poly(amine amide) ( <b>Pf1</b> ) in DMSO-d <sub>6</sub> ; (a) $^1\text{H}$ and (b) $^{13}\text{C}$ .....	74

<b>Figure 5-10:</b> NMR-spectra of synthesized poly(amine amide) ( <b>Pf2</b> ) in DMSO-d <sub>6</sub> :(a) <sup>1</sup> H and (b) <sup>13</sup> C.....	75
<b>Figure 5-11:</b> TGA of poly(amine-amide)s (a) ( <b>Pa1</b> ), (b) ( <b>Pa2</b> ), (c) ( <b>Pf1</b> ), (d), ( <b>Pf2</b> ) ....	76
<b>Figure 5-12:</b> Possible electronic transitions of p, s, and n electrons .....	82
<b>Figure 5-13:</b> UV-Vis absorption of poly(amine-amide)s in 10 <sup>-5</sup> M.....	84
<b>Figure 5-14:</b> Photoluminescence of poly(amine-amide)s with a concentration of 10 <sup>-5</sup> M in NMP.....	89
<b>Figure 5-15:</b> UV-Vis absorption spectrum of polyamide ( <b>Pa1</b> ) in (10 <sup>-5</sup> M) NMP .....	90
<b>Figure 5-16:</b> Cyclic voltammograms of (a) ferrocene as reference and (b) the cast film of poly(amine amide) ( <b>Pa1</b> ) on the indium-tin oxide(ITO)- coated glass substrate in CH <sub>3</sub> CN containing 0.1 M TBAP, with a scan rate of 0.1 V/s.....	91
<b>Figure 5-17:</b> UV-Vis absorption spectrum of polyamide ( <b>Pa1</b> ) in (10 <sup>-5</sup> M) NMP.....	94
<b>Figure 5-18:</b> Cyclic voltammograms of (a) Ferrocene as reference and (b) the cast film of poly(amine amide) ( <b>Pa1</b> ) on the indium-tin oxide(ITO)-coated glass substrate in CH <sub>3</sub> CN containing 0.1 M TBAP, with a scan rate of 0.1 V/s.....	95

## LIST OF TABLES

<b>Table 2-1:</b> Properties of commercial aromatic polyamide fibers. ....	17
<b>Table 4-1:</b> Synthesized monomers and polyamides .....	44
<b>Table 5-1:</b> Synthesized monomers and their structures.....	60
<b>Table 5-2:</b> FTIR data of the intermediates and its monomers .....	62
<b>Table 5-3:</b> <sup>1</sup> H NMR data of the synthesized monomers.....	65
<b>Table 5-4:</b> <sup>13</sup> C NMR data of synthesized monomers.....	66
<b>Table 5-5:</b> Synthesized poly(amine amide) codes.....	68
<b>Table 5-6:</b> FTIR data of the poly(amine-amide)s.....	70
<b>Table 5-7:</b> <sup>1</sup> H NMR data of synthesized poly(amine-amide)s .....	77
<b>Table 5-8:</b> <sup>13</sup> C NMR data of synthesized poly(amine-amide)s .....	78
<b>Table 5-9:</b> Solubility of aromatic polyamides .....	80
<b>Table 5-10:</b> Structures and thermal properties of the synthesized polyamides .....	85

<b>Table 5-11:</b> Thermal behavior data of the synthesized poly(amine-amide)s .....	87
<b>Table 5-12:</b> Optical properties of the poly(amine-amide)s .....	88
<b>Table 5-13:</b> Electrochemical properties of the poly(amine-amide)s .....	93

### LIST OF ABBREVIATIONS AND SYMBOLS

Alqs	Tris(8-hydroxyquinolate)aluminum(III)
BCP	2,9-Dimethyl-4,7-diphenyl-1,10-phenanthroline
CBP	4,4'-bis(9-carbazolyl)-biphenyl
CCT	Correlated color temperature
CVD	Chemical vapor deposition
CDBP	4,4'-bis(9-carbazolyl)-2,2'-dimethylbiphenyl
CES	Consumer electronics show
CIE	Commission Internationale de l'Eclairage
CRT	Cathode ray tube
CDCl <sub>3</sub> -d <sub>1</sub>	Deuterated chloroform
DMSO-d <sub>6</sub>	Dimethylsulfoxide-d <sub>6</sub>
DSC	Differential Scanning Calorimetry
DMF	N,N-dimethylformamide
DMAc	N,Ndimethylacetamide
DBTDL	Dibutyltin dilaurate
EL	Electroluminescence
EMs	Emissive materials
EMsL	Emissive materials/layer



ETMs	Electron-transport materials
ETL	Electron-transport layer
EC	Electrochromism
EIE	Electron-injector electrode
EML	Emissive material layer
GE	General Electric
HTML	Hole Transport Materials/layer
HBM	Hole blocking materials
HOMO	Highest occupied molecular orbital
HTMs	Hole transporting materials
HMPA	Hexamethylphosphoramide
ITO	Indium tin oxide
IPC	Isophthaloyl dichloride
IP	Ionization potentials
LUMO	Lowest unoccupied molecular orbital
(LED)s	Light emitting devices
mCP	N,N'-dicarbazolyl-3,5-benzene
MTDATA	4,4',4''-tris(3-methylphenylphenylamino)-triphenylamine
MPD	M-phenylenediamine
MBE	Molecular beam epitaxy
M <sub>n</sub>	Number-average molecular weight
M <sub>w</sub>	Weight-average molecular weights

$\alpha$ -NPD	4,4'-bis [N-(1-naphthyl-1)-N-phenyl-amino]biphenyl
NMP	N-methyl-2-pyrrolidone
NMR	Nuclear magnetic resonance
OA	Optically active
OLED	Organic Light Emitting Diode
OAPs	Optically active polymers
OLEMs	Organic lighting emitting materials
ODA	3,4-diaminodiphenyl ether
PLD	Pulsed laser deposition
PPV	Poly(p-phenylenevinylene)
PBD	2-(4-(biphenyl)-5-(4-tert-butylphenyl)-1,3,4-oxadiazole
POLEDs	Poly organic light emitting diodes
PAs	Polyamides
PL	Photoluminescence
PLEDs	Polymer light emitting diodes
PPPT	poly(p-phenylene terephthalamide)
PMPI	Poly(m-phenylene isophthalamide)
PPBA	Poly(p-benzamide)
PPD	p-phenylenediamine
TPP	Triphenyl phosphite
T	Triplet
T <sub>gs</sub>	Glass transition temperatures

T <sub>d</sub> 5%	Decomposition temperatures at 5% weight loss
T <sub>d</sub> 10%	Decomposition temperatures at 10% weight loss
TCTA	4,4',4''-tri(N-carbazolyl)triphenylamine
TAPC	1,1-bis [(di-4-tolylamino)phenyl]cyclohexane
TGA	Thermogravimetry analysis
TPD	N,N'-(3-methylphenyl)-1,1'-biphenyl-4,4'-diamine
TPDQ	5,5',6,6-tetraphenyl-Z-diquinoxaline
3TPYMB	Tris [3-(3-pyridyl)mesityl]borane
TPP	Triphenylphosphite
TEA	Triethylamine
TPC	Terephthaloyl dichloride
VTE	Vacuum thermal evaporation
WOLEDs	White OLEDs

## LIST OF APPENDICES

Appendix A: FTIR spectra for synthesized compounds.....	120
Appendix B: <sup>1</sup> H and <sup>13</sup> C- NMR spectra for synthesized compounds.....	125
Appendix C: DSC thermograms for synthesized compounds.....	145
Appendix D: TGA thermograms for synthesized compounds.....	150

## CHAPTER 1 : INTRODUCTION

### 1.1. Introduction

Aromatic polyamides are considered to be high-performance polymeric materials due to their superior thermal stability, good mechanical properties and chemical resistance which makes them useful for advanced technologies. They are finding increasing demand for use as advantageous replacements for metals or ceramics in currently used goods, or even as new materials in novel technological applications. They are also known as difficult processing materials because of high melting or glass transition temperatures and limited solubility in most organic solvents [1-4].

To overcome these limitations, polymer-structure modification becomes necessary such as introduction of bulky, packing-disruptive groups into the polymer backbone [5-8]. It has been demonstrated that aromatic polyamides containing three-dimensional, propeller-shaped triphenylamine (TPA) unit had good solubility in organic solvents while retaining high thermal stability [9-11]. Furthermore, TPA-based polymers are widely used as the hole-transport layer in electroluminescence (EL) devices, besides exhibiting interesting electrochromic behavior [12-18].

Fabrication of an EL device with high performance, long durability, and low driving voltage can be effectively achieved with a multilayer sandwiched structure. To balance the injection and transport of both holes and electrons, hole and electron-transporting layers are often used. Triarylamine derivatives have been used as hole transport materials for use in multilayer organic EL devices due to their relatively high mobility and their low ionization potentials [19, 20]. The feasibility of utilizing spin-coating and ink-jet printing processes for large-area EL devices and possibilities of various chemical modifications (to improve emission efficiencies and allow patterning) make polymeric materials containing triarylamine units very attractive [21]. In order to optimize the hole injection and transport

properties of classical emissive polymers like poly(*p*-phenylenevinylene)s (PPV) or poly(9,9-dialkylfluorenes) (PF), there have been several reports on PPV and PF derivatives involving hole-transporting units such as TPA groups in the emissive  $\pi$ -conjugated main chains [22] or grafting them as side chains in a polymer [23] or end-capping them onto the polymer chain-ends or the outer surface of dendritic wedges [24].

## 1.2. Research Objective

The aim of this work is to describe the synthesis and properties of new aromatic poly(amine-amide)s containing TPA moieties which has potential to be used as transporting materials in light emitting devices. The research objectives are to :

1. synthesize monomers and new poly(amine-amide)s via phosphorylation polycondensation reaction.
2. confirm the structures by FTIR,  $^1\text{H}$  and  $^{13}\text{C}$  NMR spectroscopic techniques.
3. characterize of the thermal and spectral properties were measured for these poly(amine-amide)s.
4. investigate the redox behavior of the poly(amine-amide)s by cyclic voltammetry.

## 1.3. Thesis Outline

**Chapter 1** includes an introduction of aromatic polyamides. Research objectives and thesis outline.

**Chapter 2** describes background and literature review of aromatic polyamides as hole-transport layer, which is widely used as electron acceptors in polymer light emitting devices (PLEDs). Main methods of synthesizing polyamides also are included. Special applications of the aromatic polyamides are explained in detail. An important subject was explained in this chapter about improvement of optical properties of polyamides in (PLED)s. Finally, this chapter explains the behavior of polyamides in polymer light emitting devices (PLEDs).

**Chapter 3** describes the light-emitting device (LED) as lighting source and types of these devices. Comparison of organic and inorganic devices are also demonstrated. Description of polymer organic light emitting devices (POLEDs) is simple compared to more organic layers of electro and hole transporting materials being sandwiched between two electrodes. The operation of organic transporting materials according to the energy band diagrams depends on the mechanism of the energy transfer from host to dopant. This chapter clarified how the organic light emitting diodes (OLEDs) are fabricated in different methods. Advantages and applications of organic light-emitting devices together with photophysical and photochemical processes that are encountered in the field of organic light emitting devices are expressed.

**Chapter 4** describes all the experimental procedures of synthesis starting with intermediates, carboxylic monomers and final polymers. All characterization techniques which were carried out and instruments used are explained in detail as well.

**Chapter 5** discusses the results including solubility, thermal, optical and electrochemistry properties data.

**Chapter 6** presents the concluding results of the research with recommendations to the future work. Appendices indicate the supplementary data which are related with experimental and result data.

## CHAPTER 2: BACKGROUND AND LITERATURE REVIEW

### 2.1. Aromatic Polyamides

#### 2.1.1. Aromatic Polyamide Synthesis

There are three main methods to prepare polyamides:

##### 2.1.1.1. Low -temperature Solution Method

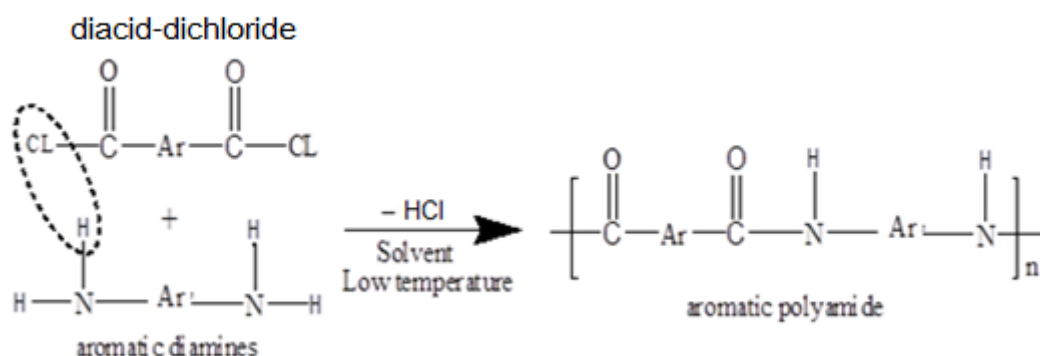
This method is most known for the preparation of aromatic polyamides. It is carried out by the reaction of diacid dichlorides with diamines at low temperatures (**Figure 2-1**). The solvents used are polar aprotic solvents like N,N-dimethylformamide (DMF), N,N-dimethylacetamide (DMAc), N-methyl-2-pyrrolidone (NMP), and hexamethylphosphoramide (HMPA).

It is often used with salts such as NaCl, CaCl<sub>2</sub>, or a mixture of salt as solubility promoters because the cations interact with the amide groups, reducing the strength of hydrogen bonds.

Poly(p-phenylene terephthalamide) (PPPT) and poly(m-phenylene isophthalamide) (PMPI) are prepared commercially by condensation of p-phenylenediamine (PPD) and terephthaloyl dichloride (TPC) or m-phenylenediamine (MPD) and isophthaloyl dichloride (IPC) using NMP as the solvent and CaCl<sub>2</sub> as the ionic component. The low temperature solution method is generally preferred when the diacid dichloride can be easily obtained from the corresponding aromatic diacid. Generally, the number-average molecular weight  $M_n$  of aromatic polyamides are in the range of  $(1 - 10) \times 10^3$  g/mol, which is typical of condensation polymers. The polydispersity of the polymers obtained by this method is approximately two for lower molecular weight polymers and nearer to three for polymers with weight-average molecular weights  $M_w > 35 \times 10^3$  g/mol.

The polycondensation reaction can also be carried out in a two-phase system at room temperature, via the interfacial polymerization [25]. The diamine and the acid dichloride monomers are dissolved in water and a water-immiscible solvent, respectively. A base and

a surfactant are usually added to the aqueous media. The mixture of immiscible solutions, upon rapid stirring, gives rise to a polymer precipitate in seconds. The reaction is extremely fast and occurs in the interface on the organic solvent side.



**Figure 2-1:** Reaction of diacid dichloride with diamine

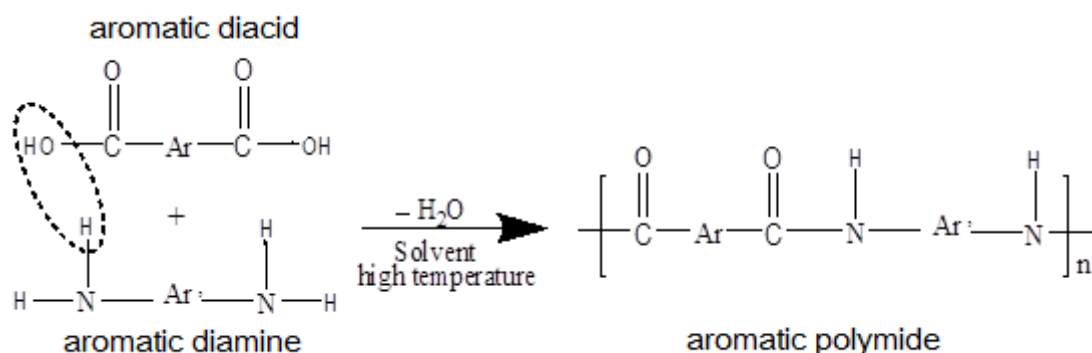
#### 2.1.1.2. High-temperature Solution Method

The direct condensation between aromatic diacids and diamines can be used (**Figure 2-2**) if the diacid dichloride cannot be obtained from the corresponding aromatic diacid or is not in good quality, i.e., if it has much moisture and is heat sensitive. The method was developed by Yamazaki et al. [26], and it is still not used for commercial purposes. Again, high purity monomers are required and an extra drawback is the side reactions that occur at the high temperatures used. Thus, to obtain an aromatic polyamide with side chains containing sensitive functional groups by this method, it is important to verify the absence of side reactions in the polymerization conditions. This can be carried out by the prior preparation of model compounds.

Recent efforts on polycondensation have been carried out under high temperature solution methods by replacing organic solvents by more environmentally friendly versions. Following this approach, the mixture of solvents used in the usual low-temperature polycondensation (DMF, DMA, NMP) and in the Yamazaki polyamidation method (NMP and pyridine) can be replaced by ionic liquids. The ionic liquids have high thermal



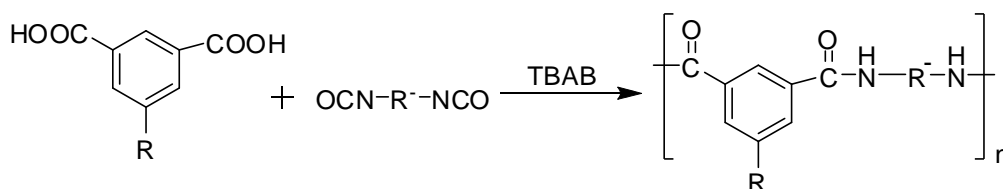
stability, low vapor pressure, are highly polar, and have a high dielectric constant, which makes them suitable to dissolve the aromatic polyamides. Thus, friendly aromatic polyamides have been prepared using ionic liquids with triphenylphosphite (TPP) to promote the direct condensation of the acid and amide groups and thus avoiding the use of harmful solvents like pyridine and NMP, and to promote the reaction of diacid and diamines at low temperatures [27-35].



**Figure 2-2:** Reaction of diacid with diamine

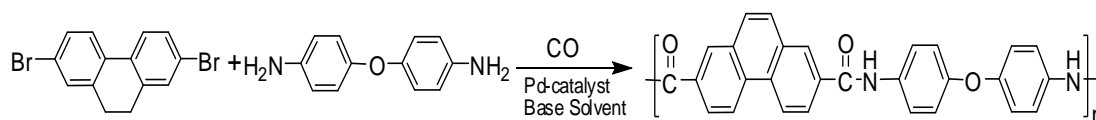
### 2.1.1.3. Alternative Polymerization Methods

There are a wide set of synthetic methods used to prepare aromatic or aliphatic–aromatic amide bonds. The reaction of diacids with diisocyanates **Figure 2-3** in the presence of tetrabutylammonium bromide (TBAB) as a molten ionic liquid under microwave irradiation conditions has been employed and was compared with polymerization in traditional solvent like N-methyl-2-pyrrolidone (NMP) [36].



**Figure 2-3:** Reaction of diacid with diisocyanate

To prepare insoluble thermosetting resins for matrix components of fiber reinforced plastics (FRP), palladium-catalyzed carbonylation-polycondensation from dihaloaryl compounds and aromatic diamines has been used [37, 38] as shown in Figure 2-4.



**Figure 2-4:** Palladium-catalyzed carbonylation-polycondensation reaction

## 2.1.2. Types of the Aromatic Polyamides

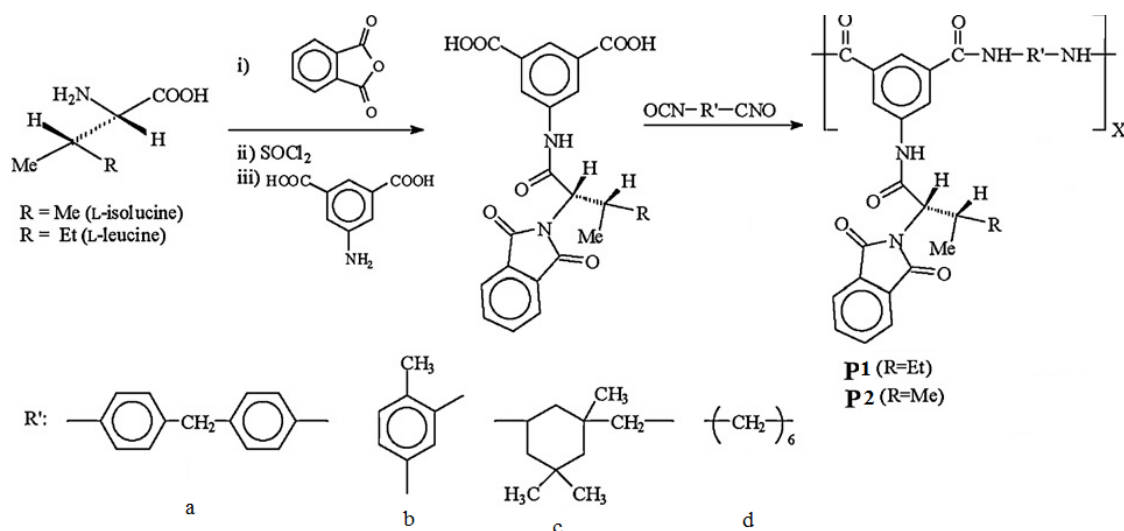
### 2.1.2.1. Optically Active Polyamides

It is obvious that many natural products are optically active. Many compounds have the same property such as drugs which are derived from natural sources. Many natural polymers, such as proteins, DNA, and polysaccharides, are also optically active. So the design, characterization and preparation of chiral polymers are of great interest [39, 40].

Optically active polymers (OAPs) are known to be employed in many applications. These include assembling chiral media for asymmetric synthesis, chiral liquid crystals in ferroelectrics, chiral stationary phases for resolution of enantiomers in chromatographic techniques, nonlinear optical devices and etc. [37].

Earlier researchers [41, 42] have synthesized pendant polyisophthalamides with a side L-isoleucine core group by using aromatic conventional high-temperature solution method using different catalysts (dibutyltin dilaurate: DBTDL, pyridine, triethylamine (TEA), or no catalysts). The best results were obtained with DBTDL. All polymers showed optical rotation  $[\alpha]$ , which verified their optical activity. Polymers prepared by different methods showed different optical rotations and this fact was attributed to the dependence of the optical rotation on the overall structure and regularity of the resulting polymer chains. Surprisingly, polymers of the same chemical structure polymerized by the same method

with different catalysts resulted in different values of  $[\alpha]$ , i.e., the  $[\alpha]_D^{25}$  is  $-28.5$  and  $+28.5$  for P1 and P2 polymers obtained by employing DBTDL as catalyst (**Figure 2-5**). However, the bulkiness of the pendant aliphatic substructure influences the polymer properties, resulting in fairly soluble materials having a low thermal stability (5% weight lost around  $210\text{--}250^\circ\text{C}$ ).

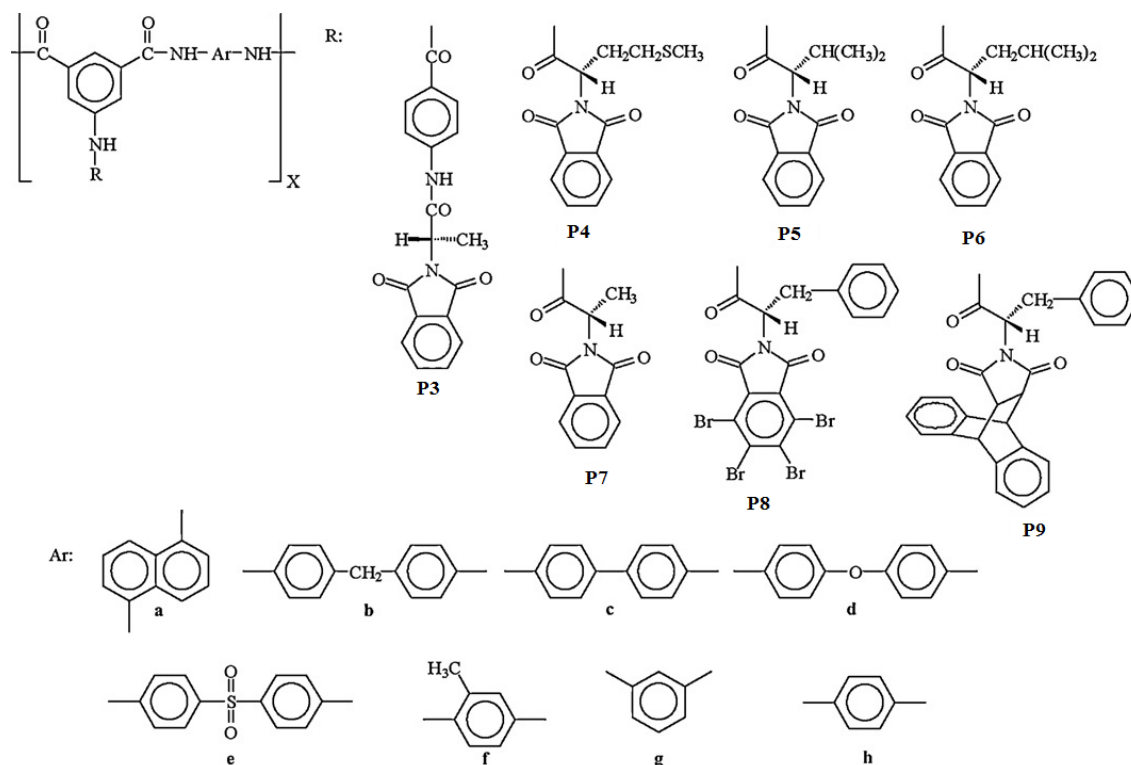


**Figure 2-5:** Synthesis of pendant polyisophthalamides

The authors claimed that since these polymers are optically active and have amino acids in the polymer architecture, they are likely biodegradable, and therefore classified as environmentally friendly polymers.

In a similar work, OAPs, specifically polyisophthalamides having a pendant L-alanine (**Figure 2-6**), (**P3**, **P7**) or methionine (**P4**) and phthalimide groups have been prepared under conventional heating by microwave methods using ionic liquids as solvents [43-45]. The microwave heating was clearly more efficient than classical thermal heating. The polymers exhibited decomposition temperatures greater than  $300^\circ\text{C}$  ( $T_{d5}$  between  $270$  and  $380^\circ\text{C}$ ) and  $T_g$ s between  $113$  and  $208^\circ\text{C}$ . The limiting oxygen index (LOI) was estimated for P16 using the van Krevelen and Hoftyzer equation [46] ( $\text{LOI} = 17.5 \times 0.4\text{CR}$ , where CR is the char yield obtained by TGA), and was greater than 35, thus classifying the

polymers as self-extinguishing. In a similar fashion, OAPs derived from 5-(2-phthalimidyl-3-methylbutanoylamino)isophthalic acid or (2S)-4-[(4-methyl-2-phthalimidylpentanoylamino)benzoylamino]isophthalic acid and aromatic diamides (**P5**, **P6**) were described and characterized. In this line, **P8**, depicts similar polymer structures containing a pendant perbromophthalimidyl moiety, giving optically active flame retardant polyamides as products. The  $[\alpha]_D^{25}$  values ranged from  $-75.8$  to  $-122.4^\circ\text{C}$ , T<sub>g</sub>s from  $197$  to  $236^\circ\text{C}$ , and the LOIs were over 65%. The authors expanded the study of these kinds of materials to other bulky pendant structures, **P9**, where the polyamides showed moderate T<sub>d</sub>10 s ranging from  $340$  to  $385^\circ\text{C}$ , and T<sub>g</sub>s over  $180^\circ\text{C}$ .



**Figure 2-6:** Structures of polyisophthalamides having a pendant L-alanine and methionine

#### 2.1.2.2. Luminescent and Electrochromic Polyamides

Luminescent materials have the characteristic of light-emitting phenomena. There are different types of luminescence, such as electroluminescence (EL) or photoluminescence (PL) phenomena. When these materials are exposed to an electric current or absorption of

photons, re-radiation will occur [47,48]. Besides having luminescent properties, the film formation properties and outstanding mechanical properties of aromatic polyamides make them applicable for the production of polymer light-emitting diodes (PLEDs). Some luminescent materials also show electrochromism (EC), a phenomenon in which materials exhibit a reversible change in optical properties when they are oxidized and reduced. Electrochromic materials are now being used in different applications like mirrors, displays, windows and earth-tone chameleon materials [49].

### **2.1.3. Improvement of Optical Properties of Polyamides**

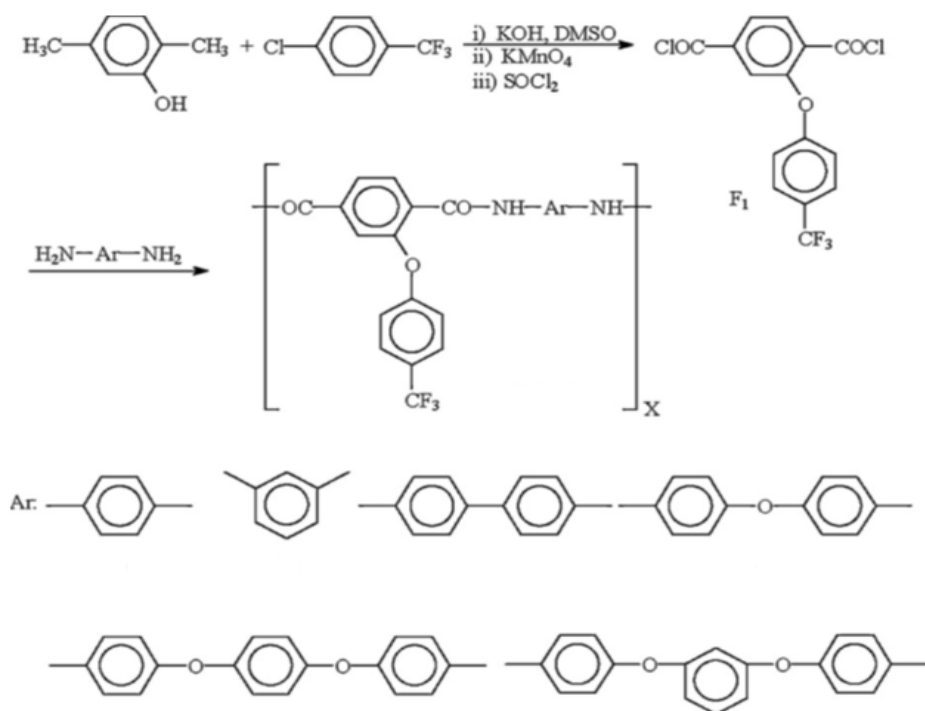
Improvements on the properties of polyamides containing the TPA-based monomer have been carried out by Hsiao et al. [50] by insertion of bulky groups such as 1,3,4-oxadiazole, naphthyl, phenyl and tert-butyl groups.

The optical properties of the polyamides containing tert-butyl groups were investigated by UV-vis and PL spectroscopy. The polymers showed strong UV-vis absorption bands at 314 - 361 nm in DMA solution, and their PL spectra exhibited emission peaks around 421 - 430 nm, which is in the blue region. The electrochemical (EC) characteristics were also measured, and when increasing the potential from 0 to 1.10 V, the characteristic absorbance peak at 356 nm for polyamide decreased gradually. The film color became green. The polyamides had high  $T_g$  values between 282 and 302°C, and decomposition temperature ranged from 458 to 498°C, while char yields were greater than 60% additionally.

#### **2.1.3.1. Polyamides with Fluorinated and Chlorinated Substituents**

The presence of fluoro and chloro groups in the polymer structures makes them resistant to flame, solvents, acid, and bases, which is desirable for a number of applications. Moreover, the trifluoromethyl group  $CF_3$ , plays an important role in achieving good solubility and electrical and dielectric performance. Sheng et al. [51] have reported on fluorinated aromatic polyamides derived from an asymmetric monomer, 2-(4-trifluoromethoxyphenyl)

terephthaloyl chloride, polymerized with various aromatic diamines (**Figure 2-7**). The resultant polyamide was amorphous and readily soluble in polar aprotic solvents, and some were soluble in THF upon heating. They gave flexible and tough films upon casting. The  $T_g$  values ranged from 222 to 294 °C, and their decomposition temperature values were greater than 442°C in nitrogen. Moreover, the films were highly transparent, as measured in terms of UV–vis absorption cut-off wavelength (330–371 nm).

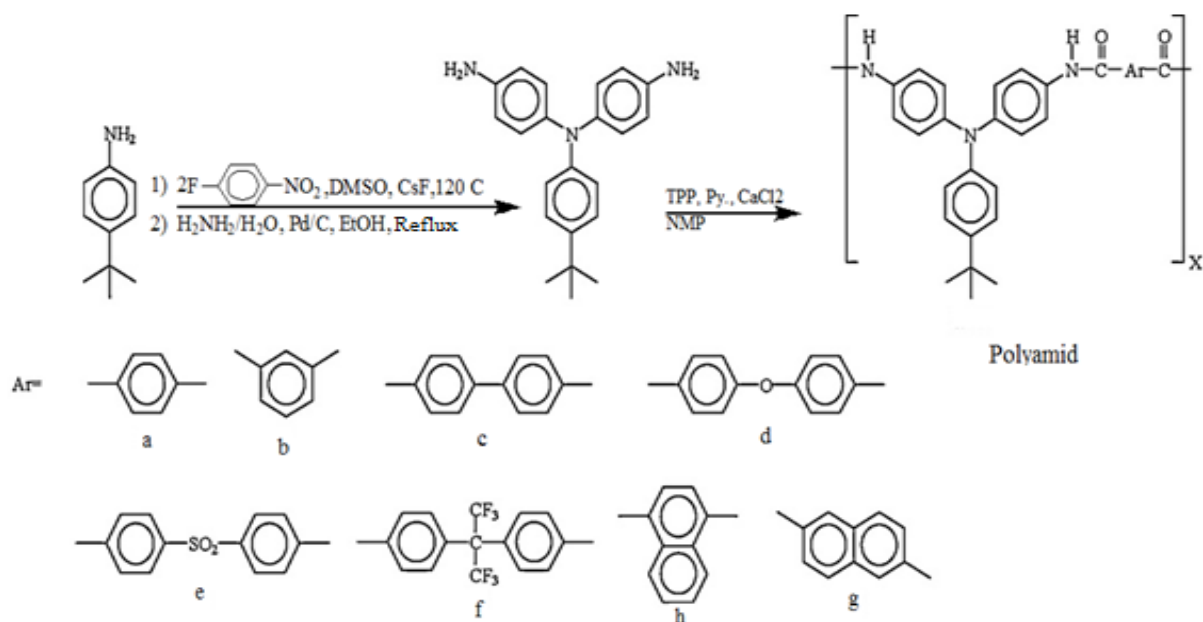


**Figure 2-7:** Halogenated polyamides

#### 2.1.3.2. Polyamides with Bulky Pendant Groups

Most research efforts are currently focused on the chemical modification of the composition of these materials with the objective of improving their processing ability and, more specifically the solubility in organic solvents. The incorporation of bulky pendant groups can provide beneficial effects for solubility, because this approach produces a separation of chains, a weakening of hydrogen bonding, and a lowering of chain packing with a gain of free volume, which decrease the  $T_g$ s (**Figure 2-8**). On the contrary, bulky

side groups also restrict molecular mobility, so that the overall observable effect is an increase in  $T_g$ s.



**Figure 2-8:** Improvement of optical properties of PLEDs using bulky groups

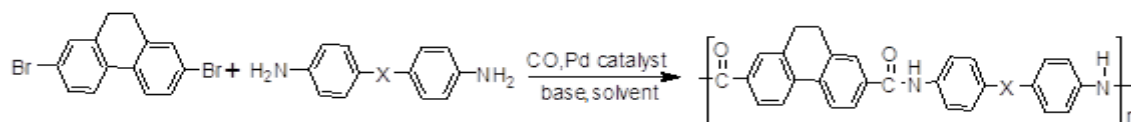
#### 2.1.3.3. Polyamides with Segmented Blocks

Segmented block polymers contain alternating blocks, or segments, having distinct chemical entities of different properties, and usually include hard and soft segments. The soft segments contribute to the flexibility, while the hard segments, which are glassy or semicrystalline, serve as physical or virtual crosslinking points. The mechanical and thermal properties of polymers depend on the chemical nature and proportion of the hard segment. The softening temperature or melting point increasing with the number of physical crosslinks between the hard segment chains.

#### 2.1.3.4. Unclassified Polyamide Structures

This section of unclassified polyamides is included to accommodate recent discoveries. Kubota et al [37]. prepared rigid biphenyl-containing aramids via a one-step procedure from dihalobiphenyl and aromatic diamine by palladium-catalyzed carbonylation polycondensation as shown in **Figure 2-9**. Parameters such as base, solvent, palladium-

phosphine catalyst, and CO pressure had a significant impact on the average molecular weight for the polyamides formed from the reaction of 2,7-dibromo-9,10-dihydrophenanthrene and 4,4'-diaminodiphenyl ether. Under optimum conditions, the polyamide was obtained in 99% yield and had a high molecular weight ( $M_w = 128 \times 10^3$ ) with the thermal stability for thermal decomposition  $T_{d10}$  varied between 450 and 470 °C.



**Figure 2-9:** Unclassified polyamide structures

#### 2.1.4. Behavior of Polyamides in PLEDs

Many researches have been carried out in the preparation of blue light-emitting polymers because blue light can be converted to green or red using proper dyes, which means a blue PLED alone is capable of generating all colors, while green or red cannot emit blue light. As a result, the 1,3,4-oxadiazole rings are promising chemical moieties for introduction into the polymer backbone or in the pendant structure as these rings have an electron-withdrawing character, which facilitates the injection and transport of electrons [52,53]. The polyamide derived from the diamine with TPA group reveal excellent electrochromic contrast and coloration efficiency, changing color from the pale yellowish neutral, to green, and then to the blue oxidized forms during positive scanning potentials from 0.0 to 1.2 V. The incorporation of bulky naphthyl groups into the polymer side of the electrochromic materials resulted in lighter-colored polymers, thus enhancing the coloration efficiency at higher contrasts [54]. The most widely studied EC polyamides are polymers with a triphenylamine moiety, a well-known high-efficiency chromophore. Since the one-electron oxidation product of triphenylamine is not stable due to the para-para tail-to-tail coupling, which yields tetraphenylbenzidine and resulting in the lost of two protons



per dimer, monomers containing electron-rich para TPA moieties have been prepared as substitutes on the pendant phenyl ring, thus providing stable radical cations upon oxidation [55-57].

#### **2.1.5. Aromatic Poly(amine-amide)s in Light Emitting Devices**

Aromatic poly(amine-amide)s are an important type of hole transporting materials (HTMs) which are widely used as an electron donator in light emitting devices (LEDs) or polymer light emitting devices (PLEDs). They have relatively high mobility and low ionization potentials (IP) [58-63] and are easily oxidized to form stable radical cations [2]. Aromatic polyamides are well accepted as high-performance polymeric materials for their excellent mechanical properties, high thermal stability, and good chemical resistance [64]. The use of conjugated polymers in the polymer light-emitting devices (PLEDs) has received a great deal of concern in the industry because of several appealing advantages. The most efficient devices using PLEDs is an architecture with a thin-film multilayer structure consisting of a hole-transporting layer, an emitting layer and an electron-transporting layer sandwiched between two metal electrodes [65]. Charge carriers (holes and electrons) are injected separately from the anode and cathode, recombine in the emitting layer and thus emit light between two electrodes [66].

Many emitting materials have been designed and used in LEDs. However, high-performance light emitting ones are rare because of the intrinsic wide band-gap required for such materials. Many hole transporting materials have been tried for light-emission [67].

#### **2.1.6. Commercial Promatic Polyamides**

The simplest and best known commercial aromatic polyamides are poly(p-phenylene terephthalamide) (PPPT) and poly(m-phenylene isophthalamide) (PMPI) as shown in **Figure 2-10**. Both can be transformed using their solutions, by wet spinning into flame to form cut-resistant, and high tensile strength synthetic fibers or they can be cast into

varnishes or enamels yielding similar properties. The transformed materials have applications in advanced fabrics, coatings and fillers, as advanced composites in the aerospace and armament industry, as asbestos substitutes, electrical insulation, bullet-proof body armor, industrial filters, and protective and sport clothing, etc.

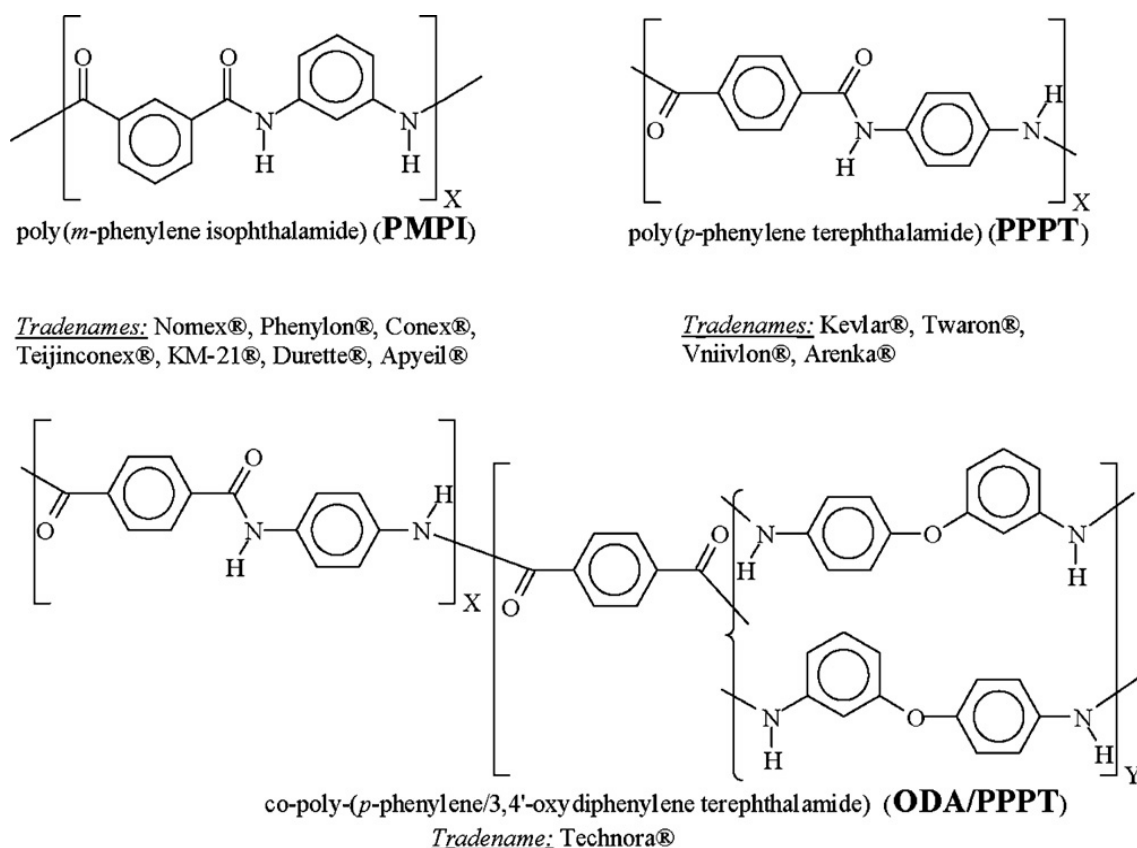
As a result, recent basic and applied researches have focused on enhancing their process ability and solubility in order to broaden the scope of the technological applications of these materials. There is currently a huge research effort directed toward exploiting the special high performance characteristics of the polyamides to obtain electro- or photoluminescent materials, reverse osmosis, gas or ion-exchange membranes, optically active (OA) materials, nanocomposites, etc. with superior thermo mechanical performances.

The first commercial para oriented polyamide was poly(p-benzamide) (PPBA) ('Fiber B). It was replaced in the market by (PPPT) in 1970 under the trade name of 'Kevlar.

Their synthesis was performed by polycondensation method at low temperatures in a solution of terephthaloyl dichloride (TPC) and p-phenylenediamine (PPD) in hexamethylphosphoramide (HMPA). After that, the solvent was successfully replaced by an N-methyl-2-pyrrolidone (NMP) in  $\text{CaCl}_2$  as an agent system. The PPPT has a high-performance properties due to its chemical structure. Its aromatic structure and all-para substitutions cause stiffness-like macromolecules with a high contact energy and a high crystallization tendency due to the very favorable intramolecular hydrogen bonds. PPPT fibers can be transformed into materials and composites having superior thermal and mechanical resistance. Because of that reason, all aromatic polyamides with all-meta orientation in the phenylene ring, such as PMPI, have less linear structures and low in its contact energy and crystallization tendency. Thus, PMPI is a high-performance polymer, with high thermal and mechanical resistances. Because of that reason, all aromatic polyamides with all-meta orientation in the phenylene ring, such as PMPI, have less linear

structures and a concomitant reduction in its cohesive energy and crystallization tendency. Thus, PMPI is a high-performance polymer, with high thermal and mechanical resistances. The copolymerization of terephthaloyl dichloride (TPC) with PPD and 3,4-diaminodiphenyl ether (ODA) gives rise to a relatively soluble polymer, ODA/PPPT as shown in **Figure 2-10**, commercialized under the trade name of Technora since 1987. The asymmetry of the monomer ODA and the copolymerization give rise to a less ordered material with lower adhesive energy.

The properties of the commercial aromatic polyamides fibers (crystal lattice parameters, density, equilibrium moisture content, tensile properties at a room and at an elevated temperatures, thermal properties and chemical resistance) and the properties of the commercial aramid films were well summarized by Gallini [68], Ozawa and Matsuda [69], Tanner et al. [70] and Yarn. Table 2-1 describes the summary of these properties.



**Figure 2-10:** Structures of (PPPT) and (PMPI)

**Table 2-1:** Properties of commercial aromatic polyamide fiber

Property of Polymer	PMPI	PPPT	ODA/PPPT
Density (g/cm <sup>3</sup> )	1.38	1.44	1.39
Water uptake (%), at 65% RH	5.2	3.9	4.0
Thermal properties T <sub>g</sub> (°C)	275	≡	-
T <sub>m</sub> (°C)	365 d <sup>a</sup>	>500 d <sup>a</sup>	>500 d <sup>a</sup>
T <sub>d</sub> (°C, in N <sub>2</sub> )	400–430	520–540	500
Tensile properties <sup>b</sup>	–	-	-
Strength (GPa)	0.59 - 0.86	2.9 - 3.0	-3.4
Modulus (GPa)	7.9 - 12.1	70 - 112	72
Elongation (%)	≡	-	-
Crystallinity	Highly crystalline	Highly crystalline	Highly oriented but less Crystalline (higher flexibility of the copolymer chain and loose crystalline structure)
Flammability (L.O.I.)	29	29	-5

a: Decomposes (d)

b: The comparison of the mechanical properties of oriented fibers with the properties reported for synthetic polyamides, usually obtained from unoriented films obtained by casting, is not usually straightforward

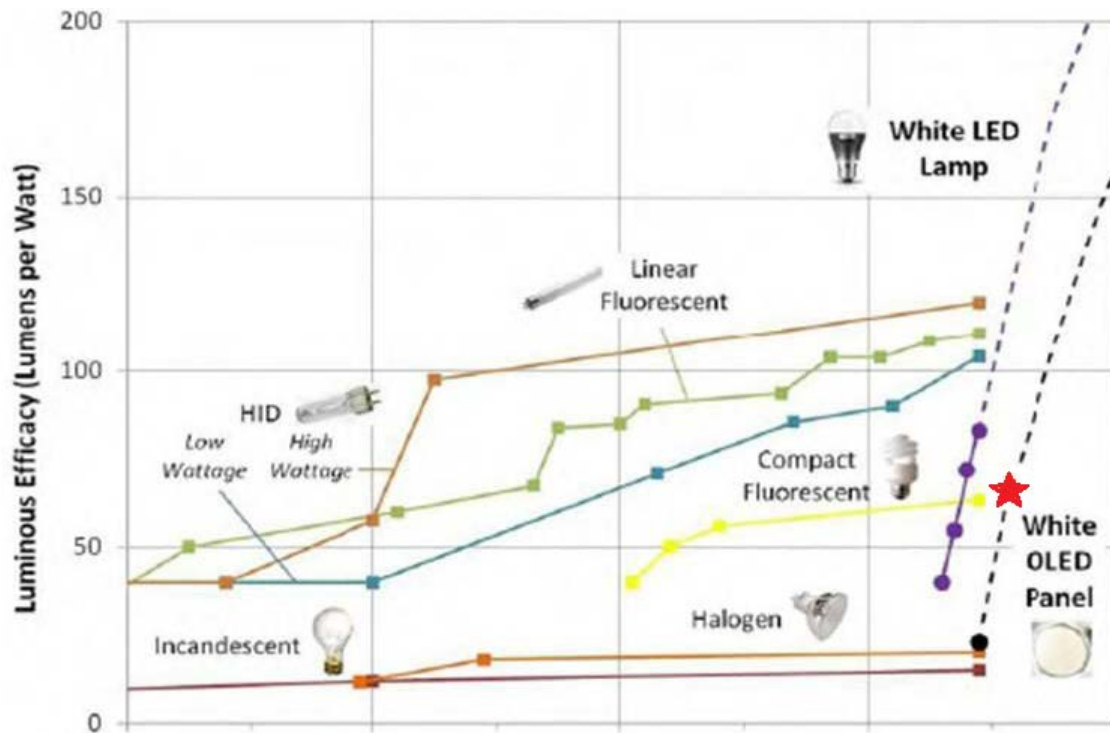
### CHAPTER 3: POLY ORGANIC LIGHT EMITTING DIODES (POLEDs)

Worldwide total energy consumption is steadily growing every year, especially with the recent increase of small mobile electronics. In order to satisfy both the limited energy resource problem and the environmentally clean energy issue, there have been continuous efforts to harvest natural energy sources such as water, wind, and sunlight. Also, highly energy-efficient rechargeable batteries such as Li-ion batteries and fuel/solar cells are intensively under investigation to meet the modern sustainable energy initiatives [71-73]. On the other hand, low electrical power consuming electronic devices are also expected to potentially reduce the demands of the energy grid. Therefore, the research which involves a high efficiency and low power consuming electronics becomes a high demand.

It was reported that approximately 22% of the total electricity consumed in the United States is transformed into lighting, and it is estimated that as much as 1,000 terawatt-hours (TWh) of electricity will be consumed by lighting by the year of 2025 [74]. If there were a lighting source that could convert the electrical energy into the visible light with 50% conversion efficiency, it would save energy consumption in the US by approximately 620 billion kilowatt-hours per year, which can eliminate about 70 nuclear plants on the US soil [75]. The common incandescent light bulb, for example, which was invented in the nineteenth century by heating a filament over 3000°C, has a power conversion efficiency (PCE) as low as 5% (i.e. 95% of electrically supplied energy is lost as a heat). As a comparison, the fluorescent tube, another common light source which excites a coated phosphor by discharging gas, has a better PCE reaching as much as approximately 20% corresponding to a high power efficiency ( $\eta P$ ) up to 100 lm/W at a room temperature ( $\sim 25^\circ\text{C}$ ). However, fluorescent tubes contain some amounts of mercury which is an environmentally hazardous material and also typically have 40 ~ 60 lm/W at elevated temperatures of operation (around 35°C) [76].

Solid-state lighting (SSL) is a highly energy-efficient light-emitting device (LED) based on semiconducting materials. Conventional LEDs are comprised of inorganic semiconductors; mostly group III-nitride, which have direct band gaps, converting the electrical energy directly into the visible light with less indirect energy losses. Although almost 100% internal quantum efficiency could be achieved using inorganic LEDs [77], there are still a few issues such as high material and fabrication cost, low color rendering index (CRI) for white light sources and device scalability. Nevertheless, the inorganic LED market has been increasing at an enormous rate in the last few years [78].

Organic light-emitting devices (OLEDs) convert the electrical power into light by using the organic semiconductors such as small molecule or polymer semiconducting materials. Since their first introduction by Tang and Vanslyke in 1987 at Eastman Kodak [79], an extensive research has been conducted among in academia and industry to achieve high efficiency and stable OLEDs. Compared to inorganic LEDs, OLEDs can be cheaper, easily scalable, and even tunable in electrical/optical properties, suggesting an excellent next-generation light source for either flat panel displays or SSL. However, a low efficiency and device stability are the most important issues for OLEDs in order to replace most existing light sources in the world. The classic power efficiencies and current progress of several white light sources including inorganic and organic LEDs are shown in **Figure 3-1**, and the power efficiency of white OLEDs (WOLEDs), demonstrated in this work without coupling enhancement methods, is also indicated by the red star [80].



**Figure 3-1:** Historical and predicted power efficiencies for various light sources [81]

### 3.1. Use of Poly Organic Light Emitting Diodes (POLEDs)

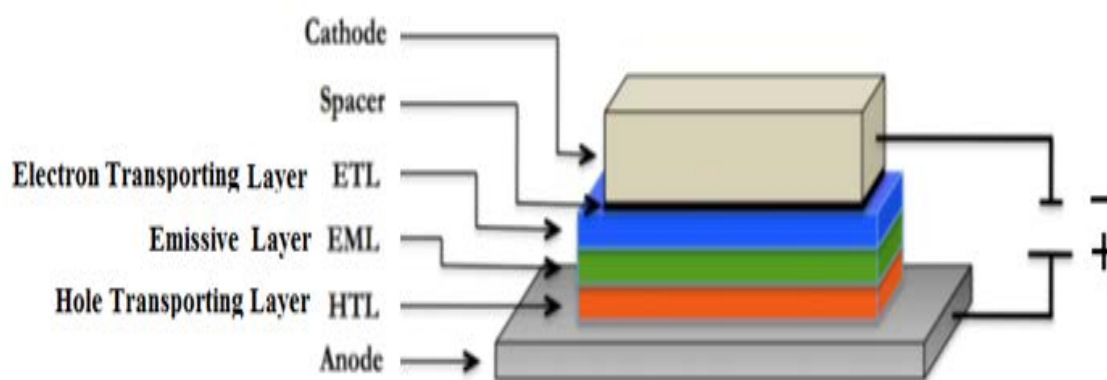
Use of POLEDs began in the 1960s with a single-layer device configuration where the light-emitting crystal was placed between two liquid electrode. After ten years, Tang and Van Slyke [81] reported superior device performance using two thin layers of amorphous organic compounds sandwiched between a transparent hole-injecting anode and a reflective electron-injecting cathode. Shortly afterwards Adachi et al [82]. reported a three-layer structure with separate layers for a hole and electron transport, and an emissive layer where recombination would occur, making fabrication of multicolor OLEDs possible.

### 3.2. POLEDs Structure

Organic Light Emitting Diodes (OLEDs) [83] are electroluminescent display devices made out of stacked organic thin films sandwiched between two metal electrodes. The total thickness of an OLED is less than 500 nm (for a typical OLED architecture) making it the most compact flat panel display on the market. Unlike LCD displays, OLED displays do not require any back lighting and can operate in broader temperature ranges. OLED

displays are lighter, brighter, have wider viewing angles ( $160^\circ$ ), faster response time, and low turn on voltages compared to the LCD displays [Tullo 2006]. The operation of OLEDs relies on molecular excitation and radiative relaxation (or decay) of conjugated organic molecules (chromophores). When a voltage is applied across the OLED, the luminescent (fluorescent or phosphorescent chromophores) within the emissive layer get promoted to the excited state of the specific chromophore by recombination of opposite charge carriers. Radiative relaxation of the excited chromophore back to the ground state results in the generation of photons with energies defined by the chromophores electronic structure. An efficient pathway of obtaining pure colored emission in OLEDs is accomplished by choosing the correct host-dopant system, where a proper energy match between the host and dopant allows for energy transfer to the emissive species thus allowing for pure RGB, white or IR emission.

The assembly of POLEDs is simple in that one or more organic layers of electro and hole transporting materials are sandwiched between two electrodes which is transparent as shown in **Figure 3-2**.



**Figure 3-2:** General structure of POLED [84]

### 3.2.1. Electron-Injector Electrode (EIE) (cathode)

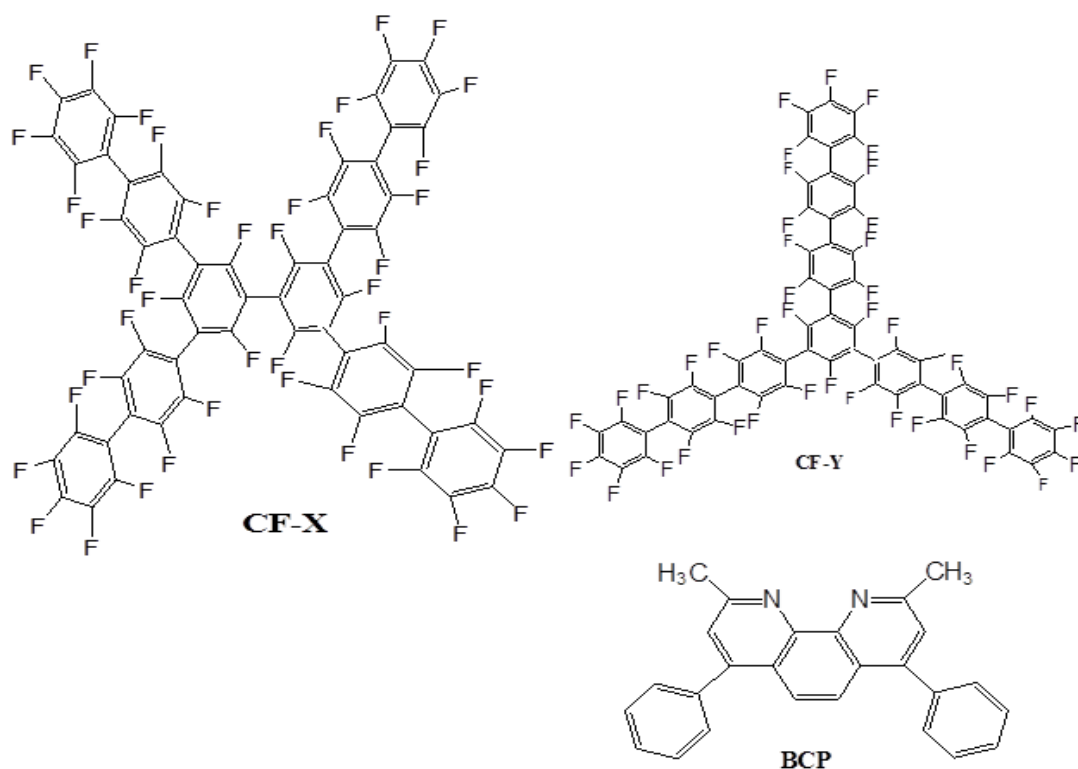
Traditionally, a pure metal or an alloyed metal with a low work function and high optical reflective surface is preferred as a cathode, such as (Al), (Ca) or Mg-Ag alloy,  $\text{MgF}_2$  [85,



86]. Most of these electrode materials are too reactive to be suitable as electron injecting electrodes, However, in order to overcome this reactivity, most researchers are currently using co-evaporated or Al composite electrodes [87]. A series of alkali metal ( $\text{Li}^+$ ,  $\text{Na}^+$ ,  $\text{K}^+$ ,  $\text{Rb}^+$ , and  $\text{Cs}^+$ ) acetates and metal fluorides were also be used [88]. Bilayer devices typically have an organic buffer layer used as an electron transporter which helps in several ways; (i) it moves the recombination region away from the cathode to minimize emission quenching, (ii) it reduces the injection barrier height between the cathode and the EML, and (iii) it confines the holes and improves the probability of recombination with the electrons, thus resulting in a higher light output.

### 3.2.2. Hole Blocking/Exciton Blocking Materials (HBMs/EBMs)

For a high efficiency OLEDs, a good balance of charges and their recombination in the emissive layer is important. Varying the transport materials, their thicknesses and location can be adjusted to optimize the device efficiency. Introduction of a hole blocking layer or an exciton blocking layer can significantly enhance recombination of carriers by blocking the holes in the emissive region [89]. Blocking materials used for hole blocking should have a good electron transporting capability and a deep HOMO level to prevent the leakage of holes by posing as a barrier for their transport. The compound 2,9-dimethyl-4,7-diphenyl-1,10-phenanthroline (BCP) which chemical structure shown in **Figure 3-3** has been used as a hole blocker with a higher electron mobility than Tris-(8-hydroxyquinoline)aluminum ( $\text{Alq}_3$ ) ( $\sim 5.2 \times 10^{-4} \text{ cm}^2 \text{V}^{-1} \text{s}^{-1}$ ) and HOMO-LUMO levels of -6.5 eV and -3.0 eV respectively see **Figure 3-4**. Starburst shaped perfluorinated phenylene, ( $\text{C}_{60}\text{F}_{42}$ -X shaped or  $\text{C}_{60}\text{F}_{42}$ -Y shaped) structures, have also been used as a hole blockers/exciton blockers and an electron transporters owing to their low lying LUMOs and HOMOs, lower sublimation temperature, and thermal and chemical stability from strong C-F bonds [90, 91].



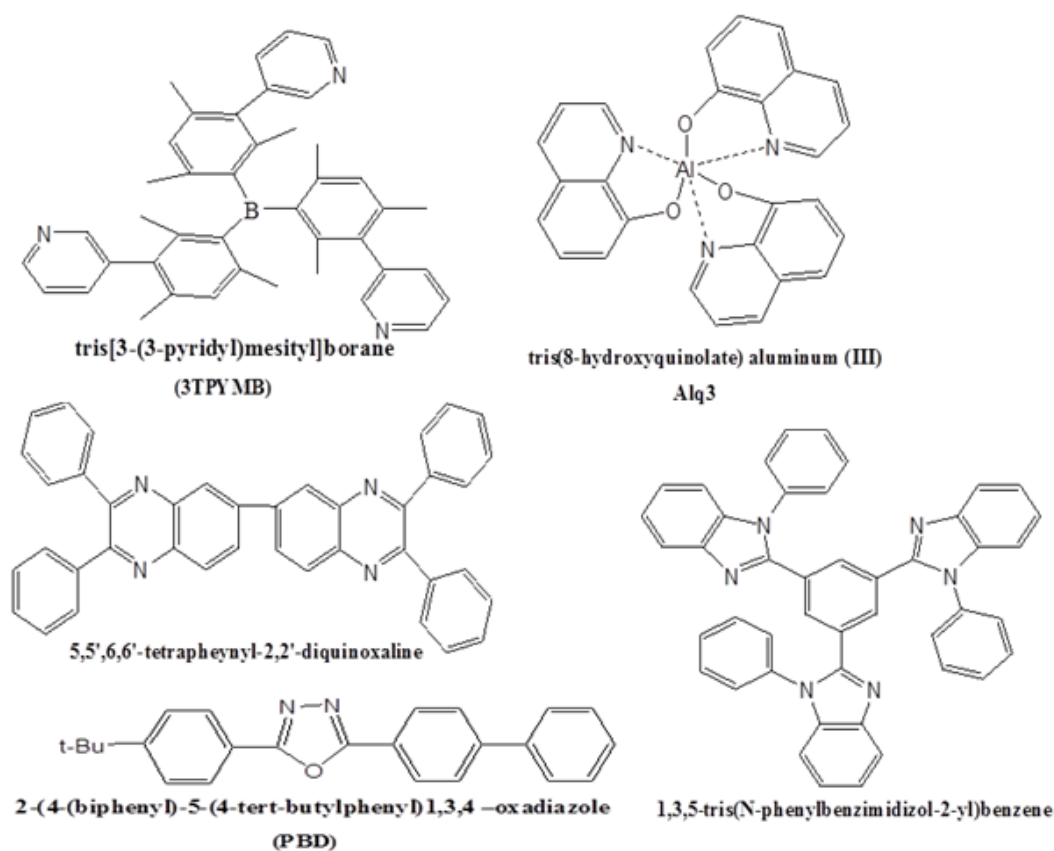
**Figure 3-3:** Chemical structures some hole blockers/exciton blocking materials

### 3.2.3. Electron-Transport Materials/Layer (ETMs/ETL)

Most organic semiconductors (small molecules or polymers) tend to have a hole mobility higher than their electron mobility [92] that electron rich moieties should be present. An order for a molecule to transport electrons, the molecule should have the following properties; (i) a suitable electron affinity and ionization potential (LUMO and HOMO levels) relative to the emitter allowing efficient injection of electrons from the cathode. (ii) high electron mobility ( $\mu_e > 10^{-5} \text{ cm}^2 \text{ V}^{-1} \text{ s}^{-1}$ ), to move the recombination zone away from the cathode. (iii) high glass transition temperatures ( $T_g$ ) and thermal stability to prevent operation-induced crystallization which leads to poor device stability and reduced lifetime [82]. The electron transport in amorphous organic molecules occurs by carrier hopping between spatially localized states [93].

Electron transport (n-type) materials have an electron-poor conjugated-electron systems. Common examples of these materials are quinoxaline-containing structures, such as 5,5,6,6-tetraphenyl-Z-diquinoxaline (TPDQ), and metal complexes, such as tris(8-

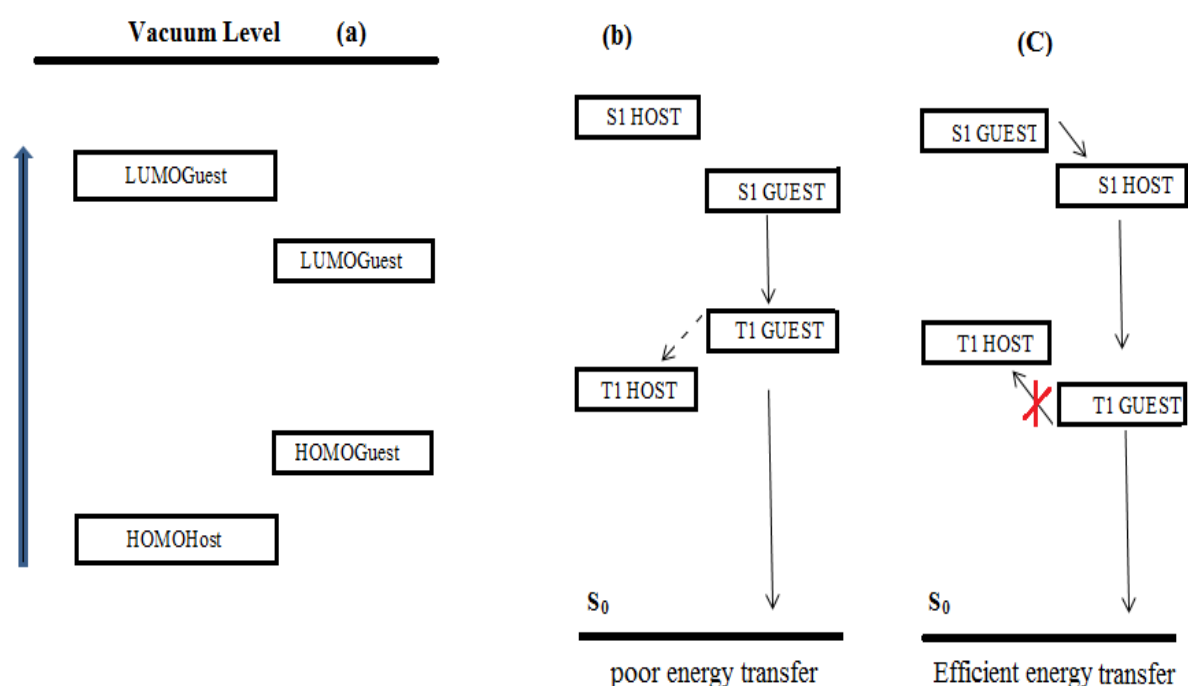
hydroxyquinolate) aluminum(III) (Alqs). An electron transporting molecule, tris [3-(3-pyridyl)mesityl]borane (3TPYMB) was recently developed by Tanaka [94]. These materials transport negative charge because they are more easily reduced and are difficult to oxidize. Few good examples of n-type materials have been investigated; however, several researchers are investigating structural modification of existing materials to create electron-poor conjugated electron systems, such as poly(p-phenylenevinylene) (PPV) derivatized with cyano-substituents that withdraw electrons from this polymer's conjugated backbone. The oxadiazole molecule 2-(4-(biphenyl)-5-(4-tert-butylphenyl)1,3,4 – oxadiazole (PBD) was first used as an electron transporter by Adachi et. al. [95]. Due to its low  $T_g$ , crystallization of thin films over time led to reduced device lifetimes. Later, this problem was overcome by blending PBD in PPV based electroluminescent polymers at 20 wt% concentrations [96]. **Figure 3-4** shows some common ETMs.



**Figure 3-4:** Some common electron-transport materials (ETMs)

### 3.2.4. Emissive Materials (EMs)

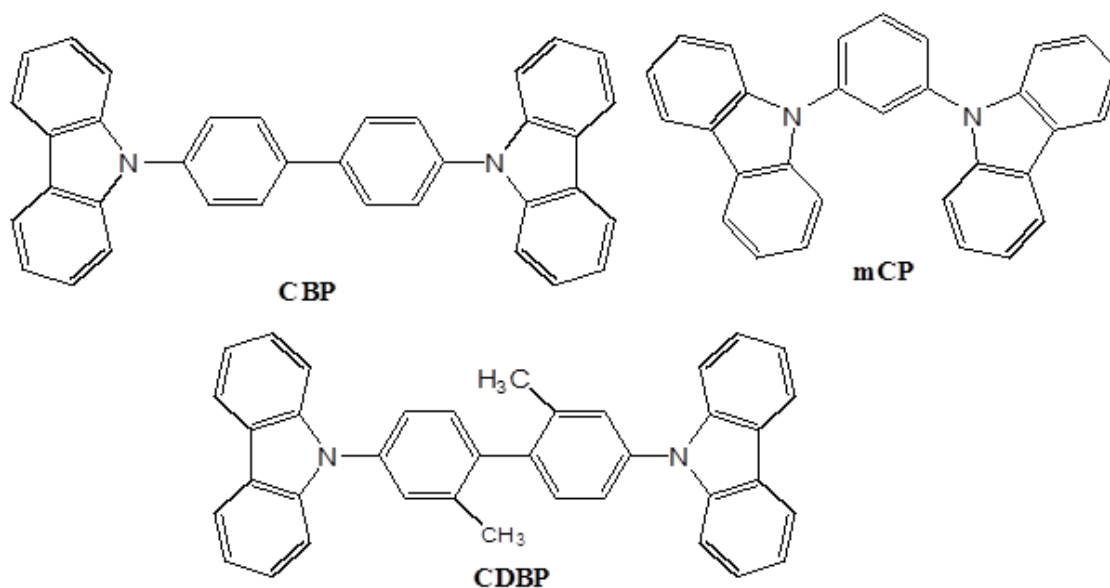
EMs layer is the most important region in OLED components and the layer where the holes and the electrons recombine typically consists of molecules that have high photoluminescence efficiency. The emissive layer in high efficiency OLEDs is a mixture of a matrix molecule (host) doped with phosphorescent emissive dopants (guest) in small concentrations, commonly known as a host-guest system [97-99] as shown in **Figure 3-5**.



**Figure 3-5:** Energy level relationships and energy transfers in a host-guest system: (a) favorable HOMO-LUMO level alignment (b) Poor energy transfer from G→T1H (c) Efficient energy transfer (T1G→S<sub>0</sub>) in phosphorescent host-guest systems [100].

The emissive layer (EML) should consist of molecules capable of transporting both holes and electrons equally so that the injected charges can move through the layer to recombine and emit photons. Host materials are required to have a wide band-gap for exothermic energy transfer to the emissive dopant, good hole and electron conduction and a higher triplet energy level than the guest [100]. Most of the hosts are suitable for green and red triplet emitters that have small band-gaps, but achieving high efficiency with blue phosphorescent emitters requires a host with a wider band-gap and also a triplet energy >

2.7eV. Several carbazole based host molecules, such as 4,4'-bis(9-carbazolyl)-biphenyl (CBP), N,N'-dicarbazolyl-3,5-benzene (mCP) and more recently 4,4'-bis(9-carbazolyl)-2,2'-dimethylbiphenyl (CDBP), with the highest triplet energy ( $\sim 3.0$  eV) known for carbazole based hosts have been used to demonstrate the importance of exciton confinement with a higher host triplet energy and a larger band gap [101] structures of which are shown in **Figure 3-6**.

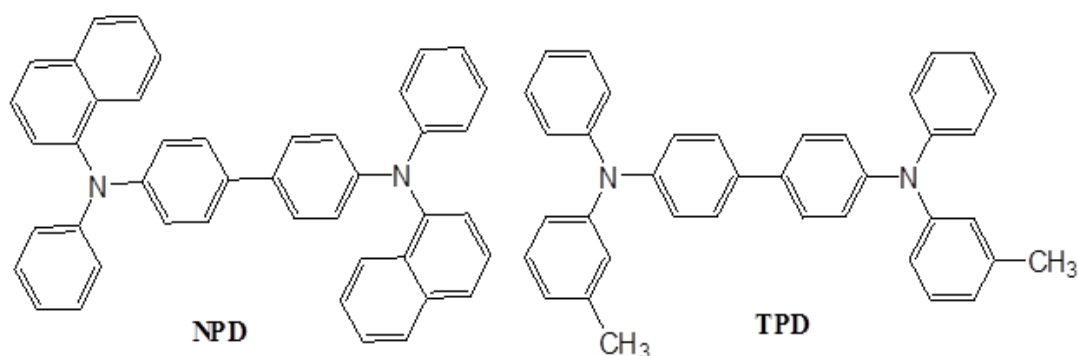


**Figure 3-6:** Some commonly known compounds as a host-guest system

### 3.2.5. Hole Transport Materials (HTMs)

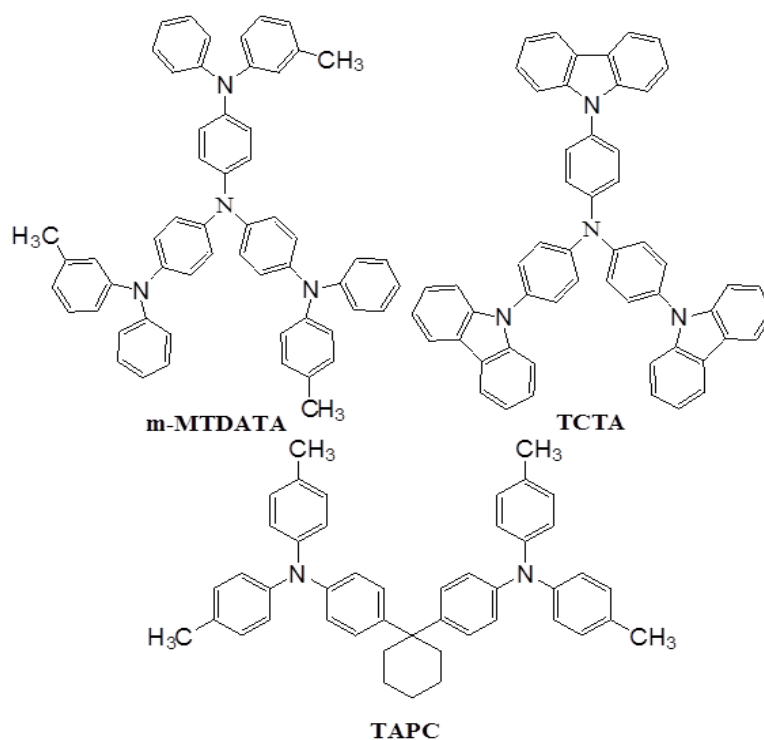
A good hole transporting material is a molecule rich in  $\pi$  electrons which transports positively charged carriers holes. The common characteristic of all hole transporting materials is their electron donating capability. These materials capable to provide a conductive pathway for the holes to transport into the emissive layer to recombine with electrons injected from the cathode, transported by the (ETM) to generate photons. HTMs are easily oxidizable and typically have shallow HOMO levels, between -5.0 eV and -6.0 eV. These molecules should also have a low LUMO level, that it can prevent electrons from migrating to the anode under an external applied field. These materials should

possess high thermal and thin film morphological stabilities. The most commonly used HTMs are the triarylamine family [100]. The best performing triarylamines with a biphenyl backbone are N,N'-(3-methylphenyl)-1,1'-biphenyl-4,4'-diamine (TPD) and 4,4'-bis [N-(1-naphthyl-1)-N-phenyl-amino]-biphenyl ( $\alpha$ -NPD) because of their availability in high purity, good electrochemical and thermal stabilities, good film-forming properties and adequate hole mobilities for OLED applications [102 ]. Chemical structure of these materials is shown in **Figure 3-7**.



**Figure 3-7:** Chemical structure of some HTMs

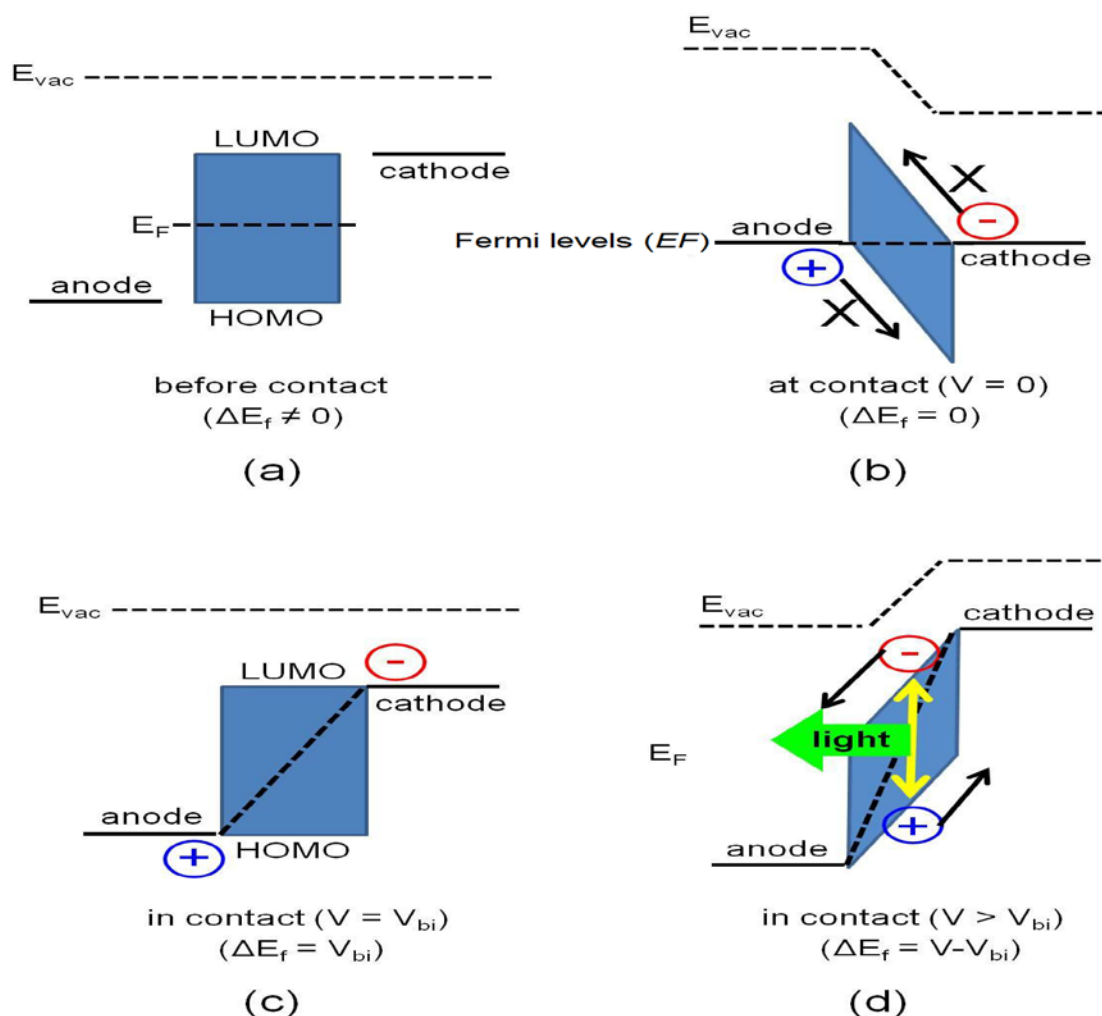
To modified these materials, several studies perform by Shirota et al. [103] lead to synthesis of amorphous molecular materials, introduction of bulky and heavy substituents in order to enlarge molecular size for attaining and increasing the  $T_g$  by incorporating a rigid moiety or a molecular intermolecular hydrogen bonding site into non-planar molecules and by increasing the molecular materials synthesized as multi using for example: 4,4',4''-tris(3-methylphenylphenylamino)-triphenylamine (m-MTDATA) and 4,4',4''-tri(N-carbazolyl)triphenylamine (TCTA). These two compound are commonly used starburst hole transporting materials which are also used as hole injection materials [104] and 1,1-bis [(di-4-tolylamino)phenyl]cyclohexane (TAPC) as a hole transporter as well as an electron and exciton blocker. **Figure 3-8** shows some of the structures of these materials.



**Figure 3-8:** Some starburst hole transporting materials

### 3.3. Energy Band Diagrams of OLEDs Operation

Figure 3-9 (a)-(d) illustrate the energy band diagrams for the operation processes of the OLED. The OLED is simplified as a single organic layer structure with the anode and the cathode at both electrical contacts. Fermi levels ( $E_F$ ) are not aligned before the electrical contact by anode and cathode as shown in **Figure 3-9** (a). After the electrical contact, there is an equilibrium state with aligned  $E_F$ . However, a charge injection into the organic layer is still not preferable due to the built-in potential barrier shown in **Figure 3-9** (b).



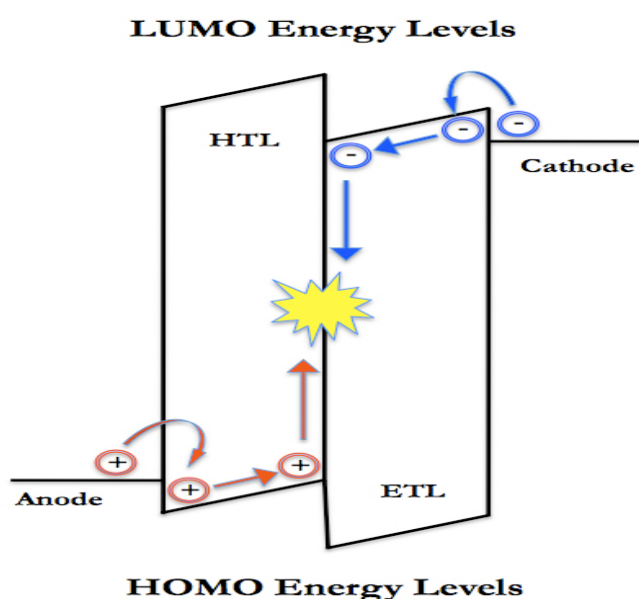
**Figure 3-9:** Schematic energy band diagrams about OLEDs operation. For simplicity, single organic layer is assumed between two electrodes; (a) before the electrical contact, (b) after the electrical contact, (c) with the applied voltage bias through both electrodes, charge carriers are ready to be injected at  $V=V_{bi}$ , and (d) charge carriers are finally injected into the organic layer at  $V>V_{bi}$ , forming excitons and emitting the light.

When the voltage bias is applied to the electrodes, charge carriers are ready to be injected into the organic layer at  $V=V_{bi}$  as shown in **Figure 3-9** (c), and finally injected to the organic layer at  $V>V_{bi}$  as shown in **Figure 3-9** (d). The holes move upward through the HOMO level and electrons transport downward through the LUMO level of the organic layer, respectively. Once the charge carriers meet each other in the organic layer, they become energetically bound each other (Columbic interaction), form excitations, and generate light-emission through the radiative relaxation in the organic layer.



### 3.4. Operation-base of POLEDs

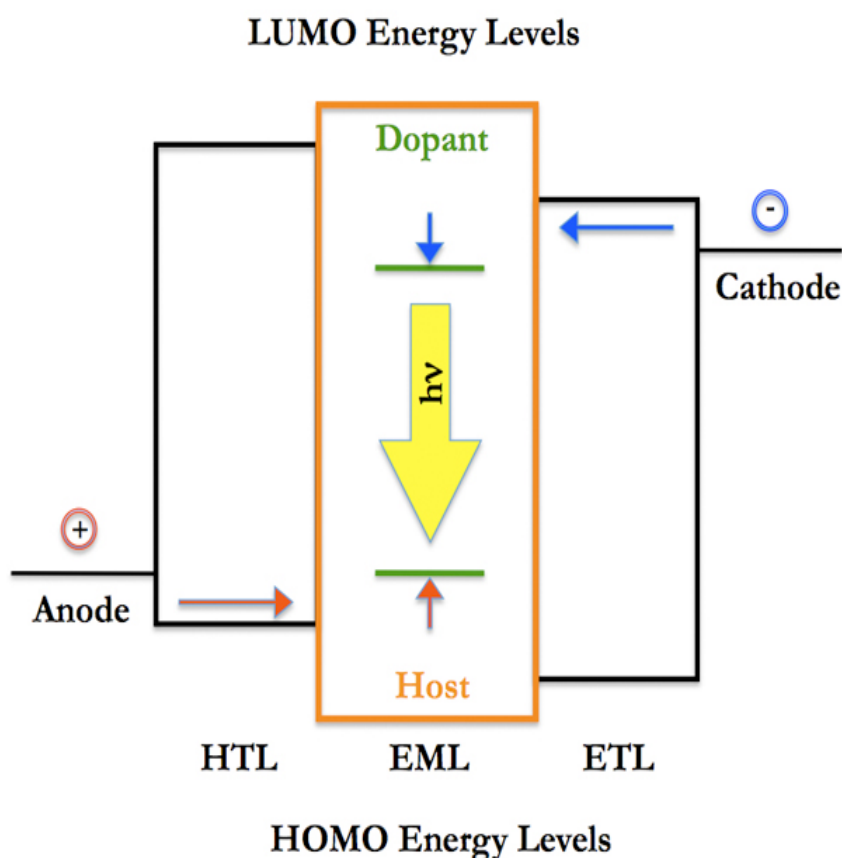
Hole injection occurs when one electron is removed from the HOMO of hole-transporters, resulting in a positively charged radical cation. Similarly, the electron transport layer is expected to transport electrons from the cathode. The electron transport process adds one electron into the LUMO of electrontransporters, making the ETL molecule a negatively charged radical anion (**Figure 3-10**). The emission from this OLED device comes from the green emitter, Alq3. This is due to the fact that Alq3 has a smaller HOMO-LUMO energy gap compared with diamine, resulting in preferential energy transfer from diamine to Alq3.



**Figure 3-10:** The energy diagram of a double heterostructure device. Holes (red circles) and electron (blue circles) are injected from their respective electrodes into the HOMO and LUMO of the organic molecules. The holes and electrons migrate along the interface, forming an exciton at that interface and radiative decaying through the emission of a photon.

Additionally, diamine transports holes faster than Alq3 transports electrons, therefore the excitons (a loosely bound hole and electron pair) are generated within the Alq3 layer, near the diamine/Alq3 interface. One of the drawbacks of using Alq3 pistine film as emissive layer, is the severe self-quenching of excitons in the pistine film. This problem can be overcome by doping an emissive dye into the ETL, thus creating a new layer called the light emitting layer (EML) [105].

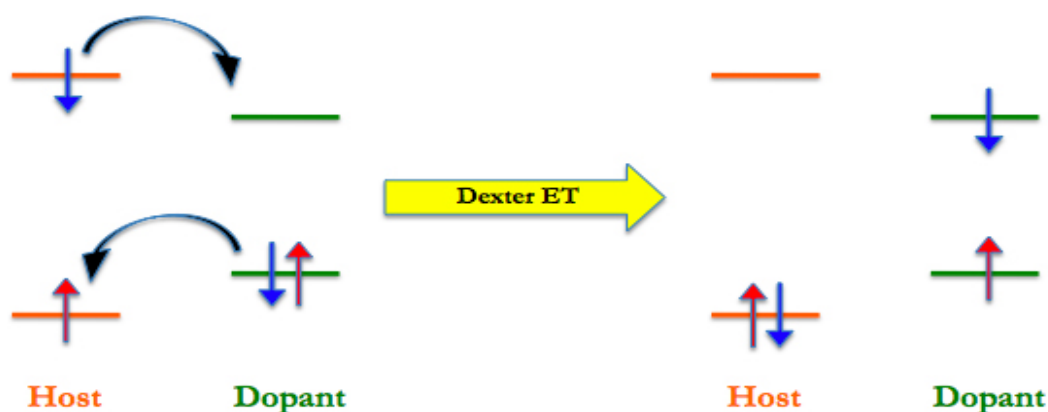
Inside of the EML, energy will transfer readily from the host to a dopant with a smaller optical gap resulting in an efficient emission from the dopant (**Figure 3-11**). The self-quenching of excitons is also suppressed by lowering the concentration of excitons and thus device efficiency is improved. An additional benefit of doping is to control emission colors of OLEDs by doping different emissive dyes [106].



**Figure 3-11:** Energy diagram of an OLED with HTL, EML (containing host (orange) and dopant (green) energy levels) and ETL.

### 3.5. Energy Transfer in OLEDs

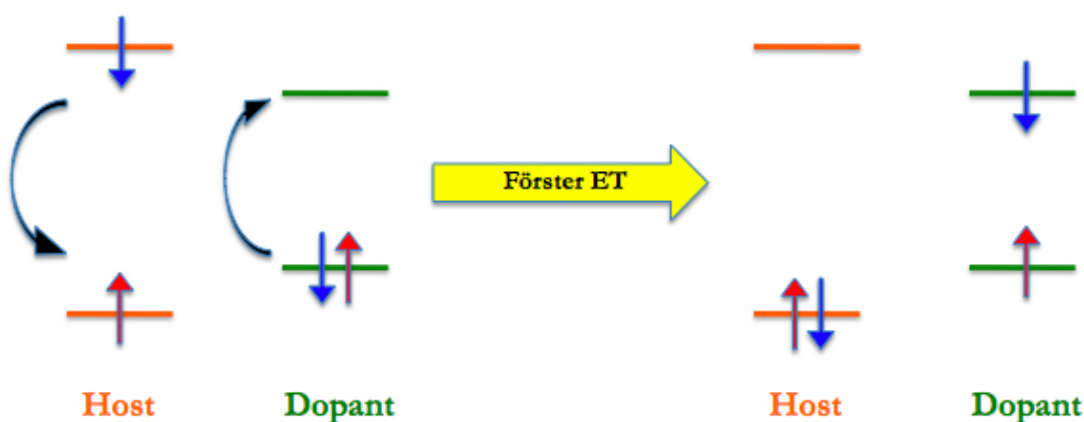
There are two distinct mechanisms for the energy transfer from host to dopant: Förster mechanism or Dexter electron exchange. In the Dexter electron exchange (**Figure 3-12**), the exciton hops directly between molecules in a concerted energy transfer (ET).



**Figure 3-12:** Dexter energy transfer from host to dopant

This is a short-range process dependant on the overlap of molecular orbitals of neighboring molecules. It also preserves the symmetry of the host and dopant pair. Thus, a triplet–singlet energy transfer is not possible by a Dexter mechanism. A change in spin-symmetry is possible if the host exciton breaks up and reforms on the dopant by incoherent electron exchange [107]. However, this process is considered to be relatively unlikely as it requires the dissociation of the host exciton, which in most molecular systems has a binding energy of 1 eV [107].

The Förster energy transfer process relies on the electrostatic interaction between a host and dopant molecule (**Figure 3-13**).



**Figure 3-13:** Förster energy transfer from host to dopant

In this mechanism, an excited host molecule with oscillating dipoles creates an electromagnetic disturbance. When a dopant molecule in the ground state comes in the vicinity of this electromagnetic disturbance, due to coulombic interaction, the dopant starts oscillating at the same frequency as the oscillating dipole of the host. This energy transfer from the host to the dopant occurs through dipole-dipole coupling between the transition dipole moments of the excited host and the ground state dopant. In the process, as the excited host relaxes to the ground state, it transfers the energy to the dopant via coulombic interaction. The Förster energy transfer process may occur in long distances (up to 100Å) and does not require any physical contact between the orbitals of the host and the dopant molecules.

### **3.6. Fabrication of OLEDs**

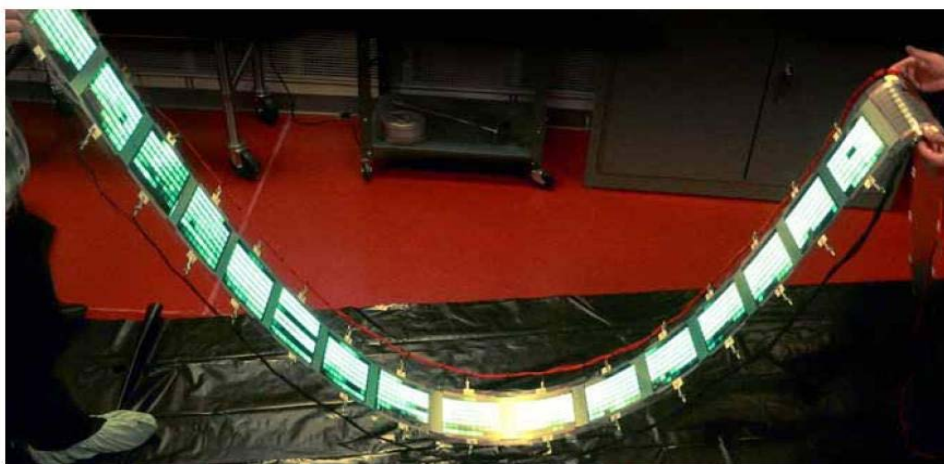
Organic Light Emitting Diodes (OLEDs) are most commonly fabricated in a bottom-emitting configuration where the anode material, stack of organic molecules and a metal cathode are sequentially deposited on a transparent substrate such as glass. The photons generated by the recombination of holes and electrons exit through the glass substrate. For high performance, reproducibility and reliability of OLEDs is extremely critical to optimize and carefully control all process conditions. These processes include thorough cleaning procedures for substrate preparation, monitoring and controlling organic layer thicknesses as well as composition, proper encapsulation methods and a complete protocol for measuring the optical and electrical characteristics of the OLEDs.

#### **3.6.1. Substrate Preparation**

The commonly used substrates are glass (borosilicate or aluminosilicate glass) and plastic films such as polyethylene terephthalate (PET) or polyethylene naphthalate (PEN), based on the application and requirements [100]. Typically, plastic films are used for large-area, flexible display or lighting panels because they are light-weight and inexpensive. Roll-to-

roll printing of polymer LEDs (PLEDs) has been demonstrated by the OLED research team at General Electric [108] as shown in **Figure 3-14**.

Large-display OLED panels have also been fabricated on glass substrates for residential and commercial lighting.



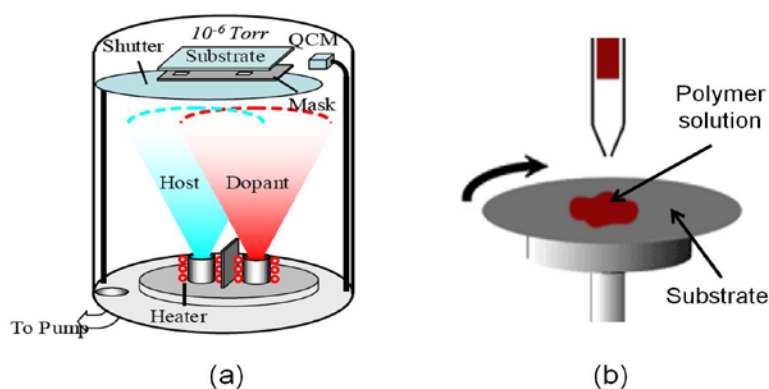
**Figure 3-14:** One of the first examples of a roll-to-roll PLED on plastic

### 3.6.2. Device Fabrication

Depending on the size of the organic molecules which are used for the thin film growth OLEDs can be divided into two types; small-molecule OLEDs (SMOLEDs) and polymer OLEDs (PLEDs). Small molecule is defined by a molecular weight approximately less than 1000 g/mol, whereas polymer has long and complicated structures with the molecular weight approximately more than 1000 g/mol. There have been many different methods to grow organic thin films such as vacuum thermal evaporation (VTE), spin-coating, organic vapor jet printing, spraying method, inkjet printing, and even a roll-to-roll processing. Among those methods, the VTE is commonly used to fabricate SMOLEDs, whilst the spin-coating is most widely used for research into PLEDs.

**Figure 3-15** (a) illustrates the VTE system in which a sufficient amount of electrical current through the source boat heats up and sublimates organic materials in a vacuum environment. The ballistic molecular thin film deposition is possible with tens of

centimeter scale mean free path under typical chamber pressure of  $10^{-6} \sim 10^{-7}$  Torr. A quartz crystal monitor (QCM, coated with a thin gold layer) provides accurate film thickness control up to the  $0.1 \text{ \AA/s}$ . **Figure 3-15** (b) schematically shows the spin-coating process where polymer materials are completely dissolved in a specific solvent and dropped onto the substrate in order to evenly disperse the polymer solution. A thermal annealing process is typically required to completely evaporate the solvent residue after spin-coating. The thickness of a polymer thin film can be accurately controlled by adjusting the spin speed and the polymer concentration. The VTE has an advantage for fabricating OLEDs with multilayered structure and doped layers, whereas the spin-coating method is more cost-efficient than the VTE.



**Figure 3-15:** Schematic illustration of organic thin film growth processes; (a) a vacuum thermal evaporation (VTE) and (b) a spin-coating methods.

### 3.7. Advantages of Organic Light-Emitting Devices

There are many advantages to organic Light-Emitting Materials. Firstly, organic materials are more cost-effective than inorganic semiconductors due to the nearly unlimited synthetic abundance of organic materials and the thinner film thickness, typically  $\sim 100 \text{ nm}$  thick. Secondly, organic thin films can be easily deposited using various simple fabrication methods such as vacuum thermal evaporation (VTE), spin-coating, inkjet printing [109,110] and even roll-to-roll process [111-117] compared to the typical inorganic thin

film growth methods such as molecular beam epitaxy (MBE), chemical vapor deposition (CVD) [118] and pulsed laser deposition (PLD). Thirdly, the extremely thin film thickness and flexibility of organic materials make OLEDs suitable for flexible device applications as shown in **Figure 3-16** [119].

OLEDs also have excellent display performances such as a fast response time, a wide viewing angle, a high contrast and low power consumption compared to the properties of their main competitor, liquid crystal display (LCD).



**Figure 3-16:** Examples of flexible OLEDs applications, (a) Flexible OLEDs by Universal display corporation, (b) Flexible OLEDs on garments.

### 3.8. Applications of Organic Light-Emitting Devices

There are two major application areas in OLEDs. The first application area is the flat panel display device where OLEDs competes with the LCD and the other area is the next generation Solid-State-Lighting SSL source which could ultimately replace fluorescent tubes. Both of applications can be currently found in the commercial consumer market.

#### 3.8.1. Flat Panel Display

There are many different types of display devices such as the cathode ray tube (CRT), the plasma display panel (PDP) and the liquid crystal display (LCD). The LCD is the most prevalent display device up to now, but the demand for the OLED display is tremendously



growing due to the excellent light-emitting qualities compared to the LCD. The short radiative lifetime (typically from a few to thousand nanoseconds) of organic materials can provide much faster response time, compared to the slow response time of the LCD, which typically takes milliseconds to rotate the liquid crystal cell. The wide viewing angle (nearly 180°) of OLEDs, which is one of the most important requirements for the mobile display devices is also another important advantage. The first commercialized 11" OLED display, XEL-1 was released by Sony in 2007 as shown in **Figure 3-17** (a), followed by recent 4" active-matrix OLED (AMOLED) by Samsung mobile display (SMD) as shown in **Figure 3-17** (b). Although the relatively small-size of OLED displays have been introduced to the market up to now, such large-size prototype OLED TVs (31" and 40") have also been continuously introduced in the consumer electronics show (CES) as shown in **Figure 3-17** (c). Recently, Sony and Samsung demonstrated 3-dimensional (3-D) display devices based on the LCD/PDP as shown in **Figure 3-17** (d). However, it is expected that the OLEDs would be more compatible in realizing the 3-D images due to their fast response time in making different images.

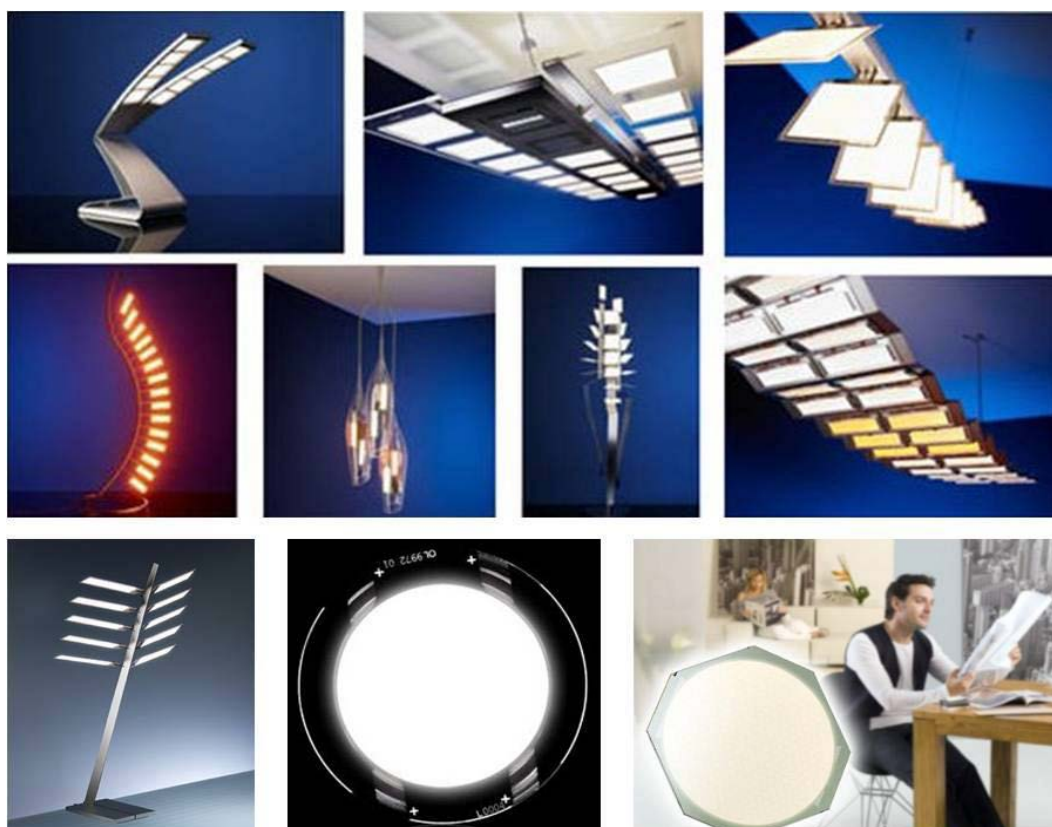


**Figure 3-17:** Various OLEDs display applications: (a) 11" OLED display, (Sony, XEL-1), (b) 4" active-matrix OLED display (Samsung Mobile Display, SMD), (c) 31" OLED TV (SMD, prototype), (d) 3-D TV based on a LCD display (SMD).



### 3.8.2. Solid-State-Lighting

The OLED lighting market is not as large yet as displays, but expected to grow significantly by 2015 [120]. The requirement for the white light source for the lighting is somewhat different than that for the display; higher brightness condition (luminance,  $L=1,000 \text{ cd/m}^2$  for the lighting vs.  $L = 100 \text{ cd/m}^2$  for the display), good color rendering index (CRI) of at least 70, matching of Commission Internationale de l'Eclairage (CIE) coordinates similar to that of a blackbody radiator, which is on the Planckian locus, and a correlated color temperature (CCT) between 2500 K and 6000 K.



**Figure 3-58:** Various OLEDs lighting applications

The adjustment of these various light-emitting properties for the efficient white light source can be easily tailored by selectively choosing different light-emitting organic molecules and optimizing the device structure of the OLEDs, consequently resulting in a wide range of the white light emissions such as warm or cool **Figure 3-18** shows various

OLED lighting products introduced by Novaled, General Electric (GE), Philips, and Osram.

### **3.9. Electronic transitions of OLEMs**

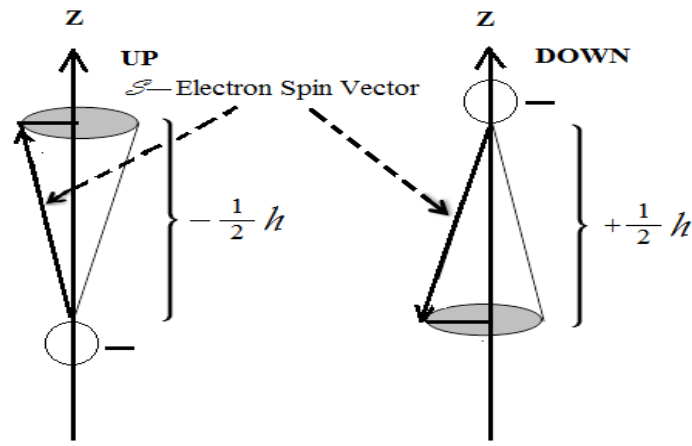
Most of the theories used to express photophysical and photochemical processes that are encountered in the field of organic light emitting devices were developed as early as in the 1920's [121-123]. Some items are required to understand and explain electronic transitions: fluorescence, phosphorescence, intersystem crossing, and internal conversion in organic materials.

#### **3.9.1. Luminescence of OLEMs**

Luminescence occurs from the emission of light when an electron in an excited electronic state moves to the lower energy vibrational bands of the ground state  $S_0$ . In the organic molecules, the absorption of UV or visible light causes excitation of the electron from occupied low energy orbital to a higher energy, unoccupied molecular orbital. This transition leads the production of a photon with lower energy and this phenomenon is known as photoluminescence [124]. On the other side, the electroluminescence is an electrical recombination of electrons and holes results in the formation of the excited electronic state of the molecular species.

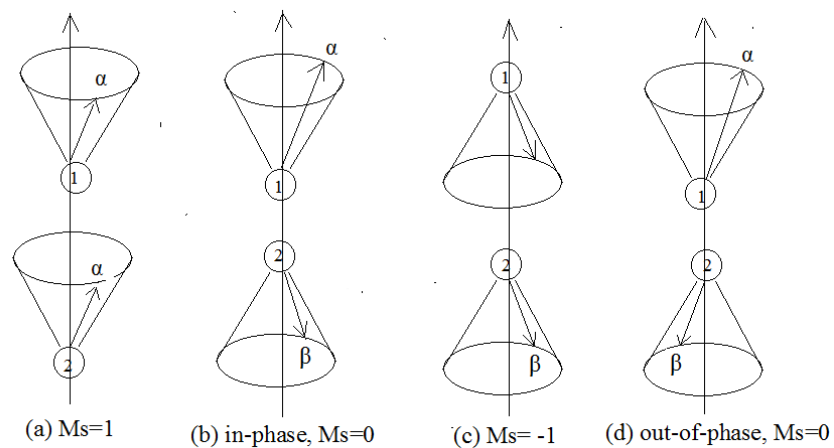
#### **3.9.2. Fluorescence and phosphorescence**

Fluorescence and phosphorescence absorption of a photon (~10-15 sec) occurs in an external magnetic field. A molecular beam of this configuration can be resolved in three different states because there are three possible alignments of the two unpaired spins resulting in a triplet state, denoted as  $T_1$ ,  $T_2$ , etc. Electrons are electrically charged particles that generate a magnetic angular momentum by spinning around an axis, known as electron spin  $S$ , as shown in **Figure 3-19**.



**Figure 3-19:** Vectorial representations of an electron's spin magnetic moment, an UP and a DOWN orientation along an arbitrary Z axis

Based on the quantum mechanics, the two allowed orientations which describe the spin angular momentum are  $+\frac{1}{2}\hbar$  and  $-\frac{1}{2}\hbar$  along an arbitrary Z axis, representing the “UP” and the “DOWN” vector or ( $\alpha$ ) and ( $\beta$ ), respectively. To understand the electron spin in triplet and singlet states, consider a two electron system, 1 and 2, with their corresponding spin vectors  $S_1$  and  $S_2$ , respectively as shown in **Figure 3-20**. The spin quantum number,  $S$ , in the triplet state is equal to 1 giving rise to three values of magnetic quantum number  $M_s = (1, 0, -1)$  and  $S=0$  results in  $M_s = 0$  for the singlet state. The spin vectors are in opposite directions and out-of-phase, whereas for a corresponding triplet state, the spin vectors are in-phase and the resultant along the x-y plane is non-zero [125].



**Figure 3-20:** Vectorial representation of the three triplet states (a, b and c) with magnetic quantum number  $M_s = (1, 0 \text{ and } -1)$  and a singlet state (d), with up and down spin vectors represented by ( $\alpha$ ) and ( $\beta$ ) respectively.

## CHAPTER 4: EXPERIMENTAL

### 4.1. Materials

4-isopropylaniline (Merck), 2,4-dimethylaniline (Acros), 4-phenoxyaniline (Merck), 4-(1H-pyrrol-1-yl)aniline (Acros), 4-fluorobenzonitrile (Acros), 60% sodium hydride (NaH) (Fluka), N,N-dimethylformamide (DMF) (Acros), potassium hydroxide (KOH) (Fluka), ethanol (Merck) and acetic acid (Merck), hydrochloric acid (Merck), p-phenylenediamine (Merck), 1,5-diaminonaphthalene (Fluka), pyridine (Merck), triphenylphosphite (Fluka), calcium chloride (Merck), N-methylpyrrolidone (NMP) (Fluka) were purchased from commercial sources and without further purification.

### 4.2. Characterization Methods and Instruments

The prepared compounds (intermediates, monomers and polyamides) were characterized by the following techniques:

#### 4.2.1. Fourier Transform Infrared Analysis (FTIR)

Infrared spectroscopy is an important analytical instrument to identify and study the presence of functional groups in a molecule and verify a pure compound or specific impurities in a compound. FTIR spectra were recorded on a Perkin Elmer FTIR RX1 spectrometer at room temperature with 4 scans from 4000 to 400  $\text{cm}^{-1}$  and resolution of 4  $\text{cm}^{-1}$ . A small sample was placed over ATR crystal and maximum pressure applied using the slip-clutch mechanism.

#### 4.2.2. UV-vis Absorption and Photoluminescence (PL) spectra

UV-vis absorption was recorded in dilute NMP solutions ( $10^{-5}\text{M}$ ) on a Cary 60 UV-vis spectrophotometer and photoluminescence spectra was detected by a Cary Eclipse spectrometer.

#### 4.2.3. Nuclear Magnetic Resonance ( $^1\text{H}$ -NMR and $^{13}\text{C}$ -NMR)

Nuclear Magnetic Resonance is a powerful analytical tool that allows molecular structure characterization including relative configuration, relative and absolute concentrations, and even intermolecular interactions.

Samples were dissolved in a deuterated solvent at a concentration of around  $10\text{ mg mL}^{-1}$  for  $^1\text{H}$ -NMR and  $100\text{ mg mL}^{-1}$  for  $^{13}\text{C}$ -NMR. The  $^1\text{H}$ -NMR and  $^{13}\text{C}$ -NMR spectra were recorded using a JEOL INM-LA 400, JNM-ECA 400 and Bruker Avance 400 spectrometers at 400 MHz and 100 MHz, respectively. The chemical shifts were referenced against TMS as 0 ppm, and the deuterated solvents; chloroform- $\text{d}_1$  ( $\text{CDCl}_3$ ) showed a typical peak at  $\delta$  value of 7.26 ppm for  $^1\text{H}$ -NMR and 77 ppm for  $^{13}\text{C}$ -NMR. Also, dimethylsulfoxide- $\text{d}_6$  (DMSO) showed a peak at 2.42ppm, 3.55ppm for  $^1\text{H}$ -NMR and 77 ppm for  $^{13}\text{C}$ -NMR due to traces of  $\text{CHCl}_3$  and DMSO in the deuterated solvents respectively.

#### 4.2.4. Differential Scanning Calorimetry (DSC)

Differential scanning calorimetry is a powerful analytical technique used to determine the glass transition temperature ( $T_g$ ).  $T_g$  is defined as a change in the heat capacity as the polymer matrix passes from the glass state to the rubber state. In other words, the  $T_g$  is the softening region of a plastic. In fact, it refers to the amorphous region of semicrystalline materials or to amorphous materials whereby the materials becomes flexible as it is heated due to the molecular motion. When a material is heated to this point and beyond, molecular motion around single bonds suddenly becomes significantly easier.

The glass transition demonstrates a thermodynamic second-order transition because at the  $T_g$  there is a heat capacity jump, but this increment of the heat capacity take places in a range of temperature not at a definite temperature [126]. In DSC,  $T_g$  is represented graphically in the thermal curve as a shift in the baseline. An amorphous polymer does not exhibit crystallization temperature ( $T_c$ ) or melting point ( $T_m$ ). DSC thermograms in

nitrogen atmosphere were obtained with a Perkin Elmer Pyris 6 DSC analyzer calibrated with indium at a scan rate of  $20^{\circ}\text{C min}^{-1}$  in a temperature range of 35 to  $350^{\circ}\text{C}$ . For the poly(amine amide) samples about 8-10 mg of sample were weighed and encapsulated in standard aluminum sample pans. The same empty pan was utilized as a reference. The first scan was to remove the thermal history of the sample. Thermal data were acquired based on the second heating run.

#### **4.2.5. Thermogravimetry Analysis (TGA)**

Thermogravimetry analysis (TGA) is used for determining the thermal stability of a substance as a technique that is defined the weight change of a material heated at a controlled rate recorded as a function of temperature or time on a thermobalance (a sensitive balance) as the sample temperature is increased in an inert atmosphere or in air. Such analysis is based on a high degree of accuracy in three measurements: weight, temperature, and temperature change. Data are recorded as a thermogram of weight versus temperature referred to as the thermogravimetry (TG) curve and a plot of the weight loss against temperature which is referred as the derivative thermogravimetric curve or (DTG). As many weight loss curves look similar, a derivative weight loss curve can be used to tell the point at which weight loss is most apparent. This is known as non-isothermal TGA. The non-isothermal technique should be used when the degradation temperature is unknown [127]. Thermal stability studies are the major application of TGA; however TGA is capable of determining the composition of materials, decomposition temperatures, activation energy and oxidative stability as well. Weight loss may result from evaporation of residual moisture, component or solvent. However, at higher temperatures weight loss is obtained from polymer decomposition. In this study, the thermal stability of macromers and synthesized copolymers were carried out using a Perkin Elmer Pyris 6 system under a steady flow of nitrogen atmosphere  $20\text{ mL min}^{-1}$  at a heating rate of  $20^{\circ}\text{C min}^{-1}$  from 50 to  $800^{\circ}\text{C}$ . The sample weight used was between 10 - 18 mg.

#### 4.2.6. Electrochemical Properties

Cyclic voltammetry was conducted with the use of a three-electrode cell in which ITO (polymer film area of about 1.0 cm x 1.0 cm) was used as a working electrode. A platinum wire was used as an auxiliary electrode. All cell potentials were taken with the use of a simple electrode Ag/AgCl and KCl as a reference electrode. Ferrocene was used as an external reference calibration (+ 0.48 V vs. Ag/AgCl).

#### 4.3. Synthesis of Monomers (Ma-Mf)

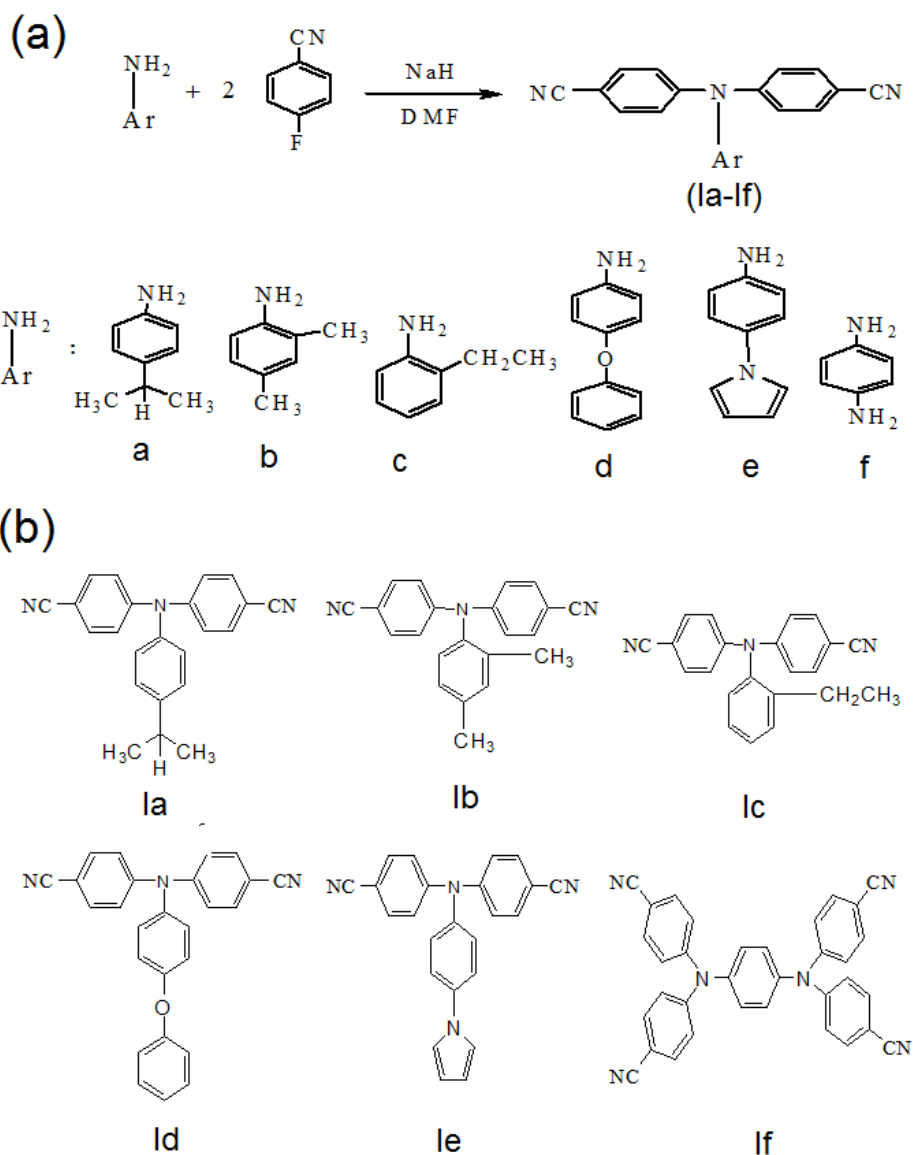
All the monomers (**Ma-Mf**) and polymers (**Pa1 – Pf1** and **Pa2 – Pf2**) synthesized in this work are shown in **Table 4.1**.

**Table 4-1:** Synthesized monomers and polyamides

Monomers	Aryldiamines	Polyamides
<b>Ma</b>	p-phenylene diamine	<b>Pa1</b>
	1,5-diamine naphthalene	<b>Pa2</b>
<b>Mb</b>	p-phenylene diamine	<b>Pb1</b>
	1,5-diamine naphthalene	<b>Pb2</b>
<b>Mc</b>	p-phenylene diamine	<b>Pc1</b>
	1,5-diamine naphthalene	<b>Pc2</b>
<b>Md</b>	p-phenylene diamine	<b>Pd1</b>
	1,5-diamine naphthalene	<b>Pd2</b>
<b>Me</b>	p-phenylene diamine	<b>Pe1</b>
	1,5-diamine naphthalene	<b>Pe2</b>
<b>Mf</b>	p-phenylene diamine	<b>Pf1</b>
	1,5-diamine naphthalene	<b>Pf2</b>

### 4.3.1 General Synthesis of Intermediates (Ia-If):

**Figure 4.1** shows the synthesis of intermediates **Ia-If** and their structures.



**Figure 4-1:** (a) Synthesis of intermediates (**Ia-If**) (b) structures of the intermediate products (**Ia-If**)

#### 4.3.1.1. Synthesis of 4, 4'-dicyano-4''-isopropyltriphenylamine (**Ia**)

A mixture of 1.40 g (0.02 mol) of sodium hydride and 80 mL of DMF was stirred at room temperature for about 30 min. To the mixture, 2.70 g (0.02 mol) of 4-isopropylaniline and 4.84 g (0.02 mol) of 4-fluorobenzonitrile were added in sequence. The mixture was heated with stirring at 120°C for 24 h under nitrogen and then precipitated into 150 mL of cold



water [128, 129]. The products were filtered and recrystallized from ethanol to give a pale yellowish solid. (3.43 g, yield: 51%), mp = 185-188°C, FTIR: 2211.4 cm<sup>-1</sup> (C≡N). <sup>1</sup>H NMR(400 MHz, CDCl<sub>3</sub>-d<sub>1</sub>, δ ppm): 7.44-7.49(d, 4H, H<sub>d</sub>), 7.19-7.23 (d, 2H, H<sub>a</sub>), 7.05-7.07 (d, 4H, H<sub>c</sub>), 6.99-7.01(d, 2H, H<sub>b</sub>), 2.84-2.94 (m, 1H, H<sub>CH</sub>), 1.20-1.28 (d, 6H, H<sub>CH<sub>3</sub></sub>). <sup>13</sup>CNMR(400 MHz, CDCl<sub>3</sub>-d<sub>1</sub>, δ ppm): 150.20 (C<sub>5</sub>), 147.47(C<sub>4</sub>), 105.38 (C<sub>8</sub>), 118.92 (C<sub>C≡N</sub>), 122.54 (C<sub>6</sub>), 126.93 (C<sub>2</sub>), 128.21 (C<sub>3</sub>), 133.40 (C<sub>7</sub>), 142.38 (C<sub>1</sub>), 33.62 (C<sub>CH</sub>), 23.84 (C<sub>CH<sub>3</sub></sub>).

#### 4.3.1.2. Synthesis of 4, 4'-dicyano-4''-2,4-dimethylaniline (Ib)

The product was filtered and recrystallized from ethanol to give a pale yellowish solid. (2.31 g, yield: 71.5%), m.p = 146-48°C, FTIR: 2222.4 cm<sup>-1</sup> (C≡N). <sup>1</sup>H NMR(400 MHz, CDCl<sub>3</sub>-d<sub>1</sub>, δ ppm): 7.67-7.73 (d, 4H, H<sub>e</sub>), 7.49-7.53 (m, 1H, H<sub>a</sub>), 7.09-7.13- (m, 5H, H<sub>b,d</sub>), 7.00-7.06 (m, 1H, H<sub>c</sub>), 2.14-2.18 (s, 3H, H<sub>CH<sub>3</sub>'</sub>), 1.23-1.29 (m, 3H, H<sub>CH<sub>3</sub>'</sub>). <sup>13</sup>C-NMR (400 MHz, CDCl<sub>3</sub>-d<sub>1</sub>, δ ppm): 150.22 (C<sub>7</sub>), 143.41 (C<sub>3</sub>), 138.68 (C<sub>1</sub>), 136.91 (C<sub>6</sub>), 135.22 (C<sub>9</sub>), 134.06 (C<sub>2</sub>), 121.81 (C<sub>4</sub>), 120.51 (C<sub>8</sub>), 119.19 (C<sub>5</sub>), 118.60 (C<sub>CN</sub>), 108.36 (C<sub>10</sub>).

#### 4.3.1.3. Synthesis of 4, 4'-dicyano-4''- 2-ethylaniline (Ic)

Pale yellowish solid. (2.81 g, yield: 77.5%), m.p = 110-112°C, FTIR: 2219 cm<sup>-1</sup> (C≡N). <sup>1</sup>H-NMR(400 MHz, CDCl<sub>3</sub>-d<sub>1</sub>, δ ppm): 7.62-7.60 (d, 4H, H<sub>f</sub>), 7.31-7.43 (m, 3H, H<sub>a,b,c</sub>), 7.05-7.20 (dd, 5H, H<sub>e,d</sub>), 2.34-2.39 (q, 2H, H<sub>CH<sub>2</sub></sub>), 0.96-0.99 (t, 3H, H<sub>CH<sub>3</sub></sub>), <sup>13</sup>C-NMR (400 MHz, CDCl<sub>3</sub>-d<sub>1</sub>, δ ppm): 150.48 (C<sub>7</sub>), 142.97 (C<sub>6</sub>), 135.38-135.31 (C<sub>1,5</sub>), 134.04 (C<sub>9</sub>), 131.34 (C<sub>2</sub>), 130.59 (C<sub>3</sub>), 129.06 (C<sub>4</sub>), 122.33 (C<sub>8</sub>), 120.54 (C<sub>CN</sub>), 105.51 (C<sub>10</sub>), 24.46 (C<sub>CH<sub>2</sub></sub>), 13.86 (C<sub>CH<sub>3</sub></sub>).

#### 4.3.1.4. Synthesis of 4, 4'-dicyano-4''-phenoxytriphenylamine (Id)

Pale yellowish solid (1.92 g, yield: 62%), m.p = 140-142 C°, FTIR: 2213.4 cm<sup>-1</sup>(C≡N). <sup>1</sup>H NMR(400 MHz, CDCl<sub>3</sub>-d<sub>1</sub>, δ ppm): 7.09-7.13 (t, 1H, H<sub>a</sub>), 7.31-7.35 (t, 2H, H<sub>b</sub>), 6.92-6.96 (d, 2H, H<sub>e</sub>), 7.00-7.09 (m, 2H, H<sub>f,c,d</sub>), 7.44-7.50 (d, 4H, H<sub>g</sub>). <sup>13</sup>C-NMR (400 MHz,

CDCl<sub>3</sub>-d<sub>1</sub>,  $\delta$  ppm): 124.04 (C<sub>1</sub>), 129.93 (C<sub>2</sub>), 119.41 (C<sub>3</sub>), 156.24 (C<sub>4</sub>), 150.11 (C<sub>5</sub>), 119.86 (C<sub>6</sub>), 128.63 (C<sub>7</sub>), 139.55 (C<sub>8</sub>), 150.44 (C<sub>9</sub>), 122.24 (C<sub>10</sub>), 133.51 (C<sub>11</sub>), 105.60 (C<sub>12</sub>), 118.87 (C<sub>CN</sub>).

#### 4.3.1.5. Synthesis of 4, 4'-dicyano-4''-(1H-pyrrol-1-yl)triphenylamine (Ie)

Pale yellowish solid. (2.72 g, yield: 76%), m.p = 148-150°C, FTIR: 2219.4 cm<sup>-1</sup> (C $\equiv$ N).

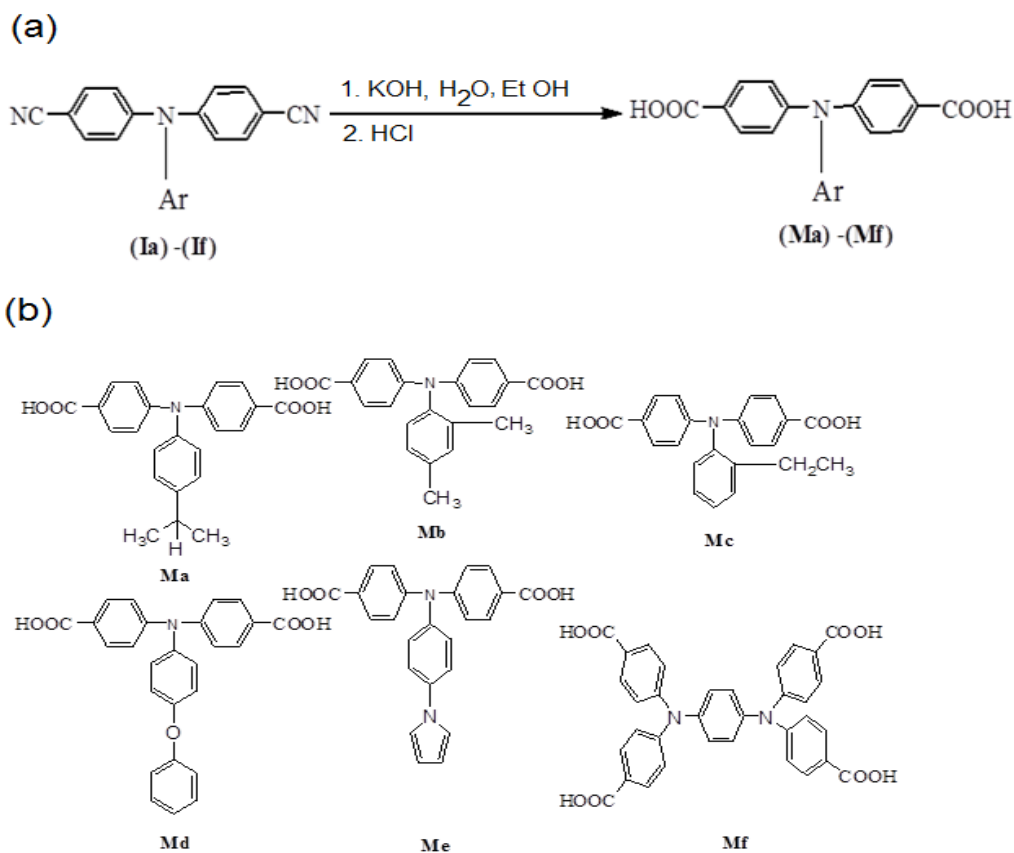
<sup>1</sup>H NMR(400 MHz, CDCl<sub>3</sub>-d<sub>1</sub>,  $\delta$  ppm): 7.44-7.56 (d, 4H, H<sub>f</sub>), 7.30-7.40 (d, 2H, H<sub>b</sub>), 7.07-7.17 (d, 2H, H<sub>c</sub>), 7.02-7.07 (d, 4H, H<sub>e</sub>), 6.97-7.02 (t, 2H, H<sub>d</sub>), 6.24-6.35 (t, 2H, H<sub>a</sub>). <sup>13</sup>C-NMR (400 MHz, CDCl<sub>3</sub>-d<sub>1</sub>,  $\delta$  ppm): 150.03(C<sub>7</sub>), 142.32 (C<sub>6</sub>), 138.84 (C<sub>3</sub>), 133.69 (C<sub>9</sub>), 128.04 (C<sub>5</sub>), 122.92 (C<sub>8</sub>), 122.05 (C<sub>4</sub>), 119.24 (C<sub>2</sub>), 118.85 (C<sub>CN</sub>), 111.03 (C<sub>1</sub>), 106.12 (C<sub>10</sub>).

#### 4.3.1.6. Synthesis of 4, 4', 4'', 4'''-(1,4-phenylenebis(azanetriyl))tetrabenzonitrile(If)

Pale yellowish solid. (3.2 g, yield: 88%), m.p = 150-152°C, FTIR: 2222 cm<sup>-1</sup> (C $\equiv$ N). <sup>1</sup>H NMR(400 MHz, CDCl<sub>3</sub>-d<sub>1</sub>,  $\delta$  ppm): 7.58-7.66 (d, 8H, H<sub>c</sub>), 7.00-7.08 (d, 8H, H<sub>b</sub>), 6.82-6.86 (s, 4H, H<sub>a</sub>). <sup>13</sup>C NMR(400 MHz, CDCl<sub>3</sub>-d<sub>1</sub>,  $\delta$  ppm): 159.22 (C<sub>3</sub>), 138.21 (C<sub>2</sub>), 135.88 (C<sub>1</sub>), 134.48 (C<sub>5</sub>), 119.69 (C<sub>4</sub>), 118.22 (C<sub>CN</sub>), 108.04 (C<sub>6</sub>).

### 4.3.2. General Synthesis of Monomers (Ma-Mf)

The monomers (**Ma-Mf**) were synthesized via the route as shown in the **Figure 4-2**.



**Figure 4-2:** (a) Synthesis of monomers (**Ma -Mf**), (b) structures of the synthesized monomers (**Ma-Mf**)

#### 4.3.2.1. Synthesis of 4,4'-dicarboxy-4''-isopropyltriphenylamine (Ma)

A mixture of 15.5 g of potassium hydroxide and 6.74 g (0.02 mol) of the dinitrile compound (**Ia**) in 60 mL of ethanol and 60 mL of distilled water was stirred at about 100°C until no further ammonia was generated. The time taken to reach this stage was about 24 h. The solution was cooled, and the pH value was adjusted by dilute hydrochloric acid to near 3. The yellowish precipitate formed was collected by filtration, washed thoroughly with water. Recrystallization from acetic acid gave pale yellow crystals (6.0 g, 80% yield); mp = 268–270°C, FTIR: 1681 cm<sup>-1</sup> (C=O), 2987 cm<sup>-1</sup> (O-H). <sup>1</sup>H NMR(400 MHz, DMSO-d<sub>6</sub>, δ ppm): 7.81-7.83 (d, 4H, H<sub>d</sub>), 7.26-7.28 (d, 2H, H<sub>a</sub>), 7.04-7.06 (d, 2H, H<sub>b</sub>), 7.00-7.02 (d, 4H, H<sub>c</sub>), 2.85-2.91 (m, 1H, H<sub>CH</sub>), 1.15-1.20 (d, 6H, H<sub>CH3</sub>), 12.62-12.78

(br, 2H, H<sub>COOH</sub>). <sup>13</sup>C NMR(400 MHz,DMSO-d<sub>6</sub>, δ ppm): 166.83 (COOH), 150.44 (C<sub>5</sub>), 145.82 (C<sub>4</sub>), 143.22 (C<sub>1</sub>), 130.97 (C<sub>7</sub>), 128.01 (C<sub>3</sub>), 124.42 (C<sub>2</sub>), 126.56 (C<sub>8</sub>), 121.86 (C<sub>6</sub>), 23.81 (CH), 23.81 (CH<sub>3</sub>).

#### 4.3.2.2. Synthesis of 4,4'-dicarboxy-4''-2,4-dimethyltriphenylamine (Mb)

Pale yellow crystals (7.3 g, 94.18% yield), m.p.= 276-278 C°, FTIR: 1683 cm<sup>-1</sup> (C=O), 2710-3321 cm<sup>-1</sup> (O-H). <sup>1</sup>H NMR (400 MHz, DMSO-d<sub>6</sub>, δ ppm): 12.73-12.89 (s, 2H, H<sub>COOH</sub>), 7.95-8.01 (d, 4H, H<sub>e</sub>), 7.80-7.84 (m, 1H, H<sub>a</sub>), 7.12-7.17 (d, 4H, H<sub>d</sub>), 6.92-6.98 (d, 1H, H<sub>b</sub>), 6.98-7.05(d, 1H, H<sub>c</sub>), 2.06-2.12 (s, 3H, H<sub>CH3''</sub>), 1.16-1.26 (s, 3H, H<sub>CH3'</sub>). <sup>13</sup>C NMR(400 MHz, DMSO-d<sub>6</sub>, δ ppm): 166.88 (C<sub>COOH</sub>), 149.86 (C<sub>7</sub>), 143.47 (C<sub>3</sub>), 132.00 (C<sub>9</sub>), 131.11 (C<sub>1</sub>), 129.00 (C<sub>2</sub>), 128.02 (C<sub>6</sub>), 122.04 (C<sub>4</sub>), 126.76 (C<sub>10</sub>), 120.29 (C<sub>5</sub>), 118.98 (C<sub>8</sub>), 33.15 (C<sub>CH3''</sub>), 23.99 (C<sub>CH3'</sub>).

#### 4.3.2.3. Synthesis of 4,4'-dicarboxy-4''- 2-ethyltriphenylamine (Mc)

The synthesis of this compound was the same to that for **Ma**. The pale yellow crystals (3.40 g, 94.2% yield) ; m.p.= 273-275°C, FTIR: 1680 cm<sup>-1</sup> (C=O), 2713-3332 cm<sup>-1</sup> (O-H). <sup>1</sup>H NMR(400 MHz, DMSO-d<sub>6</sub>, δ ppm):12.68-12.84 (s, 2H, H<sub>COOH</sub>), 7.75-7.88 (d, 4H, H<sub>f</sub>), 7.31-7.42 (m, 3H, H<sub>a,b,c</sub>), 7.07-7.17 (d, 5H, H<sub>e,d</sub>), 2.34-2.28 (q, 2H, H<sub>CH2</sub>), 0.96-0.91 (t, 3H, H<sub>CH3</sub>). <sup>13</sup>C NMR(400MHz, DMSO-d<sub>6</sub>, δ ppm): 166.81 (C<sub>COOH</sub>), 150.86 (C<sub>7</sub>), 143.25 (C<sub>6</sub>), 131.20 (C<sub>1</sub>), 131.03 (C<sub>5</sub>), 132.18 (C<sub>9</sub>), 128.50 (C<sub>2</sub>), 128.34 (C<sub>3</sub>), 128.17 (C<sub>4</sub>), 126.33 (C<sub>10</sub>), 122.16 (C<sub>8</sub>), 23.15 (C<sub>CH3</sub>), 13.23 (C<sub>CH3</sub>).

#### 4.3.2.4. Synthesis of 4, 4'-dicarboxy-4''-phenoxytriphenylamine (Md)

Pale yellow crystals (4.8 g, 80% yield); m.p.= 215—218°C, FTIR: 1670 cm<sup>-1</sup> (C=O), 3370 cm<sup>-1</sup> (O-H). <sup>1</sup>H NMR (400 MHz, DMSO-d<sub>6</sub>, δ ppm): 11.16-11.32 (s, 2H, H<sub>COOH</sub>), 7.82-7.89 (d, 4H, H<sub>g</sub>), 7.40-7.44 (t, 2H, H<sub>b</sub>), 7.19-7.50 (m, 3H, H<sub>a,c</sub>), 7.01-7.07 (m, 8H, H<sub>e,d,f</sub>). <sup>13</sup>C NMR(400 MHz, DMSO-d<sub>6</sub>, δ ppm): 166.66 (C<sub>COOH</sub>), 156.09 (C<sub>8</sub>), 145.322 (C<sub>1</sub>),

155.09 (C<sub>9</sub>), 140.52 (C<sub>5</sub>), 130.77 (C<sub>11</sub>), 129.94 (C<sub>2</sub>), 128.41 (C<sub>7</sub>), 124.49 (C<sub>4</sub>), 123.60 (C<sub>12</sub>), 121.46 (C<sub>10</sub>).

#### 4.3.2.5. Synthesis of 4,4'-dicarboxy-4''-(1H-pyrrol-1-yl)triphenylamine (Me)

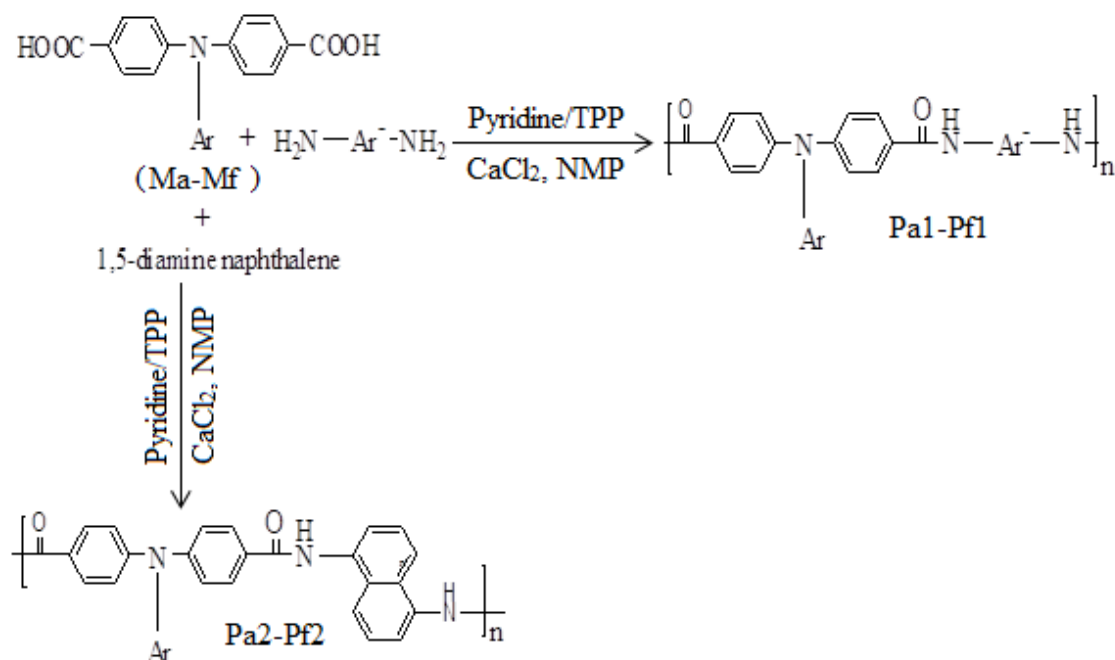
Pale yellow crystals (7.3 g, 89% yield); m.p.= 229-232°C, FTIR: 1681 cm<sup>-1</sup> (C=O), 2700-3300 cm<sup>-1</sup> (O-H). <sup>1</sup>H NMR (400 MHz, DMSO-d<sub>6</sub>, δ ppm): 11.17-11.33 (s, 2H, H<sub>COOH</sub>), 7.85-7.90 (d, 4H, H<sub>f</sub>), 7.35-7.39 (t, 2H, H<sub>b</sub>), 7.23-7.25 (d, 2H, H<sub>d</sub>), 7.60-7.67 (d, 2H, H<sub>c</sub>), 7.05-7.14 (d, 4H, H<sub>e</sub>), 6.25-6.32 (t, 2H, H<sub>a</sub>). <sup>13</sup>C NMR(400 MHz, DMSO-d<sub>6</sub>, δ ppm): 166.85 (C<sub>COOH</sub>), 150.25 (C<sub>7</sub>), 142.59 (C<sub>6</sub>), 137.25 (C<sub>3</sub>), 131.05 (C<sub>9</sub>), 127.77 (C<sub>5</sub>), 124.65 (C<sub>10</sub>), (122.02 C<sub>8</sub>), 120.91 (C<sub>4</sub>), 118.99 (C<sub>2</sub>), 110.64 (C<sub>1</sub>).

#### 4.3.2.6. Synthesis of 4,4',4'',4'''-(1,4-phenylenebis(azanetriyl))tetrabenzoic acid (Mf)

Pale yellow crystals ( 6.8 g, 90% yield); m.p.= 287—290°C, FTIR: 1682 cm<sup>-1</sup> (C=O), 3378 cm<sup>-1</sup> (O-H). <sup>1</sup>H NMR (400 MHz, DMSO-d<sub>6</sub>, δ ppm): 12.15-12.31 (s, 2H, H<sub>COOH</sub>), 7.87-7.94 (d, 8H, H<sub>c</sub>), 7.00-7.08 (d, 8H, H<sub>b</sub>), 6.50-6.54 (s, 4H, H<sub>a</sub>). <sup>13</sup>C NMR(400 MHz, DMSO-d<sub>6</sub>): 166.78 (C<sub>COOH</sub>), 158.34 (C<sub>3</sub>), 137.14 (C<sub>2</sub>), 134.78 (C<sub>1</sub>), 133.04 (C<sub>5</sub>) 123.30 (C<sub>6</sub>), 118.12 (C<sub>4</sub>).

### 4.3.3. General Synthesis of Polyamides

Polyamides (**Pa1-Pf1**) and (**Pa2-Pf2**) were synthesized via the routes as shown in **Figure 4-3**.



**Figure 4-3:** Synthetic route of the polyamides

#### 4.3.3.1. Synthesis of poly(amine amide) (**Pa1**)

The synthesis of poly(amine amide) (**Pa1**) is used as an example to illustrate the general synthetic routes. The typical procedure is as follows. A mixture of 1.14 g (3 mmol) of the dicarboxylic acid monomer (**Ma**), 0.324 g (3 mmol) of p-phenylenediamine, 0.4 g of calcium chloride, 4.5 mL of triphenyl phosphite (TPP), 1.5 mL of pyridine, and 4.5 mL of N-methyl-2-pyrrolidone (NMP) was heated with stirring at 105°C for 3 h. The resulting viscous polymer solution was poured slowly into 300 mL of stirring methanol giving rise to a stringy, fiber-like precipitate that was collected by filtration, washed thoroughly with hot water and methanol, and dried at 80°C for 24 h. The inherent viscosity of the obtained poly(amine amide) was 0.62 dL/g, measured at a concentration of 0.5 g/dL in DMAc. The IR spectrum exhibited characteristic amide absorption bands at 3309.39 cm<sup>-1</sup> (N-H

stretching), and  $1644\text{ cm}^{-1}$  (amide carbonyl).  $^1\text{H}$  NMR (400 MHz, DMSO- $d_6$ ,  $\delta$  ppm): 10.20–10.26 (s, 1H,  $\text{H}_{\text{NH-CO}}$ ), 8.00–8.08 (d, 4H,  $\text{H}_d$ ), 7.70–7.80 (s, 4H,  $\text{H}_e$ ), 7.34–7.33 (d, 2H,  $\text{H}_a$ ), 7.18–7.23 (d, 4H,  $\text{H}_c$ ), 6.54–6.63 (d, 2H,  $\text{H}_b$ ), 3.15–3.23 (m, 1H,  $\text{H}_{\text{CH}}$ ), 2.03–2.10 (s, 6H,  $\text{H}_{\text{CH}_3}$ ).  $^{13}\text{C}$  NMR(400 MHz,DMSO- $d_6$ ,  $\delta$  ppm): 166.74 (NHCO), 150.44 ( $\text{C}_5$ ), 145.82 ( $\text{C}_4$ ), 143.22 ( $\text{C}_1$ ), 131.83 ( $\text{C}_9$ ), 130.97 ( $\text{C}_7$ ), 128.23 ( $\text{C}_3$ ), 124.12 ( $\text{C}_2$ ), 126.12 ( $\text{C}_8$ ), 121.76 ( $\text{C}_6$ ), 120.02 ( $\text{C}_{10}$ ), 32.91 ( $\text{C}_{\text{CH}}$ ), 23.81 ( $\text{C}_{\text{CH}_3}$ ).

#### 4.3.3.2. Synthesis of Poly(amine amide) (Pb1)

The inherent viscosity of the obtained (**Pb1**) was 0.66 dL/g, measured at a concentration of 0.5 g/dL in DMAc. The (IR) spectrum exhibited characteristic amide absorption bands at  $3304\text{ cm}^{-1}$  (N-H stretching) and  $1644\text{ cm}^{-1}$  (amide carbonyl).  $^1\text{H}$  NMR(400 MHz, DMSO- $d_6$ ,  $\delta$  ppm): 10.23–10.31 (s, 1H,  $\text{H}_{\text{NHCO}}$ ), 8.05–7.90 (d, 5H,  $\text{H}_e$ ), 7.68–7.82 (s, 4H,  $\text{H}_f$ ), 6.95–7.55 (s, 6H,  $\text{H}_{a,b,d}$ ), 6.74–6.56 (s, 1H,  $\text{H}_c$ ), 1.92–2.02 (s, 3H,  $\text{H}_{\text{CH}_3''}$ ), 1.16–1.26 (s, 3H,  $\text{H}_{\text{CH}_3'}$ ).  $^{13}\text{C}$  NMR(400 MHz,DMSO- $d_6$ ,  $\delta$  ppm): 166.89 ( $\text{C}_{\text{CO-NH}}$ ), 149.97 ( $\text{C}_7$ ), 142.89 ( $\text{C}_3$ ), 131.91 ( $\text{C}_9$ ), 131.21 ( $\text{C}_1$ ), 129.04 ( $\text{C}_2$ ), 128.34 ( $\text{C}_6$ ), 126.45 ( $\text{C}_{10}$ ), 125.22 ( $\text{C}_{11}$ ), 123.17 ( $\text{C}_4$ ), 120.17 ( $\text{C}_5$ ), 118.12 ( $\text{C}_8$ ), 117.23 ( $\text{C}_{12}$ ), 33.45 ( $\text{C}_{\text{CH}_3''}$ ), 23.24 ( $\text{C}_{\text{CH}_3'}$ ).

#### 4.3.3.3. Synthesis of Poly(amine amide) (Pc1)

The inherent viscosity of the obtained poly(amine amide) was 0.63 dL/g, measured at a concentration of 0.5 g/dL in DMAc. The IR spectrum exhibited characteristic amide absorption bands at  $3314\text{ cm}^{-1}$  (N-H stretching) and  $1644\text{ cm}^{-1}$  (amide carbonyl).  $^1\text{H}$  NMR(400 MHz, DMSO- $d_6$ ,  $\delta$  ppm): 10.20–10.26 (s, 1H,  $\text{H}_{\text{NHCO}}$ ), 7.98–7.83 (s, 1H,  $\text{H}_{f,a}$ ), 7.40–7.34(s, 1H,  $\text{H}_{g,c}$ ), 7.13–6.73 (s, 1H,  $\text{H}_{b,e,d}$ ), 2.01–2.11 (s, 1H,  $\text{H}_{\text{CH}_2}$ ), 0.88–0.95 (s, 1H,  $\text{H}_{\text{CH}_3}$ ).  $^{13}\text{C}$  NMR(400 MHz, DMSO- $d_6$ ,  $\delta$  ppm): 166.82( $\text{C}_{\text{CO-NH}}$ ), 150.12( $\text{C}_7$ ), 142.89( $\text{C}_6$ ), 131.20 ( $\text{C}_1$ ), 131.03( $\text{C}_5$ ), 131.91( $\text{C}_9$ ), 129.17( $\text{C}_2$ ), 128.89( $\text{C}_3$ ), 127.16( $\text{C}_4$ ), 126.12( $\text{C}_{10}$ ), 125.32( $\text{C}_{11}$ ), 122.23( $\text{C}_8$ ), 121.18( $\text{C}_{12}$ ), 26.45( $\text{C}_{\text{CH}_2}$ ), 13.43( $\text{C}_{\text{CH}_3}$ ).

#### 4.3.3.4. Synthesis of Poly(amine amide) (Pd1)

The inherent viscosity of the obtained poly(amine amide) was 0.42 dL/g. The IR spectrum exhibited characteristic amide absorption bands at  $3376\text{ cm}^{-1}$  (N-H stretching) and  $1648\text{ cm}^{-1}$  (amide carbonyl).  $^1\text{H}$  NMR(400 MHz, DMSO- $\text{d}_6$ ,  $\delta$  ppm): 10.19-10.09 (s, 1H,  $\text{H}_{\text{NH-CO}}$ ), 7.86-7.98 (d, 4H,  $\text{H}_g$ ), 7.67-7.77 (s, 4H,  $\text{H}_h$ ), 7.37-7.45 (t, 1H,  $\text{H}_a$ ), 7.14-7.22 (t, 2H,  $\text{H}_b$ ), 7.02-7.14 (m, 10H,  $\text{H}_{c,d,e,f}$ ).  $^{13}\text{C}$  NMR(400 MHz, DMSO- $\text{d}_6$ ,  $\delta$  ppm): 166.95 ( $\text{C}_{\text{CONH}}$ ), 157.70 ( $\text{C}_{14}$ ), 156.37 ( $\text{C}_4$ ), 149.45 ( $\text{C}_5$ ), 148.63 ( $\text{C}_{13}$ ), 150.89 ( $\text{C}_9$ ), 142.61 ( $\text{C}_8$ ), 131.08 ( $\text{C}_{11}$ ), 130.25 ( $\text{C}_7$ ), 128.77 ( $\text{C}_2$ ), 124.57 ( $\text{C}_1$ ), 123.88 ( $\text{C}_{12}$ ), 121.76 ( $\text{C}_{10}$ ), 120.00 ( $\text{C}_3$ ), 119.12 ( $\text{C}_6$ ).

#### 4.3.3.5. Synthesis of Poly(amine amide) (Pe1)

The inherent viscosity of the obtained poly(amine amide) was 0.46 dL/g. The (IR) spectrum exhibited characteristic amide absorption bands at  $3373\text{ cm}^{-1}$  (N-H stretching) and  $1648\text{ cm}^{-1}$  (amide carbonyl).  $^1\text{H}$  NMR(400 MHz, DMSO- $\text{d}_6$ ,  $\delta$  ppm): 10.18-10.30 (s, 1H,  $\text{H}_{\text{NH-C=O}}$ ), 7.93-8.05 (d, 4H,  $\text{H}_f$ ), 7.73-7.62 (m, 8H,  $\text{H}_{g,c,b}$ ), 7.32-7.40 (d, 2H,  $\text{H}_d$ ), 7.11-7.24 (d, 2H,  $\text{H}_e$ ), 6.24-6.43 (s, 2H,  $\text{H}_a$ ).  $^{13}\text{C}$  NMR(400 MHz, DMSO- $\text{d}_6$ ,  $\delta$  ppm): 164.68 ( $\text{C}_{\text{CONH-}}$ ), 150.05 ( $\text{C}_7$ ), 143.11 ( $\text{C}_6$ ), 138.12 ( $\text{C}_3$ ), 134.75 ( $\text{C}_{11}$ ), 130.06 ( $\text{C}_9$ ), 127.16 ( $\text{C}_5$ ), 124.18 ( $\text{C}_{10}$ ), 122.34 ( $\text{C}_8$ ), 120.60 ( $\text{C}_{12}$ ), 118.09 ( $\text{C}_4$ ), 118.42 ( $\text{C}_2$ ), 110.49 ( $\text{C}_1$ ).

#### 4.3.3.6. Synthesis of Poly(amine amide) (Pf1)

The inherent viscosity of the obtained poly(amine amide) was 0.43 dL/g. The IR spectrum exhibited characteristic amide absorption bands at  $3264\text{ cm}^{-1}$  (N-H stretching) and  $1647\text{ cm}^{-1}$  (amide carbonyl).  $^1\text{H}$  NMR(400 MHz, DMSO- $\text{d}_6$ ,  $\delta$  ppm): 10.25-10.36 (s, 1H,  $\text{H}_{\text{NH-CO}}$ ), 8.04-8.16 (s, 8H,  $\text{H}_c$ ), 7.74-7.84 (s, 4H,  $\text{H}_d$ ), 7.42-7.24 (d, 8H,  $\text{H}_b$ ), 6.55-6.67 (s, 4H,  $\text{H}_a$ ).  $^{13}\text{C}$  NMR(400 MHz, DMSO- $\text{d}_6$ ,  $\delta$  ppm): 164.94 ( $\text{C}_{\text{CO-NH}}$ ), 158.75 ( $\text{C}_3$ ), 145.26 ( $\text{C}_7$ ), 135.43 ( $\text{C}_2$ ), 131.35 ( $\text{C}_1$ ), 130.52 ( $\text{C}_5$ ), 122.74 ( $\text{C}_6$ ), 121.15 ( $\text{C}_8$ ), 118.93 ( $\text{C}_4$ ).



#### 4.3.3.7. Synthesis of Poly(amine amide) (Pa2)

The inherent viscosity of the obtained poly(amine amide) was 0.75 dL/g, measured at a concentration of 0.5 g/dL in DMAc. The IR spectrum exhibited characteristic amide absorption bands at  $3364\text{cm}^{-1}$  (N-H stretching) and  $1647\text{ cm}^{-1}$  (amide carbonyl).  $^1\text{H}$  NMR(400 MHz, DMSO- $\text{d}_6$ ,  $\delta$  ppm): 10.38-10.44 (s, 1H,  $\text{H}_{\text{NH-CO}}$ ), 7.99-7.97(d, 2H,  $\text{H}_g$ ), 7.84-7.82(d, 4H,  $\text{H}_d$ ), 7.45-7.56 (s, 2H,  $\text{H}_f$ ), 7.35-7.40 (d, 2H,  $\text{H}_a$ ), 7.29-7.27(d, 2H,  $\text{H}_e$ ), 7.15-7.13(d, 4H,  $\text{H}_c$ ), 7.03-7.01(d, 2H,  $\text{H}_b$ ), 1.92-1.84(m, 1H,  $\text{H}_{\text{CH}}$ ), 1.21-1.19(d, 6H,  $\text{H}_{\text{CH}_3}$ ).  $^{13}\text{C}$  NMR(400 MHz, DMSO- $\text{d}_6$ ,  $\delta$  ppm): 166.56 ( $\text{C}_{\text{CONH}}$ ), 150.47 ( $\text{C}_5$ ), 145.68 ( $\text{C}_4$ ), 143.46 ( $\text{C}_1$ ), 131.76 ( $\text{C}_9$ ), 130.36 ( $\text{C}_7$ ), 128.33 ( $\text{C}_3$ ), 127.40 ( $\text{C}_2$ ), 126.11 ( $\text{C}_8$ ), 125.98 ( $\text{C}_{13}$ ), 125.68 ( $\text{C}_{11}$ ), 121.86 ( $\text{C}_6$ ), 110.77 ( $\text{C}_{12}$ ), 104.24 ( $\text{C}_{10}$ ), 32.82 ( $\text{C}_{\text{CH}}$ ), 23.87 ( $\text{C}_{\text{CH}_3}$ ).

#### 4.3.3.8. Synthesis of Poly(amine amide) (Pb2)

The inherent viscosity of the obtained poly(amine amide) was 0.67 dL/g, measured at a concentration of 0.5 g/dL in DMAc. The IR spectrum exhibited characteristic amide absorption bands at  $3364\text{cm}^{-1}$  (N-H stretching) and  $1648\text{ cm}^{-1}$  (amide carbonyl).  $^1\text{H}$  NMR(400 MHz, DMSO- $\text{d}_6$ ,  $\delta$  ppm): 10.41-10.50 (s, 1H,  $\text{H}_{\text{NH-CO}}$ ), 8.07-8.21(s, 6H,  $\text{H}_{e,h}$ ), 7.94-7.88 (d, 2H,  $\text{H}_g$ ), 7.55-7.24 (d, 2H,  $\text{H}_f$ ), 7.20-7.06 (d, 6H,  $\text{H}_{a,b,d}$ ), 6.68-6.64 (d, 2H,  $\text{H}_c$ ), 1.98-1.76 (s, 3H,  $\text{H}_{\text{CH}_3''}$ ), 1.23-0.92 (s, 3H,  $\text{H}_{\text{CH}_3'}$ ).  $^{13}\text{C}$  NMR(400 MHz, DMSO- $\text{d}_6$ ,  $\delta$  ppm): 166.86 ( $\text{C}_{\text{CONH}}$ ), 150.54( $\text{C}_7$ ), 143.73 ( $\text{C}_3$ ), 132.71 ( $\text{C}_{11}$ ), 131.75 ( $\text{C}_9$ ), 131.12 ( $\text{C}_1$ ), 130.76 ( $\text{C}_2$ ), 128.58 ( $\text{C}_6$ ), 126.67 ( $\text{C}_{10}$ ), 125.87 ( $\text{C}_{15}$ ), 124.77 ( $\text{C}_{13}$ ), 122.57 ( $\text{C}_4$ ), 121.82 ( $\text{C}_5$ ), 118.82 ( $\text{C}_8$ ), 110.23 ( $\text{C}_{14}$ ), 107.63 ( $\text{C}_{12}$ ), , 33.07 ( $\text{C}_{\text{CH}_3''}$ ), 23.65 ( $\text{C}_{\text{CH}_3'}$ ).

#### 4.3.3.9. Synthesis of Poly(amine amide) (Pc2)

The inherent viscosity of the obtained poly(amine amide) was 0.88 dL/g, measured at a concentration of 0.5 g/dL in DMAc. The IR spectrum exhibited characteristic amide absorption bands at  $3357\text{ cm}^{-1}$  (N-H stretching) and  $1648\text{ cm}^{-1}$  (amide carbonyl).  $^1\text{H}$  NMR(400 MHz, DMSO- $\text{d}_6$ ,  $\delta$  ppm): 10.38-10.48 (s, 1H,  $\text{H}_{\text{NHCO}}$ ), 8.12-8.08 (s, 7H,  $\text{H}_{f,a,i}$ ), 7.88-7.86 (d, 2H,  $\text{H}_h$ ), 7.64-7.50 (d, 2H,  $\text{H}_{g,c}$ ), 7.19-7.00(d, 5H,  $\text{H}_{e,d}$ ), 6.66-6.64 (d, 1H,

H<sub>b</sub>), 2.06 (q, 1H, H<sub>CH2</sub>), 0.97 (t, 1H, H<sub>CH3</sub>). <sup>13</sup>C NMR(400 MHz, DMSO-d<sub>6</sub>, δ ppm): 165.92 (C<sub>CONH</sub>), 150.24 (C<sub>7</sub>), 142.56 (C<sub>6</sub>), 132.05 (C<sub>5</sub>), 131.85 (C<sub>1</sub>), 131.24 (C<sub>11</sub>), 130.86 (C<sub>9</sub>), 131.12 (C<sub>2</sub>), 130.76 (C<sub>3</sub>), 128.58 (C<sub>4</sub>), 126.56 (C<sub>10</sub>), 124.06 (C<sub>15</sub>), 121.77 (C<sub>13</sub>), 118.57 (C<sub>8</sub>), 110.32 (C<sub>14</sub>), 106.81 (C<sub>12</sub>), 26.43 (C<sub>CH2</sub>), 13.63 (C<sub>CH3</sub>).

#### 4.3.3.10. Synthesis of Poly(amine amide) (Pd2)

The inherent viscosity of the obtained poly(amine amide) was 0.65 dL/g, measured at a concentration of 0.5 g/dL in DMAc. The IR spectrum exhibited characteristic amide absorption bands at 3372 cm<sup>-1</sup> (N-H stretching) and 1646 cm<sup>-1</sup> (amide carbonyl). <sup>1</sup>H NMR(400 MHz, DMSO-d<sub>6</sub>, δ ppm): 10.34-10.44 (s, 1H, H<sub>NH-CO</sub>), 8.10-8.07 (m, 4H, H<sub>g,i</sub>), 7.93-7.91 (d, 2H, H<sub>j</sub>), 7.61-7.56 (t, 2H, H<sub>b</sub>), 7.45-7.41 (m, 3H, H<sub>a,c</sub>), 7.26-7.17 (m, 8H, H<sub>h,f,e</sub>), 7.11-7.09 (d, 2H, H<sub>d</sub>). <sup>13</sup>C NMR(400 MHz, DMSO-d<sub>6</sub>, δ ppm): 165.63 (C<sub>CO-NH</sub>), 156.54 (C<sub>4</sub>), 150.59 (C<sub>9</sub>), 149.71 (C<sub>5</sub>), 141.25 (C<sub>8</sub>), 131.97 (C<sub>13</sub>), 130.21 (C<sub>11</sub>), 129.57 (C<sub>7</sub>), 128.30 (C<sub>2</sub>), 125.49 (C<sub>15</sub>), 124.23 (C<sub>1</sub>), 123.77 (C<sub>12</sub>), 121.94 (C<sub>10</sub>), 120.77 (C<sub>17</sub>), 120.07 (C<sub>3</sub>), 118.88 (C<sub>6</sub>), 111.82 (C<sub>16</sub>), 107.87 (C<sub>14</sub>).

#### 4.3.3.11. Synthesis of Poly(amine amide) (Pe2)

The inherent viscosity of the obtained poly(amine amide) was 0.66 dL/g, measured at a concentration of 0.66 g/dL in DMAc. The IR spectrum exhibited characteristic amide absorption bands at 3370 cm<sup>-1</sup> (N-H stretching) and 1646 cm<sup>-1</sup> (amide carbonyl). <sup>1</sup>H NMR(400 MHz, DMSO-d<sub>6</sub>, δ ppm): 10.40-10.49 (s, 1H, H<sub>NH-CO</sub>), 8.12-7.94 (m, 6H, H<sub>f,i</sub>), 7.69-7.65 (m, 6H, H<sub>b,c,h</sub>), 7.39-7.22 (m, 8H, H<sub>d,e,g</sub>), 6.25-6.34 (s, 2H, H<sub>a</sub>). <sup>13</sup>C NMR(400 MHz, DMSO-d<sub>6</sub>, δ ppm): 166.06 (C<sub>CO-NH</sub>), 150.08 (C<sub>7</sub>), 143.59 (C<sub>6</sub>), 137.45 (C<sub>11</sub>), 134.85 (C<sub>3</sub>), 130.13 (C<sub>9</sub>), 128.84 (C<sub>10</sub>), 127.74 (C<sub>13</sub>), 124.56 (C<sub>5</sub>), 122.77 (C<sub>2</sub>), 121.12 (C<sub>4</sub>), 119.57 (C<sub>8</sub>), 119.14 (C<sub>15</sub>), 111.23 (C<sub>14</sub>), 108.21 (C<sub>1</sub>), 103.34 (C<sub>12</sub>).

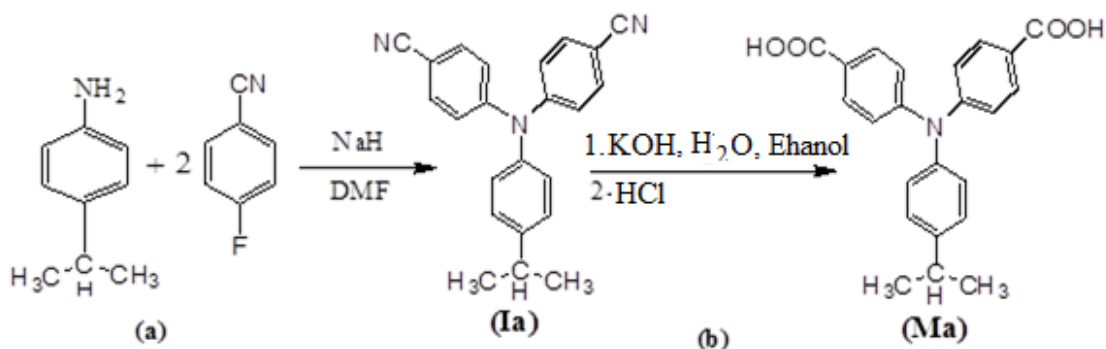
#### 4.3.3.12. Synthesis of Poly(amine amide) (Pf2)

The inherent viscosity of the obtained poly(amine amide) was 0.71 dL/g, measured at a concentration of 0.71 g/dL in DMAc. The IR spectrum exhibited characteristic amide absorption bands at  $3370\text{ cm}^{-1}$  (N-H stretching) and  $1644\text{ cm}^{-1}$  (amide carbonyl).  $^1\text{H}$  NMR(400 MHz, DMSO- $\text{d}_6$ ,  $\delta$  ppm): 10.47-10.58 (s, 1H,  $\text{H}_{\text{NH-CO}}$ ), 8.23-8.21 (d, 8H,  $\text{H}_e$ ), 8.12-7.88 (d, 2H,  $\text{H}_e$ ), 7.73-7.59 (d, 2H,  $\text{H}_f$ ), 7.18-7.12 (d, 2H,  $\text{H}_d$ ), 7.18-7.38(d, 8H,  $\text{H}_b$ ), 6.70-6.77 (s, 4H,  $\text{H}_a$ ).  $^{13}\text{C}$  NMR(400 MHz, DMSO- $\text{d}_6$ ,  $\delta$  ppm): 165.90 ( $\text{C}_{\text{CO-NH}}$ ), 159.34 ( $\text{C}_3$ ), 134.62 ( $\text{C}_7$ ), 132.30 ( $\text{C}_2$ ), 130.78 ( $\text{C}_5$ ), 126.02 ( $\text{C}_9$ ), 122.45 ( $\text{C}_6$ ), 119.60 ( $\text{C}_{11}$ ), 119.09 ( $\text{C}_4$ ), 118.69 ( $\text{C}_{10}$ ), 115.67 ( $\text{C}_8$ ), 131.80 ( $\text{C}_1$ ).

## CHAPTER 5: RESULTS AND DISCUSSION

### 5.1. Monomer synthesis

The new aromatic dicarboxylic acids having alkyl and aryl substituted triphenylamine units (**Ma-Mf**), were synthesized by the amination reaction of the substituted aromatic amines (**a-f**) with 4-fluorobenzonitrile in the presence of NaH as a strong base and DMF as a polar solvent followed by the alkaline hydrolysis of the dicyano intermediates (**Ia-I f**) respectively. In this study, 4-isopropylaniline (**a**) is used as an example for the discussion of this synthesis as shown in **Figure 5-1** (a) 4,4'-dicarboxy-4''-isopropyltriphenylamine (**Ma**) was synthesized by the amination reaction of 4-isopropylaniline with 4-fluorobenzonitrile. The resultant intermediate dicyano compound (**Ia**) was hydrolyzed by an alkaline medium to produce the monomer (**Ma**) as shown in Figure 5-1 (b).



**Figure 5-1:** Synthesis routes of (a) intermediate **Ia** and (b) its monomer **Ma**

The reaction starts via the aromatic nucleophilic fluoro-displacement reaction of 4-fluorobenzonitrile with aniline-derivatives using sodium hydride as the base as shown in **Figure 5-2** (a). This is followed by phenylation hydrolysis of the dinitrile intermediates **Ia**, **Ib**, **Ic**, **Id**, **Ie**, **If** as shown in **Figure 5-2** (b).

The amine group with nonbonding electrons of the aromatic amine functions as the nucleophile and attacks the carbon atom of C-F of the aromatic fluoride, displacing the fluoride and creating the new C-N bond. In the acid/base reaction, the base (excess amine)

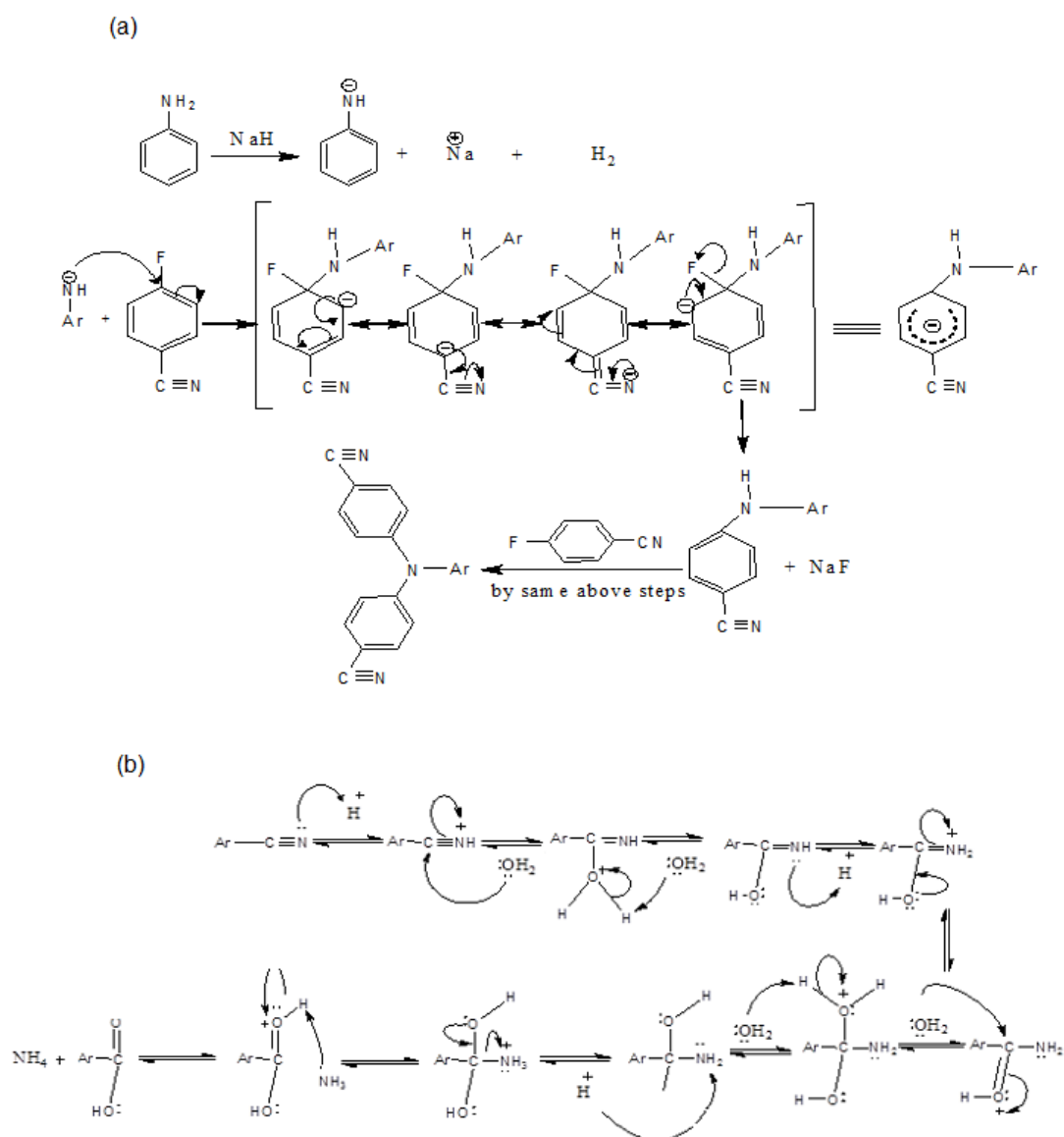
deprotonates the positive N (ammonium) center creating the phenylation product, which is a secondary amine. The tertiary aromatic amine is produced by the same way. In the next step, the nitrile tertiary aromatic amine hydrolyses to the carboxylic compound in alkaline medium in three different steps:

Step 1: An acid/base reaction to activate the nitrile, protonation makes it more electrophilic. The O from water functions as the nucleophile attacking the electrophilic C in the  $C\equiv N$ , with the electrons moving towards the positive center.

Step 2: An acid/base reaction to deprotonate the oxygen that comes from the water molecule. The remaining task is tautomerisation at N and O centers, then protonating the N to give  $-NH_2$ .

Step 3: The electrons of an adjacent O is used to neutralize the positive charge at N and form the  $\pi$  bond in the  $C=O$ . Finally an acid/base reaction and deprotonation of the oxonium ion gives the carbonyl in the amide intermediate which will form the acid.

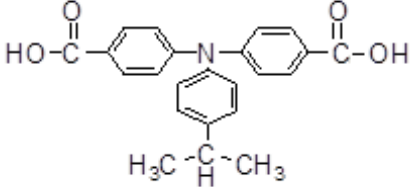
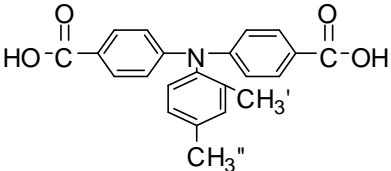
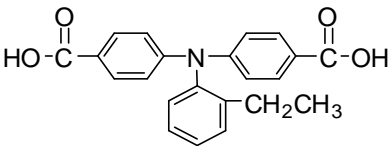
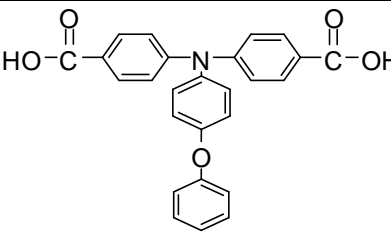
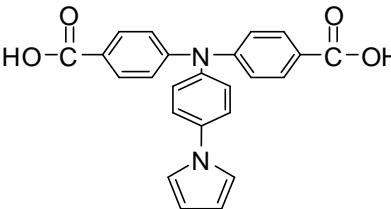
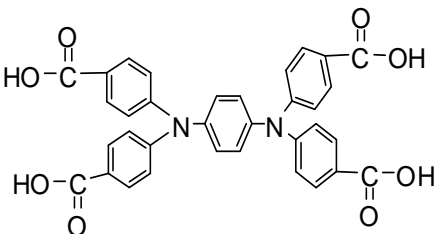
The other nitrile tertiary aromatic amines similarly undergo hydrolysis to form carboxylic derivatives thus giving the overall dicarboxylic compounds.



**Figure 5-2:** Reaction mechanism of (a) the aromatic nucleophilic fluoro-displacement reaction and (b) the hydrolysis of nitrile intermediate to the carboxylic compound

**Table 5-1** shows the structures of synthesized monomers with their melting points and yields.

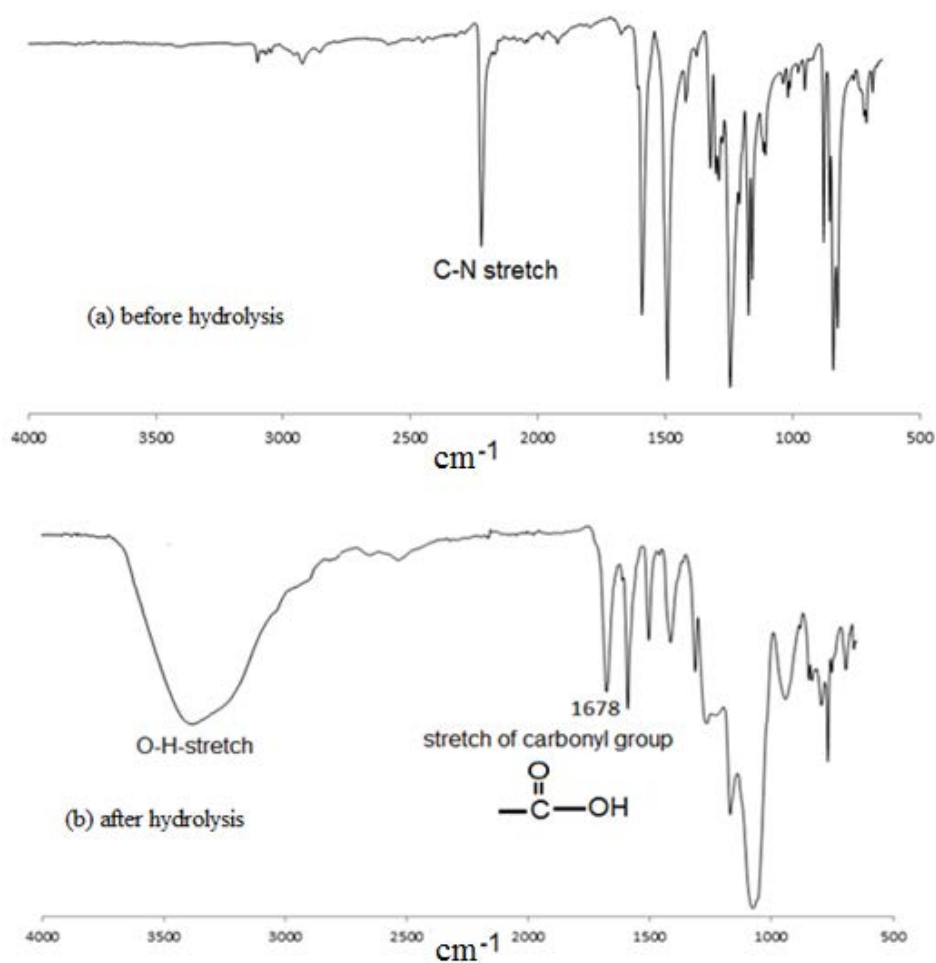
**Table 5-1:** Synthesized Monomers and their Structures

Monomer structures	Monomers codes	m.p (°C)	Yield %
	<b>Ma</b>	268—270	80
	<b>Mb</b>	276—278	94
	<b>Mc</b>	273—275	94
	<b>Md</b>	215—218	80
	<b>Me</b>	229—232	89
	<b>Mf</b>	287—290	90

## 5.2. Characterization of the synthesized monomers

### 5.2.1. FTIR spectra of synthesized monomers

The FTIR spectroscopic technique was used to identify the chemical structures of the intermediate dicyano compound (**Ia**) and the dicarboxylic acid monomer (**Ma**). **Table 5-2** shows all the FTIR data for synthesized intermediates and their monomers.



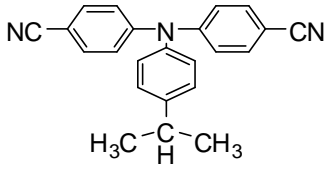

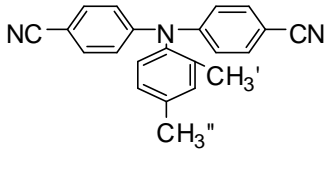
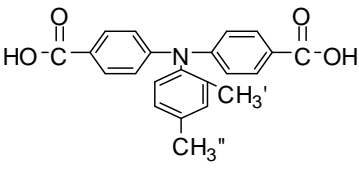
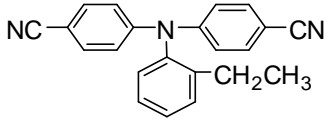
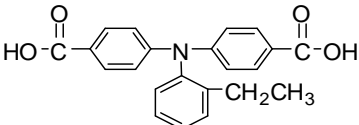
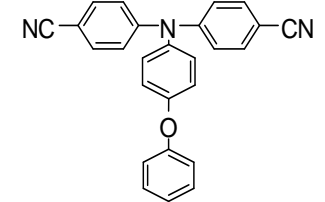
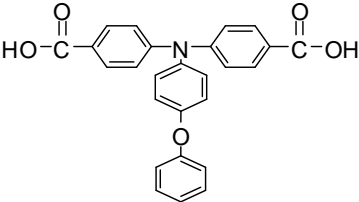
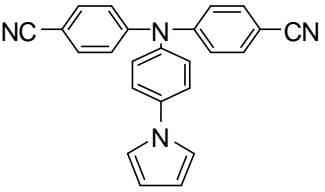
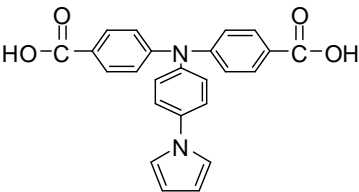
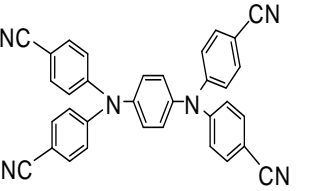
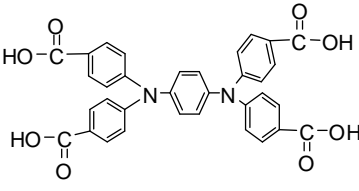
**Figure 5-2:** FTIR spectra of compound **Ma** (a) before and (b) after hydrolysis

The FTIR spectra of compound **Ia** gave a cyano group characteristic band at 2221 cm<sup>-1</sup> (C≡N stretching) as shown in **Figure 5-3** (a). After hydrolysis, the cyano group absorption peak disappeared, and the carboxylic acid group showed a typical carbonyl absorption



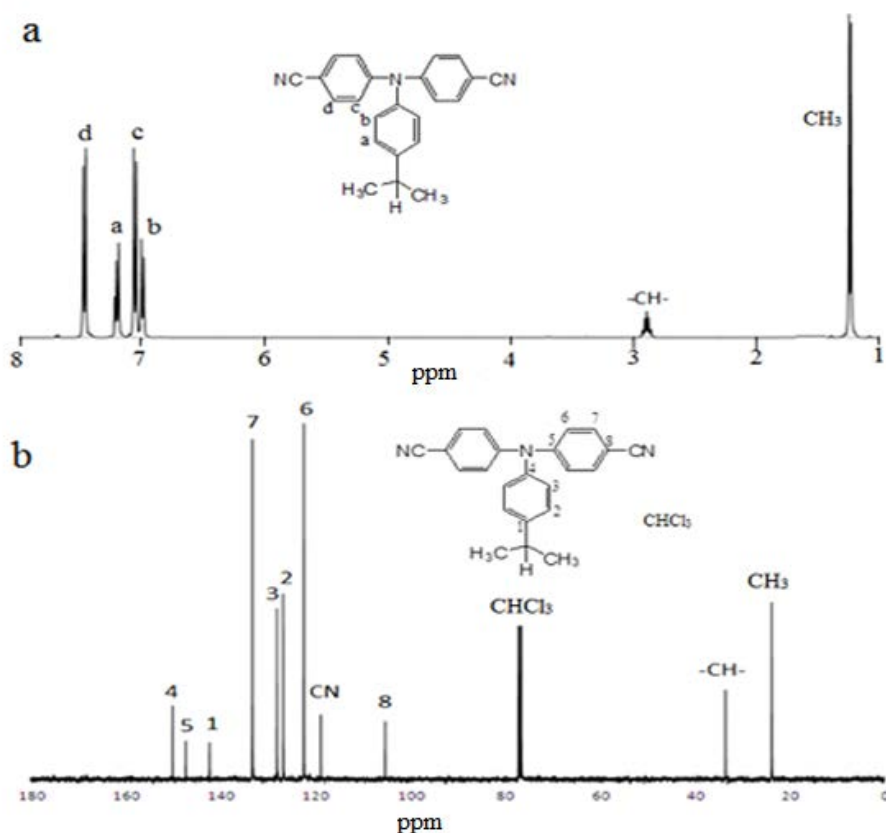
band at  $1678\text{ cm}^{-1}$  (C=O stretching) together with the appearance of broad bands around  $2700\text{--}3400\text{ cm}^{-1}$  (O-H stretching) (**Figure 5-3 (b)**).

**Table 5-2:** FTIR data of the intermediates and its monomers

I- structure	I	$\nu_{\text{CN}}$	M- structure	M	$\nu_{\text{OH}}$	$\nu_{\text{CO}}$
	<b>Ia</b>	2211		<b>Ma</b>	2981	1681
	<b>Ib</b>	2222		<b>Mb</b>	2710 to 3321	1683
	<b>Ic</b>	2219		<b>Mc</b>	2855	1680
	<b>Id</b>	2213		<b>Md</b>	3370	1670
	<b>Ie</b>	2219		<b>Me</b>	2700 to 3300	1681
	<b>If</b>	2222		<b>Mf</b>	3378	1682

### 5.2.2. NMR spectrum of synthesized monomers

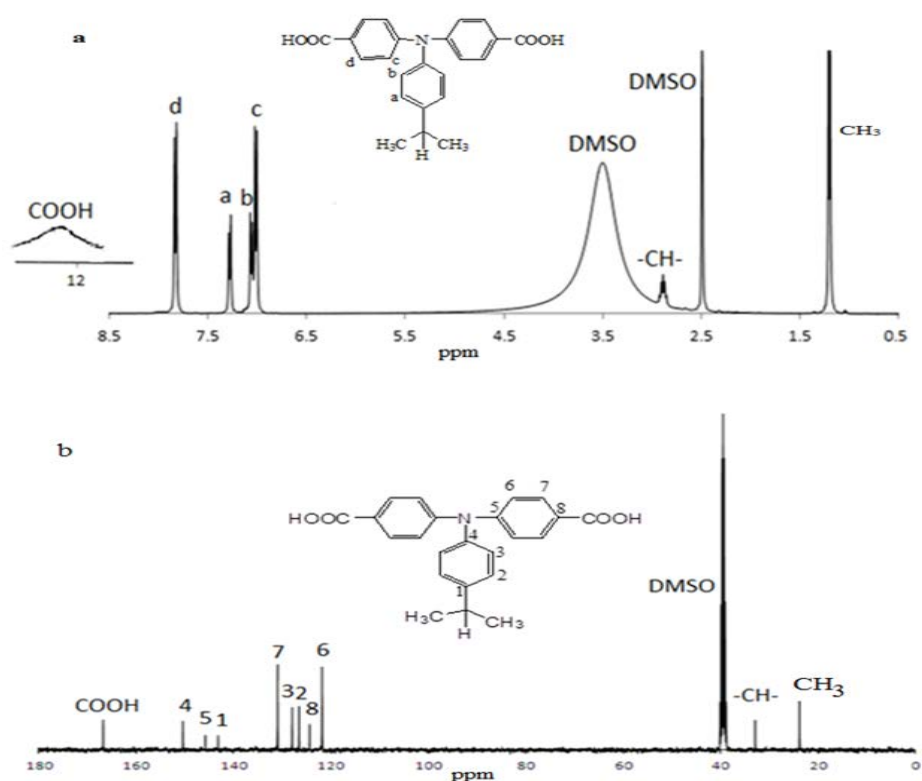
Structures of compounds (**Ia**) and (**Ma**) were also confirmed by high-resolution NMR spectra. In  $^1\text{H}$ -NMR spectrum as shown in **Figure 5-4** (a), intense doublet peaks, at 7.44-7.49 (d, 4H,  $\text{H}_d$ ) and 7.05-7.07 (d, 4H,  $\text{H}_c$ ) were obtained due to four phenylene protons (d) and (c) respectively which appeared together with a doublet peak at 7.19 - 7.23 (d, 2H,  $\text{H}_a$ ) due to two protons of (a) and another doublet peak at 6.99 - 7.01 (d, 2H,  $\text{H}_b$ ) for two protons of (b). A multiplet peak of one proton is assigned to CH at 2.84 - 2.94 (m, 1H,  $\text{H}_{\text{CH}}$ ) and a doublet peak of six protons of the two methyl groups ( $2\text{CH}_3$ ) at 1.20 - 1.28 (d, 6H,  $\text{H}_{\text{CH}_3}$ ). The  $^{13}\text{C}$  NMR spectra as shown in **Figure 5-4** (b) confirmed that the chemical shifting of C-atoms and that the cyano groups were completely converted into the carboxylic acid groups by the disappearance of the resonance peak for the cyano carbon at 118.92 ppm and by the appearance of the carboxylic peak at 166.8 ppm.



**Figure 5-3:** NMR spectrum of compound **Ia** and its molecular structure (a)  $^1\text{H}$  and (b)  $^{13}\text{C}$

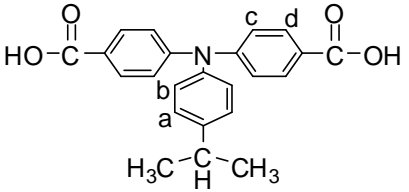
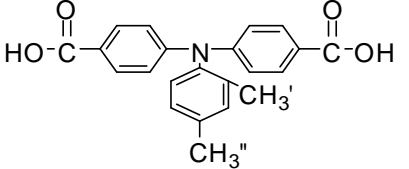
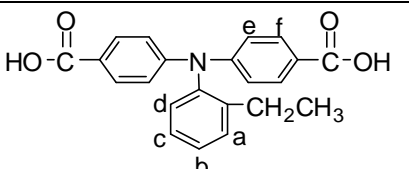
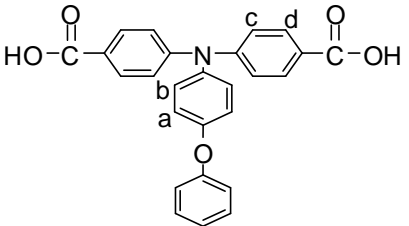
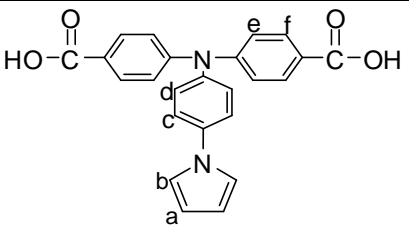
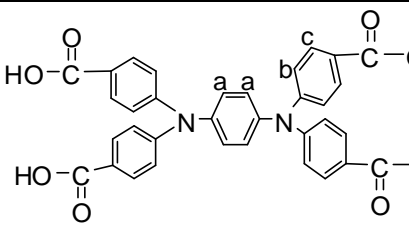
**Figure 5-5** (a) exhibits a very broad singlet peak due to the proton of carboxylic group which is hardly observable because of the replacement of hydrogen atoms of (COOH) by deuterium of DMSO solvent, and formation of H-bonding.

Other important evidence of this change is the shifting of the carbon resonance signals of C<sub>8</sub> adjacent to the cyano or carboxyl group. The C<sub>8</sub> of dinitrile (**Ia**) resonated at a higher field (105.4 ppm) than the other aromatic carbons because of the anisotropic shielding by the  $\pi$ -electrons of C $\equiv$ N. After hydrolysis, the resonance peak of C<sub>8</sub> shifted to a lower field (126.56 ppm) because of the lack of an anisotropic field (**Figure 5-5** (b)). Monomers (**Md** and **Me**) and their intermediates have the same NMR character peaks to **Ma** except they have different peaks assigned to the phenoxy and N-pyroll groups respectively. The triplet peaks 7.09-7.13 (t, 1H, H<sub>a</sub>), 7.31-7.35 (t, 2H, H<sub>b</sub>), and multiplet peak of 7.00-7.09 (m, 8H, H<sub>f,c,d</sub>) respectively are assigned to the a, b, c, d, f hydrogen atoms of the phenoxy ring in the **Id** intermediate and peaks 7.40-7.44 (t, 2H, H<sub>b</sub>), 7.19-7.50(m, 3H, H<sub>a,c</sub>) are due to a, b, c hydrogen atoms in the phenoxy ring of the **Md** monomer as shown in the **Table 5-3**.

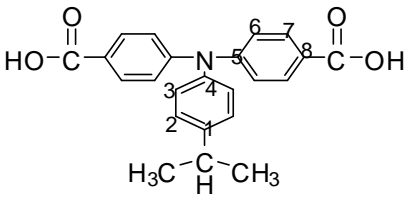
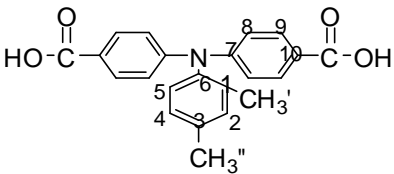
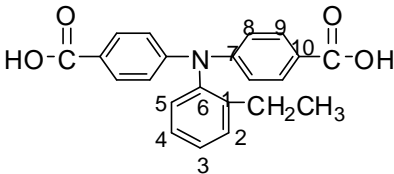
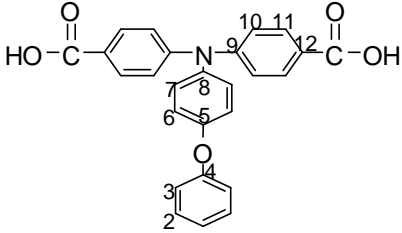
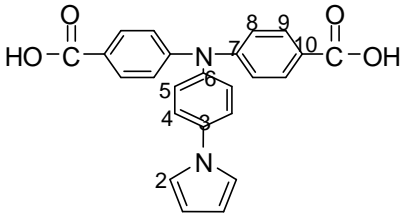
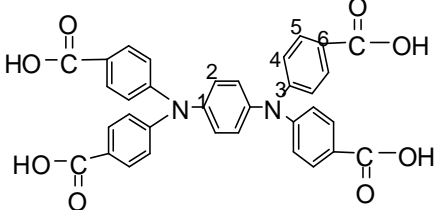


**Figure 5-4:** NMR spectrum of compound (Ma) and its molecular structure (a) <sup>1</sup>H and (b) <sup>13</sup>C

**Table 5-3:** <sup>1</sup>H NMR data of the synthesized monomers

Monomer structure	Code	( $\delta$ ) / ppm
	<b>Ma</b>	$H_a$ : 7.26-7.28 $H_b$ : 7.04-7.06 $H_c$ : 7.00-7.02 $H_d$ : 7.81-7.83 $H_{2COOH}$ : 12.62-12.78 $H_{CH}$ : 2.85-2.91 $H_{2CH_3}$ : 1.16-1.26
	<b>Mb</b>	$H_a$ : 7.80-7.84 $H_b$ : 6.92-6.98 $H_c$ : 6.98-7.05 $H_d$ : 7.12-7.17 $H_{CH_3'}$ : 1.16-1.26 $H_{CH_3''}$ : 2.06-2.12 $H_{2COOH}$ : 12.73-12.89
	<b>Mc</b>	$H_{a,b,c}$ : 7.31-7.42 $H_{e,d}$ : 7.07-7.17 $H_f$ : 7.75-7.88 $H_{CH_2}$ : 2.34-2.28 $H_{2COOH}$ : 12.68-12.84
	<b>Md</b>	$H_{a,c}$ : 7.19-7.50 $H_b$ : 7.40-7.44 $H_{e,d,f}$ : 7.01-7.07 $H_g$ : 7.82-7.89 $H_{2COOH}$ : 11.16-11.32
	<b>Me</b>	$H_a$ : 6.25-6.32 $H_b$ : 7.35-7.39 $H_c$ : 7.60-7.67 $H_d$ : 7.23-7.25 $H_e$ : 7.05-7.14 $H_f$ : 7.85-7.90 $H_{COOH}$ : 11.17-11.33
	<b>Mf</b>	$H_a$ : 6.50-6.54 $H_b$ : 7.00-7.08 $H_c$ : 7.87-7.94 $H_{COOH}$ : 12.15-12.31

**Table 5-4:**  $^{13}\text{C}$  NMR data of synthesized monomers

Monomer structure	Code	( $\delta$ ) / ppm
	<b>Ma</b>	143.22(C <sub>1</sub> ) 124.42(C <sub>2</sub> ) 128.01(C <sub>3</sub> ) 145.82(C <sub>4</sub> ) 150.44(C <sub>5</sub> ) 121.86(C <sub>6</sub> ) 130.97(C <sub>7</sub> ) 23.81(CH) 126.56(C <sub>8</sub> ) 23.81(CH <sub>3</sub> ) 166.83(COOH)
	<b>Mb</b>	131.11(C <sub>1</sub> ) 128.02(C <sub>6</sub> ) 129.00(C <sub>2</sub> ) 149.86(C <sub>7</sub> ) 143.47(C <sub>3</sub> ) 118.98(C <sub>8</sub> ) 122.04(C <sub>4</sub> ) 132.00(C <sub>9</sub> ) 120.29(C <sub>5</sub> ) 126.76(C <sub>10</sub> ) 33.15(C <sub>CH3'</sub> ) 23.99(C <sub>CH3''</sub> )
	<b>Mc</b>	131.20(C <sub>1</sub> ) 128.50(C <sub>2</sub> ) 128.34(C <sub>3</sub> ) 128.17(C <sub>4</sub> ) 131.03(C <sub>5</sub> ) 143.25(C <sub>6</sub> ) 150.86(C <sub>7</sub> ) 122.16(C <sub>8</sub> ) 132.18(C <sub>9</sub> ) 126.33(C <sub>10</sub> ) 3.23(C <sub>CH3</sub> ) 23.15(C <sub>CH3</sub> ) 166.81(C <sub>COOH</sub> )
	<b>Md</b>	145.322(C <sub>1</sub> ) 129.94(C <sub>2</sub> ) 118.78(C <sub>3</sub> ) 124.49(C <sub>4</sub> ) 140.52(C <sub>5</sub> ) 119.66(C <sub>6</sub> ) 128.41(C <sub>7</sub> ) 156.09(C <sub>8</sub> ) 155.09(C <sub>9</sub> ) 121.46(C <sub>10</sub> ) 123.60(C <sub>12</sub> ) 166.66(C <sub>COOH</sub> ) 130.77(C <sub>11</sub> )
	<b>Me</b>	110.64 (C <sub>1</sub> ) 118.99(C <sub>2</sub> ) 137.25(C <sub>3</sub> ) 120.91(C <sub>4</sub> ) 127.77(C <sub>5</sub> ) 142.59(C <sub>6</sub> ) 150.25(C <sub>7</sub> ) 122.02(C <sub>8</sub> ) 131.05(C <sub>9</sub> ) 124.65(C <sub>10</sub> ) 166.85(C <sub>COOH</sub> )
	<b>Mf</b>	134.78(C <sub>1</sub> ) 137.14(C <sub>2</sub> ) 158.34(C <sub>3</sub> ) 118.12(C <sub>4</sub> ) 133.04(C <sub>5</sub> ) 123.30(C <sub>6</sub> ) 166.78(C <sub>COOH</sub> )

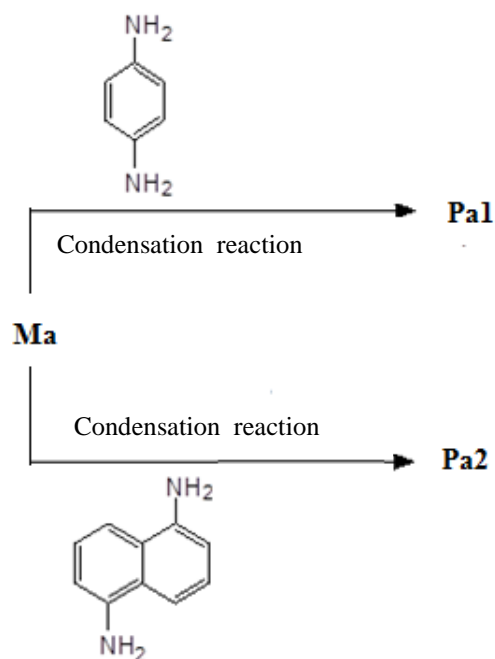
With reference to **Ie** and **Me** compounds which have N-pyrrole ring, the hydrogen peaks in **Ie** compound are triplet and doublet peaks 6.29 (t, 2H, H<sub>a</sub>), 7.33 (d, 2H, H<sub>b</sub>) respectively because of a and b hydrogen atoms of pyrrole ring. After converting of **Ie** intermediate to

its monomer, the peaks of a and b H- atoms are 6.29 (t, 2H, H<sub>a</sub>), and 7.64 (t, 2H, H<sub>b</sub>) respectively.

### 5.3. Poly(amine amide)s synthesis

As mentioned earlier, the most common methods for the preparation of aromatic polyamides are the reaction of diacid chlorides with diamines at low temperatures or direct condensation reactions in solution of aromatic diacids with diamines at high temperatures. The solvents used are polar aprotic solvents and salts are often used as solubility promoters because the cations interact with the amide groups to decrease the strength of the interchain hydrogen bonds. Triphenylphosphite (TPP) and pyridine are also used as condensing agents to promote condensation reaction.

**Table 5-5** shows the codes of the synthesized poly(amine amide)s in this study. A series of new aromatic poly(amine amide)s with aryltriphenylamine (ATPA) units were prepared by the direct polycondensation reactions of the dicarboxylic acid monomers with various aromatic diamines (p-phenylenediamine, 1,5-diaminenaphthalene) using triphenylphosphite (TPP) where pyridine and CaCl<sub>2</sub> act as condensing agents as mentioned in the Experimental (**Figure 4-5**). All the polymerizations proceeded homogeneously throughout the reaction and afforded clear, highly viscous polymer solutions. These polymers precipitated in a tough, fiber-like form when the resulting polymer solutions were slowly poured out into methanol with stirring.



**Figure 5-5:** Synthetic routes of poly(amine-amide)s (**Pa1** and **Pa2**)

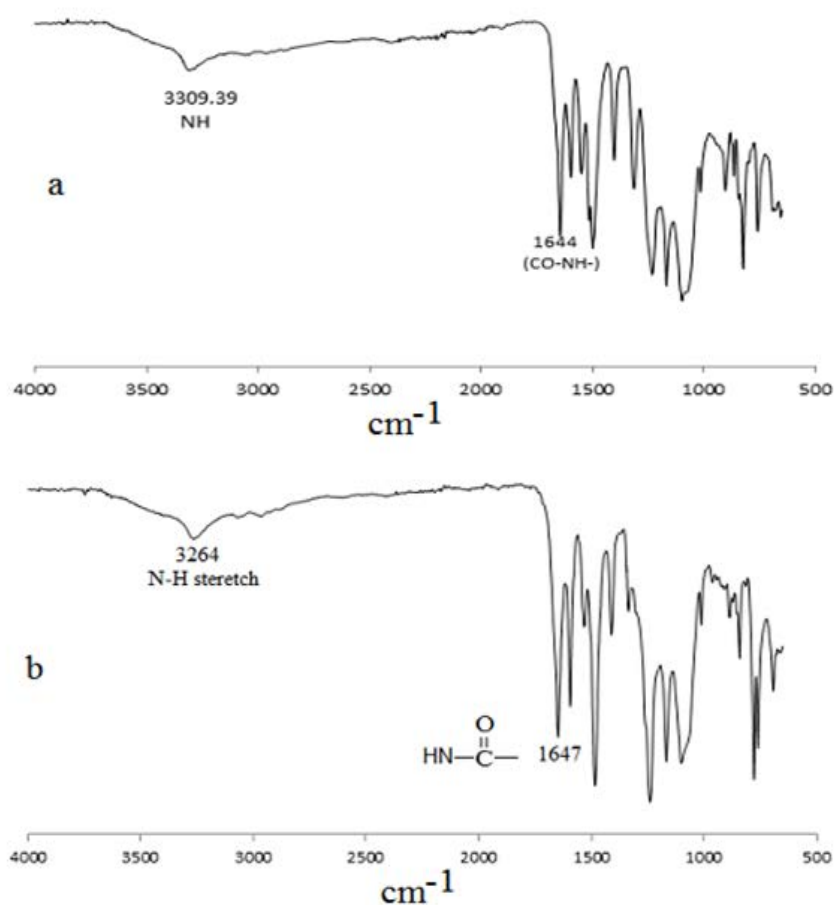
These poly(amine amide)s were obtained in almost quantitative yields (55 - 60)% with the inherent viscosity  $\eta_{inh}$  values in the range of 0.42 - 0.81 dL/g as shown in **Table 5-5**. All the polymers can be solution-cast into flexible and tough films.

**Table 5-5:** Synthesized poly(amine amide) codes

monomer code	diamine code	polymer code	viscosity (dL/g)	diamine code	polymer code	viscosity (dL/g)
<b>Ma</b>	1	<b>Pa1</b>	0.62	2	<b>Pa2</b>	0.75
<b>Mb</b>	1	<b>Pb1</b>	0.66	2	<b>Pb2</b>	0.67
<b>Mc</b>	1	<b>Pc1</b>	0.63	2	<b>Pc2</b>	0.81
<b>Md</b>	1	<b>Pd1</b>	0.42	2	<b>Pd2</b>	0.65
<b>Me</b>	1	<b>Pe1</b>	0.46	2	<b>Pe2</b>	0.48
<b>Mf</b>	1	<b>Pf1</b>	0.43	2	<b>Pf2</b>	0.48

### 5.3.1. FTIR spectra of synthesized poly(amine amide)s

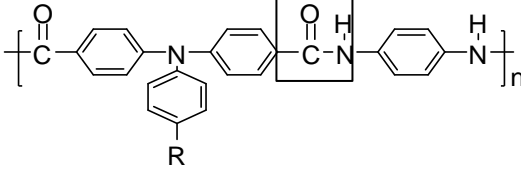
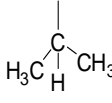
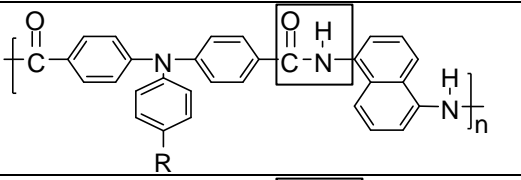
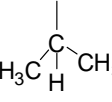
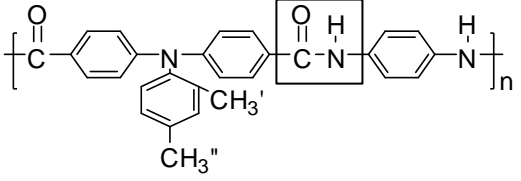
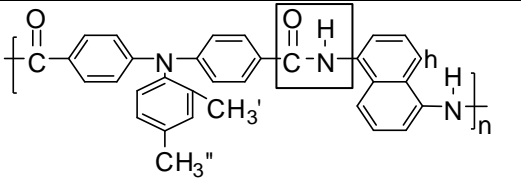
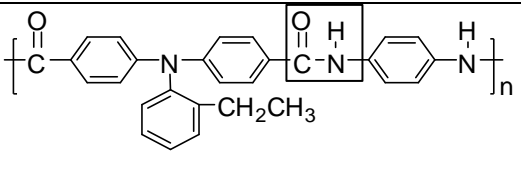
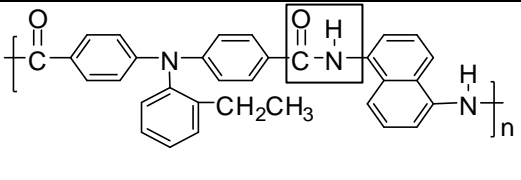
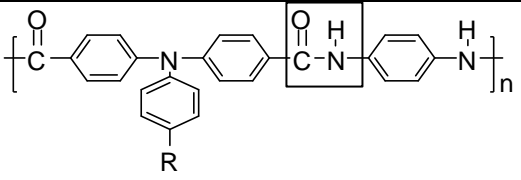
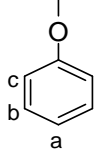
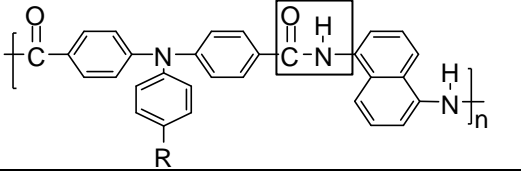
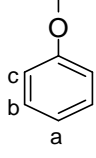
Structural features of these poly(amine-amide)s were verified by FTIR spectra based on characteristic absorption bands observed around 3309 (N-H stretching) and 1644  $\text{cm}^{-1}$  (C=O stretching of amide group) for polymer, **Pa1**. **Figure 5-7** (a) and (b) illustrate a typical FTIR spectra of the representative poly(amine amide)s **Pa1** and **Pa2** respectively. **Table 5-6** shows FTIR data of the synthesized poly(amine amide)s.



**Figure 5-7:** FTIR spectra of the representative poly(amine amide) (a) **Pa1** and (b) **Pa2**



**Table 5-6:** FTIR data of the Poly(amine amide)s

Poly(amine amide) structure	Code	R	NH-stretch (cm <sup>-1</sup> )	CO-stretch (cm <sup>-1</sup> )
	<b>Pa1</b>		3309	1644
	<b>Pa2</b>		3264	1647
	<b>Pb1</b>	-	3302	1647
	<b>Pb2</b>	-	3268	1647
	<b>Pc1</b>	-	3319	1648
	<b>Pc2</b>	-	3263	1648
	<b>Pd1</b>		3376	1649
	<b>Pd2</b>		3372	1647

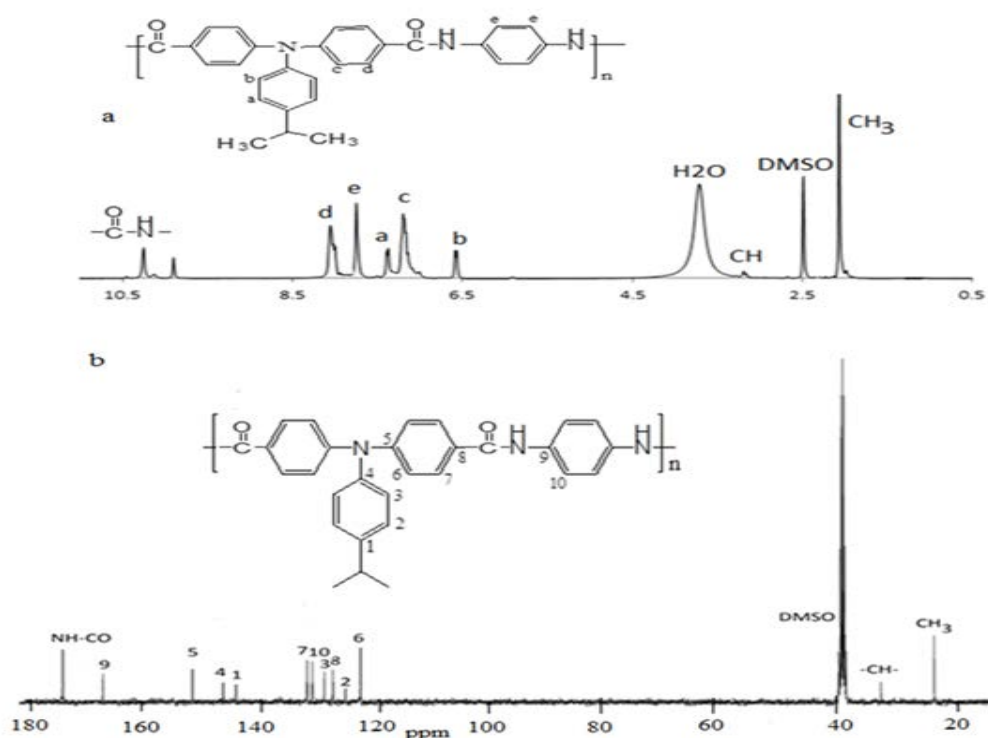
	<b>Pe1</b>		3262	1647
	<b>Pe2</b>		3254	1647
	<b>Pf1</b>	-	3264	1647
	<b>Pf2</b>	-	3264	1647

### 5.3.2. NMR spectra of the synthesized poly(amine amide)s

$^1\text{H}$  and  $^{13}\text{C}$  NMR techniques were used to characterize the synthesized polyamides in  $\text{DMSO-d}_6$ . Assignments of each proton and the spectra agree well with the proposed molecular structure of polyamides as shown in the **Figures 5-8** (a,b), **5.9** (a,b) and **5-10** (a,b).

In  $^1\text{H}$  NMR spectrum, the broad proton peaks of the dicarboxylic monomer groups located at 12.62 - 12.78 ppm were completely absent after polymerization. Meanwhile, there is an appearance of singlet peak at a higher field region at 10.20 - 10.26 ppm and 10.38 - 10.46 ppm which is ascribed to the amide group  $-\overset{\text{O}}{\parallel}{\text{C}}-\text{NH}-$  proton of the resultant poly(amine amide)s **Pa1** and **Pa2** respectively. The doublet peaks in the regions of 7.18 - 7.23 ppm and 8.00 - 8.08 ppm are assigned to the four protons c and d in the triphenyl amine group respectively. The signals in the region of 7.70 - 7.80 ppm are attributed to four equivalent

protons e of the phenylene diamine group. As for **Pa2**, two doublet peaks at 7.29 - 7.27 ppm attributed to protons e and g was observed together with triplet peak signal at 7.45 - 7.56 ppm assigned to the two protons f in naphthalene segment. The signals 7.34 - 7.33 ppm and 6.54 - 6.63 ppm of the two doublet peaks are assigned to the protons in the positions a and b respectively. Finally, the doublet peak of the six protons of two methyl groups at 2.03 - 2.10 ppm and multiplet peak of CH group appears in the region (3.15-3.23 ppm) as shown in **Figures 5-8 (a) and 5-9 (a)**.

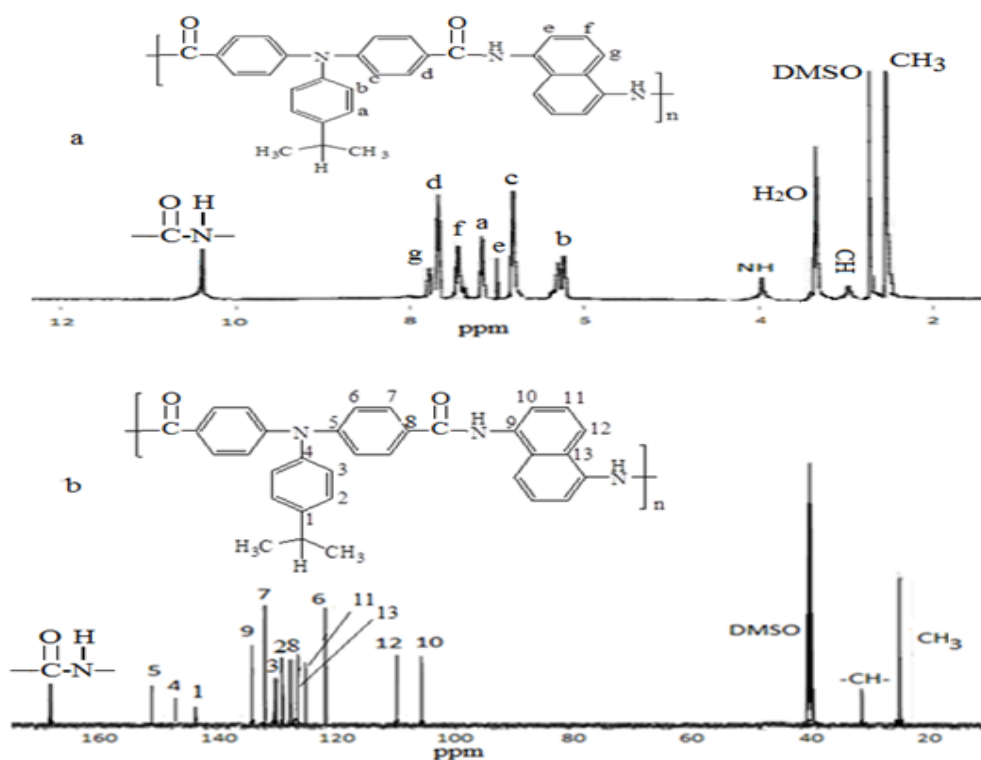


**Figure 5-8:** NMR-spectrum of poly(amine amide), **Pa1**, in DMSO- $d_6$  (a)  $^1H$  and (b)  $^{13}C$

**Figures 5-8 (b) and 5-9 (b)** show the  $^{13}C$  NMR spectra of **Pa1** and **Pa2** respectively. The main peak at the most downfield region at 166.74 ppm is due to the carbon atom in the amide carbonyl group of the polyamide. These carbon atoms have higher chemical shifting because of the  $sp^2$  resonance between carbonyl group attached to a highly electronegative nitrogen atom. The first ring of the TPA exhibited  $^{13}C$  NMR peaks, assigned to carbon atoms 1, 2, 3, and 4 at the regions 143.22, 124.12, 128.23 and 145.82 ppm respectively. The second ring have four peaks of carbon atoms at the regions 150.44, 121.76, 130.97 and

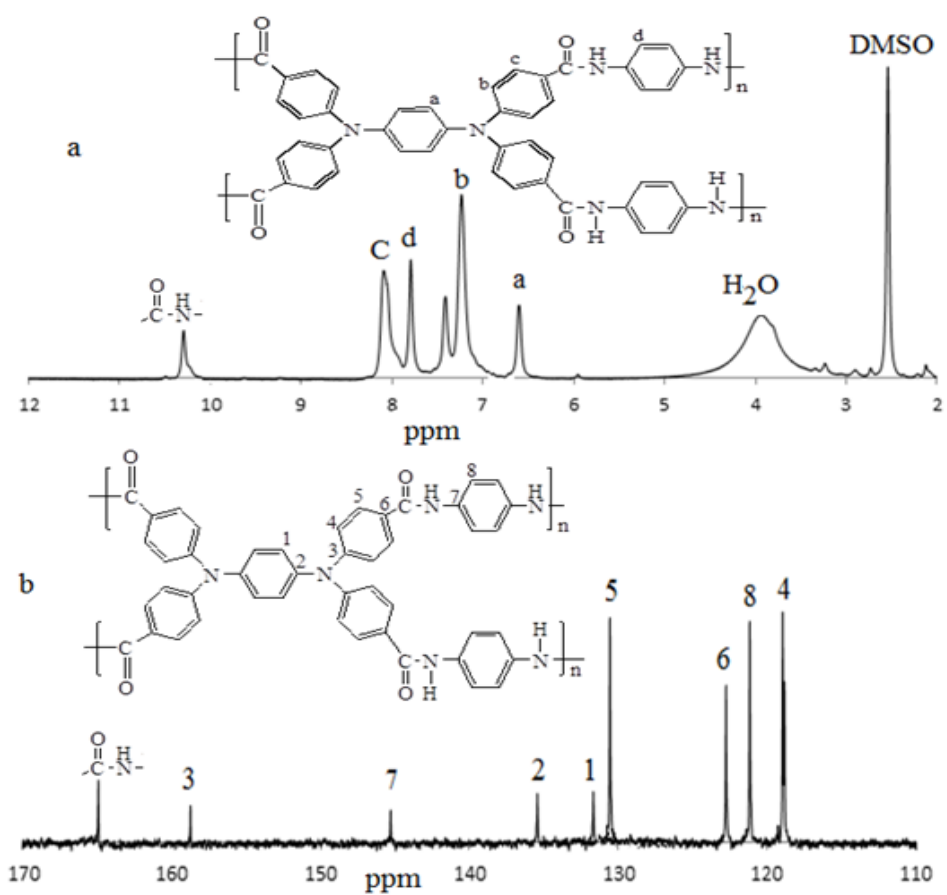
126.12 ppm. The C<sub>9</sub> atom has a peak at the region 131.83 ppm and four equivalents C<sub>10</sub> atoms have a signal at 120.02 ppm. New peaks in **Pa2** are assigned to C<sub>9</sub> at 131.76 ppm and atoms 104.24 (C<sub>10</sub>), 125.98 (C<sub>13</sub>), 110.77 (C<sub>12</sub>) and 125.68 (C<sub>11</sub>) in the naphthalene segment.

Poly(amine amide)s **Pb1**, **Pb2**, **Pc1**, and **Pc2** have same NMR characters except peaks of groups on the ring of triphenylamine. In **Pb1** and **Pb2** <sup>1</sup>H NMR spectra there are two singlet peaks of protons of methyl groups CH<sub>3</sub>' and CH<sub>3</sub>'' at regions 1.16 - 1.26 ppm and 1.92 - 2.02 ppm respectively. Peaks at 23.65 ppm and 33.07 ppm are the signals of <sup>13</sup>C NMR peaks assigned to the same methyl groups. With respect to **Pc1** and **Pc2**, there are two <sup>1</sup>H NMR peaks assigned to CH<sub>2</sub> protons of ethyl group with a tetra peak at chemical shift of 2.01 - 2.11 ppm and <sup>13</sup>C NMR peak signal at 26.45 ppm. CH<sub>3</sub> protons have triplet peak at 0.88 - 0.95 ppm in <sup>1</sup>H NMR and in <sup>13</sup>C NMR peak appeared at region 13.43 ppm. New peaks in **Pd1** and **Pd2** are due to phenylene protons of phenoxy group which have two doublet peaks, one of H<sub>c</sub> at the region 6.92 - 6.99 ppm and other of H<sub>b</sub> at signal 7.14 - 7.22 ppm. The last peak is a triplet peak of H<sub>a</sub> at 7.37 - 7.45 ppm. Phenoxy group in **Pa1** and **Pa2** have three <sup>13</sup>C NMR peaks of carbons numbered C<sub>1</sub>, C<sub>2</sub> and C<sub>3</sub> with chemical shifts of 124.57, 128.77 and 120.00 ppm respectively. <sup>1</sup>H NMR peaks of pyrrole group in **Pe2** are singlet peak of proton (a) at signal 6.24 - 6.43 ppm and peak assigned to proton (b) peak mixed with multiplet peaks b, g, c at region 7.73 - 7.62 ppm. Two <sup>13</sup>C NMR peaks assigned to C<sub>1</sub> and C<sub>2</sub> at signal 110.49 ppm and 118.42 ppm respectively.

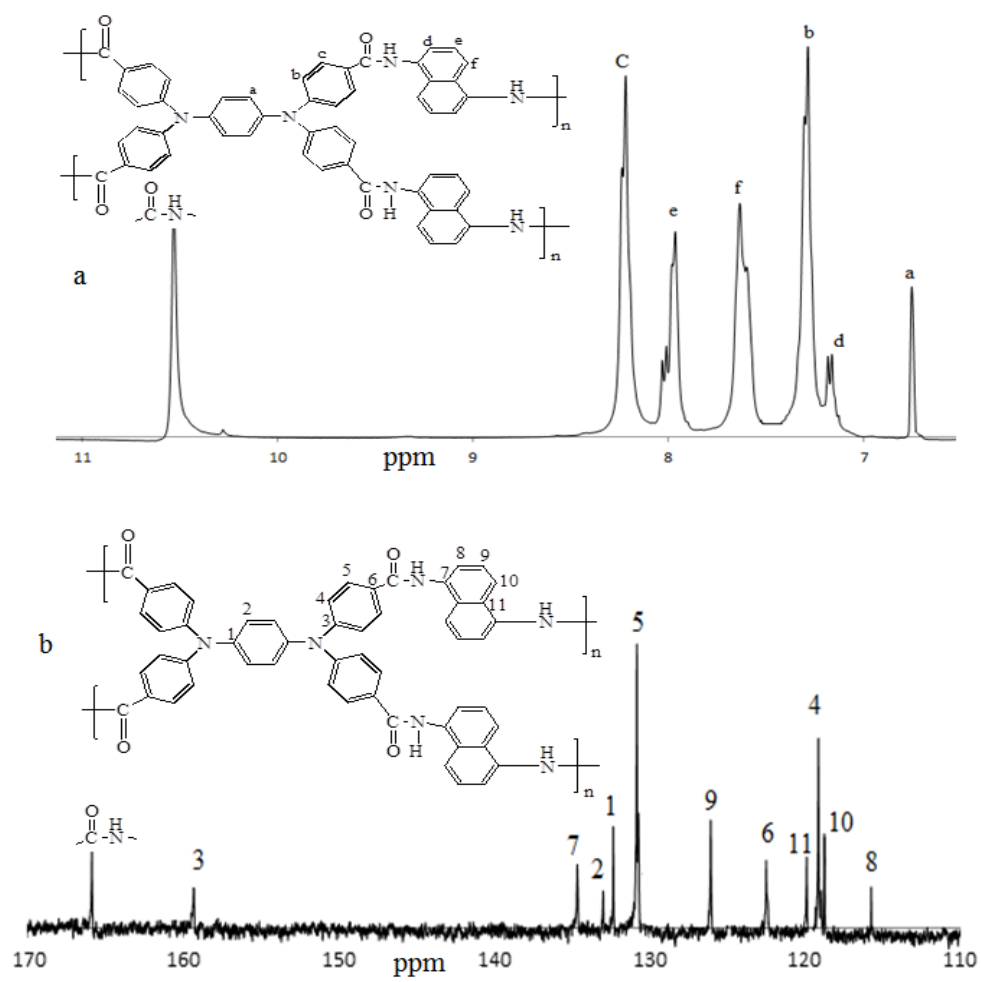


**Figure 5-9:** NMR-spectra of synthesized poly(amine amide) (**Pa2**) in DMSO- $d_6$ ; (a)  $^1H$  and (b)  $^{13}C$

Finally,  $^1H$  NMR peaks of **Pf1**, **Pf2** are singlet peaks assigned to 4 protons in position (a) in region 6.55 - 6.67 ppm and two doublet peaks attributed to 8 protons at region 7.24 - 7.42 ppm of H<sub>b</sub> and 8 protons at region 8.04 - 8.16 ppm of H<sub>c</sub>. Another singlet peak is assigned to 8 protons in position (d) at region 7.74-7.84 ppm as shown in **Figure 5-10**. On the other hand, new peaks in the naphthalene segment of **Pf2** are observed as doublet peak at 7.18-7.16 ppm of H<sub>d</sub> and triplet peak at 8.12-7.84 ppm of H<sub>e</sub>. Another doublet peak at region 7.63-7.59 ppm is assigned to H<sub>f</sub>.  $^{13}C$  NMR peaks in the naphthalene segment of **Pf2** are 134.62 ppm (C<sub>7</sub>), 115.67 ppm (C<sub>8</sub>), 126.02 ppm (C<sub>9</sub>), 118.69 ppm (C<sub>10</sub>) and 119.60 ppm (C<sub>11</sub>) as shown in **Figure 5-11** (a), (b).



**Figure 5-10** NMR-spectra of synthesized poly(amine amide) (**Pf1**) in DMSO- $d_6$ ; (a)  $^1H$  and (b)  $^{13}C$



**Figure 5-11:** NMR-spectra of synthesized poly(amine amide) (**Pf2**) in DMSO-d<sub>6</sub>: (a) <sup>1</sup>H and (b) <sup>13</sup>C

**Table 5-7:** <sup>1</sup>H NMR data of Synthesized Poly(amine amide)s

Poly(amine amide)s structure	code	R	<sup>1</sup> H NMR shift (δ) ppm
	<b>Pa1</b>		NH:10.20–10.26 H <sub>a</sub> : 7.34-7.33 H <sub>b</sub> : 6.54-6.63 H <sub>c</sub> : 7.18-7.23 H <sub>d</sub> : 8.00-8.08 H <sub>e</sub> : 7.70-7.80 H <sub>CH</sub> : 3.15-3.23 H <sub>CH3</sub> : 2.03-2.10
	<b>Pa2</b>		NH:10.38-10.44 H <sub>e</sub> : 7.29-7.27 H <sub>a</sub> : 7.35-7.40 H <sub>f</sub> : 7.45-7.56 H <sub>b</sub> : 7.03-7.01 H <sub>g</sub> : 7.99-7.97 H <sub>c</sub> : 7.15-7.13 H <sub>CH</sub> : 1.92-1.84 H <sub>d</sub> : 7.84-7.82 H <sub>CH3</sub> : 1.21-1.19
	<b>Pb1</b>	-	NH:10.23-10.31 H <sub>a,b,d</sub> : 7.17-7.23 H <sub>c</sub> : 6.74-6.56 H <sub>e</sub> : 8.05-7.90 H <sub>f</sub> : 7.68-7.82 H <sub>CH3</sub> : 1.92-2.02 H <sub>CH3</sub> : 1.16-1.26
	<b>Pb2</b>	-	NH:10.41-10.50 H <sub>e,h</sub> : 8.07-8.21 H <sub>a,b,d</sub> : 7.20-7.06 H <sub>c</sub> : 6.68-6.64 H <sub>f</sub> : 7.55-7.24 H <sub>g</sub> : 7.94-7.88
	<b>Pc1</b>	-	NH:10.20-10.26 H <sub>g,c</sub> : 7.40-7.34 H <sub>f,a</sub> : 7.98-7.83 H <sub>CH2</sub> : 2.01-2.11 H <sub>b,e,d</sub> : 7.13-6.73 H <sub>CH3</sub> : 0.88-0.95
	<b>Pc2</b>	-	NH:10.38-10.48 H <sub>g,c</sub> : 7.64-7.50 H <sub>f,a,i</sub> : 8.12-8.08 H <sub>e,d</sub> : 7.19-7.00 H <sub>b</sub> : 6.66-6.64 H <sub>h</sub> : 7.88-7.86
	<b>Pd1</b>		NH:10.19-10.09 H <sub>g</sub> : 7.86-7.98 H <sub>c,d,e,f</sub> : 7.02-7.14 H <sub>h</sub> : 7.14-7.22 H <sub>a</sub> : 7.37-7.45 H <sub>h</sub> : 7.67-7.77
	<b>Pd2</b>		NH:10.34-10.44 H <sub>h,f,e</sub> : 7.26-7.17 H <sub>a,c</sub> : 7.34-7.33 H <sub>g,i</sub> : 8.10-8.07 H <sub>b</sub> : 7.61-7.56 H <sub>j</sub> : 7.93-7.91 H <sub>d</sub> : 7.11-7.09
	<b>Pe1</b>		NH:10.18-10.30 H <sub>d</sub> : 7.32-7.40 H <sub>a</sub> : 6.24-6.43 H <sub>e</sub> : 7.11-7.24 H <sub>g,c,b</sub> : 7.73-7.62 H <sub>f</sub> : 7.93-8.05
	<b>Pe2</b>		NH:10.40-10.49 H <sub>d,e,g</sub> : 7.39-7.22 H <sub>a</sub> : 6.25-6.34 H <sub>f,i</sub> : 8.12-7.94 H <sub>b,c,h</sub> : 7.69-7.65



	<b>Pf1</b>	-	NH: 10.25-10.36    H <sub>c</sub> : 8.04-8.16 H <sub>a</sub> : 7.34-7.33    H <sub>d</sub> : 7.74-7.84 H <sub>b</sub> : 7.42-7.24
	<b>Pf2</b>	-	NH: 10.20-10.26    H <sub>d</sub> : 7.18-7.12 H <sub>a</sub> : 6.70-6.77    H <sub>e</sub> : 8.12-7.88 H <sub>b</sub> : 7.18-7.38    H <sub>f</sub> : 7.73-7.59 H <sub>c</sub> : 8.23-8.21

**Table 5-8:** <sup>13</sup>C NMR data of synthesized poly(amine amide)s

Poly(amine-amide)s structure	code	R	<sup>13</sup> C NMR shift (δ) ppm
	<b>Pa1</b>		C=O : 166.74 C <sub>1</sub> :143.22    C <sub>2</sub> :124.12    C <sub>3</sub> :128.23 C <sub>4</sub> :145.82 C <sub>5</sub> :150.44    C <sub>6</sub> :121.76    C <sub>7</sub> :130.97 C <sub>8</sub> :126.12 C <sub>9</sub> :131.83    C <sub>10</sub> :120.02    C <sub>CH</sub> :32.91 C <sub>CH3</sub> :23.81
	<b>Pa2</b>		C=O : 166.56 C <sub>1</sub> :131.21    C <sub>2</sub> :129.04 C <sub>3</sub> :142.89    C <sub>4</sub> :123.17 C <sub>5</sub> :150.47    C <sub>6</sub> :121.86    C <sub>7</sub> :130.36 C <sub>8</sub> :126.11 C <sub>9</sub> :131.76    C <sub>10</sub> :104.24    C <sub>11</sub> :125.68 C <sub>12</sub> :110.77 C <sub>13</sub> :125.98    C <sub>CH</sub> :32.82    C <sub>CH3</sub> :23.87
	<b>Pb1</b>	-	C=O : 166.89 C <sub>1</sub> :143.22    C <sub>2</sub> :121.76    C <sub>3</sub> :124.12 C <sub>4</sub> :130.97 C <sub>5</sub> :120.17    C <sub>6</sub> :128.34    C <sub>7</sub> :149.97 C <sub>8</sub> :118.12 C <sub>9</sub> :131.91    C <sub>10</sub> :126.45    C <sub>11</sub> :125.22 C <sub>12</sub> :117.23 C <sub>CH3</sub> :23.24    C <sub>CH3</sub> ':33.45
	<b>Pb2</b>	-	C=O :166.86    C <sub>1</sub> :131.12    C <sub>2</sub> :130.76 C <sub>3</sub> :143.73    C <sub>4</sub> :122.57    C <sub>5</sub> :121.82 C <sub>6</sub> :128.58    C <sub>7</sub> :150.54    C <sub>8</sub> :118.82 C <sub>9</sub> :131.75    C <sub>10</sub> :126.67    C <sub>11</sub> :132.71 C <sub>12</sub> :107.63    C <sub>13</sub> :124.77    C <sub>14</sub> :110.23 C <sub>15</sub> :125.87    C <sub>CH3</sub> :23.65    C <sub>CH3</sub> ':33.07
	<b>Pc1</b>	-	-C=O: 166.82    C <sub>1</sub> :131.20    C <sub>2</sub> :129.17 C <sub>3</sub> :128.89    C <sub>4</sub> :127.16    C <sub>5</sub> :131.03 C <sub>6</sub> :142.89 C <sub>7</sub> :150.12    C <sub>8</sub> :122.23    C <sub>9</sub> :131.91 C <sub>10</sub> :126.12 C <sub>11</sub> :125.32    C <sub>12</sub> :121.18 C <sub>CH2</sub> :26.45    C <sub>CH3</sub> :13.43

	<b>Pc2</b>	-	-C=O : 165.92 C <sub>1</sub> :131.85 C <sub>2</sub> :131.12 C <sub>3</sub> :130.76 C <sub>4</sub> :128.58 C <sub>5</sub> :132.05 C <sub>6</sub> :142.56 C <sub>7</sub> :150.24 C <sub>8</sub> :118.57 C <sub>9</sub> :130.86 C <sub>10</sub> :126.56 C <sub>11</sub> :131.24 C <sub>12</sub> :106.81 C <sub>13</sub> :121.77 C <sub>14</sub> :110.32 C <sub>15</sub> :124.06 C <sub>CH2</sub> :26.43 C <sub>CH3</sub> :13.63
	<b>Pd2</b>		-C=O : 165.63 C <sub>1</sub> :124.23 C <sub>2</sub> :128.30 C <sub>3</sub> :120.07 C <sub>4</sub> :156.54 C <sub>5</sub> :149.71 C <sub>6</sub> :118.88 C <sub>7</sub> :129.57 C <sub>8</sub> :141.25 C <sub>9</sub> :150.59 C <sub>10</sub> :121.94 C <sub>11</sub> :130.21 C <sub>12</sub> :123.77 C <sub>13</sub> :123.77 C <sub>14</sub> :107.87 C <sub>15</sub> :125.49 C <sub>16</sub> :111.82 C <sub>17</sub> :120.77
	<b>Pe1</b>		-C=O : 164.68 C <sub>1</sub> :110.49 C <sub>2</sub> :118.42 C <sub>3</sub> :138.12 C <sub>4</sub> :118.09 C <sub>5</sub> :127.16 C <sub>6</sub> :143.11 C <sub>7</sub> :150.05 C <sub>8</sub> :122.34 C <sub>9</sub> :130.06 C <sub>10</sub> :124.18 C <sub>11</sub> :134.75 C <sub>12</sub> :120.60
	<b>Pe2</b>		C=O : 166.06 C <sub>1</sub> :108.21 C <sub>2</sub> :122.77 C <sub>3</sub> :134.85 C <sub>4</sub> :121.12 C <sub>5</sub> :124.56 C <sub>6</sub> :143.59 C <sub>7</sub> :150.08 C <sub>8</sub> :119.57 C <sub>9</sub> :130.13 C <sub>10</sub> :128.84 C <sub>11</sub> :137.45 C <sub>12</sub> :103.34 C <sub>13</sub> :127.74 C <sub>14</sub> :111.23 C <sub>15</sub> :119.14
	<b>Pf1</b>	-	C=O : 164.94 C <sub>1</sub> :131.35 C <sub>2</sub> :135.43 C <sub>3</sub> :158.75 C <sub>4</sub> :118.93 C <sub>5</sub> :130.52 C <sub>6</sub> :122.74 C <sub>7</sub> :145.26 C <sub>8</sub> :121.15
	<b>Pf2</b>	-	C=O : 165.90 C <sub>1</sub> :131.80 C <sub>2</sub> :132.30 C <sub>3</sub> :159.34 C <sub>4</sub> :119.09 C <sub>5</sub> :130.78 C <sub>6</sub> :122.45 C <sub>7</sub> :134.62 C <sub>8</sub> :115.67 C <sub>9</sub> :126.02 C <sub>10</sub> :118.69 C <sub>11</sub> :119.60

## 5.4. Solubility

The qualitative solubility properties of the synthesized poly(amine-amide)s in several organic solvents at 10% (w/v) are summarized in Table 5-9. All the polymers exhibited excellent solubility in polar organic solvents NMP, DMF, DMSO and DMAc. The enhanced solubility can be attributed to the presence of the triarylamine unit.

Polymers **Pa2**, **Pb2**, **Pc2**, **Pd2**, **Pe2** and **Pf2**, have more solubility than others because the more bulky pendant naphthalene group chromophores in the repeating unit leads to the increase in free volume in the polymer chains that allow more solvent to come in. Furthermore, they are more flexible. The excellent solubility makes these polymers convenient to be processed to articles by spin-coating.

**Table 5-9:** Solubility of Aromatic Polyamides

Polymer Code	$\eta_{inh}^a$ (dL/g)	Solvents						
		NMP	DMAc	DMF	DMSO	m-Cresol	THF	CHCl <sub>3</sub>
<b>Pa1</b>	0.62	++	++	++	+	-	-	-
<b>Pb1</b>	0.66	++	++	++	++	-	-	-
<b>Pc1</b>	0.63	++	++	++	++	-	-	-
<b>Pd1</b>	0.42	++	++	++	++	-	-	-
<b>Pe1</b>	0.46	++	++	++	++	-	-	-
<b>Pf1</b>	0.43	++	++	++	++	-	-	-
<b>Pa2</b>	0.75	++	++	++	++	+	-	-
<b>Pb2</b>	0.67	++	++	++	++	+	-	-
<b>Pc2</b>	0.88	++	++	++	++	+	-	-
<b>Pd2</b>	0.65	++	++	++	++	+	-	-
<b>Pe2</b>	0.66	++	++	++	++	+	-	-
<b>Pf2</b>	0.71	++	++	++	+++	+	-	-

++: soluble at room temperature, +: soluble on heating, -: insoluble even on heating.

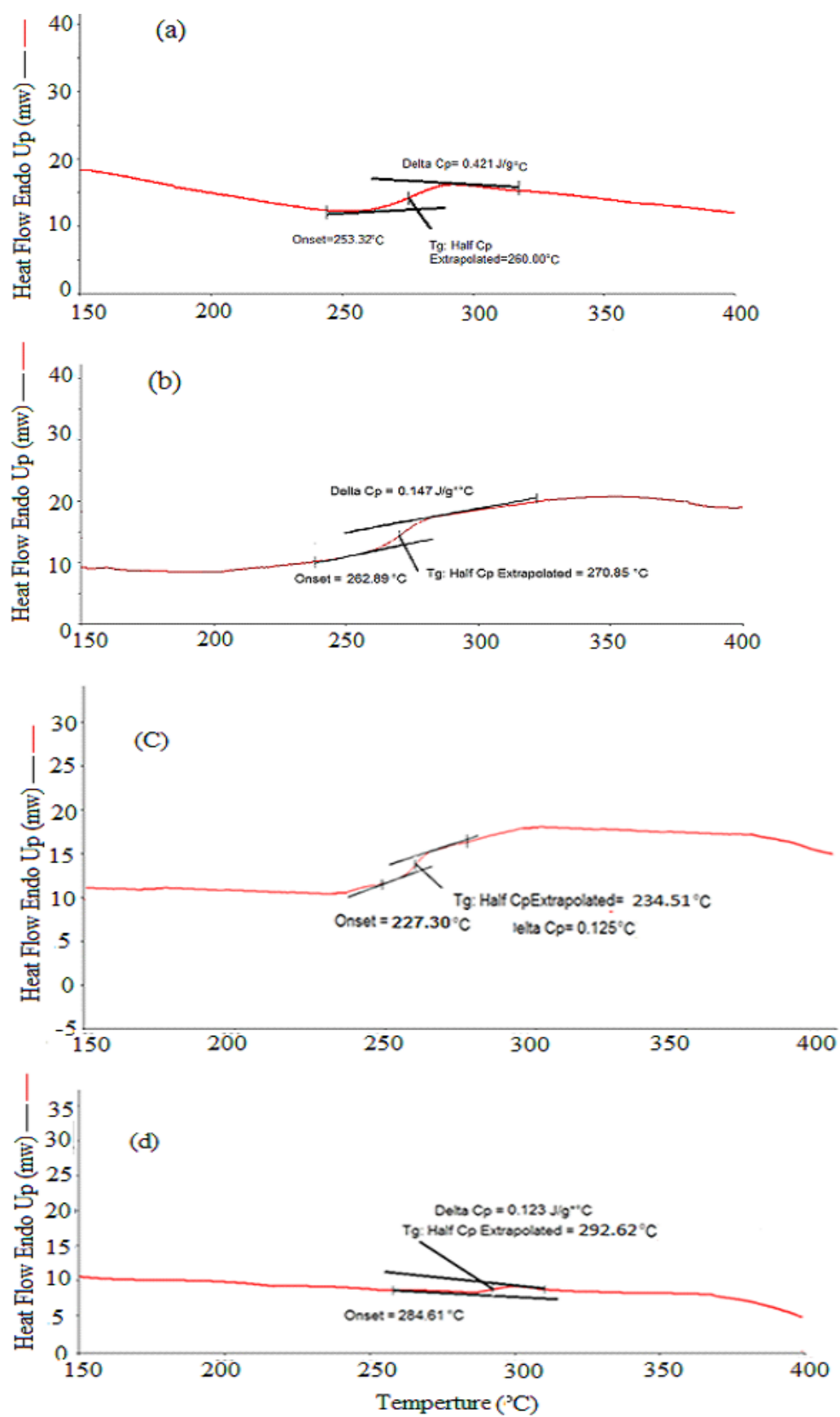
a: viscosity measured at a polymer concentration of 0.5 g/dL in DMAc at 30°C.

## 5.5. Thermal properties

DSC and TGA were used to investigate the thermal properties of all the synthesized poly(amine-amide)s, the thermal behavior data of these poly(amine-amide)s are summarized in **Table 5.10**. They showed high glass transition temperatures ( $T_g$ ), in the range of 292.6 - 234.5°C as determined by DSC. **Figures 5.12** (a), (b), (c) and (d) show DSC of synthesized poly(amine-amide)s **Pa1**, **Pa2**, **Pb1** and **Pf2** respectively.

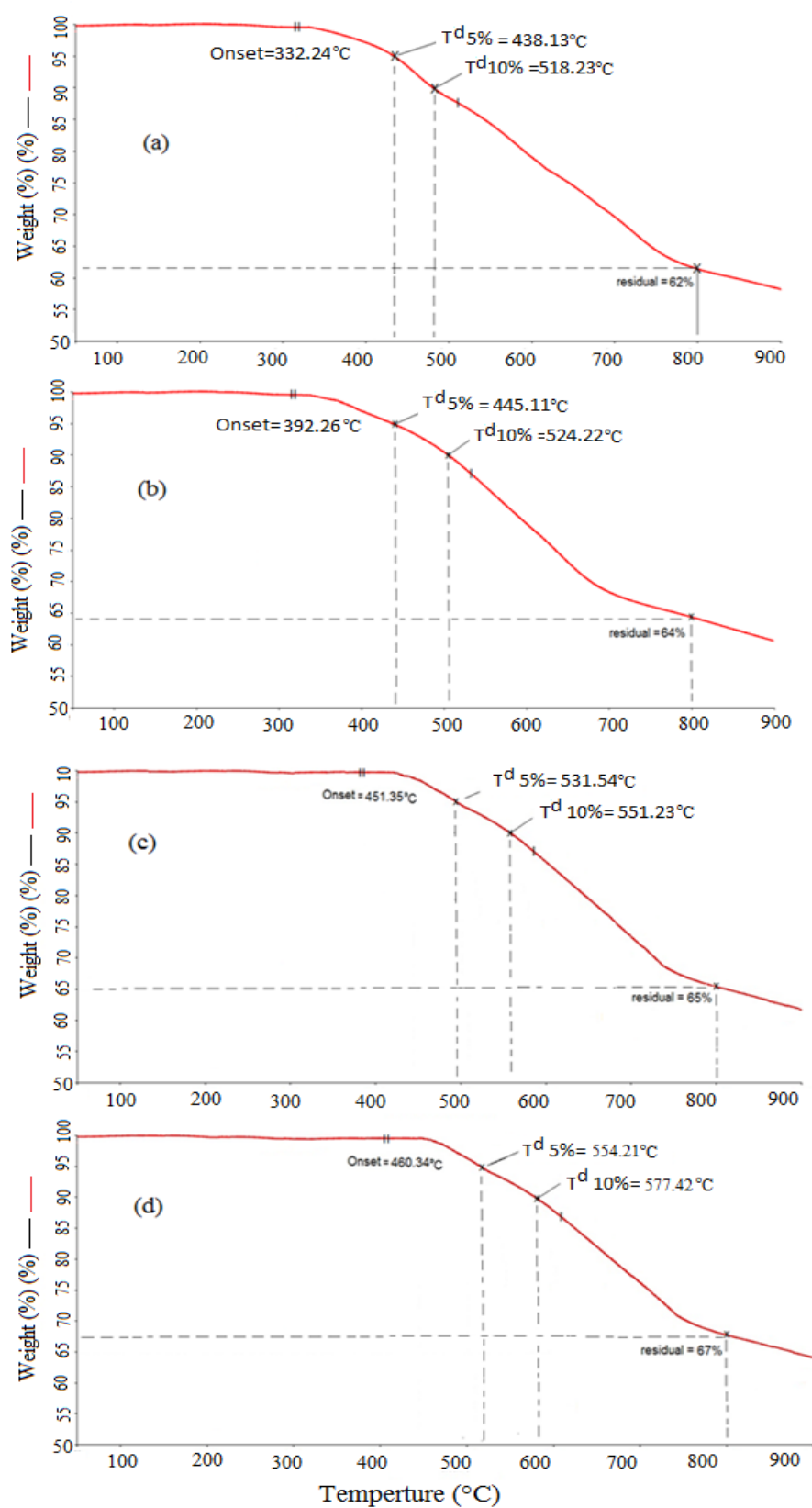
The  $T_g$  values of these poly(amine-amide)s generally decreased with decreasing stiffness of the diamine component. Therefore polymers with phenylene diamine exhibited low  $T_g$  value due to less rigidity than polymers with 1,5-diamine. **Table 5-10** shows that the lowest  $T_g$  value (234.5°C) of poly(amine amide) (**Pc1**) can be explained in terms of the flexibility and high rotation of its diamine moiety in the main chain (**Figure 5-12** (c)). Poly(amine amide) **Pf2** exhibited the highest  $T_g$  value (292.6°C) in this series of polymers because of the presence of four rigid 1,5-diamine naphthalene component leading to increase in amide links as shown in **Figure 5-12** (d).

It can be summarized that the glass transition ( $T_g$ ) of all polyamides with more aromatic rings have higher  $T_g$  than others with low aromatic rings. Polyamides with higher stiff diamine components have higher  $T_g$ . Polyamides with more amide links have higher  $T_g$  (**Table 5-10**).



**Figure 5-12:** DSC of poly(amine amide)s (a) **Pa1**, (b) **Pa2**, (c) **Pc1**, (d) **Pf2**

The thermal degradation behavior of the poly(amine amide)s at a heating rate of 20°C in nitrogen atmosphere has been investigated by TGA analysis. The minimum onset temperature at which the polymers started to degrade was 313.6°C up to 460.3°C. **Figure 5.13** (a) and (b) show the TGA curves of poly(amine amide)s (**Pa1**) and (**Pa2**) respectively. The decomposition temperatures ( $T_d$ ) at 5% and 10% weight losses are given in **Table 5-10**. All the poly(amine-amide)s exhibited good thermal stability with insignificant weight loss up to 400°C in nitrogen. The 5% weight-loss temperatures in nitrogen were recorded in the range of 340.4 - 554.2 °C and 401.2 - 577.4°C for 10% weight-loss. Polymers with 1,5-diamine naphthalene exhibited higher thermal stability compared to phenylene diamine due to their high aromatic content which results from naphthalene rings.

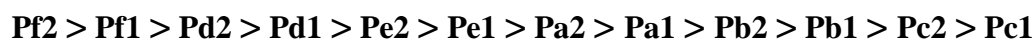


**Figure 5-13:** TGA of poly(amine-amide)s (a) **Pa1**, (b) **Pa2**, (c) **Pf1**, (d), **Pf2**

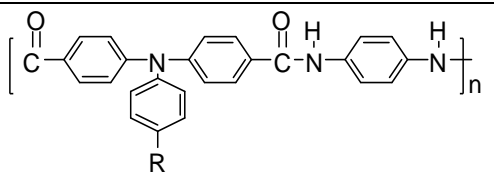
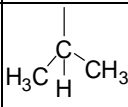
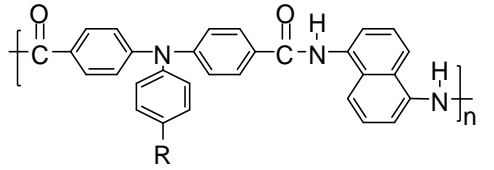
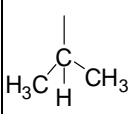
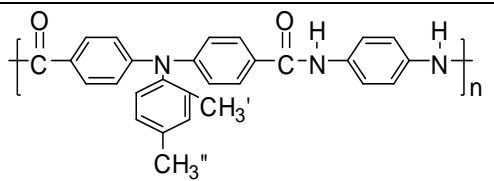
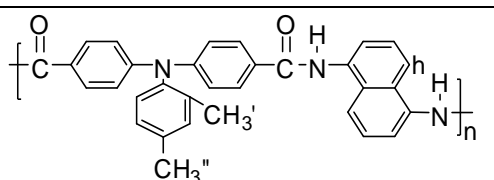
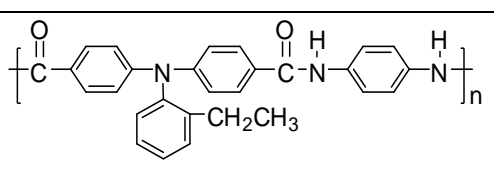
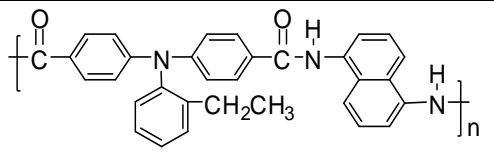
On the other hand, four amides links in **Pf1** and **Pf2** polyamides lead to more cross-linking in the chain of the polymer relative to other polyamides which will increase the thermal

stability of polymers **Pf1** and **Pf2** as shown in **Figure 5-13** (c) and (d). All polymers revealed residual yields in nitrogen of more than 60% at 800°C. **Table 5-10** summarizes the relation between structures of the synthesized polyamides and their thermal stabilities.

From the above results, the thermal stability order of the synthesized polyamides is:



**Table 5-10:** Structures and thermal properties of the synthesized polyamides

poly(amine amide)s structure	code	R	T <sub>g</sub>	TGA	
				T <sub>d</sub> 5%	T <sub>d</sub> 10%
	<b>Pa1</b>		255.00	438.13	518.23
	<b>Pa2</b>		260.85	445.11	524.22
	<b>Pb1</b>	-	248.32	355.12	512.10
	<b>Pb2</b>	-	254.45	386.64	516.16
	<b>Pc1</b>	-	234.51	340.35	401.22
	<b>Pc2</b>	-	240.46	351.14	506.21



	<b>Pd1</b>		277.72	480.54	538.20
	<b>Pd2</b>		281.32	496.34	540.34
	<b>Pe1</b>		271.28	470.54	530.20
	<b>Pe2</b>		276.20	481.54	534.21
	<b>Pf1</b>	-	288.79	531.54	551.23
	<b>Pf2</b>	-	292.62	554.21	577.42

**Table 5-11:** Thermal behavior data of the synthesized poly(amine-amide)s

Polymer Code	Onset (°C) <sup>a</sup>	T <sub>g</sub> (°C) <sup>b</sup>	Onset (°C) <sup>c</sup>	T <sup>d</sup> 5% (°C) <sup>d</sup>	T <sup>d</sup> 10% (°C) <sup>d</sup>	Char. (%) <sup>e</sup>
(Pa1)	253.3	255.0	332.2	438.1	518.2	62
(Pa2)	262.8	260.8	392.2	445.1	524.2	64
(Pb1)	242.0	248.3	335.4	355.1	512.1	63
(Pb2)	256.9	254.4	386.0	386.6	516.1	64
(Pc1)	241.3	234.5	331.6	340.3	401.2	64
(Pc2)	251.1	240.4	398.1	351.1	506.2	64
(Pd1)	261.3	277.7	432.1	480.5	538.2	67
(Pd2)	271.4	281.3	449.1	496.3	540.3	67
(Pe1)	251.7	271.2	422.1	470.5	530.2	67
(Pe2)	269.9	276.2	436.1	481.5	534.2	67
(Pf1)	274.7	288.7	451.3	531.5	551.2	65
(Pf2)	294.6	292.6	460.3	554.2	577.4	67

a: onset temp, recorded by DSC.

b: The midpoint temperature of baseline shift on the subsequent DSC trace (from 30 to 350) °C at heating rate 20 °C/min ) was defined as T<sub>g</sub>.

c: Onset temperature of the degradation polymer

d: Decomposition temperature at which a 5% or 10% weight loss was recorded by TGA at a heating rate of 20 °C/min.

e: Residual weight percentages at 800°C under nitrogen flow.

## 5.6. Optical properties

The optical properties of the synthesized poly(amine amide)s were investigated by UV-Vis and photoluminescence spectroscopy (PL). The results are summarized in **Table 5-12**.

**Table 5-12: Optical properties of the poly(amine amide)s**

Polymer Code	$\lambda_{\text{abs max}}$ (nm)a	$\lambda_{\text{abs onset}}$ (nm)a	$\lambda_{\text{PL}}$ (nm)b
<b>Pa1</b>	355	403	438
<b>Pa2</b>	328	397	431
<b>Pb1</b>	354	400	437
<b>Pb2</b>	318	395	430
<b>Pc1</b>	353	405	436
<b>Pc2</b>	320	395	429
<b>Pd1</b>	363	399	446
<b>Pd2</b>	355	407	440
<b>Pe1</b>	360	399	447
<b>Pe2</b>	351	405	442
<b>Pf1</b>	313	399	488
<b>Pf2</b>	305	403	486

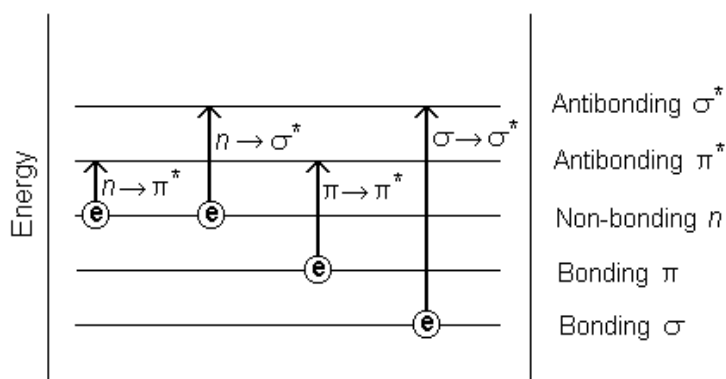
a: UV-vis absorption measurements in NMP ( $1 \times 10^{-5}$  M).

b: PL spectra measurements in NMP ( $1 \times 10^{-5}$  M).

The dilute solutions of these poly(amine amide)s in concentrations of  $10^{-5}$  M in NMP (N-Methyl-2-pyrrolidone) exhibited strong UV-Vis absorption bands in the range of 305–363 nm assignable to the (n- $\pi^*$ ) transitions resulting from the conjugation between the aromatic rings and nitrogen atoms in the triphenylamine and ( $\pi$ - $\pi^*$ ) transitions in the triphenylamine and the naphthalene chromosphere [130].

Many molecules absorb ultraviolet or visible light. Absorbance is directly proportional to the path length,  $b$ , and the concentration,  $c$ , of the absorbing species. *Beer's Law* states that:  $A = \epsilon bc$ , where  $\epsilon$  is a constant of the proportionality or known as the *absorptivity*.

Electrons in a sigma or pi bonding orbital that are excited to the corresponding anti bonding orbital requires energy in the range of 200-700 nm of the UV-Vis spectra as shown in **Figure 5-14**.



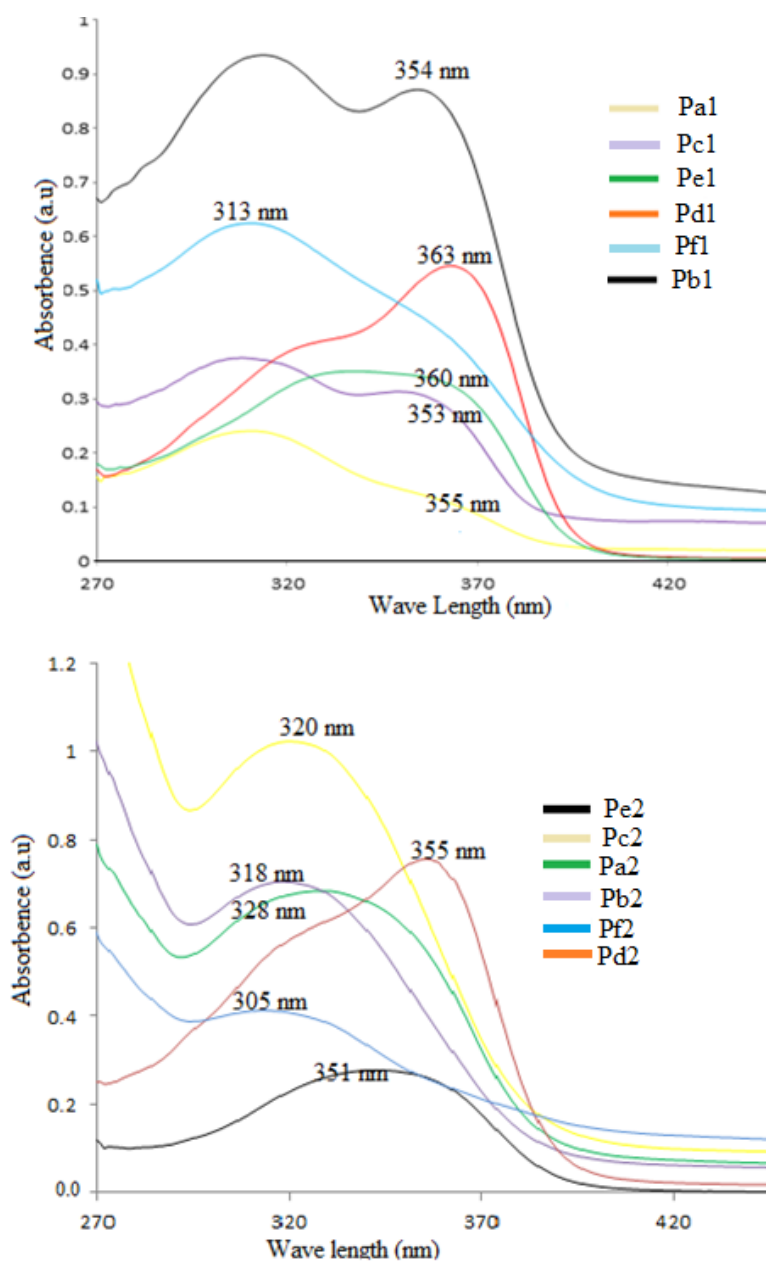
**Figure 5-14:** Possible electronic transitions of p, s and n electrons

Polyamides with 1,5-naphthalene diamine have lower UV-Vis  $\lambda_{\text{abs}}$  max absorption than that with phenylene diamine because they have ( $n\text{-}\pi^*$ ) electronic transitions and more ( $\pi\text{-}\pi^*$ ) transitions from additional 1,5-naphthalene so they require more absorbance energy for transition than polyamides with phenylene diamine (**Figure 5-15**). Polyamides with high max wavelength ( $\lambda_{\text{abs}}$  max) require low absorption energies.

Referring to **Figure 5-14**, polyamides **Pa1**, **Pb1** and **Pc1** have ( $n\text{-}\pi^*$ ) and ( $\pi\text{-}\pi^*$ ) transition band into TPA group so they have max absorbance in approximate wave length. Polyamides **Pa2**, **Pb2** and **Pc2** also showed approximate values also but polyamides **Pd1**, **Pe1**, **Pd2** and **Pe2** have max absorbance shifted to higher wave lengths because of the electron withdrawing groups and the resonance of phenoxy ( $\text{-O-Ph}$ ) into **Pd1**, **Pd2** and (N-pyrrole) into **Pe1**, **Pe2**.

The lowest UV-vis  $\lambda_{\text{abs}}$  max observed at 313 nm and 305 nm in polyamides **Pf1** and **Pf2** respectively is attributed to the presence of one excess nitrogen atom. Incorporation of a high conjugated N-phenyl and phenyl groups into the backbones of these polyamides leads to a requirement of more UV-Vis absorption energies for these transitions (**Figure 5-15**). The effect of the substituent groups,  $\text{CH}_3\text{CH}_2\text{-}$ ,  $\text{CH}_3\text{-CH-CH}_3$  and  $\text{-CH}_3$  in the rings of the triphenyl groups are unobservable.

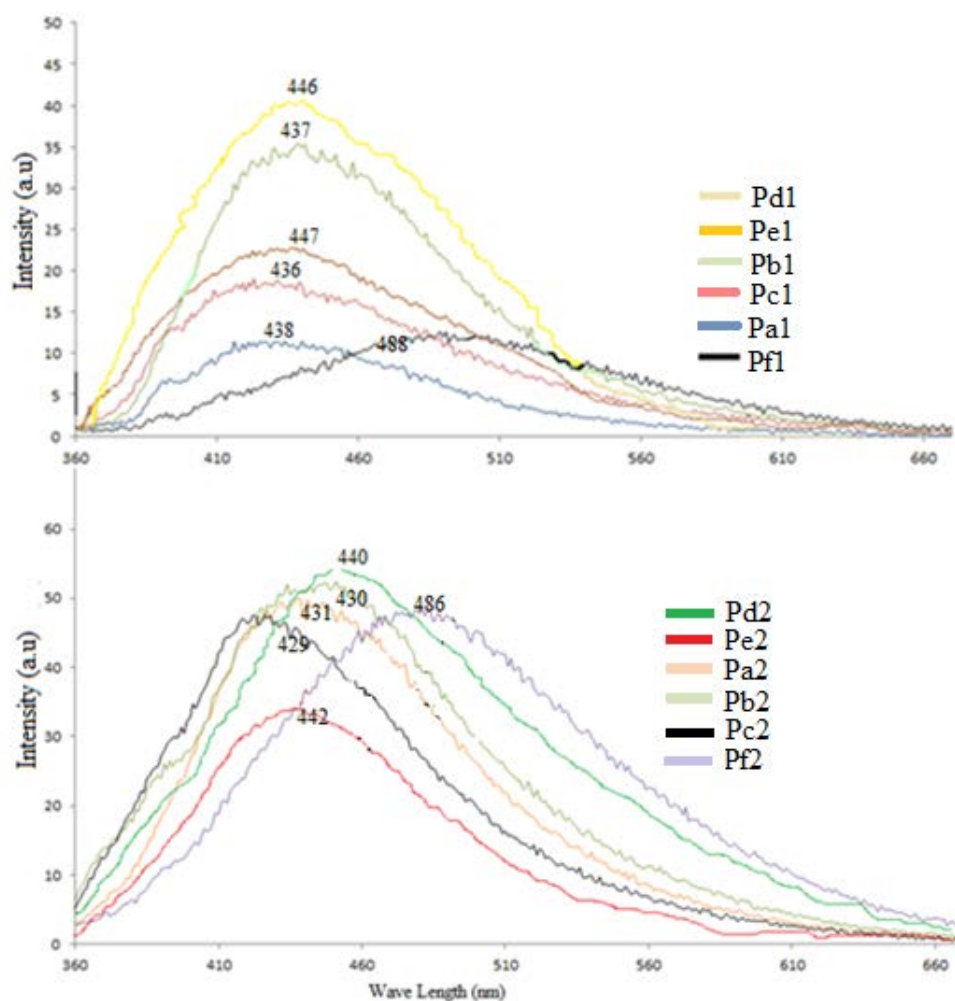
**Figure 5-15** shows that polyamides with phenylene groups have peaks with two separate tops resulting from ( $n-\pi^*$ ) and ( $\pi-\pi^*$ ) transition band while polyamides with 1,5-naphthalene have incorporated peak tops because of the more ( $\pi-\pi^*$ ) transitions.



**Figure 5-15:** UV-vis absorption of poly(amine amide)s in  $10^{-5}$  M NMP

Polyamide spectra in NMP solution showed PL emission bands around 429 - 488 nm in the blue region (**Figure 5-16**). The PL spectra in the blue region can be explained from the decreased intra and inter molecular electronic interactions. The bulky crank of triphenyl

group is effective in decreasing charge transfer formation within or between polymer chains through steric hindrance.



**Figure 5-26:** Photoluminescence of poly(amine amide)s with a concentration of  $10^{-5}$  M in NMP.

Polyamides **Pa1**, **Pb1** and **Pc1** have approximate PL values but additional 1,5-naphthalene in polyamides **Pa2**, **Pb2** and **Pc2** increases the excitation of  $\pi$ -electrons which leads to the decreases of the  $\lambda_{PL}$  of these polyamides. Polyamides **Pe1** and **Pd1** have electron withdrawing groups which lead to the decreased excitation of p-electrons resulting in an increase in the  $\lambda_{PL}$ . Polyamides **Pd2** and **Pe2** have low  $\lambda_{PL}$  values. **Pf1** and **Pf2** have the highest PL wavelength due to the low excitation of n and  $\pi$ -electrons in phenyl and 1,5-naphthalene which have more benzene rings, thus leading to higher diffusion of electrons

(n and  $\pi$ -electrons) into benzene rings. Therefore, the PL will have a low energy and a high wavelength ( $\lambda_{\text{PL}}$ ).

### 5.7. Electrochemical Properties

The redox behavior of poly(amine amide)s was investigated by cyclic voltammetry (CV) where the cast films on an ITO-coated glass substrate as a working electrode and dry acetonitrile containing 0.1 M of tetrabutylammonium perchlorate ( $\text{Bu}_4\text{NH}_4\text{ClO}_4$ ) as an electrolyte. All the poly(amine amide)s showed one reversible oxidation redox couple. **Figure 5-18** shows a typical cyclic voltammetry curve for poly(amine amide) (**Pa1**) recorded at a scanning rate of 0.1 V/s at the oxidation half-wave potential of  $E_{1/2} = 1.13$  V in the oxidative scan corresponding to the removal of two electrons from the nitrogen atoms at triarylamine structure in each repeating unit to yield stable delocalized poly(amine amide)<sup>2+</sup> [131]. Because of the electrochemical stability of the films and a good adhesion between the polymer and ITO substrate, the polyamide (**Pa1**) exhibited a good reversibility of electrochromic characteristics as shown by sixteen continuous scans between 0.0 - 1.60 V changing the color from original pale yellowish to blue (**Figure 5-18**). The energy of the HOMO and LUMO levels of the corresponding poly(amine amide)s can be determined from the oxidation half-wave potential  $E_{1/2}$  and the onset absorption wavelength of the UV-Vis absorption ( $\lambda_{\text{abs}}$  onset) of the solution [132]. The results are listed in **Table 5-13**. The external ferrocene/ferrocenium ( $\text{Fc}/\text{Fc}^+$ ) redox standard  $E_{1/2}$  was 0.41 V vs Ag/AgCl in  $\text{CH}_3\text{CN}$ , and the HOMO energy for the  $\text{Fc}/\text{Fc}^+$  standard was 4.80 eV.

**Table 5-13:** Electrochemical properties of the poly(amine-amide)s

Polymer Code	E <sub>1/2</sub> V vs. Ag/AgCl	λ <sub>abs, onset</sub> (nm)	E <sub>Homo</sub> <sup>a</sup> (eV)	E <sub>Lumo</sub> <sup>b</sup> (eV)	E <sub>Homo-Lumo</sub> <sup>c</sup> gap (eV)
<b>Pa1</b>	1.13	403	5.52	2.44	3.08
<b>Pa2</b>	1.13	397	5.51	2.39	3.12
<b>Pb1</b>	1.11	400	5.50	2.40	3.10
<b>Pb2</b>	1.09	395	5.48	2.35	3.15
<b>Pc1</b>	1.10	405	5.49	2.43	3.06
<b>Pc2</b>	1.09	395	5.48	2.33	3.15
<b>Pd1</b>	1.18	403	5.57	2.49	3.08
<b>Pd2</b>	1.19	399	5.58	2.47	3.11
<b>Pe1</b>	1.21	405	5.60	2.54	3.06
<b>Pe2</b>	1.20	399	5.59	2.55	3.04
<b>Pf1</b>	1.25	407	5.64	2.60	3.04
<b>Pf2</b>	1.27	407	5.66	2.62	3.04

a: The HOMO energy levels were calculated from cyclic voltammetry and were referenced to ferrocene/ferrocenium couple (4.8 eV).

b: E<sub>Lumo</sub> = E<sub>Homo</sub> – E<sub>gap</sub>.

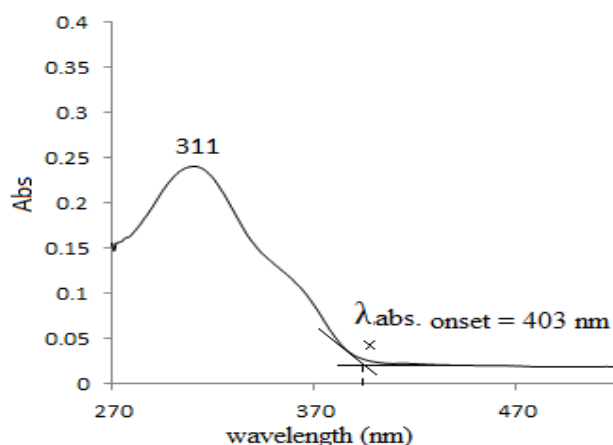
c: Energy gap data

Optical band energy can be calculated by the equation:

$$E_{\text{gap}} = \frac{1242}{\lambda_{\text{abs onset}}} \dots\dots\dots 1$$

where 1242 is a constant, λ<sub>abs onset</sub> is the onset wavelength which can be calculated by intersection of two tangents on the absorption edges as shown in **Figure 5-17**.





**Figure 5-37:** Uv-Vis absorption spectrum of polyamide (Pa1) in ( $10^{-5}$  M) NMP

Therefore, the HOMO energy for Pa1 can be calculated as follows:

$$E_{\text{HOMO}} = [E_{1/2} - E_{1/2}(\text{ref.}) + 4.8] \text{ eV} \dots\dots\dots 2$$

where  $E_{1/2}$  is the oxidation half-wave potential which can be determined from the relation:

$$E_{1/2} = (E_{\text{red}} + E_{\text{ox}}) / 2 \dots\dots\dots 3$$

where  $E_{\text{red}}$  and  $E_{\text{ox}}$  are the potentials of cathode and anode respectively.

$E_{1/2}$  (ref.) is the external standard oxidation energy of ferrocene/ferrocenium ion couple under the same experimental conditions. Its value is 0.41 V versus Ag/AgCl in  $\text{CH}_3\text{CN}$ .

From application of equations 1, 2, 3 above:

$$E_{1/2} = (E_{\text{red}} + E_{\text{ox}}) / 2$$

$$E_{1/2} = 0.95 \text{ V} + 1.31 \text{ V} / 2 = 1.13 \text{ V}$$

$$E_{\text{HOMO}} = [E_{1/2} - E_{1/2}(\text{ref.}) + 4.8] \text{ eV} = [1.13 \text{ V} - 0.41 \text{ V} + 4.8] \text{ eV}$$

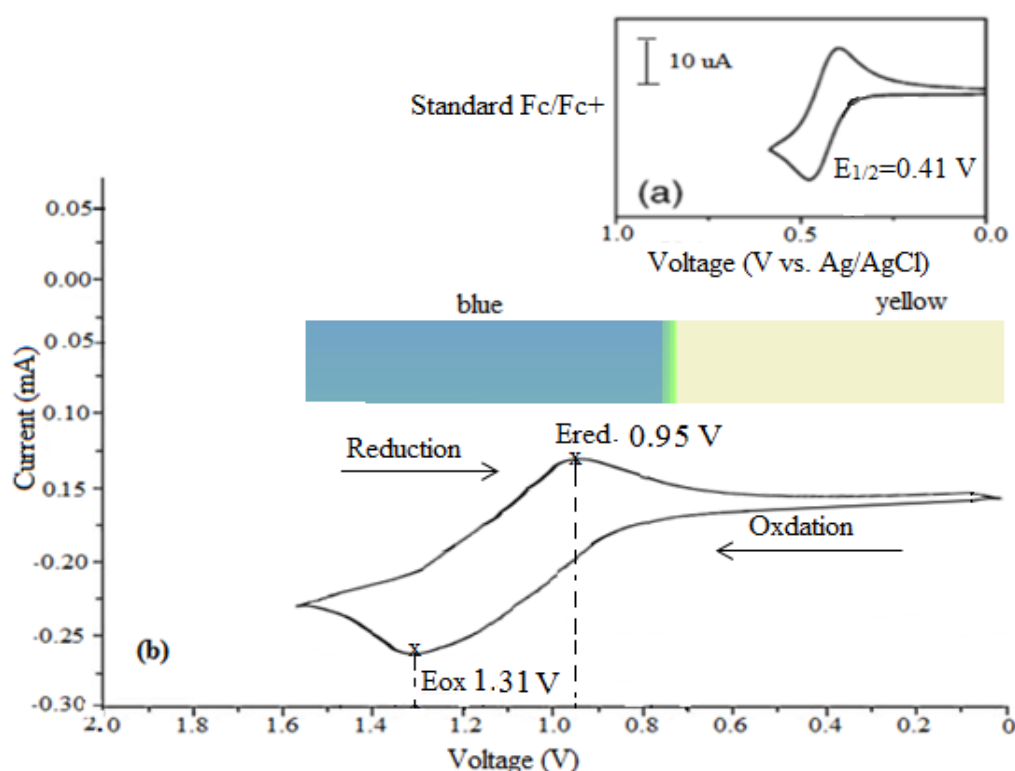
$$E_{\text{HOMO}} = 5.52 \text{ eV}$$

$$E_{\text{gap}} = 1240 / \lambda_{\text{onset}} = 1240 / 403 = 3.08 \text{ eV}$$

$$E_{\text{HOMO}} - E_{\text{gap}} = E_{\text{LUMO}}$$

$$E_{\text{LUMO}} = 5.52 - 3.08 = 2.44 \text{ eV}$$

**Table 5-13** shows that the HOMO energy values of polyamides **Pa1**, **Pa2**, **Pb1**, **Pb2** and **Pc2** are lower and have approximately similar values because the triarylamine in each repeating unit has electron donating alkyl groups ( $\text{CH}_3\text{-CH-CH}_3$ ,  $\text{CH}_3$ ,  $\text{-CH}_2\text{-CH}_3$ ). These alkyl groups help to stabilize the  $(\text{polyamine-amide})^{2+}$  which is the result of the removal of two electrons from a nitrogen atom in each repeating unit in the backbone of the polyamides. Therefore these polyamides require a low energy of oxidation (considering that other amide moiety nitrogen atoms have approximately the same effect). Polyamides **Pd1**, **Pd2**, **Pe1** and **Pe2** require higher energy of oxidation because they have electron withdrawing groups ( $\text{-O-Ph}$ ) and ( $\text{-N-py}$ ) which lead to a decrease in the stability of  $(\text{polyamine-amide})^{2+}$  in each unit. On the other hand, polyamides **Pf1** and **Pf2** have one excess nitrogen atom in each unit of its backbone which means it requires a higher energy oxidation than the other polyamides.



**Figure 5-18:** Cyclic voltammograms of (a) Ferrocene as reference and (b) the cast film of poly(amine amide) (**Pa1**) on the indium-tin oxide(ITO)-coated glass substrate in  $\text{CH}_3\text{CN}$  containing 0.1 M TBAP, with a scan rate of 0.1 V/s



## CHAPTER 6: CONCLUSION AND SUGGESTIONS FOR FUTURE WORK

### 6.1 Conclusion

A series of new poly(amine-amide)s bearing triphenylamine units in the polymer main chain have been successfully prepared from a newly synthesized aromatic derived triphenylamine dicarboxylic acid, 4,4'-dicarboxy-4"-triphenylamine with two different aromatic diamines by phosphorylation polyamidation technique. All the polymers exhibited excellent solubility in polar organic solvents because of the incorporation of triarylamine and 1,5-diamine naphthalene in the backbones of these polyamides. This excellent solubility makes these polymers convenient to process into articles by spin-coating.

All the poly(amine-amide)s were amorphous with high a glass transition temperature ( $T_g$ ) in the range of 292.6 - 234.5°C and exhibited excellent thermal stability. Polymers with phenylene diamine exhibited low  $T_g$  value due to the less rigidity than compared to the polymers with 1,5-diamine. Poly(amine amide) **Pf2** exhibited the highest  $T_g$  value of 292.6°C in this polymer series because of the presence of four rigid 1,5-diamine naphthalene component leading to the increase in amide links. Polymers with 1,5-diaminenaphthalene exhibited a higher thermal stability compared to those with phenylene diamine due to their high aromatic content. Polymers **Pf1**, **Pf2** exhibited a higher thermal stability at the 551.2 and 577.4°C respectively, because due to the high amide groups which lead to the increase of rigidity. The order of thermal stability of the synthesized polyamides is:

**Pf2 > Pf1 > Pd2 > Pd1 > Pe2 > Pe1 > Pa2 > Pa1 > Pb2 > Pb1 > Pc2 > Pc1.**

The optical properties of the synthesized poly(amine-amide)s were investigated by UV-Vis and photoluminescence spectroscopy. The poly(amine-amide)s in concentration of  $10^{-5}$  M in NMP exhibited strong UV-Vis absorption bands at the range of 305 - 363 nm which is

assigned to the ( $n-\pi^*$ ) and ( $\pi-\pi^*$ ) transitions resulting from the conjugation between the aromatic rings, nitrogen atoms and the benzene rings.

Polyamides with 1,5-naphthalene diamine have lower UV-Vis  $\lambda_{\text{abs}}$  max absorption compared to those with phenylene diamine because they have ( $n-\pi^*$ ) electronic transitions and higher ( $\pi-\pi^*$ ) transitions from additional 1,5-naphthalene moiety. Therefore they require more absorbance energy for transition. The lowest UV-Vis  $\lambda_{\text{abs}}$  max of 305 nm and 313 nm in polyamides **Pf1** and **Pf2** respectively are attributed to the presence of one excess nitrogen atom. Incorporation of highly conjugated N-phenyl and phenyl groups the backbones of these polyamides lead to the requirement of more UV-Vis absorption energies for these transitions.

Polyamide spectra in NMP solution showed photoluminescence (PL) emission bands at around 429–488 nm in the blue region. Polyamides **Pa1**, **Pb1** and **Pc1** have higher PL values but the additional 1,5-naphthalene group in polyamides **Pa2**, **Pb2** and **Pc2** increase the excitation of  $\pi$ -electrons which lead to a decrease of the  $\lambda_{\text{PL}}$  of these polyamides. Polyamides **Pe1**, **Pe2**, **pd1** and **Pd2** have withdrawing groups which lead to decrease in the excitation of p-electrons while the  $\lambda_{\text{PL}}$  increased. Finally **Pf1** and **Pf2** have the highest PL wavelength due to the more benzene rings which lead to the higher diffusion of electrons ( $n$  and  $\pi$ -electrons) in benzene rings. Therefore the PL shows a low energy and a high wavelength ( $\lambda_{\text{PL}}$ ).

All the poly(amine amide)s showed one reversible oxidation redox couple recorded at a scanning rate of 0.1 V/s; the color changed from original pale yellowish to blue. The energy of the HOMO and LUMO levels of the poly(amine-amide)s were determined from the half-wave oxidation ( $E_{1/2}$ ) and the onset absorption wavelength of the UV-Vis absorption  $E_{\text{abs}}$ . Thus, these triphenylamine-containing polyamides can be applied in electroluminescent devices as hole-transporting or blue-light-emitting polymeric materials.

The HOMO energy values of polyamides **Pa1**, **Pa2**, **Pb1**, **Pb2** and **Pc2** are lower and have approximately the same values because the triarylamine in each repeating unit has electron donating alkyl groups ( $\text{CH}_3\text{-CH-CH}_3$ ,  $\text{CH}_3$ ,  $\text{-CH}_2\text{-CH}_3$ ). Polyamides **Pd1**, **Pd2**, **Pe1** and **Pe2** require higher energy of oxidation because they have electron withdrawing groups ( $\text{-O-Ph}$ ) and ( $\text{-N-Py}$ ) respectively which lead to the decrease in stability of the (polyamine-amide)<sup>2+</sup> in each unit. Polyamides **Pf1** and **Pf2** have one excess nitrogen atom in each unit of its backbone which means that it requires a higher energy of oxidation compared to the other polyamides.

## 6.2. Suggestion for future work

In the synthesis of dicyano triphenylamine the starting materials (aromatic amines) can be chosen from groups that can increase the stability of the positive ion containing free electron which is result of one electron from the nitrogen atom in the triarylamine. This will produce positive ion with a free electron,  $[\text{poly}(\text{amine-amide})]^{+\bullet}$  in each backbone unit of the polymer. The stable positive free radical ion unit could form reversible oxidation redox couple with a good separate potential. The ion (polyamine amide)<sup>2+</sup> produces a green color between the main yellowish and blue colors.

Other suggestion includes the synthesis of dicarboxylic monomers. From the literature, the oxadiazoles are good to be used as electron-transport materials/layer (ETMsL). Thus it could convert the synthesized dicarboxylic monomer to oxadiazoles compounds.

## REFERENCES

1. Cassidy, P.E., Thermally stable polymers. 1980, New York: Marcel Dekker
2. Thelakkat, M. and Schmidt, H.W., Aromatic High-Strength Fibers. 1989 New York Wiley.
3. Yarn, J.F., High performance polymers. 2008, New York: Sage Publications.
4. Eastmond, L.A., Russo, S., and Sigwald, P., Step polymerization, Comprehensive polymer science, 1989. 5(83), P 373
5. Imai Y., Synthesis of novel organic-soluble high-temperature aromatic polymers *High Perform Polym*, 1995. 7(337).
6. Imai Y., Synthesis of novel organic-soluble high-temperature aromatic polymers, *React Funct Polym*, 1996. 30(3).
7. Liou, G.S., Polyterephthalamides with naphthoxy-pendant groups, *J Polym Sci*, 2002. 40(1781).
8. Hsiao, S.H. and Liou G.S., Novel Aromatic Polyamides Bearing Pendant Diphenylamino or Carbazolyl Groups, *J Polym Sci Part A: Polym Chem*, 2004. 42, P(3302).
9. Oishi, Y., Kakimoto, M. and Imai, Y., Preparation and properties of new aromatic polyamides from 4, 4'-diaminotriphenylamine and aromatic dicarboxylic acids, *J Polym Sci Part A: Polym Chem*, 1990. 28(1763).
10. Liou, G.S., Kakimoto, M. and Imai Y., Synthesis and characterization of novel soluble triphenylamine-containing aromatic polyamides based on N,N'-bis(4-aminophenyl)-N,N'-diphenyl-1,4-phenylenediamine *J Polym Sci Part A: Polym Chem*, 2002. 40(16), P 2810-2818
11. Liou, G.S., Synthesis and properties of new soluble triphenylamine based aromatic poly (amine amide)s derived from N-N''bis(4-carboxyphenyl)-N,N'-diphenyl-1,4-phenylene diamine, *J Polym Sci Part A: Polym Chem*, 2003. 41(94).
12. Ogino, K., Kurtaja Y.-H., Oxidative coupling polymerization of 4-methyltriphenylamine, *J Macromol Rapid Commun*, 1999. 20(103).
13. Chou, M.Y., Lin, C.C., Liu, J.H., and Kuo, C.K. Electropolymerization of Starburst Triarylamines and Their Application to Electrochromism and Electroluminescence *Chem Mater*, 2001. 16(654).
14. Cheng, S.H., and Liou G.S. , Novel Aromatic Poly(Amine-Imide)s Bearing A Pendant Triphenylamine Group: Synthesis, Thermal, Photophysical, Electrochemical, and Electrochromic Characteristics, *Macromolecules*, 2005. 38(307).

15. Hsiao, S.H., Chen, H.W., and Liou, G.S., Novel aromatic polyamides and polyimides functionalized with 4-*tert*-butyltriphenylamine groups, *J Polym Sci Part A: Polym Chem*, 2006. 44(15), P4579–4592.
16. Liou, G.S., Novel high- $T_g$  poly(amine-imide)s bearing pendant *N*-phenylcarbazole units: Synthesis and photophysical, electrochemical and electrochromic properties, *J. Mater. Chem.* , 2006. 16(1831).
17. Beaupre, S., and Leclerc M., Toward the Development of New Textile/Plastic Electrochromic Cells Using Triphenylamine-Based Copolymers, *Chem Mater*, 2006. 18(4011).
18. Choi, K., and Zentel, R. , Spin-coating of designed functional planar defects in opal films: Generalized Synthesis, *Chem Mater*, 2006. 18 P 5640-5642
19. Tang, C.W., Vanslyke S.A., Electroluminescence of doped organic thin films, *J Appl Phys*, 1989. 85(3610).
20. Adachi, C.K., Tamoto, Electroluminescence of doped organic thin films, *J Appl Phys N, Appl Phys Lett*, 1995. 66 P 2679.
21. Sun, Y., Maindron, T., Dodelet, J.P., and Iorio, M.D., Synthesis and Characterization of a Blue Light Emitting Polymer Containing Both Hole and Electron Transporting Units, *Chem Mater*, 1999. 11 P 2501.
22. Liu, Y.Q., and Jen, A.K.Y., Synthesis and characterization of novel light-emitting polymer containing highly efficient hole transporting aromatic diamine, *Chem Mater*, 1998. 10(11) P 3301
23. Kido, J.M.S., and Nishide, H., A Novel Triphenylamine-Substituted Poly(*p*-phenylenevinylene): Improved Photo- and Electroluminescent Properties, *Chem Mater*, 2001. 13 P 3817.
24. Miteva, T.A.M., Knoll, W., Nothofer, U., Scherf, D.C., Muller, K., Meerholz, A., and Yasuda, D., Improving the Performance of Polyfluorene-Based Organic Light-Emitting Diodes via End-capping, *Adv Mater*, 2001. 13(565).
25. Alleyne, X.B.D., Djurovich, P.I., Adachi, C., Tsyba, I., Bau, R. and Thompson, M.E., Organometallic Complexes as Hole-Transporting Materials in Organic Light-Emitting Diodes. *Inorg Chem* , 2004. 43(5) P1697 - 1707.
26. Yamazaki, N., Higashi, F., and Kawataba, T., Studies on reactions of the N-phosphonium salts of pyridines. XI. Preparation of polypeptides and polyamides by means of triaryl phosphites in pyridine, *J Polym Sci Part A: Polym Chem*, 1974. 12(54) P 2149
27. Vygodskii, Y.S., Ionic Liquids as Novel Reaction Media for the Synthesis of Condensation Polymers, *Macromol Rapid Commun*, 2002. 23(80).
28. Mallakpour, S.D.M., Microwave step-growth polymerization of 5-(4-methyl-2-phthalimidylpentanoylamino)isophthalic acid with different diisocyanates, *Polym Adv Technol*, 2008. 19(42).



29. Mallakpour, S.Z., Safe and fast polyamidation of 5-[4-(2-phthalimidylpropanoylamino)benzoylamino]isophthalic acid with aromatic diamines in ionic liquid under microwave irradiation, *Polymer*, 2008. 49(13).
30. Mallakpour, S.Z., Polym. Use of ionic liquid and microwave irradiation as a convenient, rapid and eco-friendly method for synthesis of novel optically active and thermally stable aromatic polyamides containing *N*-phthaloyl-L-alanine pendant group, *Degrad Stab*, 2008. 93(9).
31. Mallakpour, S.M., Soluble new optically active polyamides derived from 5-(4-methyl-2-phthalimidylpentanoylamino)isophthalic acid and different diisocyanates under microwave irradiation in molten ionic liquid, *Polym Bull*, 2009. 10(4).
32. Mallakpour, S.M., Ionic liquid catalyzed synthesis of organosoluble wholly aromatic optically active polyamides, *React Funct Polym*, 2009. 69(15).
33. Mallakpour, S.S., and Majid, K., Preparation of new poly(amide-imide)s with chiral architectures via direct polyamidation reaction, *J Appl Polym Sci*, 2007. 104(2).
34. Mallakpour, S.H., Ionic liquid catalyzed synthesis of organosoluble wholly aromatic optically active polyamides, *Polym Bull*, 2009. 62(14).
35. Mallakpour, S., Hajipour, A.R., Vahabi, R., Synthesis of novel polyimides containing side-chain azo-2-naphthol moieties, *J Appl Polym Sci*, 89 (7) P 1942-1951
36. Mallakpour, S., Rafiee, Z., Expeditious synthesis of novel aromatic polyamides from 5-[3-phenyl-2-(9,10-dihydro-9,10-ethanoanthracene-11,12-dicarboximido)propanoylamino]isophthalic acid and various diamines using microwave-assisted polycondensation, *React Funct Polym*, 2009, 69 (4) P 52 - 258
37. Kubota, Y., Nakada, S., and Sugi, Y., New heat-resistant and soluble aramids synthesized by palladium-catalyzed carbonylation polycondensation, *Mater. Trans.*, 2002. 43(31) P 326
38. Rabani, G., Arno, K., Synthesis of Poly(ether-esteramide) Elastomers by a Palladium-Catalyzed Polycondensation of Aromatic Diiodides with Telechelic Diamines and Carbon Monoxide, *Macromol Rapid Commun.*, 2002. 23(5-6) P 75-379.
39. Grozea, A.D., Feng, X.D., Lu, Z.H., Aziz, H., and Hor, A.M., 2002. Metal/AlQ<sub>3</sub> interface structures. *Appl Phys Lett*, 81(4) P 766-768.
40. Lee, M.-T., Chen, H.-H., Liao, C.-H., Tsai, C.-H., and Chen, C.H., 2004. Stable styrylamine-doped blue organic electroluminescent device based on 2-methyl-9,10-di(2-naphthyl)anthracene. *Appl Phys Lett*, 85(15) P 3301-3303.

41. Taghav, M.A., Facile, microwave-assisted synthesis of novel optically active polyamides derived from 5-(3-methyl-2-halimidylpentanoylamino)isophthalic acid and different diisocyanates, *Eur Polym J*, 2008. 44(1) P 87–97
42. Mallakpour, S., Rafiee, Z., Microwave-enhanced rapid synthesis of organosoluble polyamides based on 5-(3-acetoxynaphthoylamino)-isophthalic acid, *Polym Adv Technol*, 2008. 19 (11) P1474-1478
43. Mallakpour, S., Rafiee, Z., Microwave-induced synthesis of new optically active and soluble polyamides containing pendant 4-(2-phthalimidylpropanoylamino) benzoylamino-groups, *Amino Acids*, 2009, 37 (4) P 665-672
44. Mallakpour, S., Yousefian, H., Direct polyamidation in molten tetrabutylammonium bromide: novel and efficient green media, *Polym Bull*, 2009. 60 (2-3) P 191-198
45. Mallakpour, S., Dinari, M., Preparation of thermally stable and optically active organosoluble aromatic polyamides containing l-leucine amino acid under green conditions, *Polym Bull*, 2009, 63(5) P 623-635
46. van Krevelen, H.P., *Properties of polymers*. 1976, New York: Elsevier Scientific Publishing Company.
47. Kim, D.Y., and Cho, H.N., Blue light emitting polymers, *Prog Polym Sci*, 2000. 25(8) P 1089-1139
48. Allen, G. and Vollbracht, L., *Aromatic polyamides*. Oxford: Pergamon Press: 1989. 22
49. Chang, C.W., and Liou, G.S, Novel anodic electrochromic aromatic polyamides with multi-stage oxidative coloring based on N,N,N',N'-tetraphenyl-p-phenylenediamine derivatives *J Mater Chem Lett*, 2008. 18(46) P 5638-5646
50. Hsiao, S.H, and Liou G.S., Organosoluble and colorless fluorinated poly(ether imide)s from 1,2-bis(3,4-dicarboxyphenoxy)benzene dianhydride and trifluoromethyl-substituted aromatic bis(ether amine)s *J Polym Sci A: Polym Chem*, 2006. 44(9) P 3092–3102.
51. Sheng, S.R., Liu X.L, and Song, C.S., Novel soluble fluorinated aromatic polyamides derived from 2-(4-trifluoromethylphenoxy)terephthaloyl chloride with various aromatic diamines, *Eur Polym J*, 2009. 45(6).
52. Bruma, M.H.E., Schulz, B., Köpnick, T., and Kaminorz, Y., Aromatic polymers with side oxadiazole rings as luminescent materials in LEDs *J Macromol Symp*. 2003. 199(1).
53. Bruma, M.H.E., Schulz, B., Köpnick, T., Kaminorz, Y., and Robison, J., Synthesis and study of new polyamides with side oxadiazole rings *J Appl Polym Sci*, 2003. 87(4) P 714–721

54. Liou, G.S., and Yen, H. J., Synthesis, photoluminescence, and electrochromic properties of wholly aromatic polyamides bearing naphthylamine chromophores *J. Polym Sci Part A: Polym Chem*, 2006. 44(16), P 6094–6102.
55. Wang, X., Ogino, K., Sato, H., Strzelec, K., and Miyata, S., Preparation of New Hole Transport Polymers via Copolymerization of N,N'-Diphenyl-N,N'-bis(4-alkylphenyl)benzidine (TPD) Derivatives with 1,4-Divinylbenzene. *Macromol. Chem Phys* 2002. 4(203) P 739-747
56. ng, X., Ogino, K., Sato, H., and Tan, H.M., Synthesis and Characterization Of New Triarylamine-Based Polymers, *Macromol Chem Phys*, 2001, 202 (1) P 117-125
57. Bellmann, E., Grubbs, R.H, Marder, S.R., Kippelen, B., and Peyghambarian, N., Organic two-layer light-emitting diodes based on high-T<sub>g</sub> hole-transporting polymers with different redox potentials *Chem Mater* 1999. 11 (2) P 399-407
58. Adachi, C., Nagai, K., Tamoto, N., Molecular design of hole transport materials for obtaining high durability in organic electroluminescent diodes, *Appl Phys Lett*, 1995. 66(20) P 2679-2681
59. Tang, C.W., and. VanSlyke, S.A., Organic electroluminescent diodes, *Appl Phys Lett*, 1987. 51(913).
60. Tang, C.W., and Chen, C.H., Electroluminescence of doped organic thin films *J Appl Phys*, 1989. 65(9) P 3610
61. Liaw, D.J., Liaw, B.Y., Synthesis and properties of new polyimides derived from 1,1-bis[4-(4-aminophenoxy)phenyl] cyclododecane. *Polymer* 1999, 40(9).
62. Liaw, D.J., Liaw, B.Y., Yang, C.M., Hsu, P.N., Hwang, C.Y., Synthesis and characterization of new organosoluble polyamides derived from bis[4-(4-carboxyphenoxy)phenyl] diphenylmethane. *J Polym Sci A: Polym Chem* 2001, 39(61) P 1156.
63. Kulkarni, A.P., and Jenekhe, S.A., Electron Transport Materials for Organic Light-Emitting Diodes, *J Mater Chem*, 2004. 16(23) P 4556-4573.
64. Thelakkat, M., Haarer, D., and Schmidt, H.W., Star-Shaped, Dendrimeric and Polymeric Triarylamines as Photoconductors and Hole Transport Materials for Electro-Optical Applications, *Macromol Mater and Eng*, 2002, 287 (7) P 442-461
65. Giebeler, C.H., Antoniadis, D.D. Bradley, C., and Shirota, Y. (1999). Influence of the hole transport layer on the performance of organic light-emitting diodes. *J. Appl Phys*, 85(1) P 608-615
66. Mitschke, U and Bauerle, P, The electroluminescence of organic materials *J Mater Chem*, 2000 (10) P1471-1507
67. Ohishi, T., Sugi, R, Yokoyama, A., Yokozawa, T.A., variety of poly(m-benzamide)s with low polydispersities from inductive effect-assisted chain-growth polycondensation. *J Polym Sci A: Polym Chem*, 2006,(44) P 4990 - 5003.

68. Gallini, J., Polyamides, aromatic. Encyclopedia of polymer science and technology, 2005 New York: John Wiley & Sons.
69. Ozawa, S.K., *Handbook of fiber science and technology*. 1989, New York: Wiley.
70. Tanner, D.R.P., and Knoff, W.F., *Handbook of fiber science*. 1989, New York: Wiley.
71. Dihrab, S.S., and Sopian K., Electricity generation of hybridnPV/wind systems in Iraq, *Renew. Energy*, 2010. 35(6) P 1303- 1307
72. Paska, J.P.B., and Klos, M. , Hybrid power systems – An effective way of utilising primary energy sources, *Renew Energy*, 2009. 34(11) P 2414-2421.
73. Lash,T.D., Chandrasekar, P., Osuma, A.T., Chaney, S.T., and Spence, J.D., Porphyrins with Exocyclic Rings Synthesis and Spectroscopic Characterization of Highly Modified Porphyrin Chromophores with Fused Acenaphthylene and Benzothiadiazole Rings. *J Org Chem*, 1998. 63(23) P 8455- 8469.
75. [http://www.sc.doe.gov/bes/reports/files/SSL\\_rpt.pdf](http://www.sc.doe.gov/bes/reports/files/SSL_rpt.pdf) (September 2008)
76. Kamtekar, K.T., Recent Advances in White Organic Light-Emitting Materials and Devices (WOLEDs), *Adv Mater*, 2010. 22(5) P 572-582
77. Dupont, E.H.C., Buchanan, S., Chiu, M., and Gao, M. , Efficient GaAs light-emitting diodes by photon recycling , *Appl Phys Lett*, 2000. 76(1) P 4.
78. Humphreys, C.J., Solid-State Lighting, *MRS Bull*, 2008. 33(04) P 459-470.
79. Tang, C.W., and Jianmin, S.,<sup>1</sup> Doped organic electroluminescent devices with improved stability, *Appl Phys Lett*, 1997. 70(13) P 1665
80. Eom, S.H., *High efficiency blue and white phosphorescent organic light emitting devices*. 2010, Florida: UMI. .
81. Helfrich, W., and Schneider, W.G., Recombination Radiation in Anthracene Crystals , *Phys Rev Lett*, 1965. 14, P 229.
82. Adachi, C. Tsutsui, T., and Saito, S., Blue light-emitting organic electroluminescent devices *Appl Phys Lett*, 1990. 56(9) P 799-801
83. Tang, C.W., and Jianmin, S., Anthracene derivatives for stable blue-emitting organic electroluminescence devices *Appl Phys Lett*, 1987. 80(17) P 3201
84. Dodabalapur, A., Rothberg, L., and Miller, T.M., Electroluminescence from organic semiconductors in patterned microcavities, *Electron Lett.*, 1994, 30 (12), P 1000-1002
85. Diaz, F.R.,Moreno, J.T.,agle, L.H., Synthesis, characterization and electrical properties of polyimines derived from selenophene, *Synth Met*, 1997. 91(125).

86. Kido, J.N., Bright organic electroluminescent devices with double-layer cathode, *IEEE Trans Electron Devices*, 1993. 40(7) P 1342.
87. Mason, M.G. Hung, L.S. and Tang, C.W., Characterization of treated indium–tin–oxide surfaces used in electroluminescent devices *J Appl Phys*, 1999. 3(86) P 1688
88. Jabbour, G.E., Armstrong, N.R., and Peyghambarian, N., Aluminum based cathode structure for enhanced electron injection in electroluminescent organic devices *Appl Phys Lett*, 1998, 73 (9) P 1185-1187.
89. Koppe, M., Brabec, C.J. Sariciftci, N. S. Eichen, G. Nakhmanovich, E., Ehrenfreund, O., Epstein and Heiss, W., 2001.  $\text{Er}^{3+}$  emission from organic complexes embedded in thin polymer films. *Synth Met*, 121(1-3) P 1511-1512.
90. Sakamoto, Y.S., Miura, A., Fujikawa, H., Tokito, S., and Taga, Y., Synthesis, Characterization, and Electron-Transport Property of Perfluorinated Phenylene Dendrimers, *J Amer Chem Soc*, 2000. 122(8) P1832-1833
91. Ikai, M., Suzuki, T., and Taga, Y., Highly efficient phosphorescence from organic light-emitting devices with an exciton-block layer. *Appl Phys Lett*, 2001. 79 P 156-158.
92. Antoniadis, H.M. and Hsieh, B.R., Carrier deep-trapping mobility-lifetime products in poly(*p*-phenylene vinylene), *Appl Phys Lett*, 1994. 65(16) P 2030.
93. Kotorlenko, L. A. and Gardenina, A.P, 1971. Transmission of electronic effects of substituents in vinyl esters. *Theoretical and Experimental Chemistry* 4(4) P 279-283.
94. Tanaka, D.T.T., Chiba, T., and Watanabe, Novel Electron-transport Material Containing Boron Atom with a High Triplet Excited Energy Level, S., *J Chem Lett*, 2007. 36(2) P 262-263.
95. Adachi, C., Tsutsui, T, and Saito, S., Organic electroluminescent device having a hole conductor as an emitting layer *Appl Phys Lett*, 1989. 55(15) P1489-1491
96. Cava, M.P., and Deana, A.A., 1959. Condensed Cyclobutane Aromatic Compounds. VI. The Pyrolysis of 1,3-Dihydroisothianaphthene-2,2-dioxide: A New Synthesis of Benzocyclobutene. *J Amer Chem Soc* 81(16) P 4266-4268.
97. Goushi, K.B.J., Sasabe, H., and Adachi, C., J. Triplet exciton confinement and unconfinement by adjacent hole-transport layers, *Appl Phys*, 2004. 95(12) P 7798-7802.
98. Adachi, C., Forrest, S. Lamansky, M.E., and Thompson, R.C., High-efficiency red electrophosphorescence devices, *Appl Phys Lett*, 2001. 78(11) P 1622-1624.
99. Baldo, M.A., Thompson, M.E., and Forrest, S.R., 2000. High-efficiency fluorescent organic light-emitting devices using a phosphorescent sensitizer. *Nature*, 403(6771) P 750-753.

100. Meng, Z.L., *Organic Light Emitting Materials and Devices*. 2007, Boca Raton: Taylor and Francis Group.
101. Tokito, S.S.Y., Tsuzuki, T., and Sato, F., Confinement of triplet energy on phosphorescent molecules for highly-efficient organic blue-light-emitting devices, *Appl Phys Lett*, 2003. 83(3) P 569.
102. Zhao, H.C.T., and Thayumanavan, S., Design and synthesis of stable triarylamine for hole-transport applications, *Tetrahedron Lett*, 2001. 42(27), P 4421-4424.
103. Bellmann, E.S.E., Thayumanavan, S., Barlow, S., Grubbs, R.H., and Marder, New Triarylamine-Containing Polymers as Hole Transport Materials in Organic Light-Emitting Diodes: Effect of Polymer Structure and Cross-Linking on Device Characteristics, S.R., *Chem Mater*, 1998. 10(6), P 1668-1676.
104. Jiang, X.Y., Khan, M.A., and Zhu, White OLED with high stability and low driving voltage based on a novel buffer layer MoOx W.Q. , Phys, D: *Applied Phys*, 2007. 40(18) P 5553
105. Zhang, X., Liu W., Zhu, X., Jiang, X. and Zhang, Z., Obtaining highefficiency red electrophosphorescent OLEDs by changing the thickness of light-emitting layer, *Displays*, 2007. 28(3), 150-153
106. Shoustikov, A.A., Electroluminescence color tuning by dye doping in organic light-emitting diodes, *Journal of IEEE*, 1998. 4(1).
107. Baldo, M.A., High-efficiency fluorescent organic light-emitting devices using a phosphorescent sensitizer, *Nature*, 2000. 403(6771).
108. Sharada, D.S., Muresan, A.Z., Muthukumaran, K. and Lindsey J.S., 2005. Direct Synthesis of Palladium Porphyrins from Acyldipyrrromethanes. *J Org Chem*, **70**(9) P 3500-3510.
109. Segal, M., Baldo, M.A., Holmes, R.J., Forrest S.R., and Soos, Z.G. 2003. Excitonic singlet-triplet ratios in molecular and polymeric organic materials. *Physical Review B* 68(7) P 075211.
110. Andersson, P., and Berggren, M., Printable All-Organic Electrochromic Active-Matrix Displays, *Adv Funct Mater*, 2007. 17(16) P 3074-3082.
111. Krebs, F.C., All solution roll-to-roll processed polymer solar cells free from indium-tin-oxide and vacuum coating steps, *Org Electron*, 2009. 10(5), P 761-768.
112. Krebs, F.C., Wadstrom, M., and Pedersen M. S. , Manufacture, integration and demonstration of polymer solar cells in a lamp for the "Lighting Africa" initiative *Energy Environ Sci*, 2010. 3 P 512-525.
113. Krebs, F.C., Fabrication and processing of polymer solar cells: A review of printing and coating techniques, *Energ Mat Sol*, 2009. 93 P 394-412.
114. Krebs, F.C., Roll-to-roll fabrication of monolithic large-area polymer solar cells free from indium-tin-oxide, *Sol Energy Mater Sol Cells* (2009) 93 P 1636-1641.

115. Krebs, F.C., A roll-to-roll process to flexible polymer solar cells: model studies, manufacture and operational stability studies, *Mater Chem*, 2009. 19 P 5442-5451.
116. Krebs, F.C., Upscaling of polymer solar cell fabrication using full roll-to-roll processing. *Nanoscale*, 2010. 2 P 873-886.
117. Krebs, F.C., Upscaling of polymer solar cell fabrication using full roll-to-roll processing *ACS Applied Mater Inter*, 2010. 2(6) P 873-886.
118. Barr, M.C., Chelawat, H., Ozaydin-Ince, G., Petruczuk, C.D., Sreenivasan, R., Tenhaeff, W.E., Trujillo, N.J., Vaddiraju, S., and Gleason, K.K. , Development of hybrid organic-inorganic light emitting diodes using conducting polymers deposited by oxidative chemical vapor deposition process, *Adv Mater*, 2010. 22 P 1993.
119. Someya, T.S., Effect of pentacene–dielectric affinity on pentacene thin film growth morphology in organic field-effect transistors, *Adv Mater*, 2010. 22 P2228
120. Choi J.H., Choi, S.J., and Lee, H.H. , Whole device printing for full colour displays with organic light emitting diodes, *Nanotechnology*, 2006. 17(9) P 2246.
121. Mason, M.G., Lee, S.T., Wong, K.W., and Wang, M., Characterization of treated indium–tin–oxide surfaces used in electroluminescent devices, *J Applied Phys*, 1999. 86(3) P1688.
122. Naka, S., and Tsutsu, T., High electron mobility in bathophenanthroline *Applied Physics Letters*, 2000. 76(2) P197.
123. Wenthold, P.G., Hrovat, D.A., Weston, B., Thatcher, and Lineberger, W.C., Transition-State Spectroscopy of Cyclooctatetraene. *Science*, 1996.272(5267) P 1456-1459.
124. Pope, M., Electroluminescence in Organic Crystals, *J Chem Phys*, 1963. 38(8) P 2042.
125. Turro, N.J., *Modern Molecular Photochemistry*, 1991, New York: Wiley.
126. Menczel, J.D.P., *Thermal analysis of polymer, fundamentals and applications*, 2009, New York: Wiley.
127. Wendlandt, W., *Thermal Analysis*, 1986, New York: Wiley.
128. Liou, G.S., Blue-light-emitting and anodically electrochromic materials of new wholly aromatic polyamides derived from the high-efficiency chromophore 4,4'-dicarboxy-4''-methyltriphenylamine, *Polym Sci Part A: Polym Chem*, 2006. 44(13) P 4095-4107.
129. Oishi, Y., Imai, Y., Novel synthetic methods for condensation polymers using silylated nucleophilic monomers. *Prog Polym Sci*, 1989 14 (93) P 173.
130. Rozhkov, V.V., Khajepour, M., and. Vinogradov, S.A., 2003. Luminescent Zn and Pd Tetranaphthaloporphyryns. *Inorg Chem*, 42(14) P 4253-4255.

131. Selby, T.D., and Blackstock S.C., Patterned Redox Arrays of Polyarylamines I. Synthesis and Electrochemistry of a *p*-Phenylenediamine and Arylamino-Appended *p*-Phenylenediamine Arrays, *Chem Mater*, 2002. 14(4) P 1685-1690.
132. Leeuw, D.M., and Einerhand, R.E., Stability of n-type doped conducting polymers and consequences for polymeric microelectronic devices, *Synth Met*, 1997. 87(1) P 53-59.



## LIST OF PUBLICATIONS

1. Azhar Kamil Rashid, Rosiyah Binti Yahya and Phang Sook Wai, Synthesis, Characterization, Effect of Triaryl Ring Substituents Groups on Thermal and Spectral Properties of New Soluble Triphenylamine-Based Aromatic Polyamides, *Asian Journal of Chemistry*, 2014, 26(1), P 85-92.
2. Azhar Kamil Rashid, Rosiyah Binti Yahya and Phang Sook Wai, Synthesis of Spectral, Thermal and Electrochemical Properties of New Thermally Stable Blue Light Emitting Materials Based Aromatic Polyamides, *Asian Journal of Chemistry*, 2014, 26(13), P 3854-3862

## APPENDICES

### Appendix A: FTIR spectra for synthesized compounds

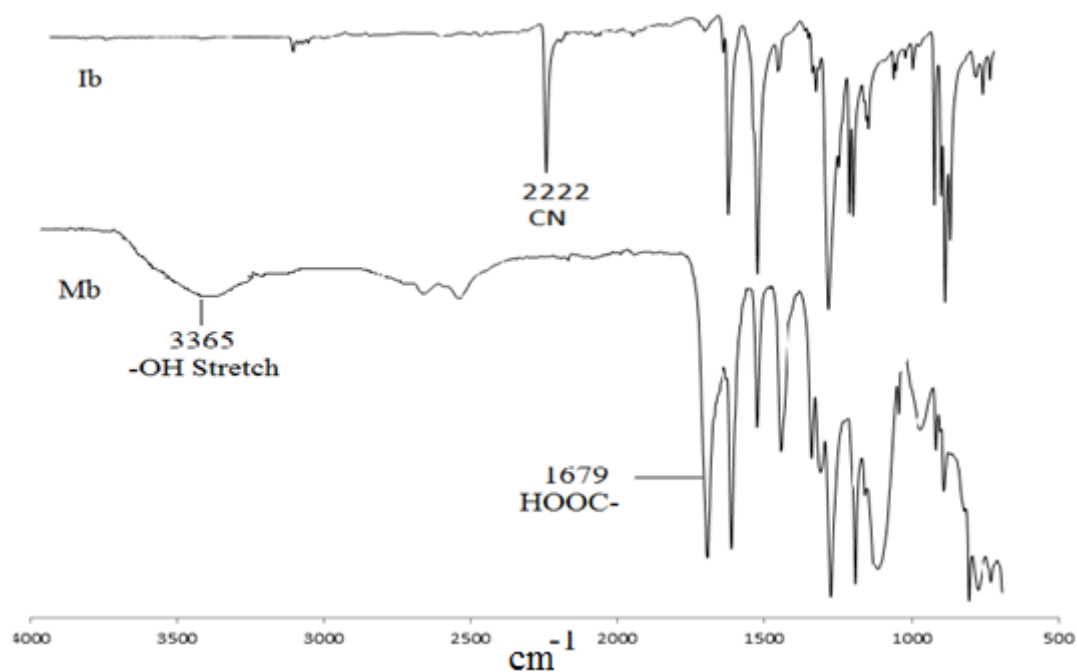


Figure 1: FTIR spectra for Ib, Mb

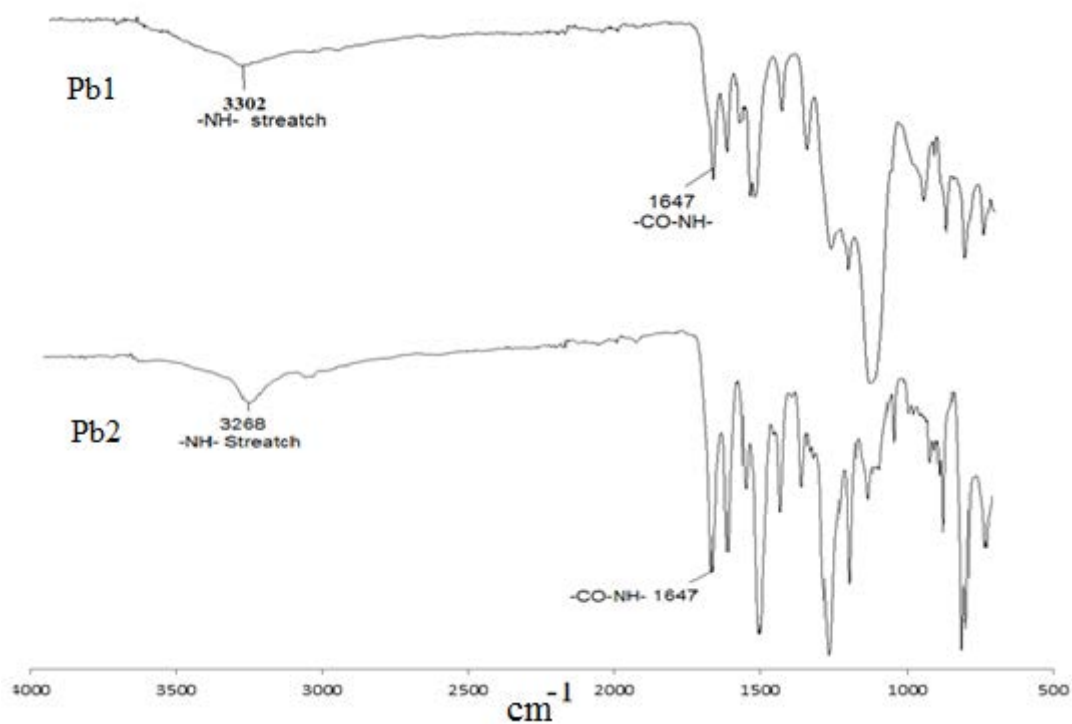
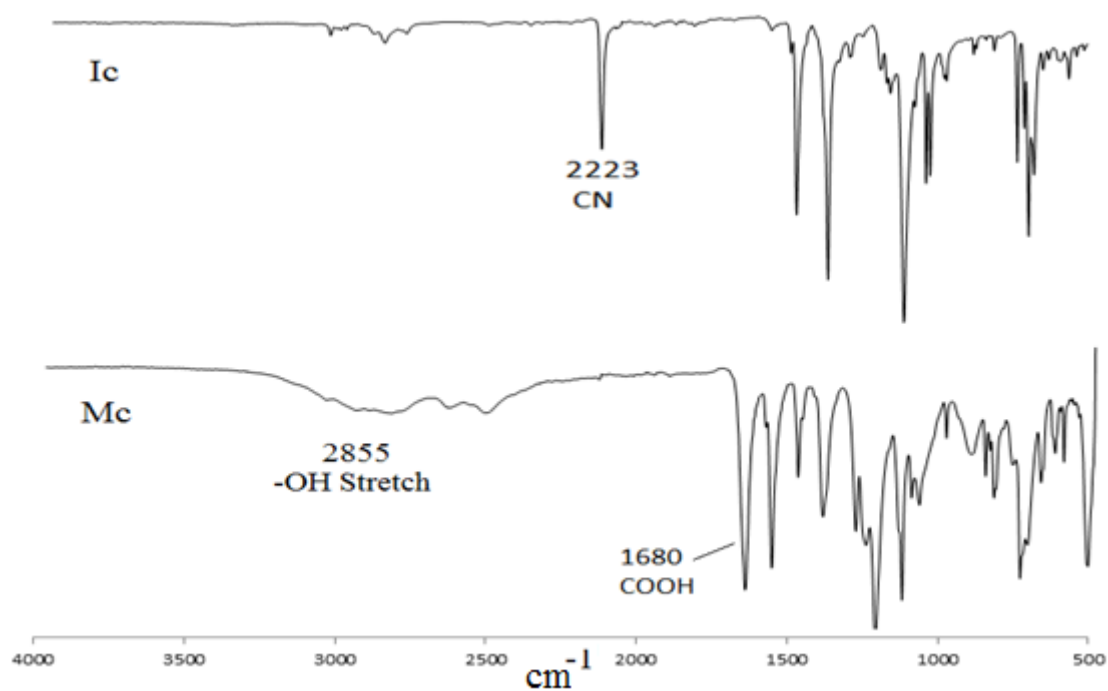
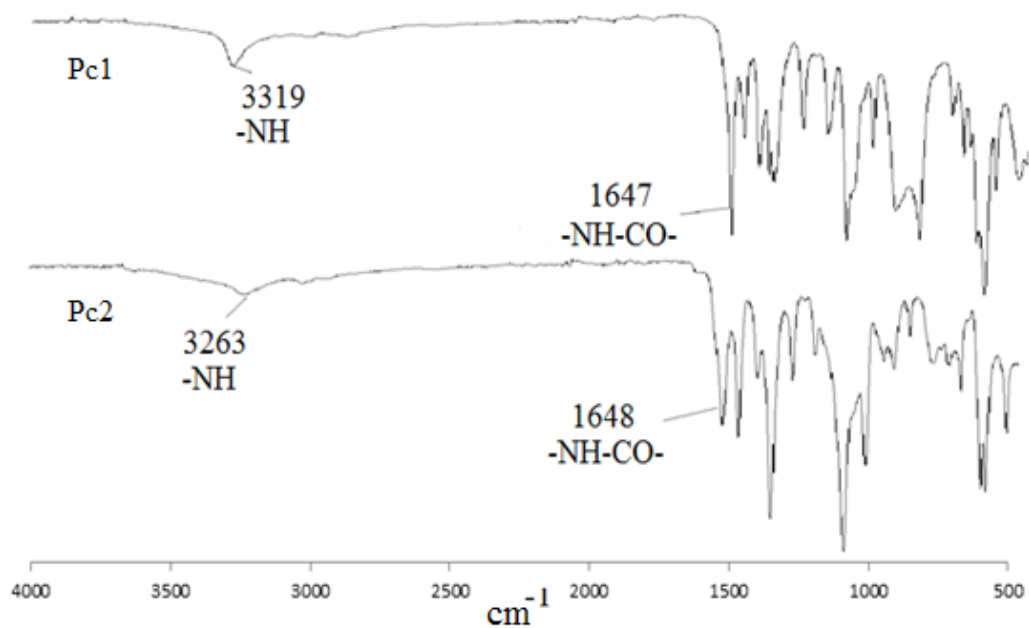


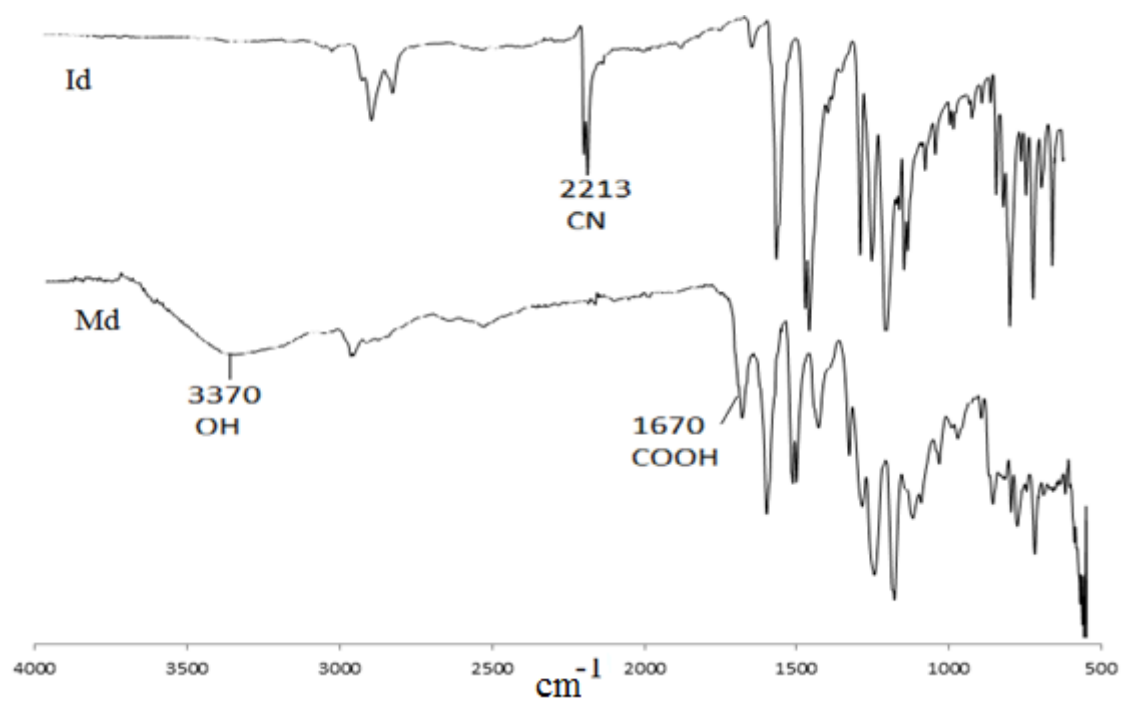
Figure 2: FTIR spectra for Pb1, Pb2



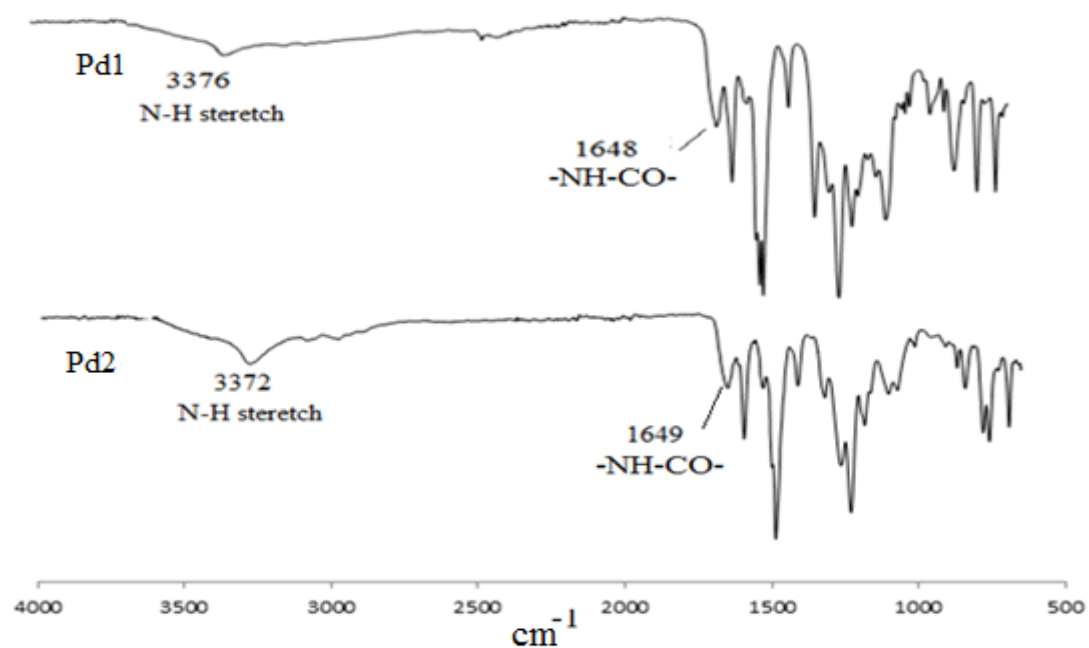
**Figure 3:** FTIR spectra for **Ic**, **Mc**



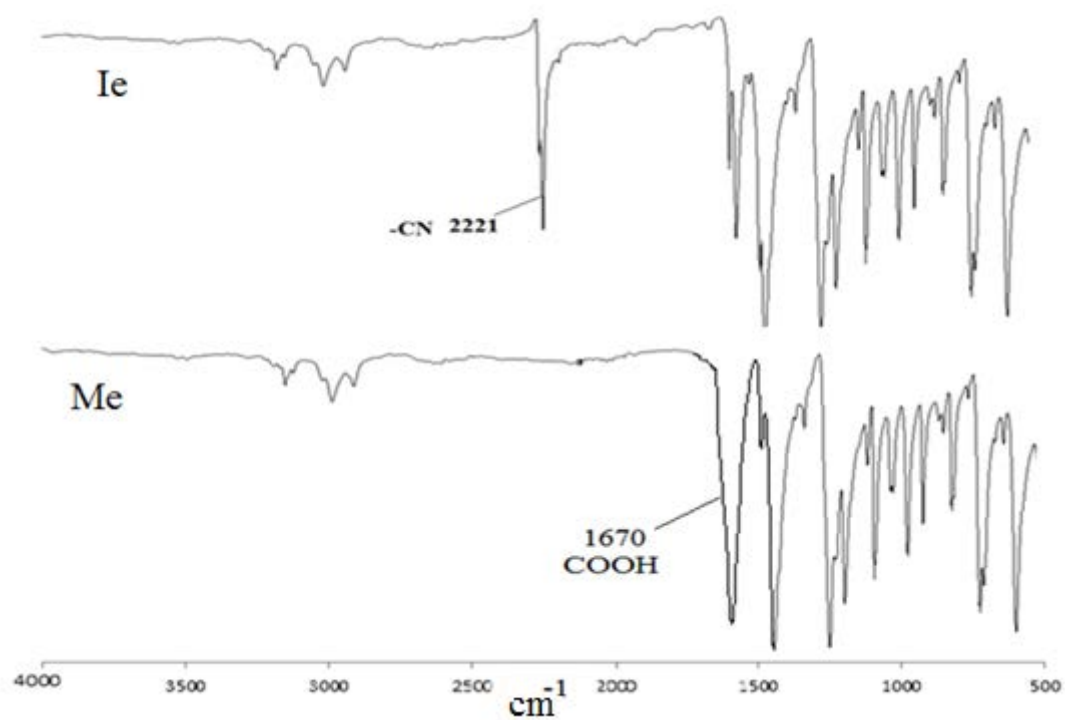
**Figure 4:** FTIR spectra for **Pc1**, **Pc2**



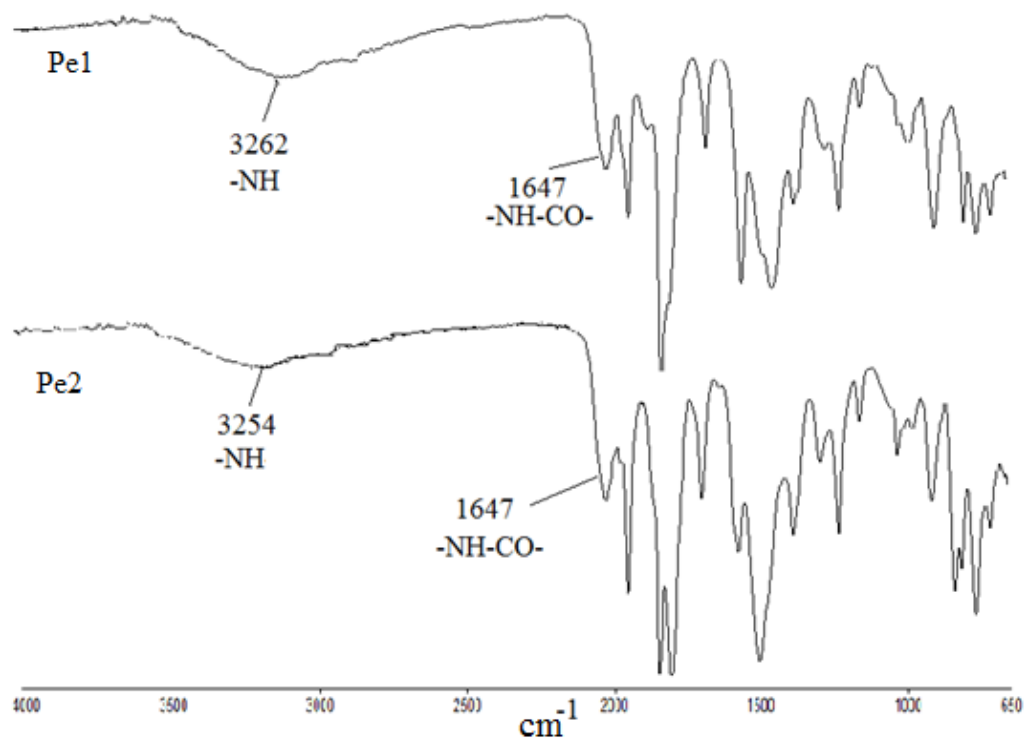
**Figure 5:** FTIR spectra for **Id, Md**



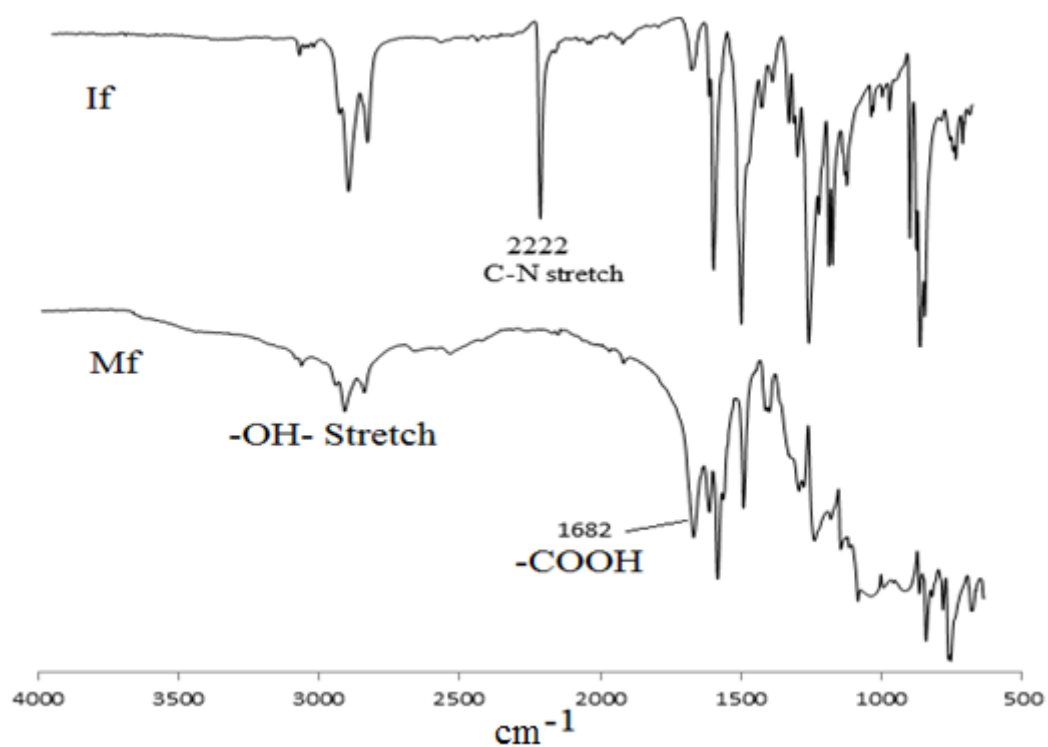
**Figure 6:** FTIR spectra for **Pd1, Pd2**



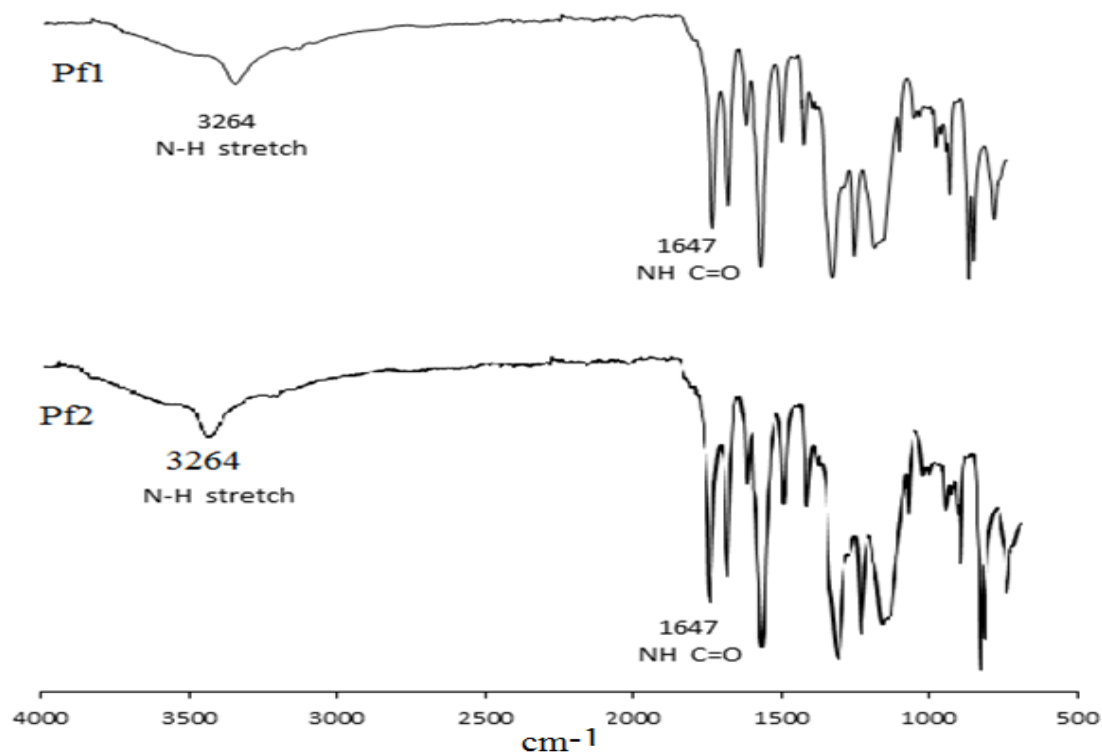
**Figure 7:** FTIR spectra for **Ie** , **Me**



**Figure 8:** FTIR spectra for **Pe1**, **Pe2**

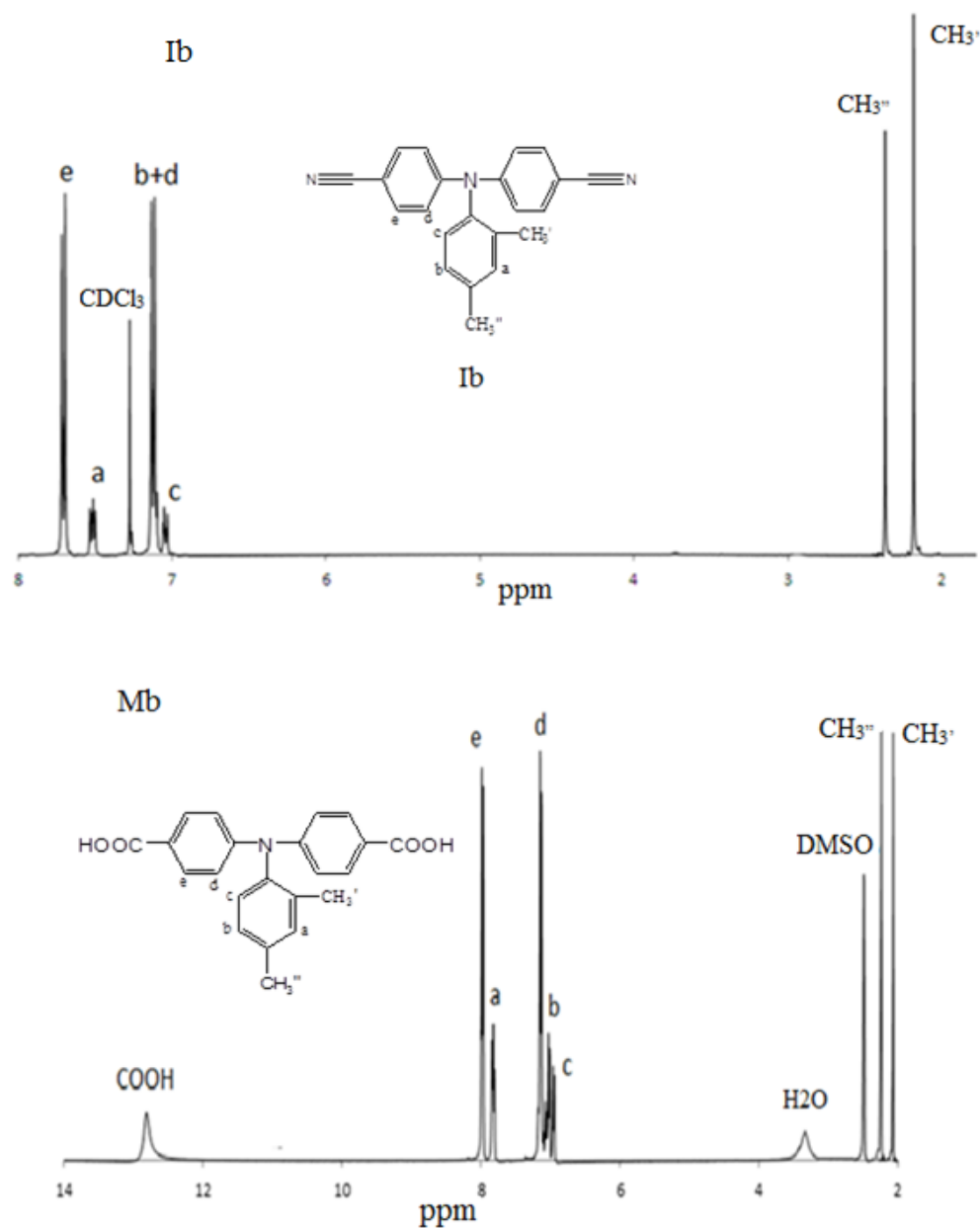


**Figure 9:** FTIR spectra for If, Mf

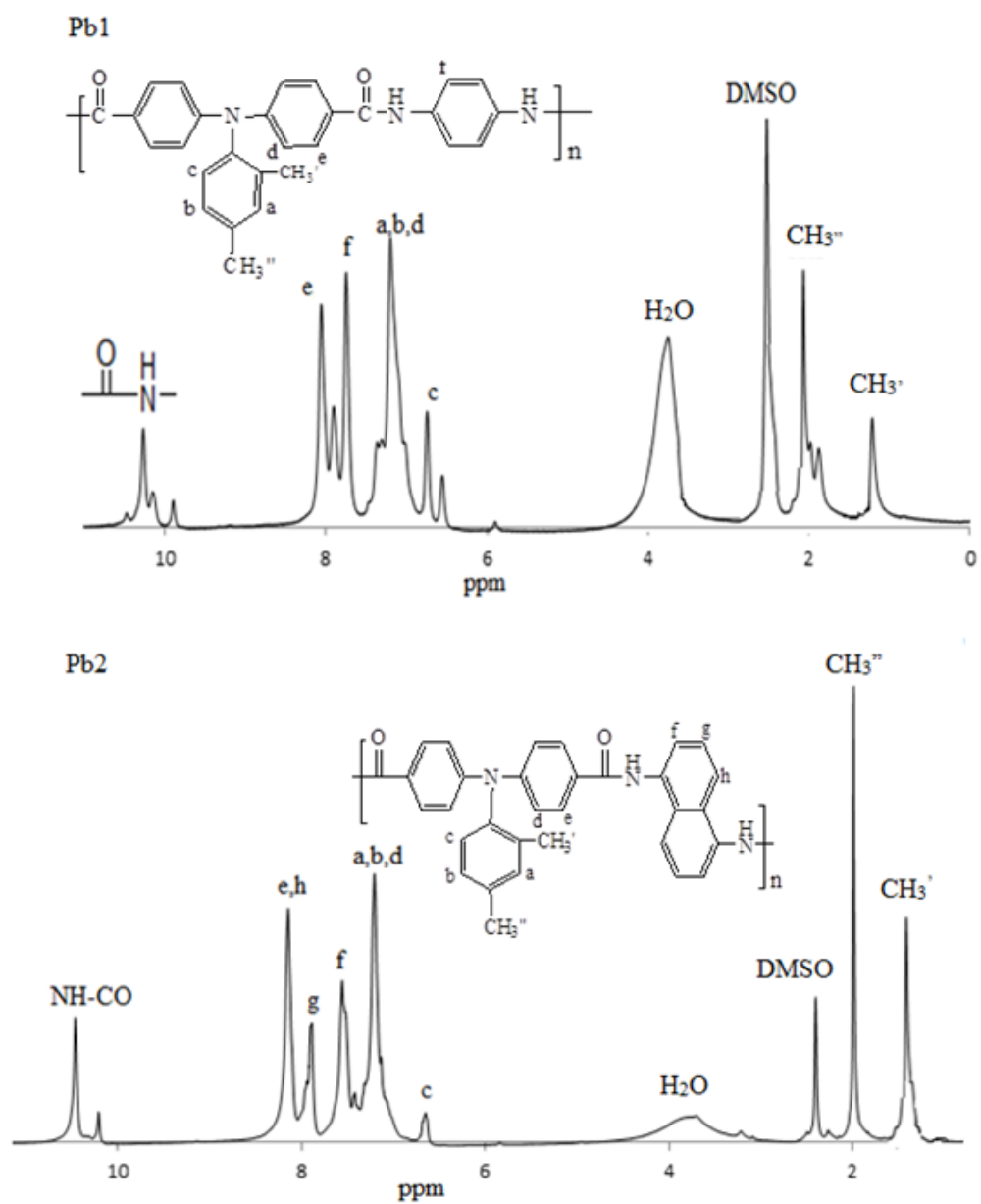


**Figure 10:** FTIR spectra for Pf1, Pf2

Appendix B:  $^1\text{H}$  and  $^{13}\text{C}$ - NMR spectra for synthesized compounds

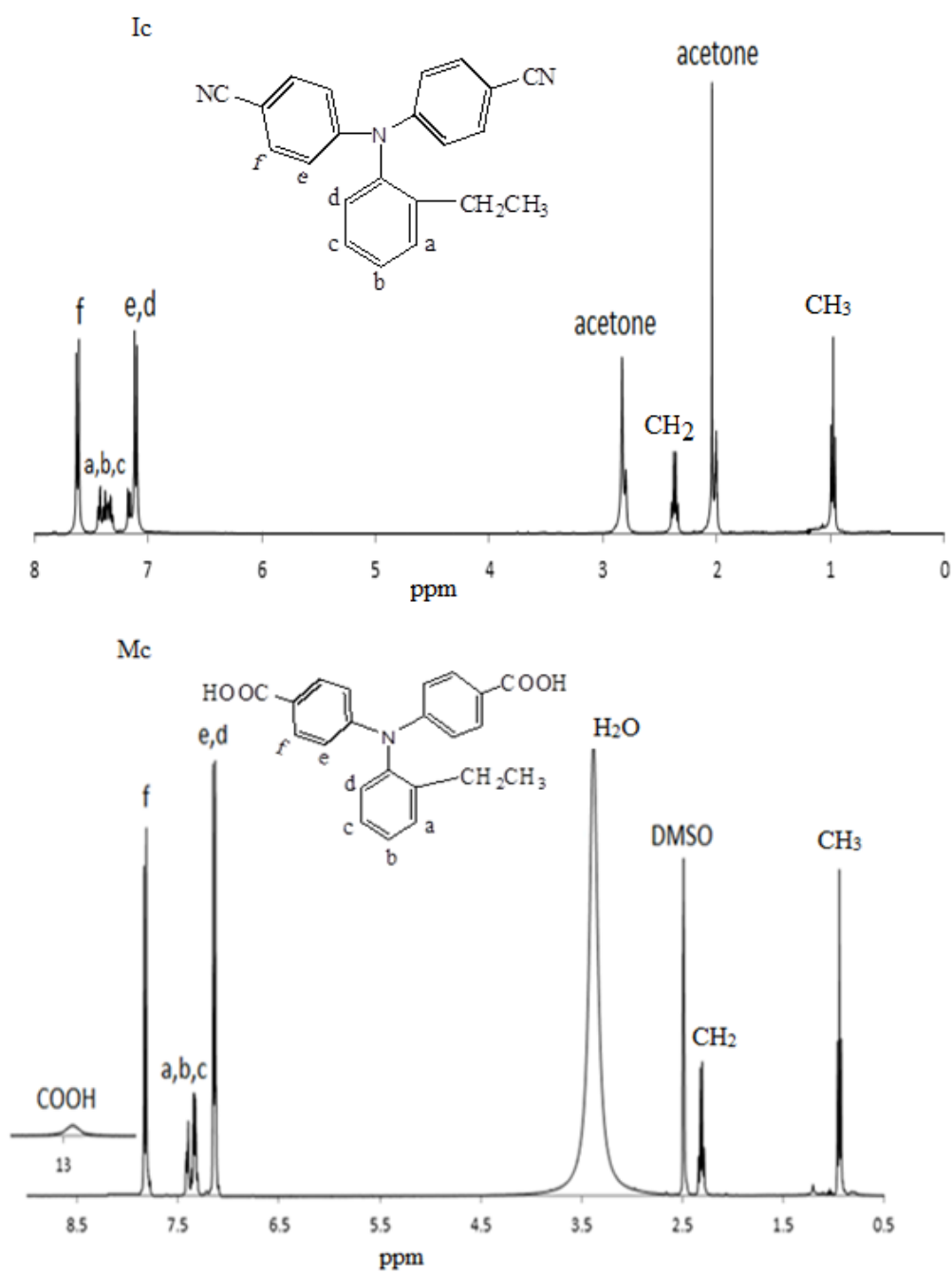


**Figure 1:**  $^1\text{H}$  NMR spectra for **Ib**, **Mb**

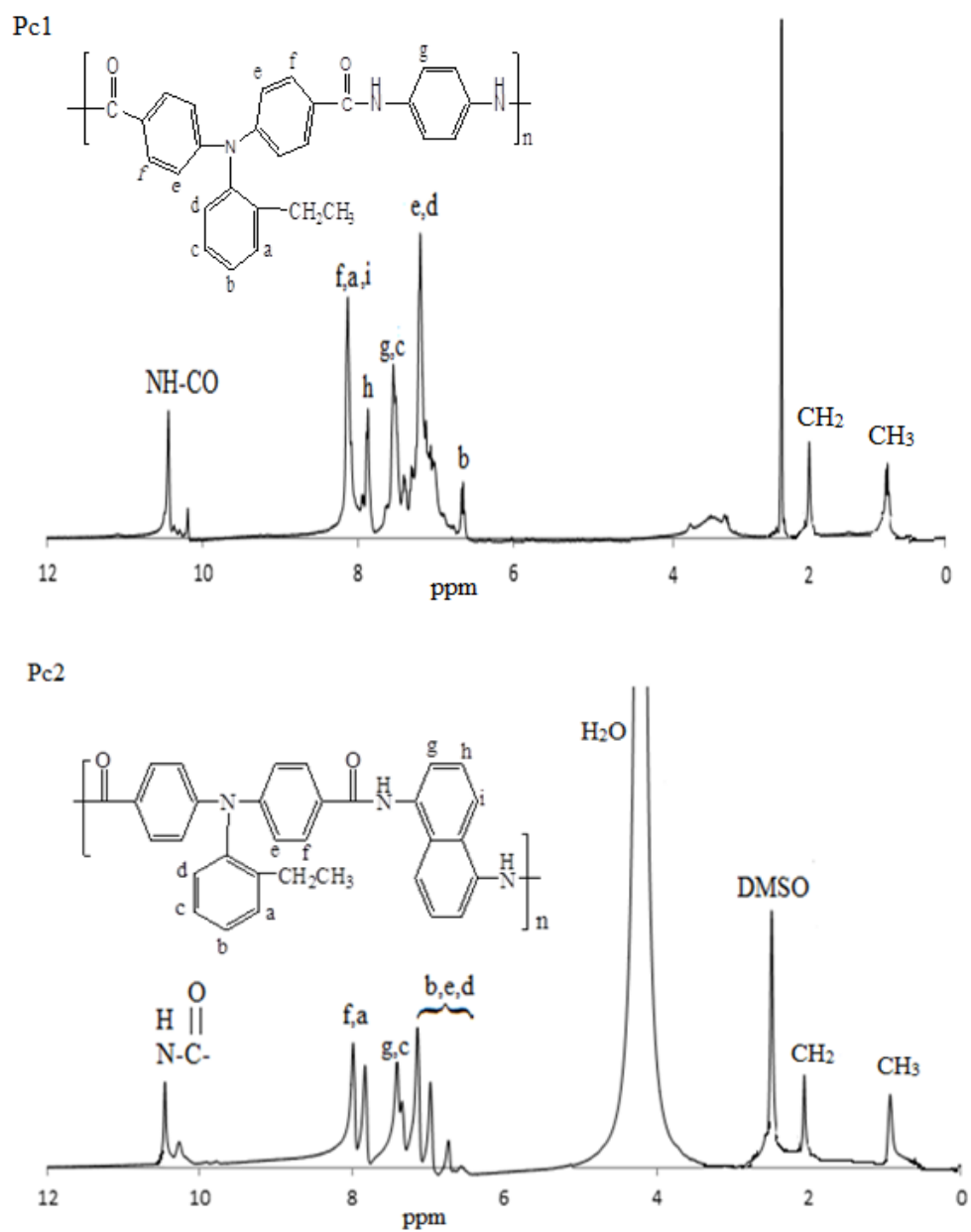


**Figure 2:**  $^1\text{H}$  NMR spectra for **Pb1**, **Pb2**

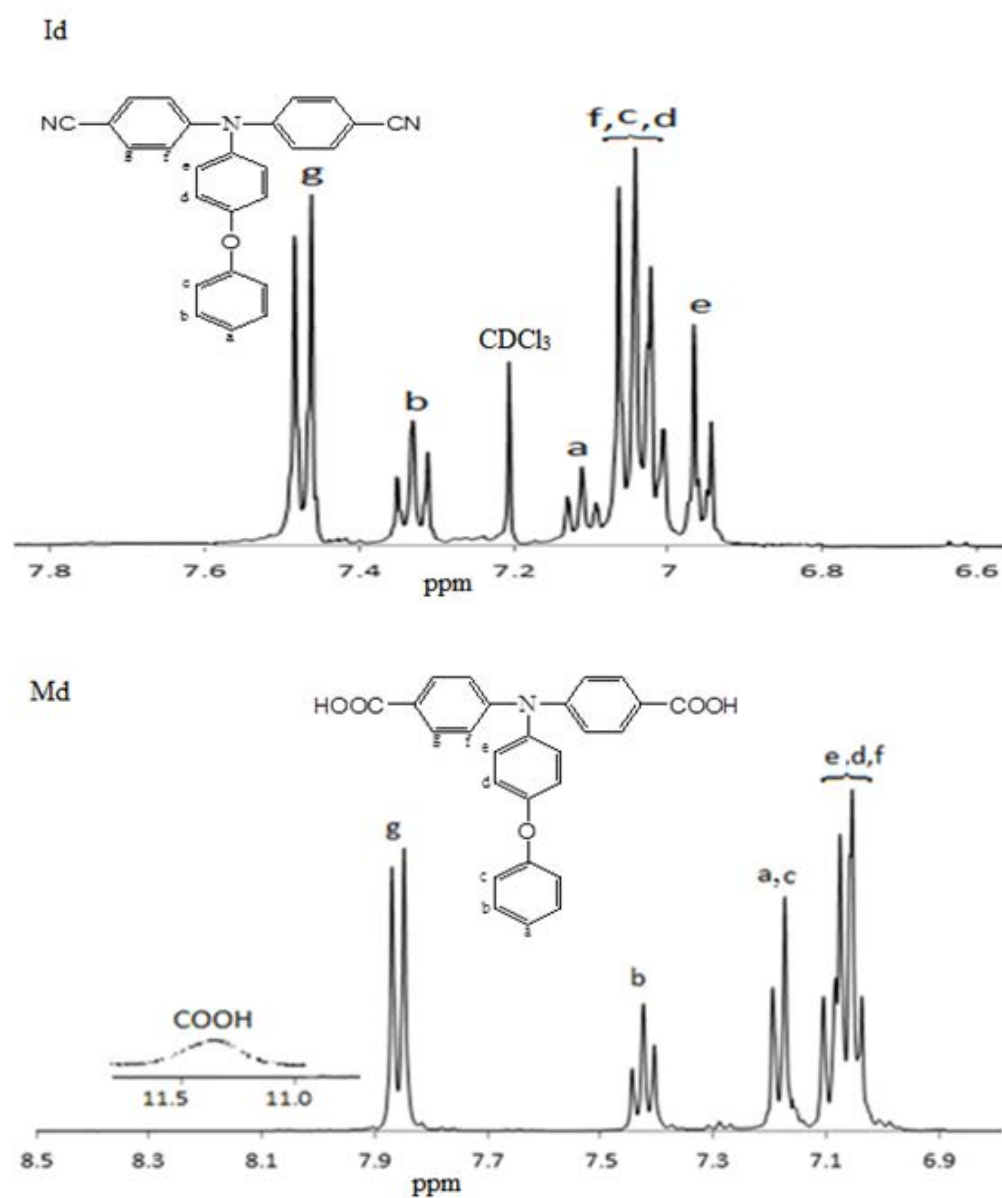




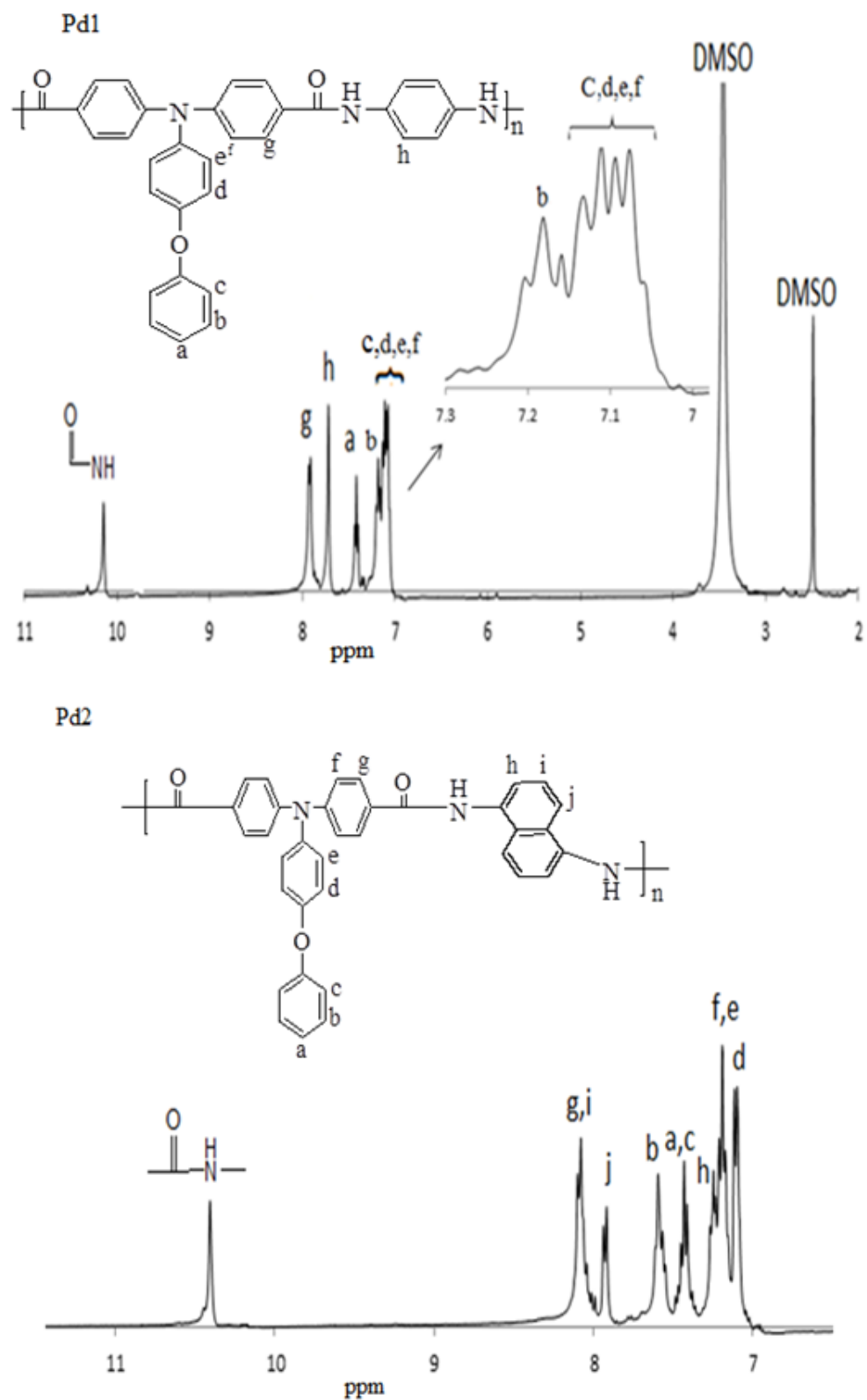
**Figure 3:**  $^1\text{H}$  NMR spectra for **Ic**, **Mc**



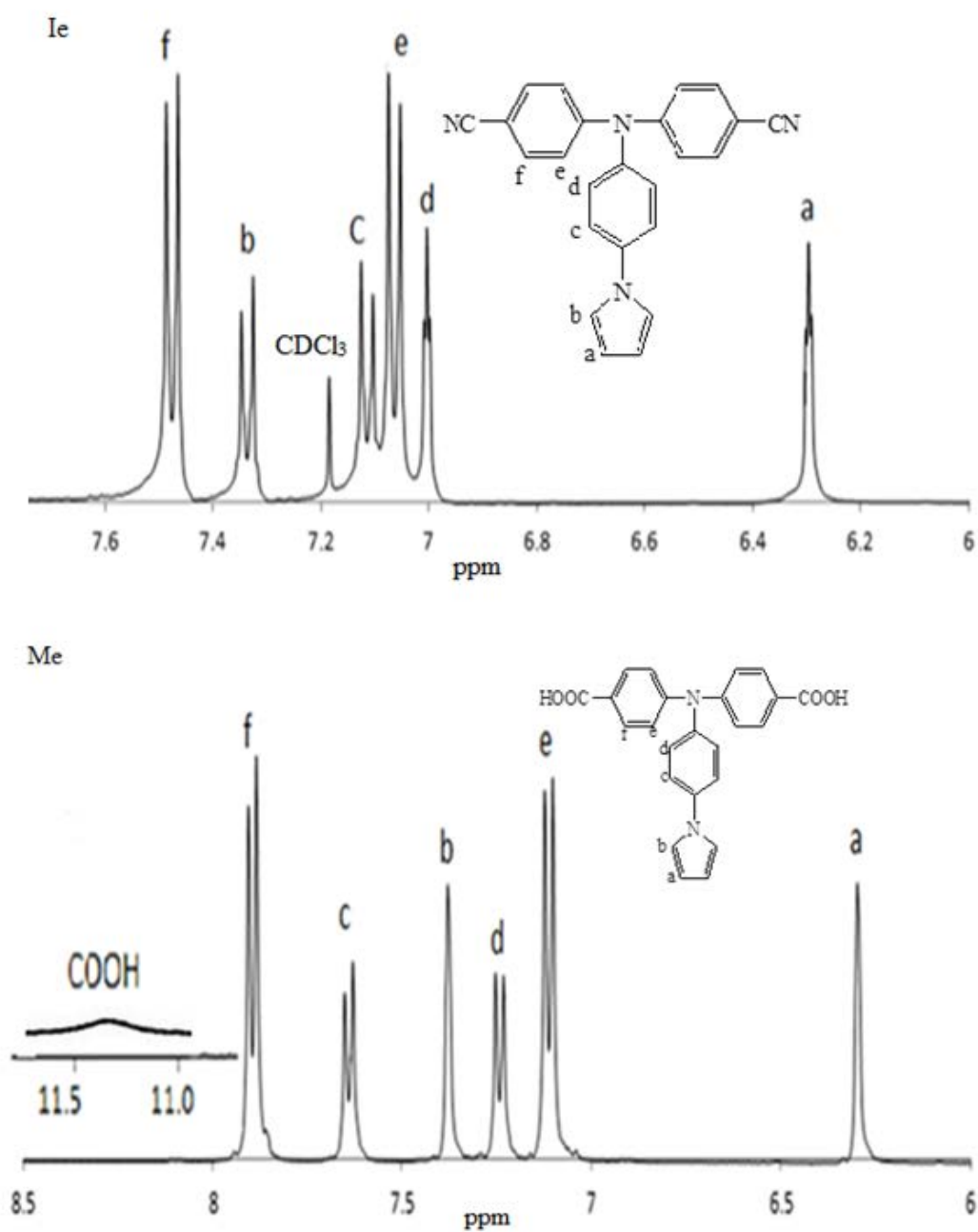
**Figure 4:**  $^1\text{H}$  NMR spectra for **Pc1**, **Pc2**



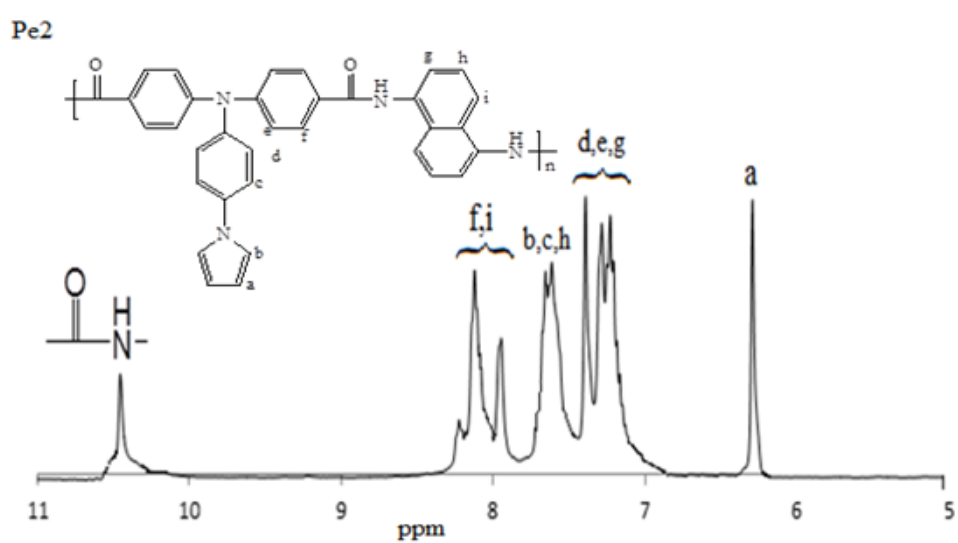
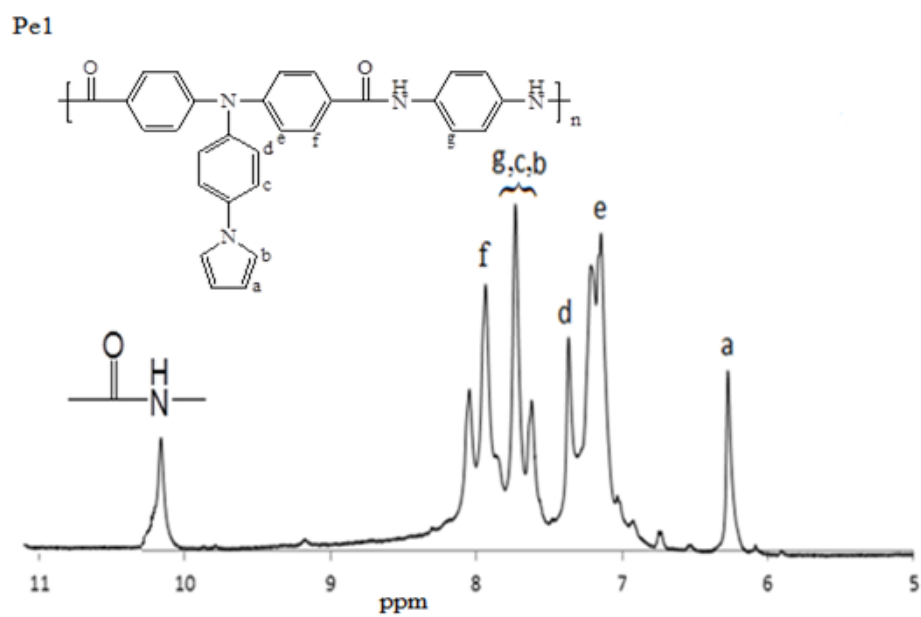
**Figure 5:** <sup>1</sup>H NMR spectra for **1d**, **Md**



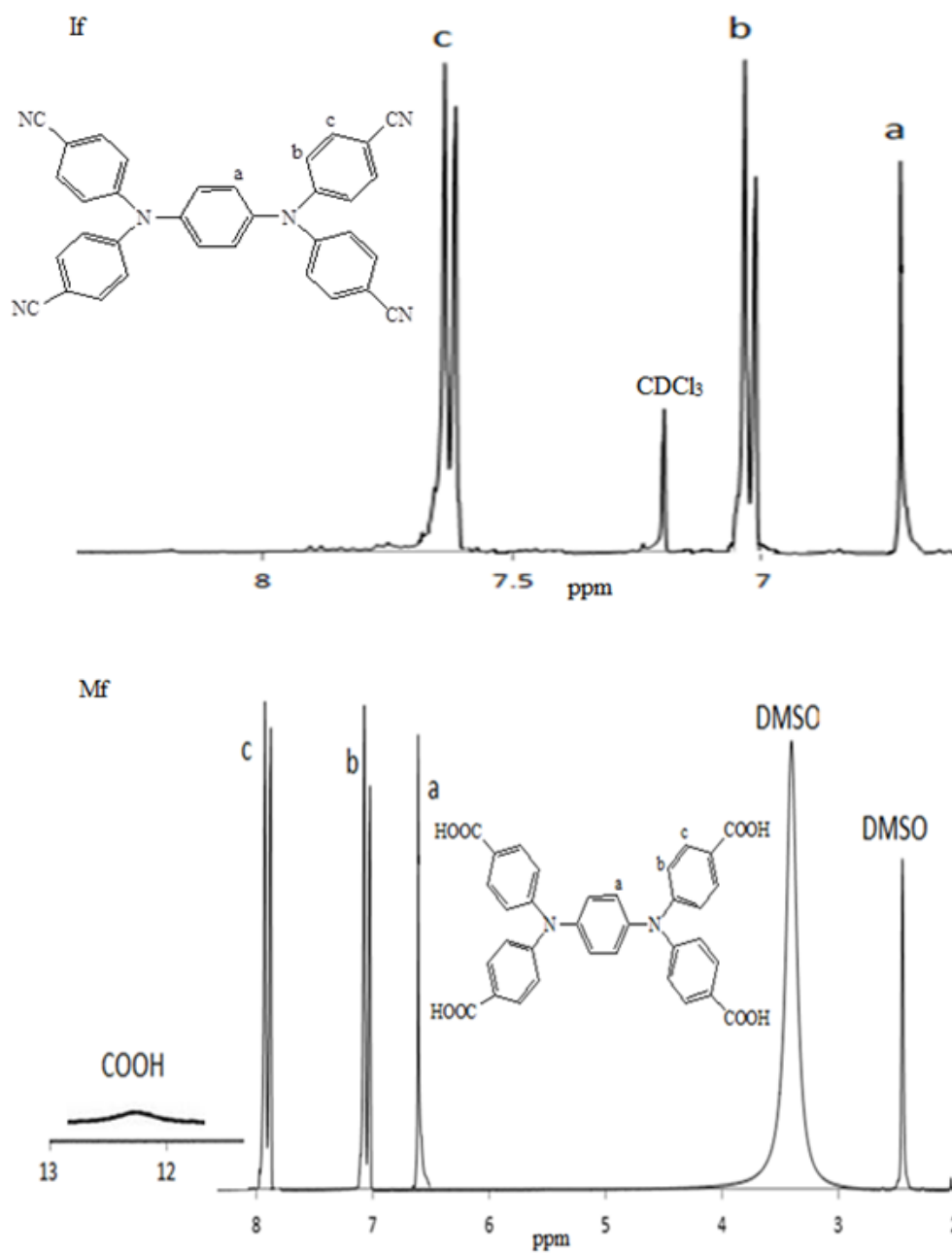
**Figure 6:**  $^1\text{H}$  NMR spectra for **Pd1**, **Pd2**



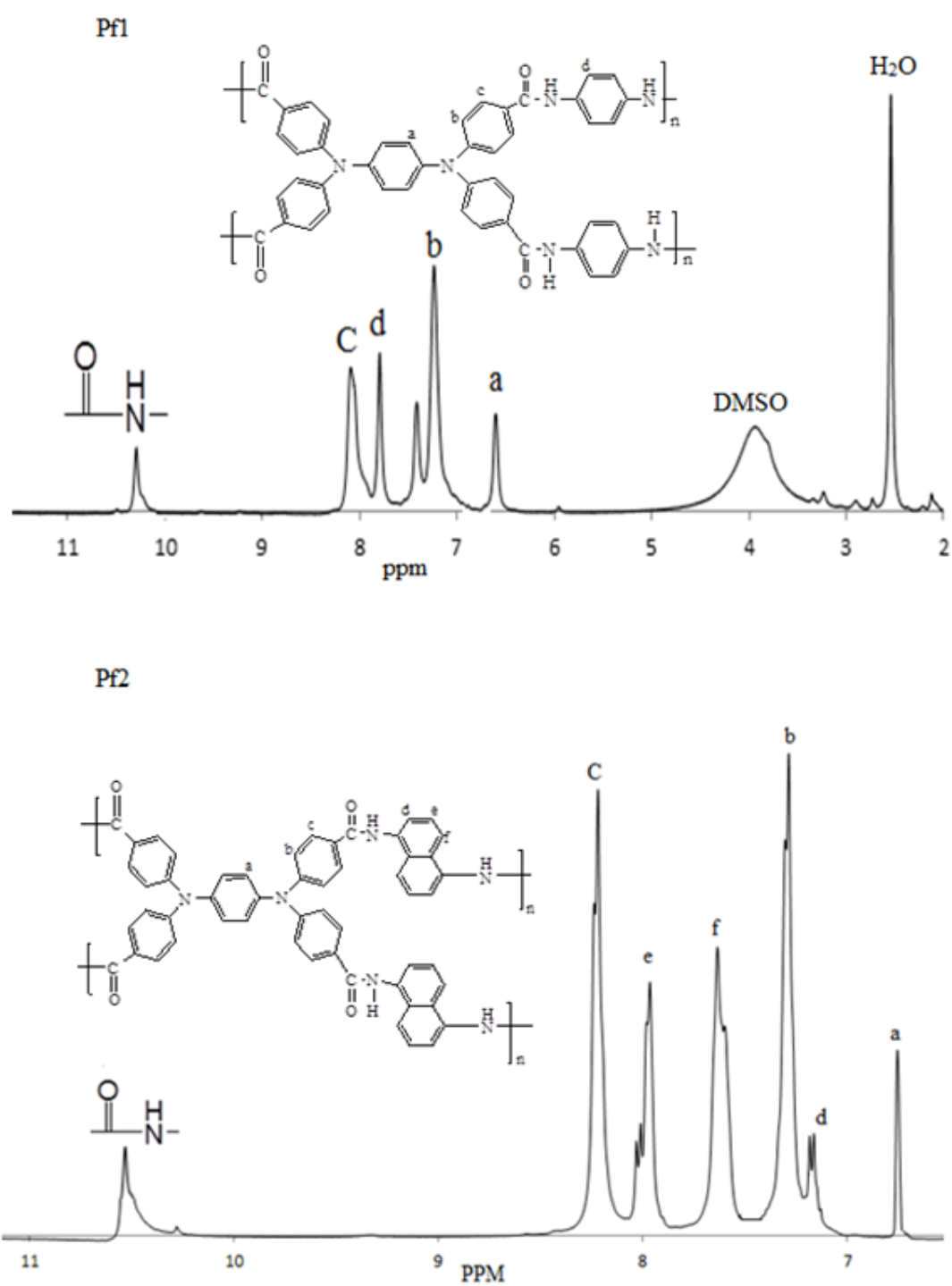
**Figure 7:** <sup>1</sup>H NMR spectra for **Ie**, **Me**



**Figure 8:**  $^1\text{H}$  NMR spectra for **pe1**, **Pe2**

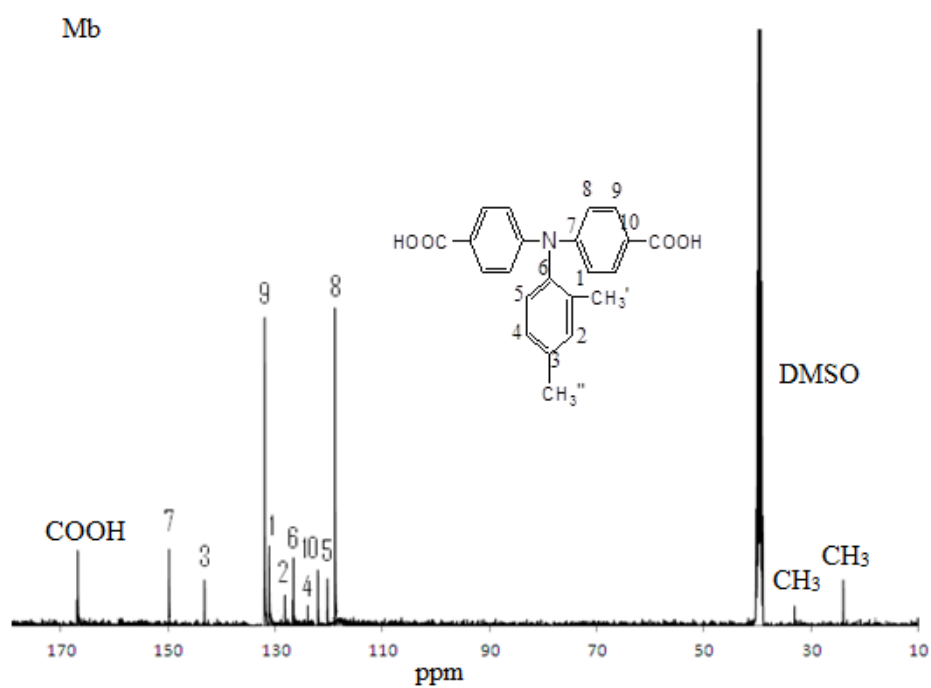
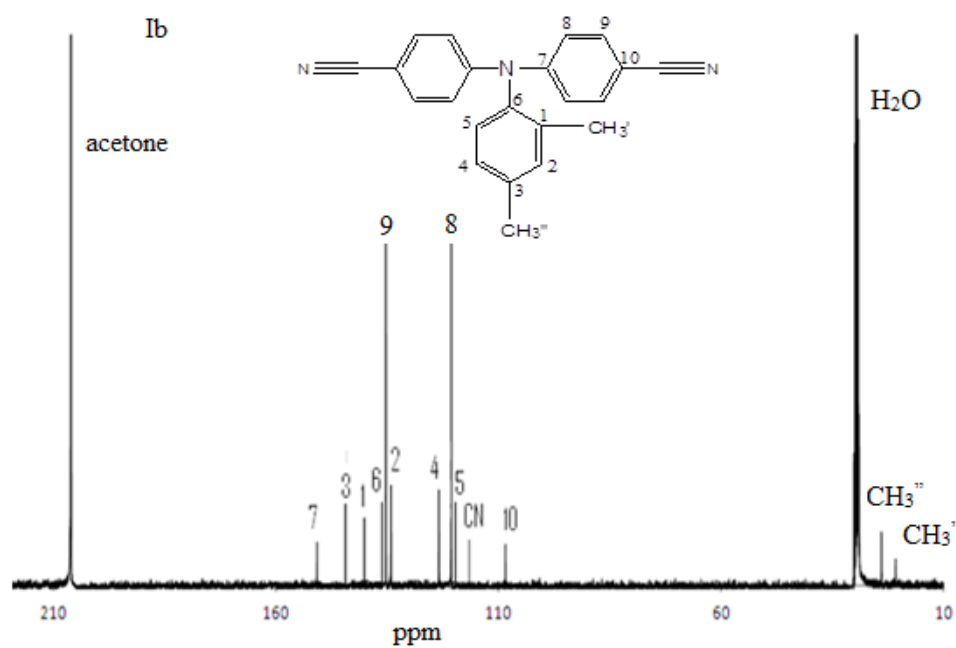


**Figure 9:**  $^1\text{H}$  NMR spectra for **If**, **Mf**

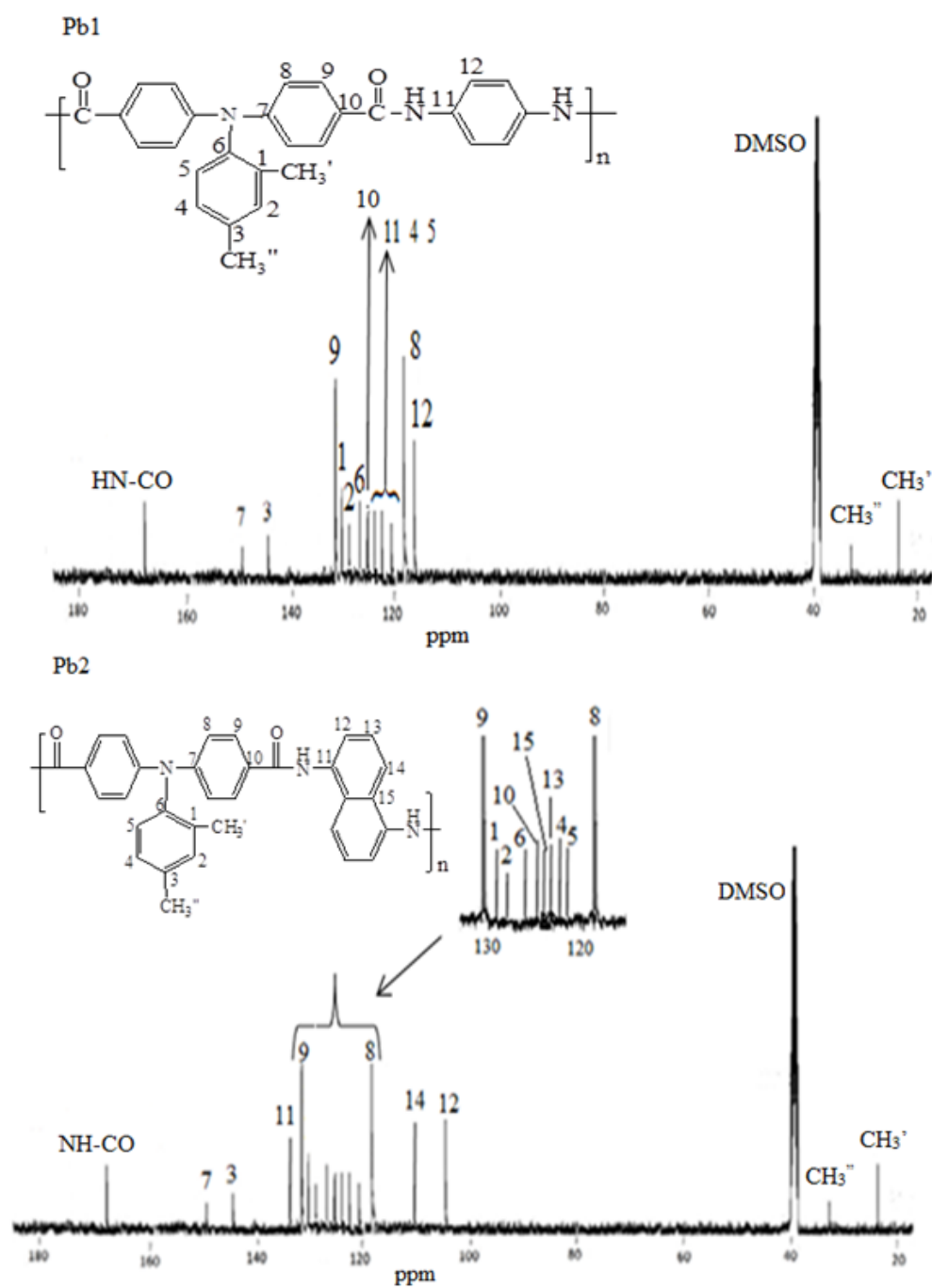


**Figure 10:**  $^1\text{H}$  NMR spectra for **Pf1**, **Pf2**

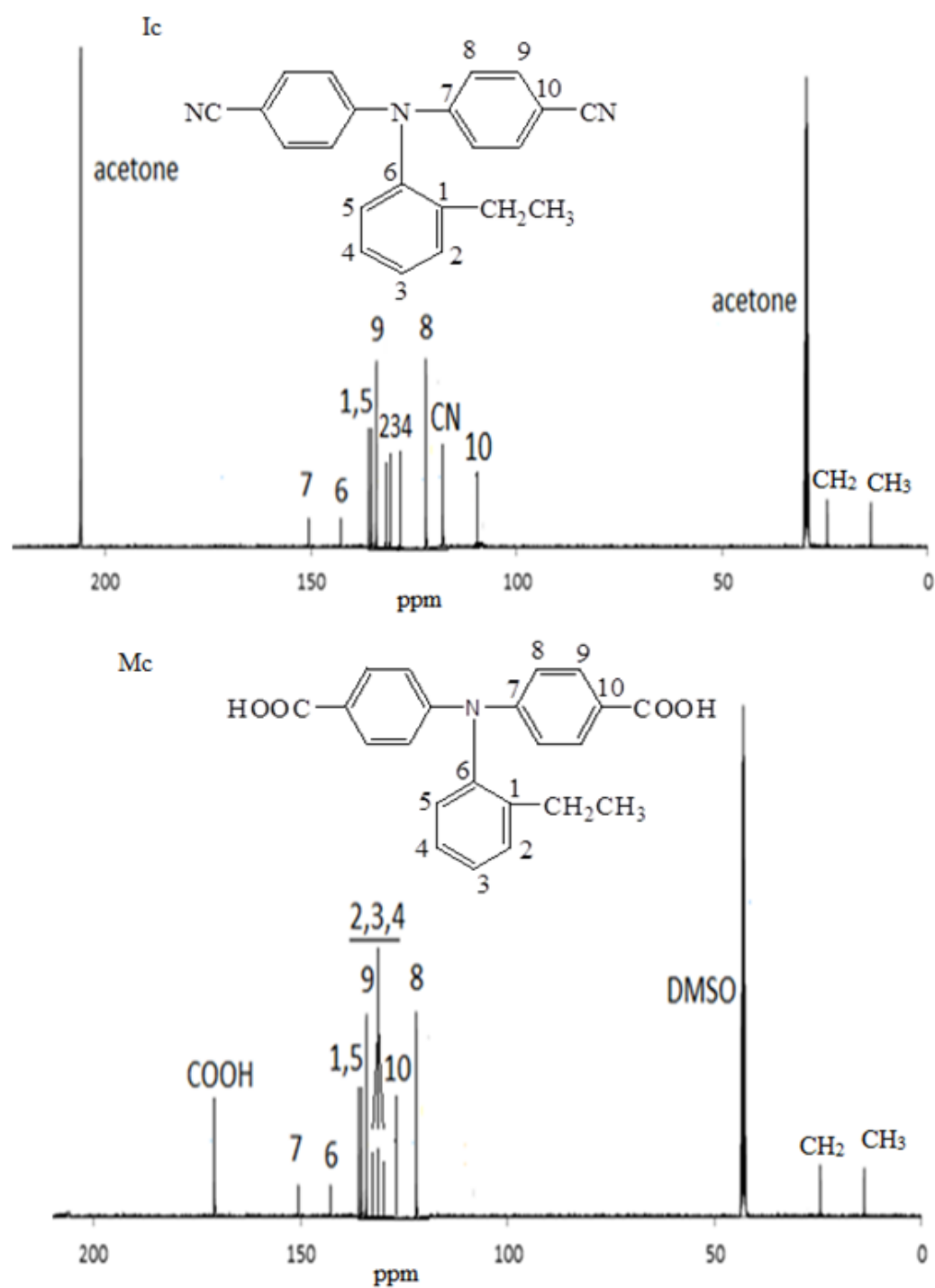




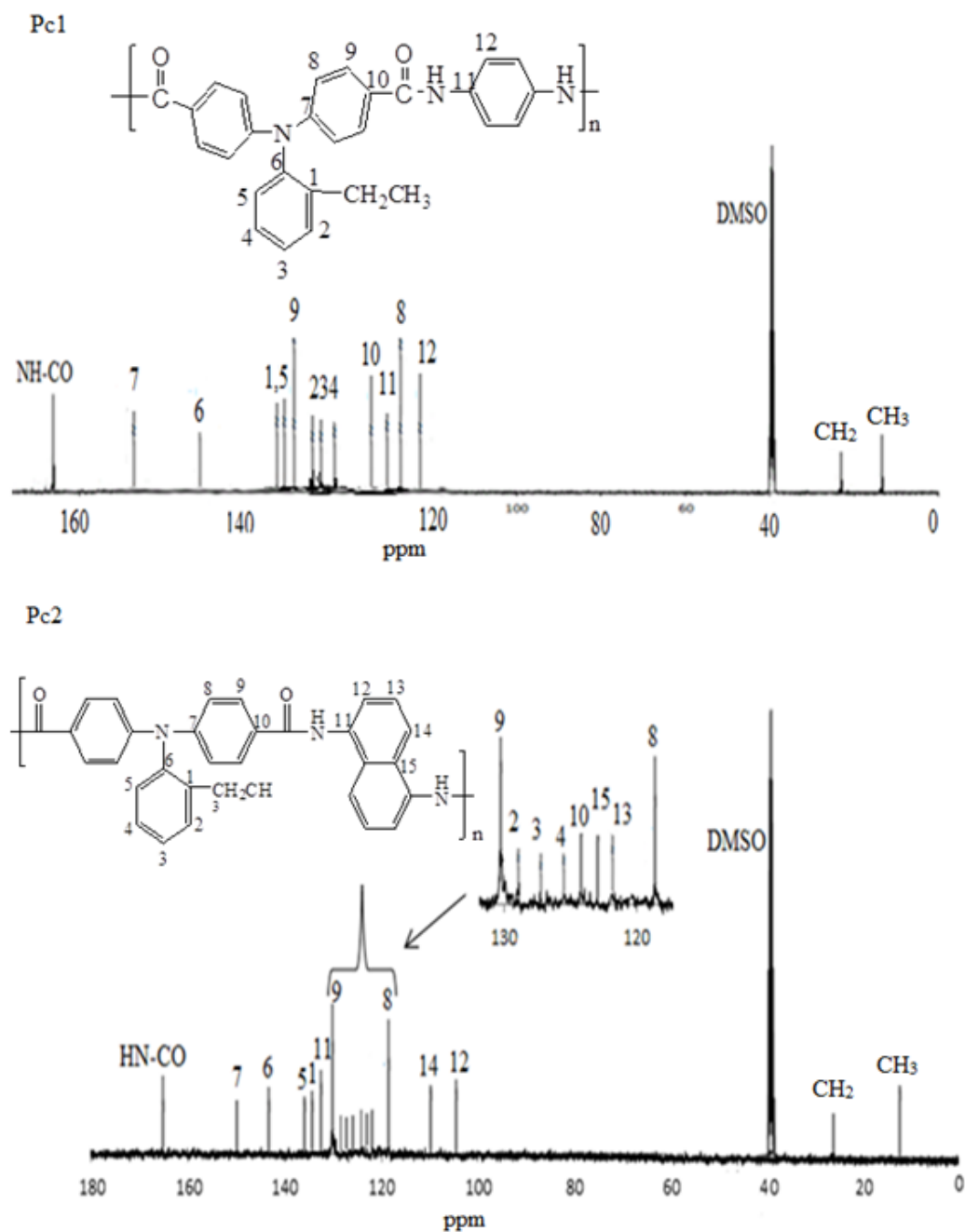
**Figure 11:** <sup>13</sup>C NMR spectra for **Ib**, **Mb**



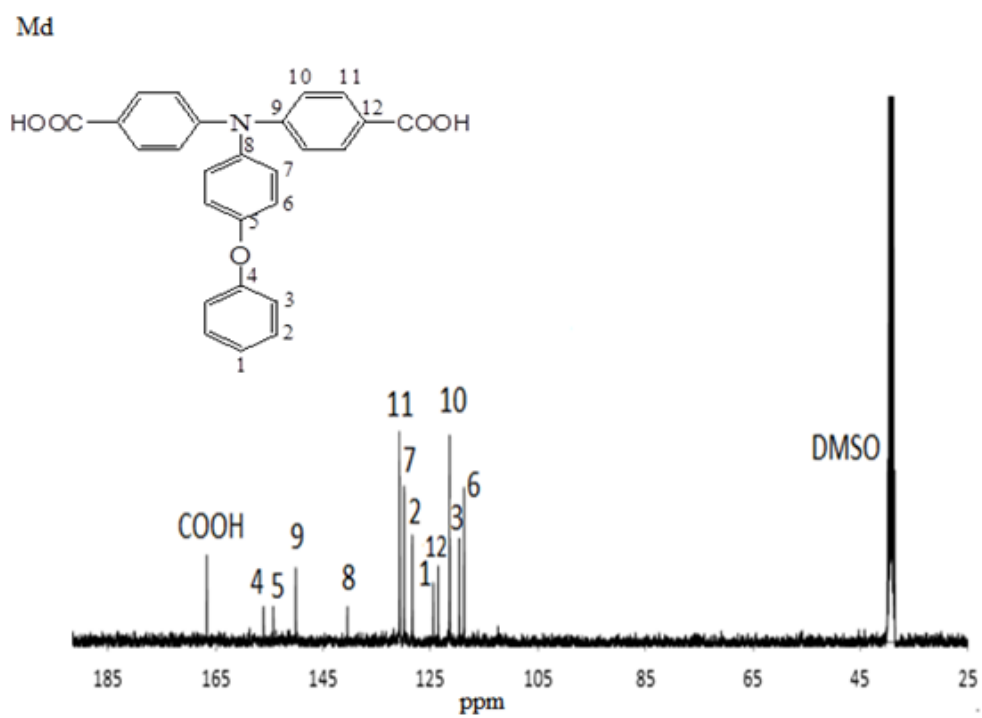
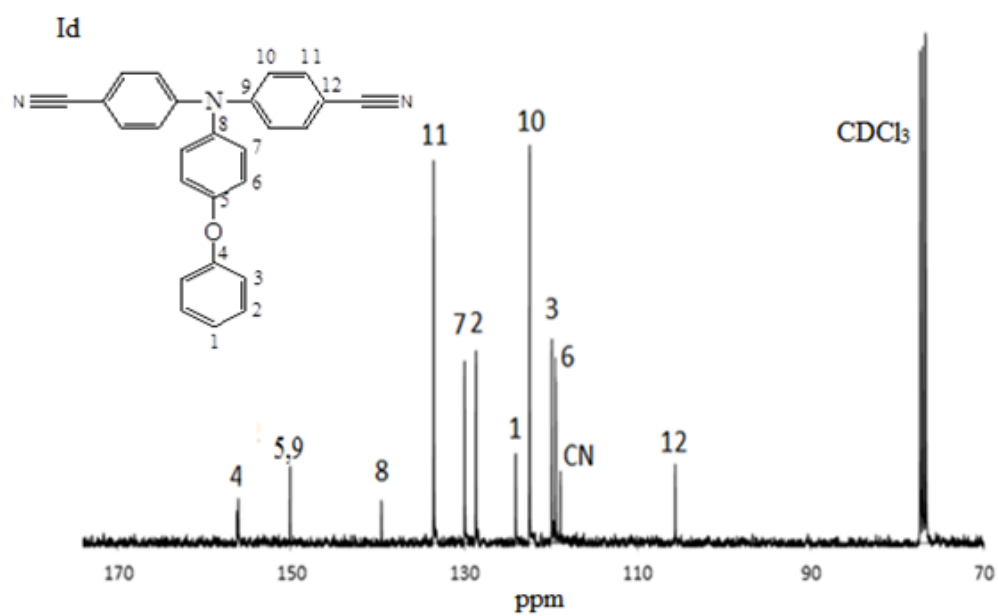
**Figure 12:**  $^{13}\text{C}$  NMR spectra for **Pb1**, **Pb2**



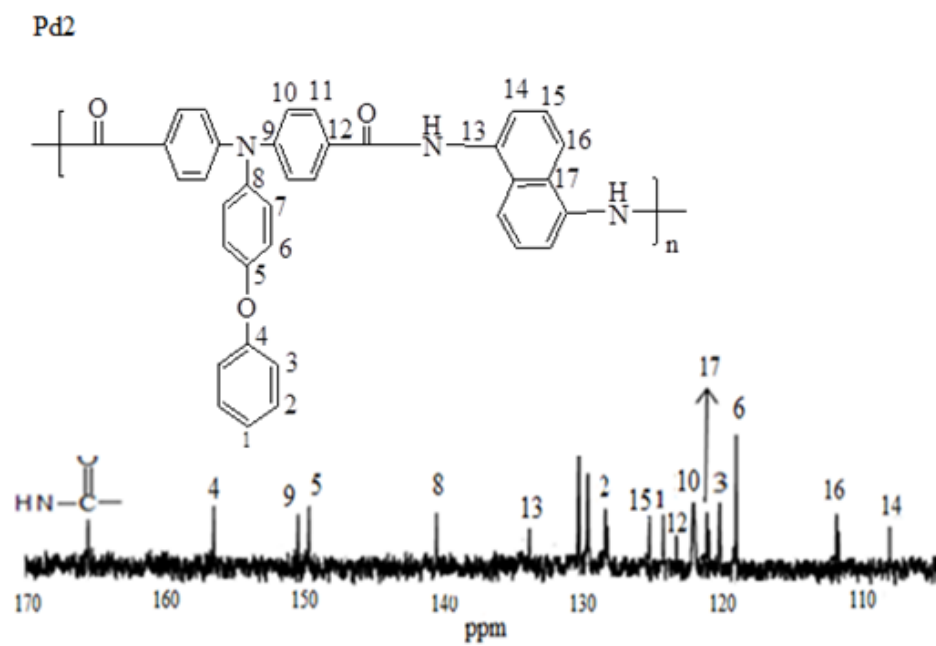
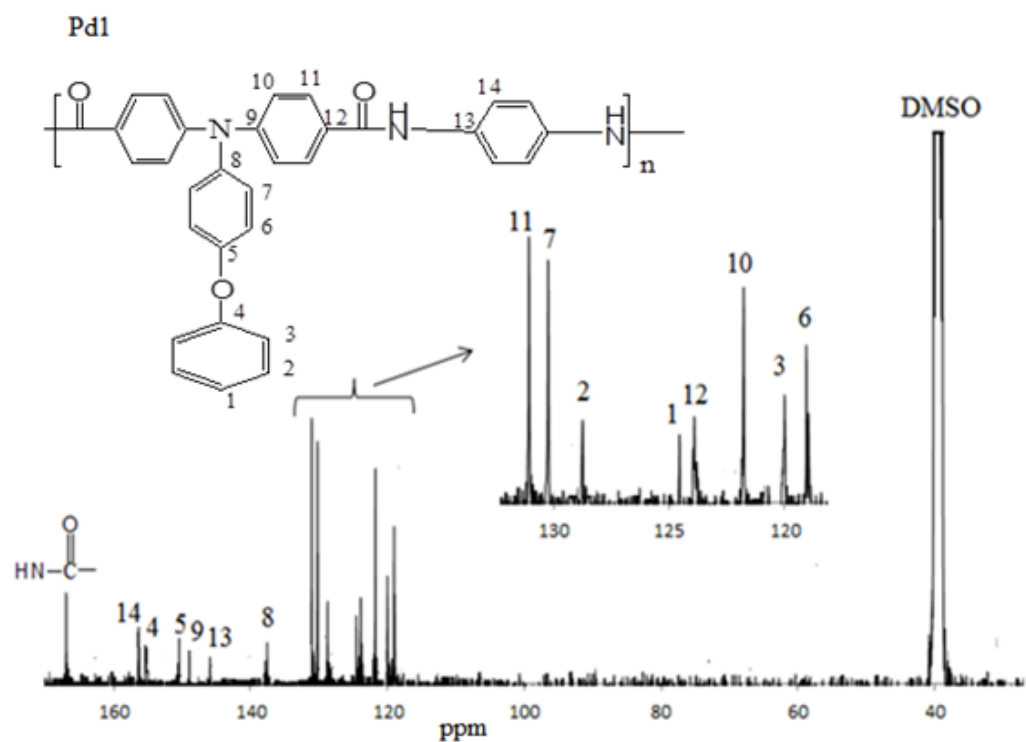
**Figure 13:**  $^{13}\text{C}$  NMR spectra for **Ic**, **Mc**



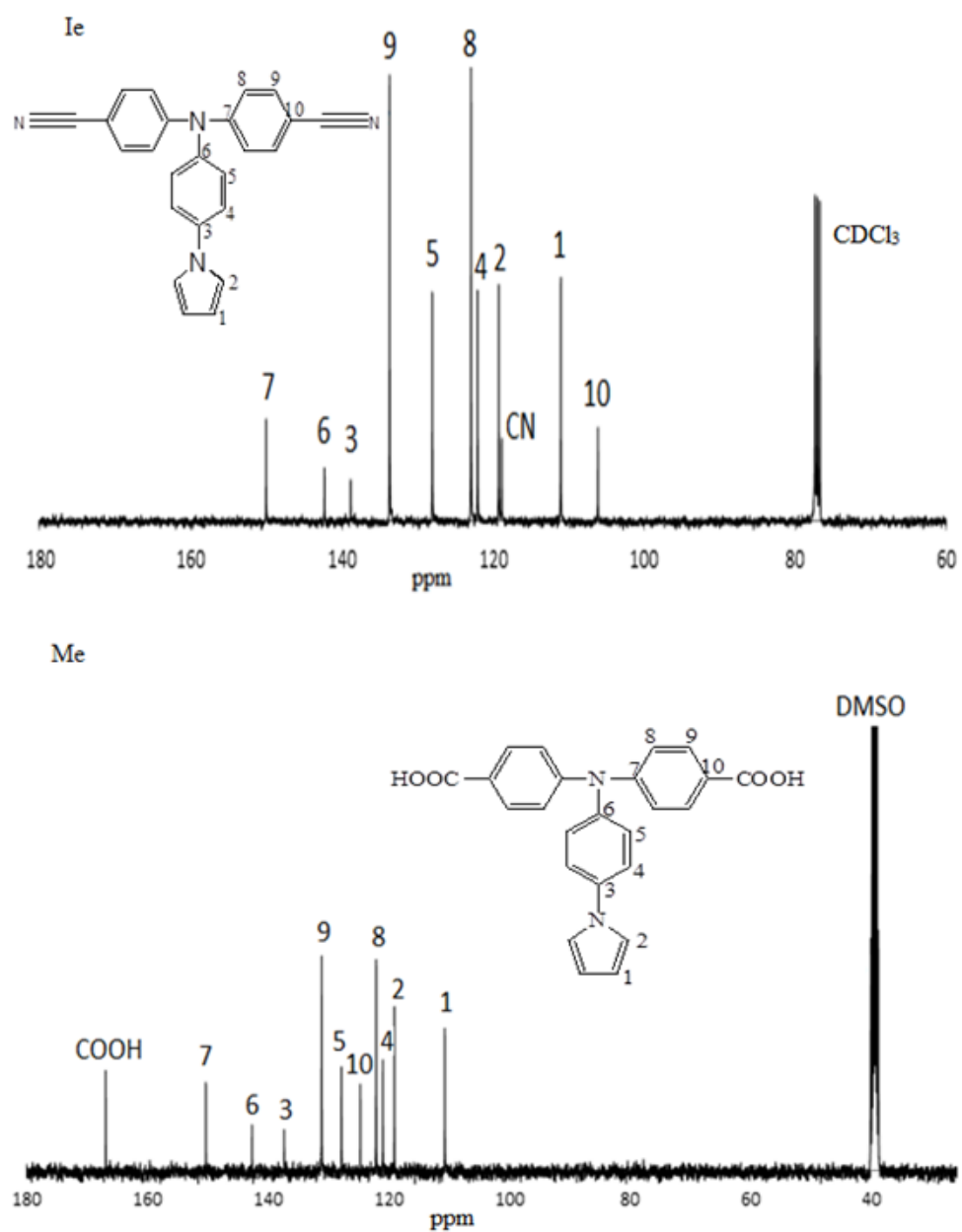
**Figure 14:**  $^{13}\text{C}$  NMR spectra for **Pc1**, **Pc2**



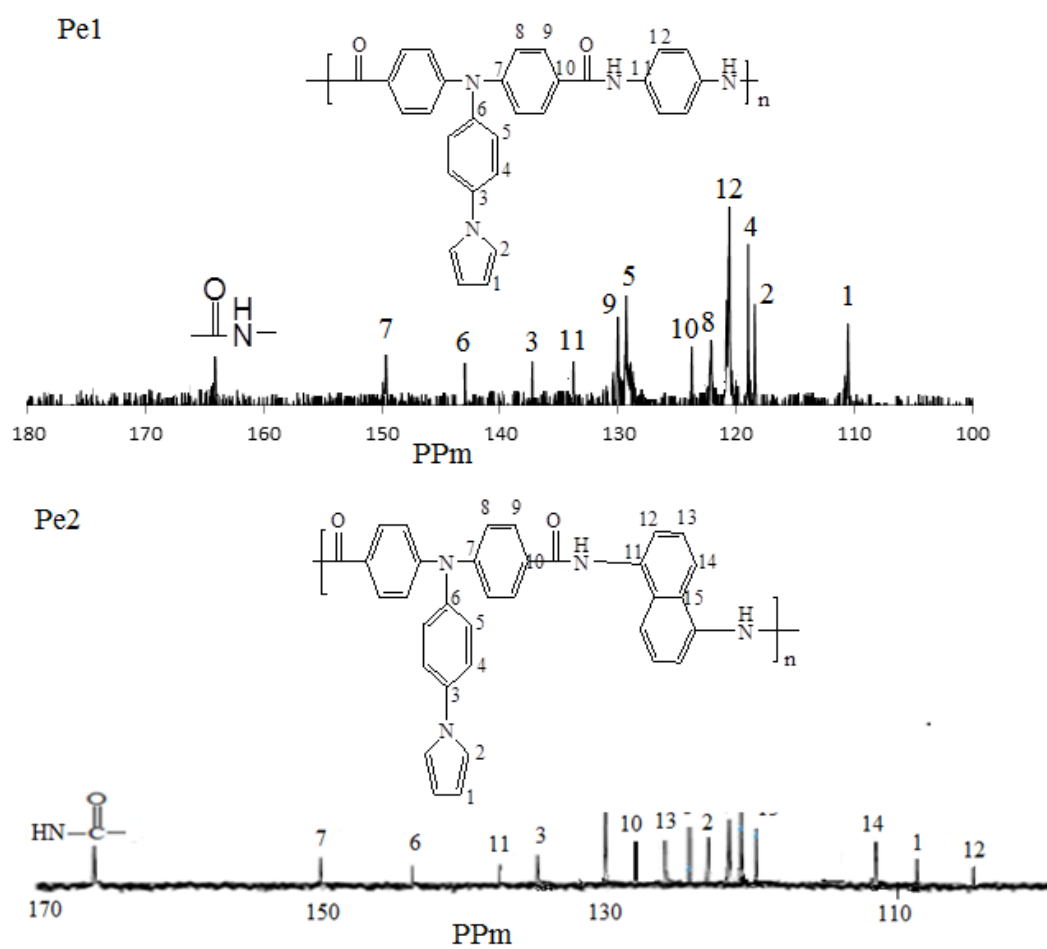
**Figure 15:**  $^{13}\text{C}$  NMR spectra for **Id**, **Md**



**Figure 16:** <sup>13</sup>C NMR spectra for Pd1, Pd2

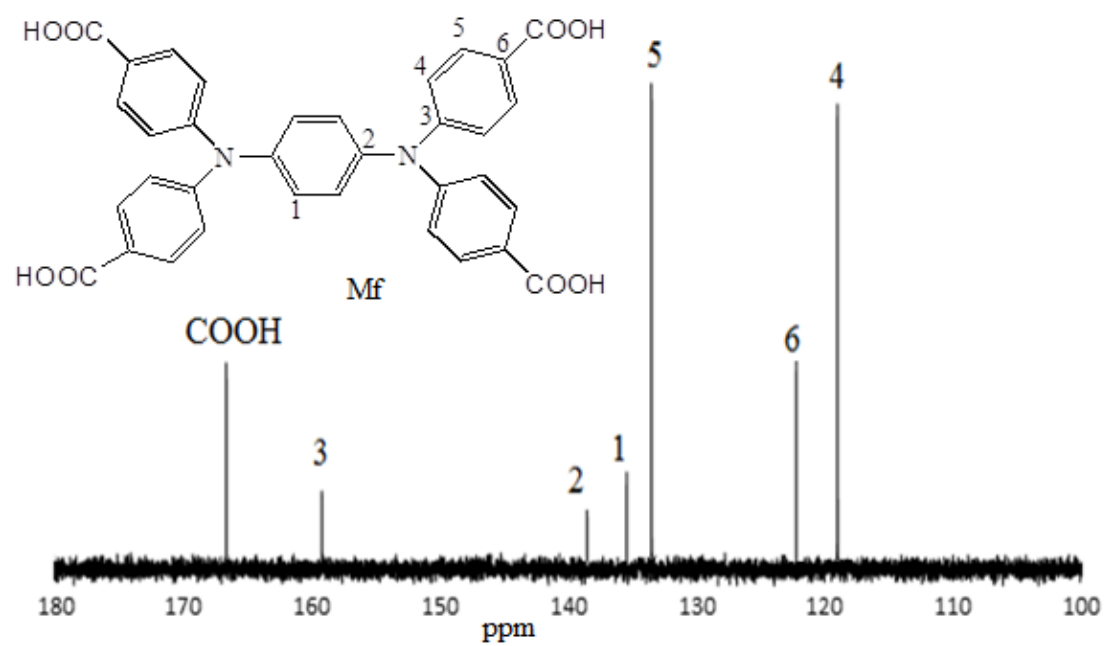
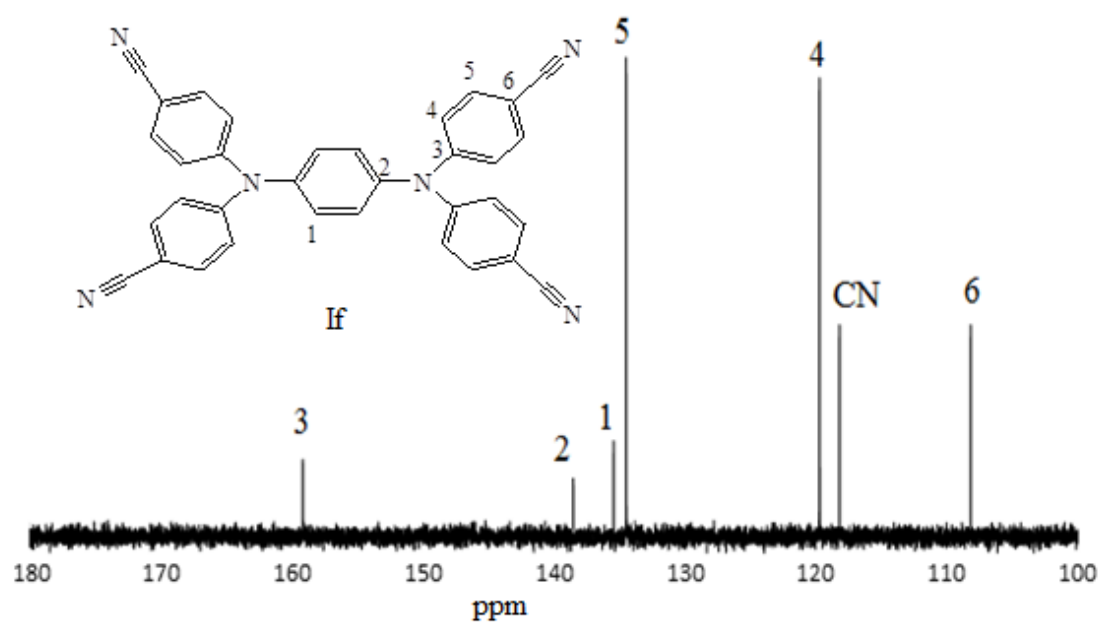


**Figure 17:**  $^{13}\text{C}$  NMR spectra for **Ie**, **Me**

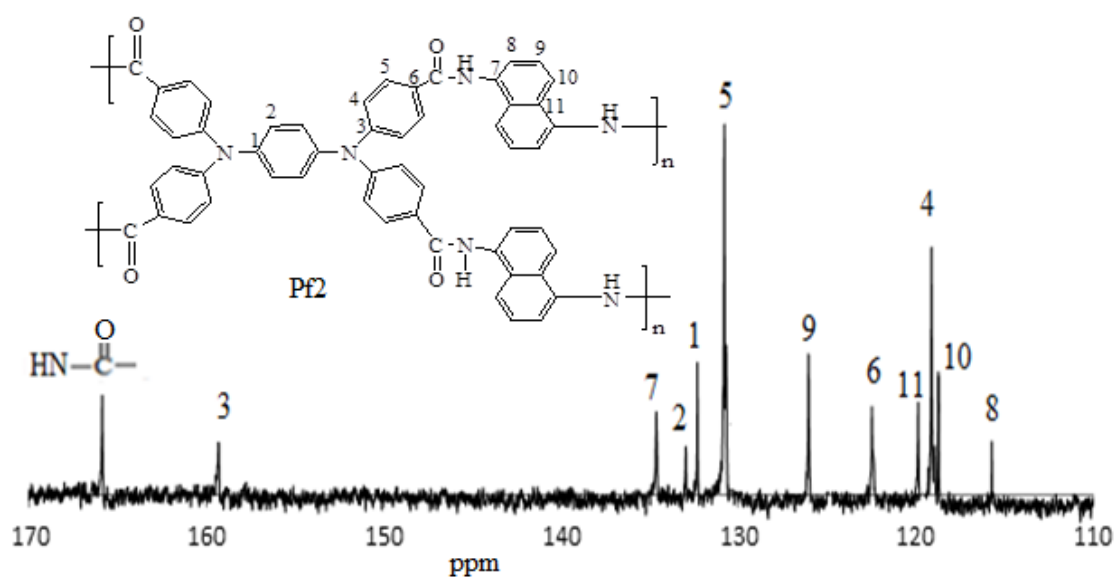
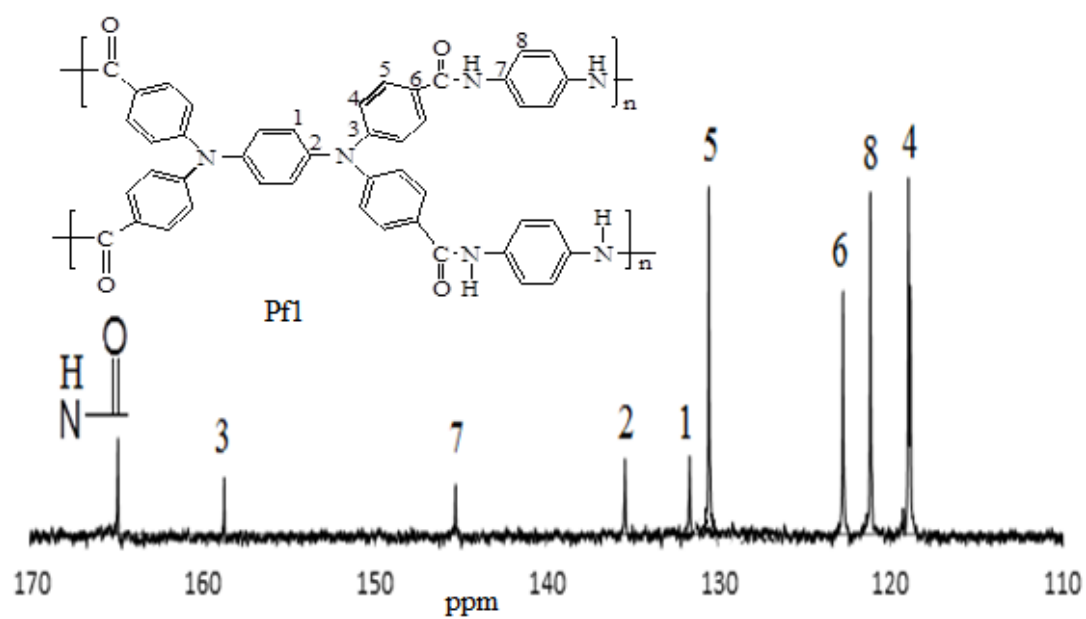


**Figure 18:**  $^{13}\text{C}$  NMR spectra for **Pe1**, **Pe2**



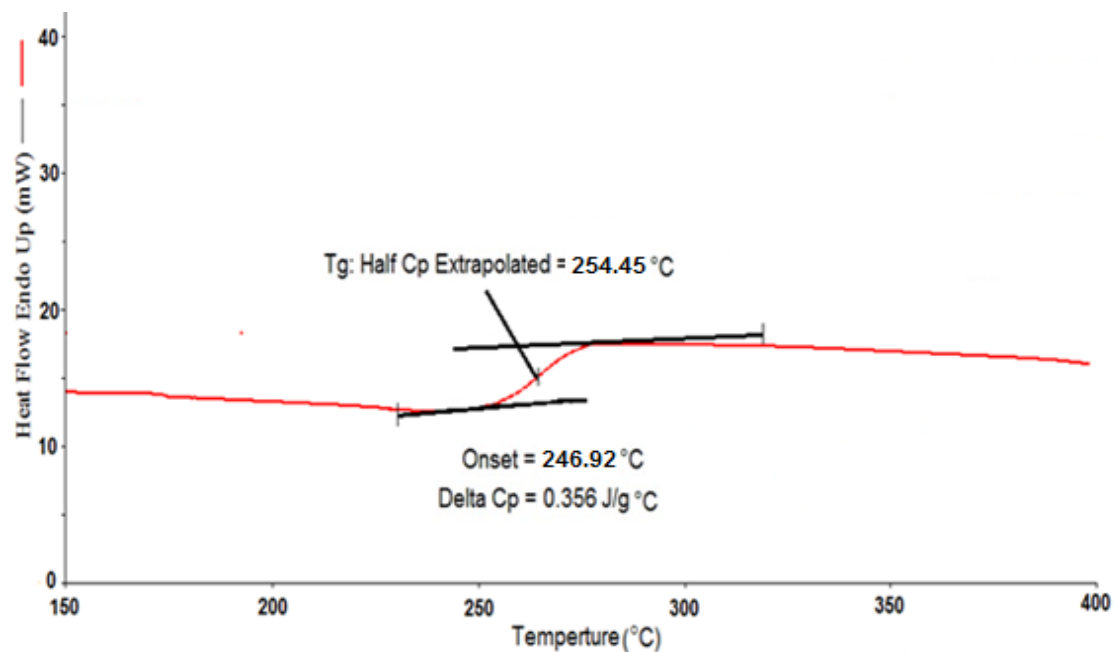


**Figure 19:**  $^{13}\text{C}$  NMR spectra for **If**, **Mf**

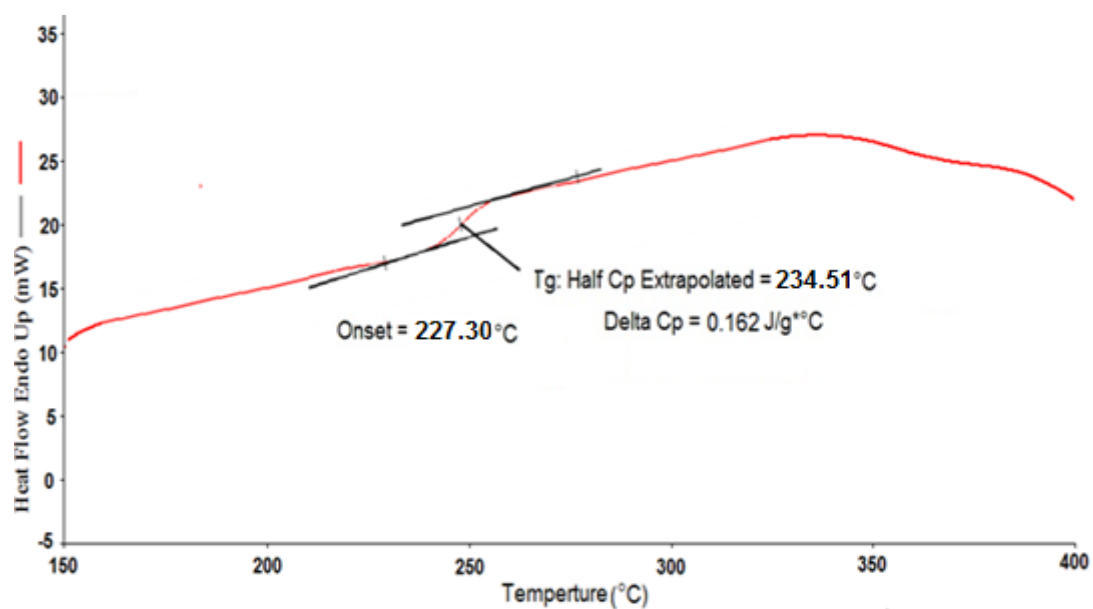


**Figure 20:**  $^{13}\text{C}$  NMR spectra for **Pf1**, **Pf2**

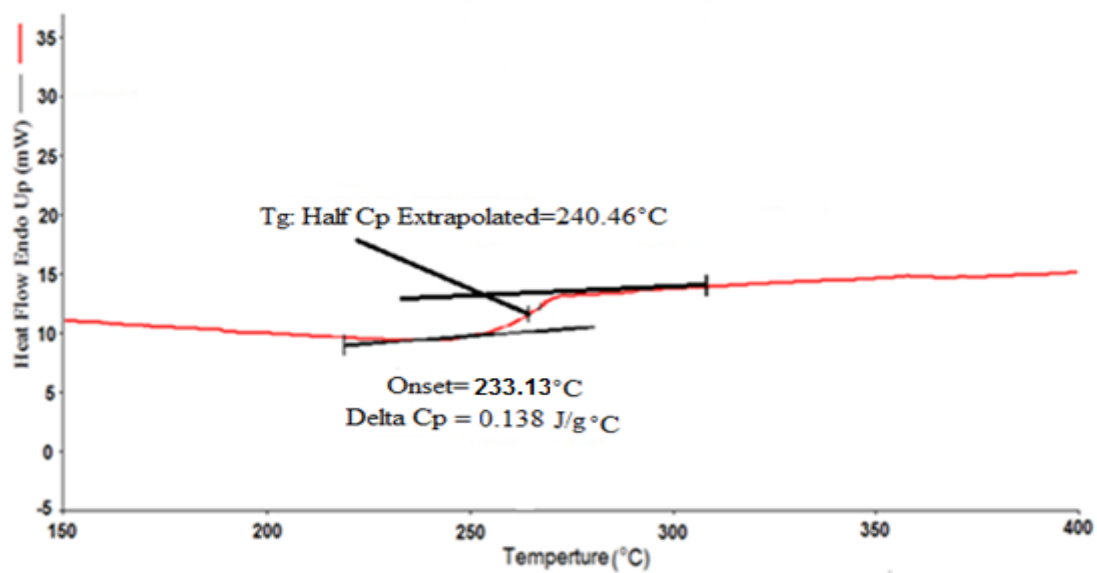
## Appendix C: DSC thermograms for the synthesized polyamides



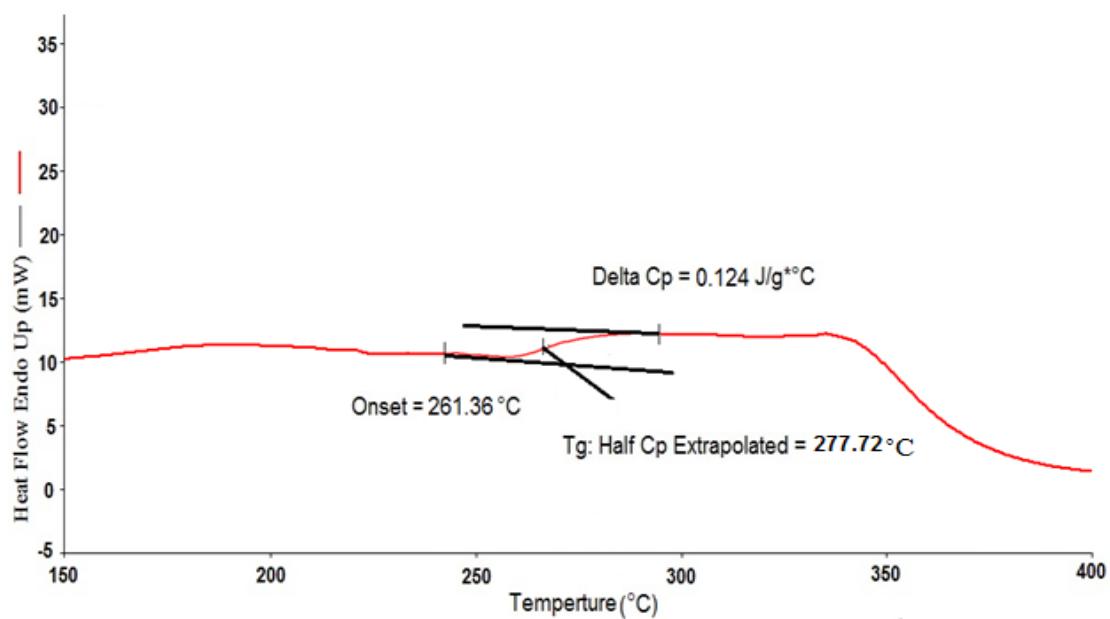
**Figure 1:** DSC trace of **Pb2**



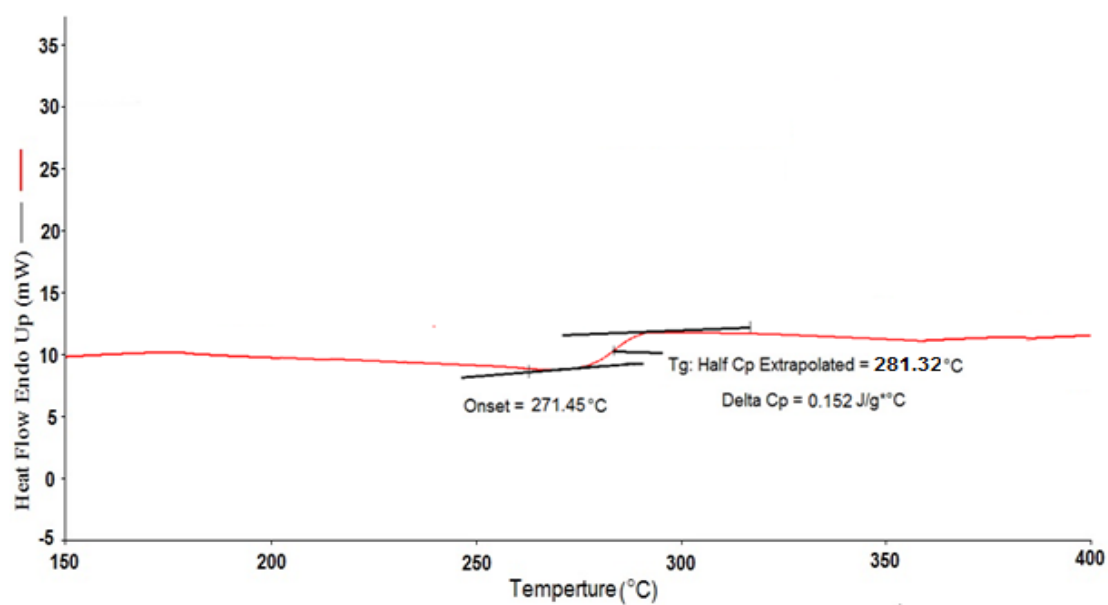
**Figure 2:** DSC trace of **Pc1**



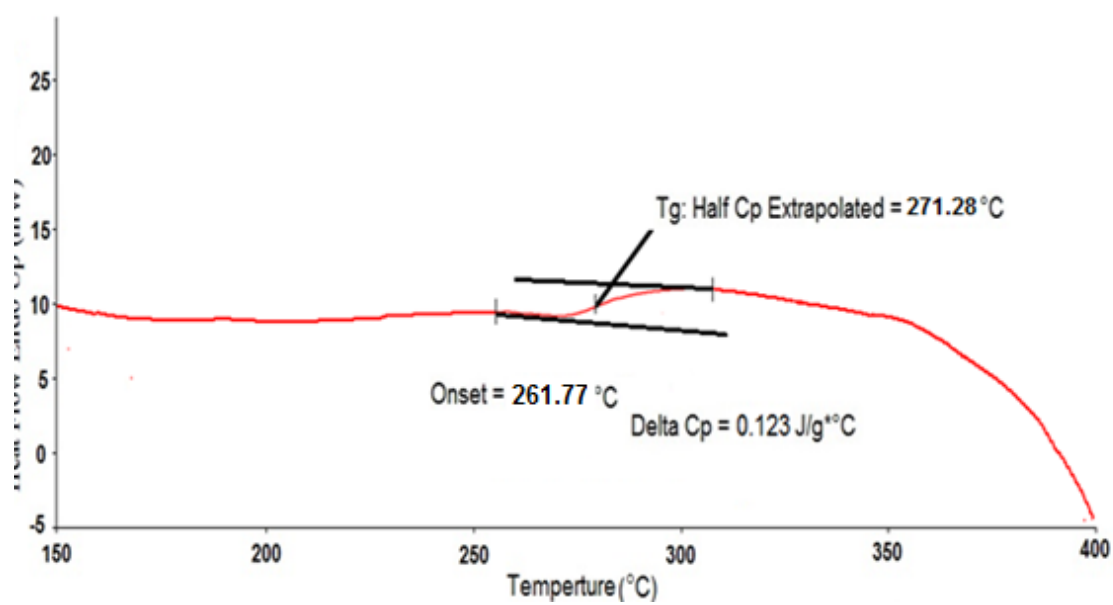
**Figure 3: DSC trace of Pc2**



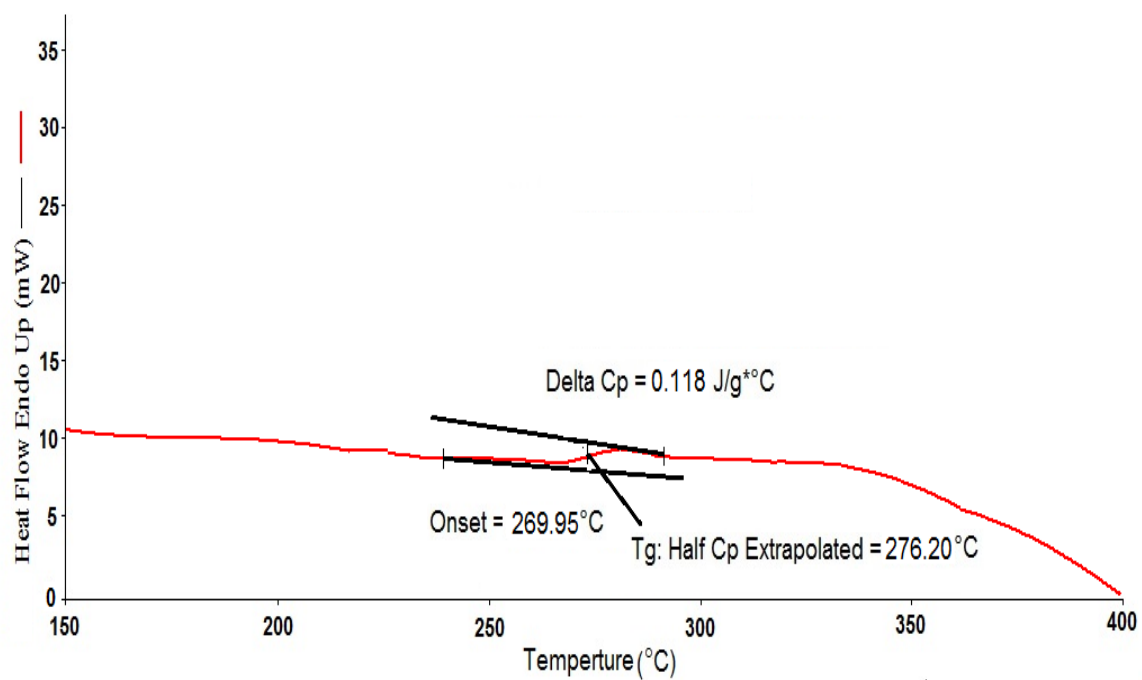
**Figure 4: DSC trace of Pd1**



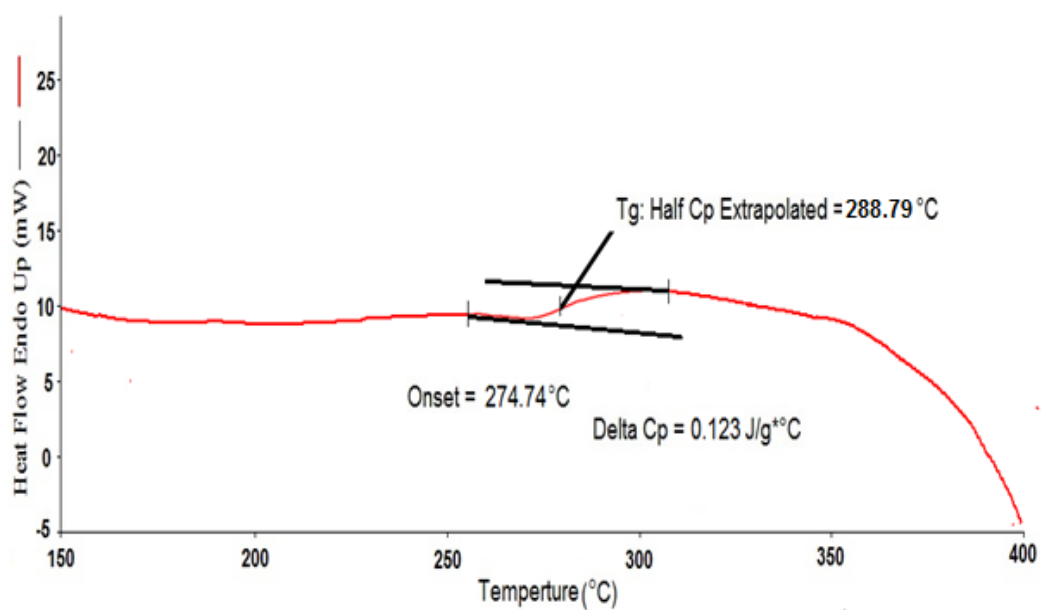
**Figure 5: DSC trace of Pd2**



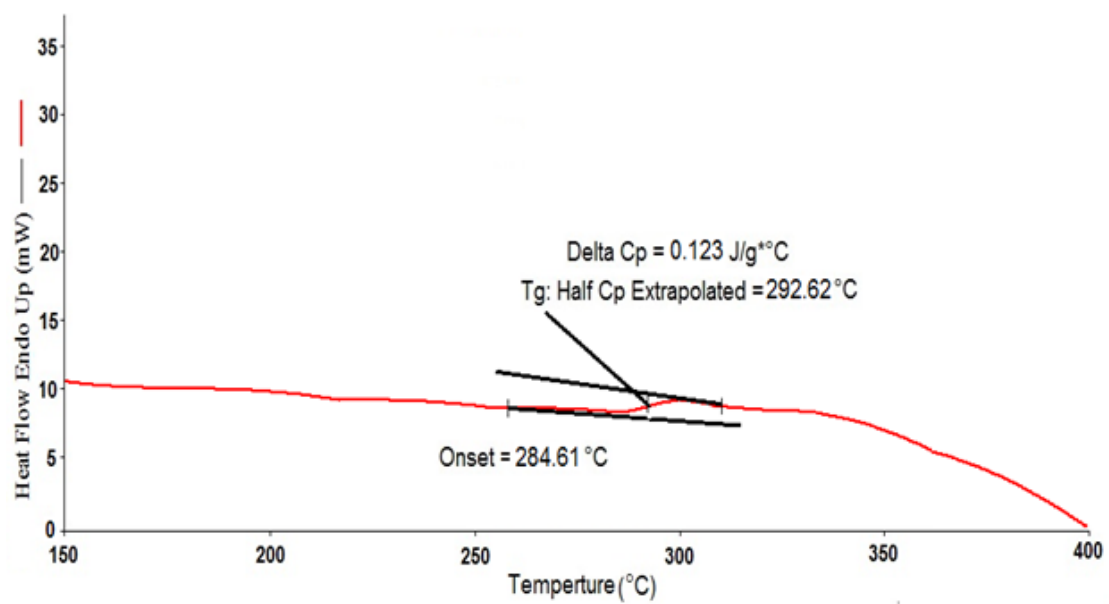
**Figure 6: DSC trace of Pe1**



**Figure7:** DSC trace of **Pe2**



**Figure 8:** DSC trace of **Pf1**



**Figure 9:** DSC trace of **Pf2**

## Appendix D: TGA thermograms for the synthesized polyamides

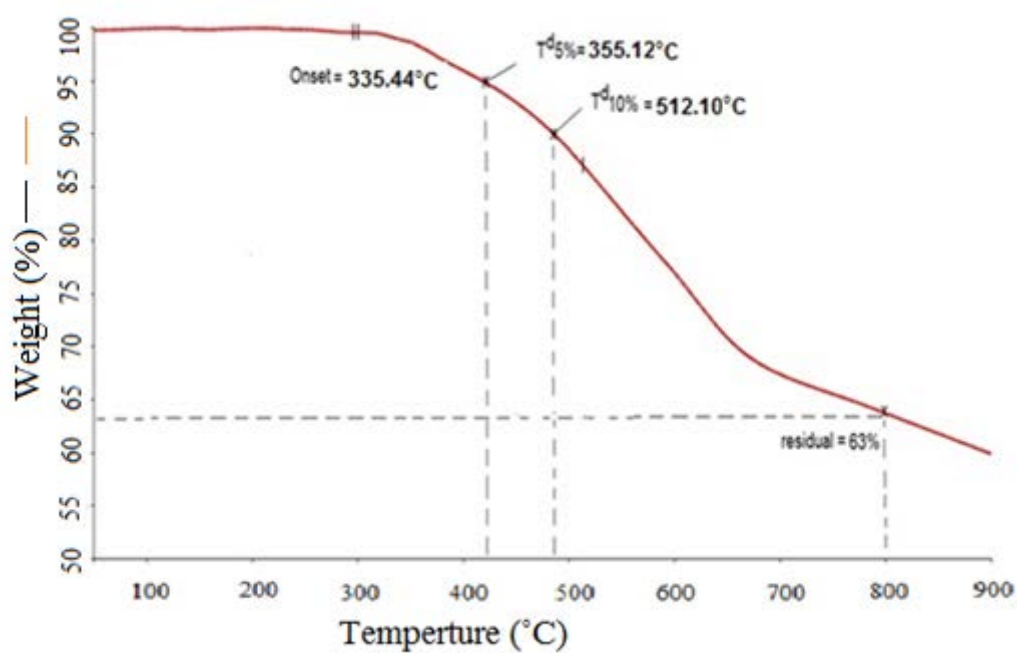


Figure 1: TGA thermogram for Pb1

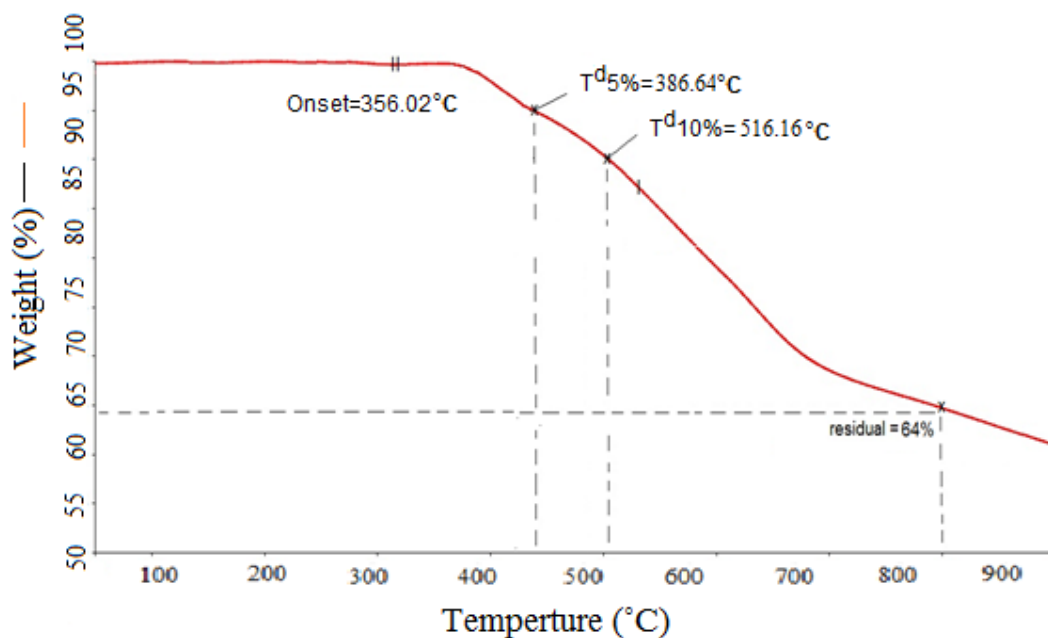
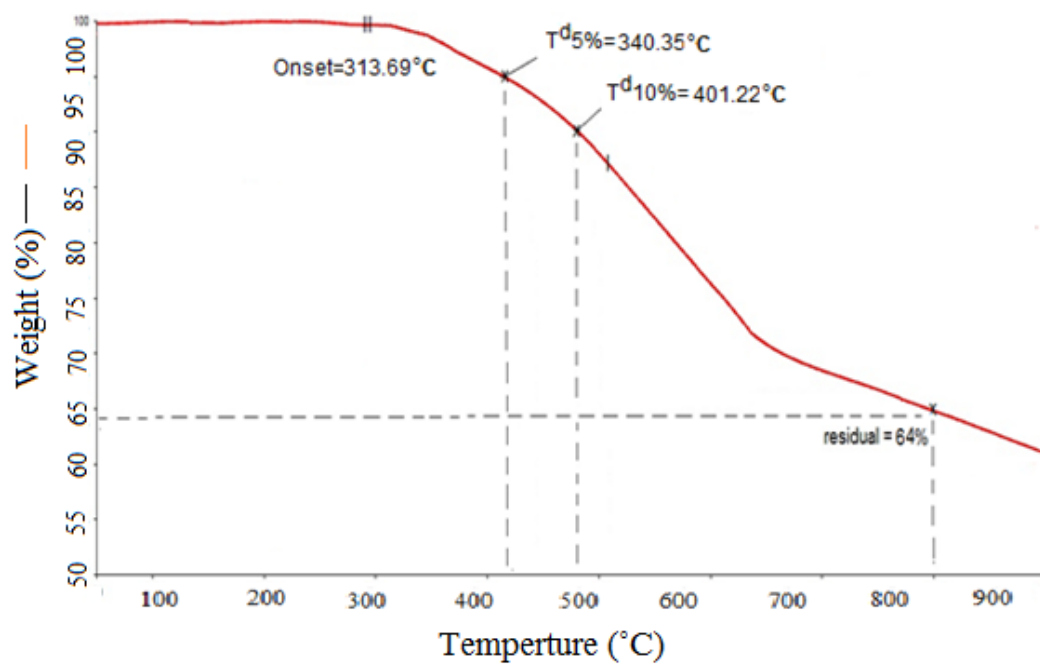
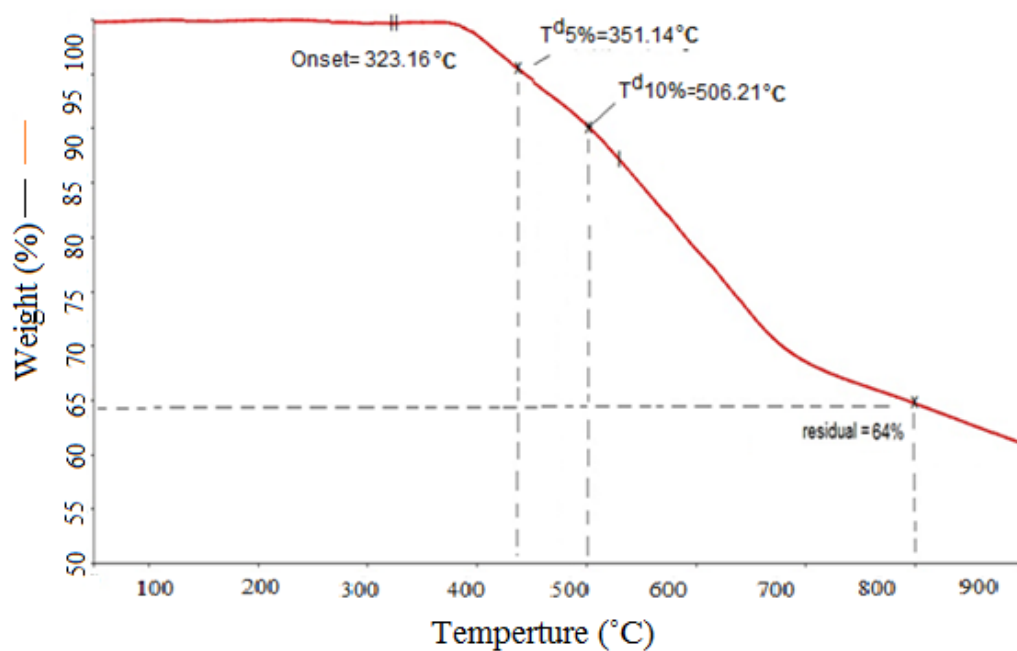


Figure 2: TGA thermogram for Pb2

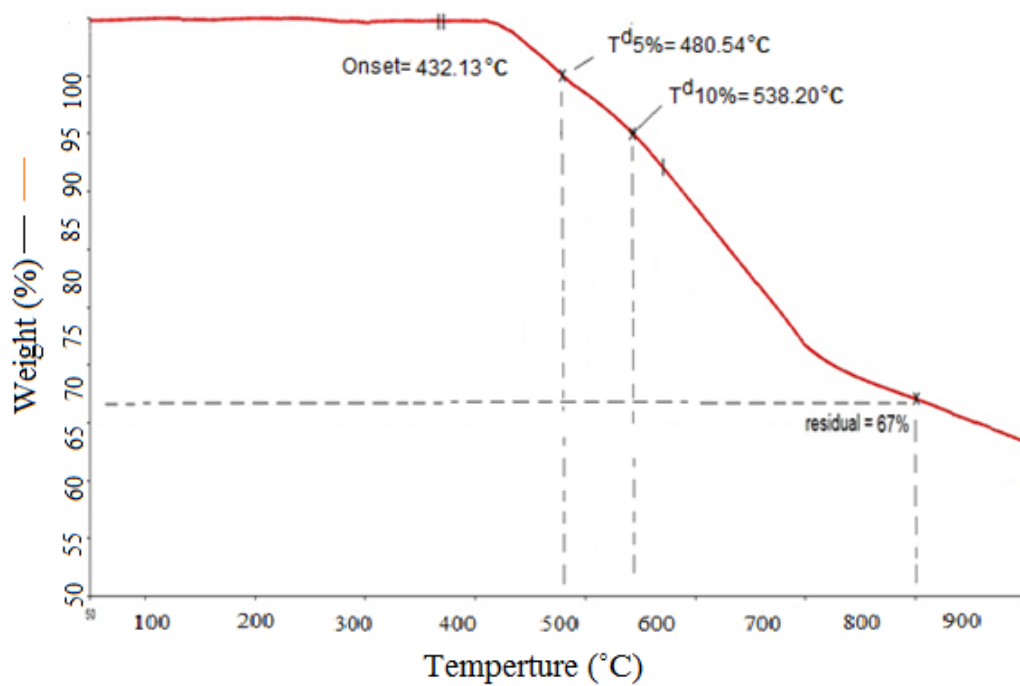




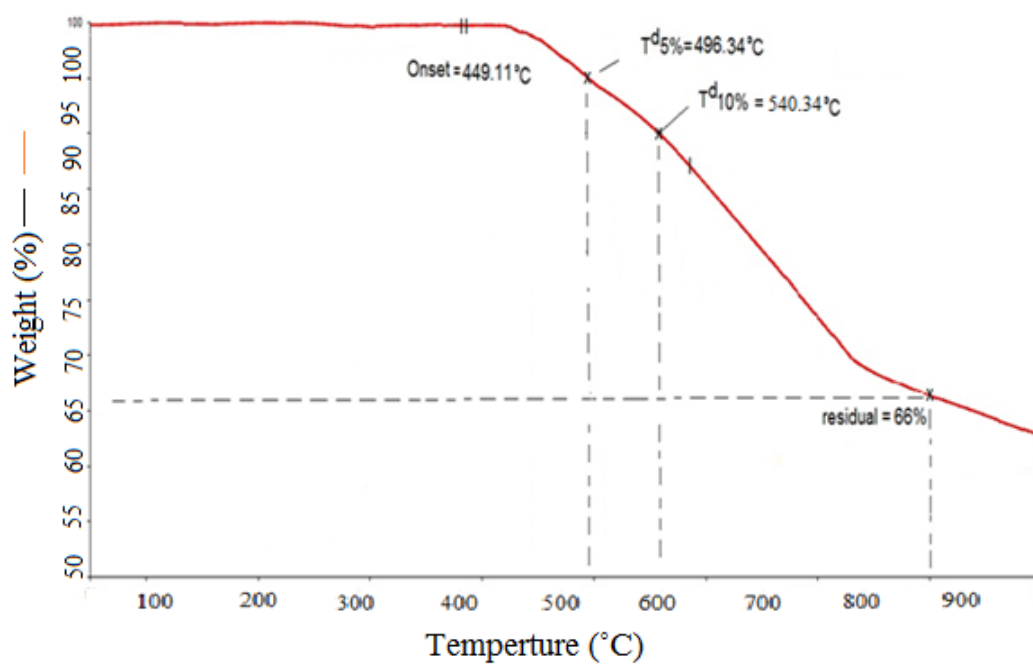
**Figure 3:** TGA thermogram for **Pc1**



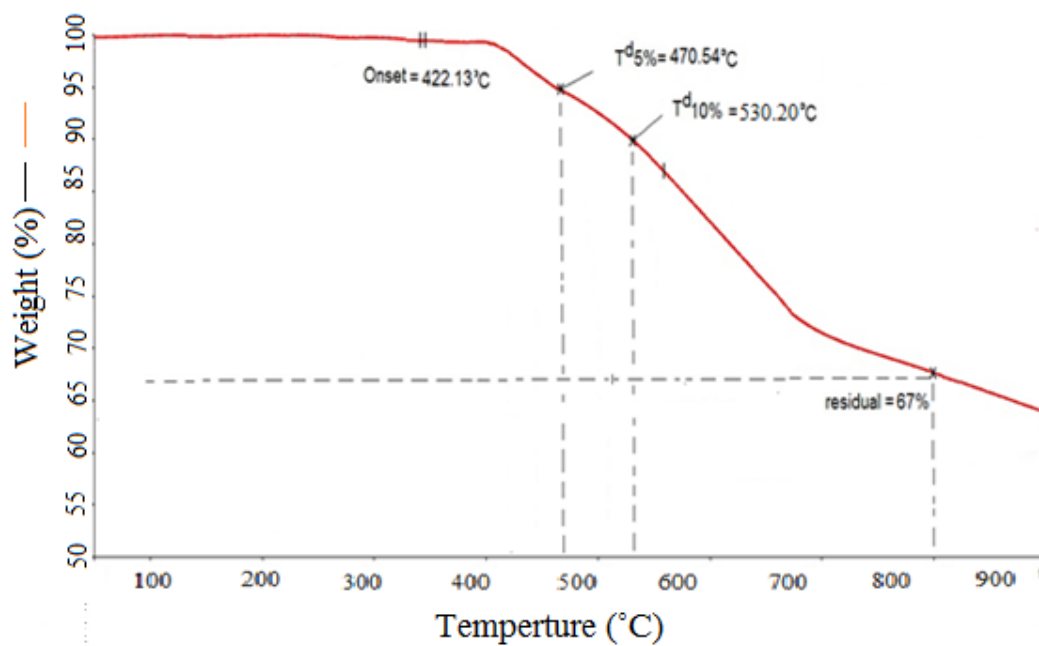
**Figure 4:** TGA thermogram for **Pc2**



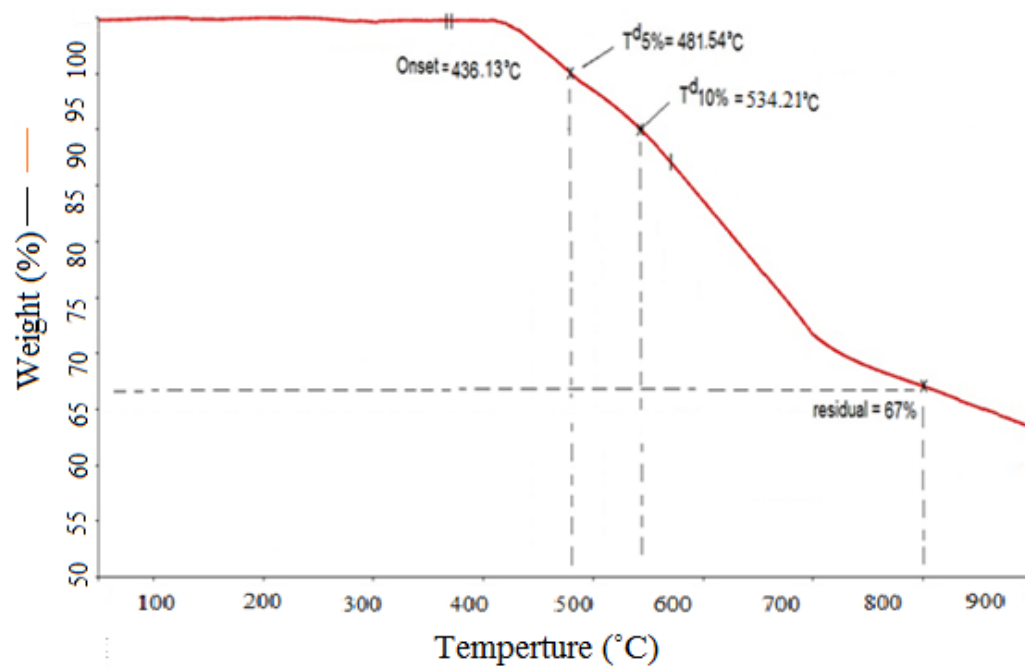
**Figure 5:** TGA thermogram for **Pd1**



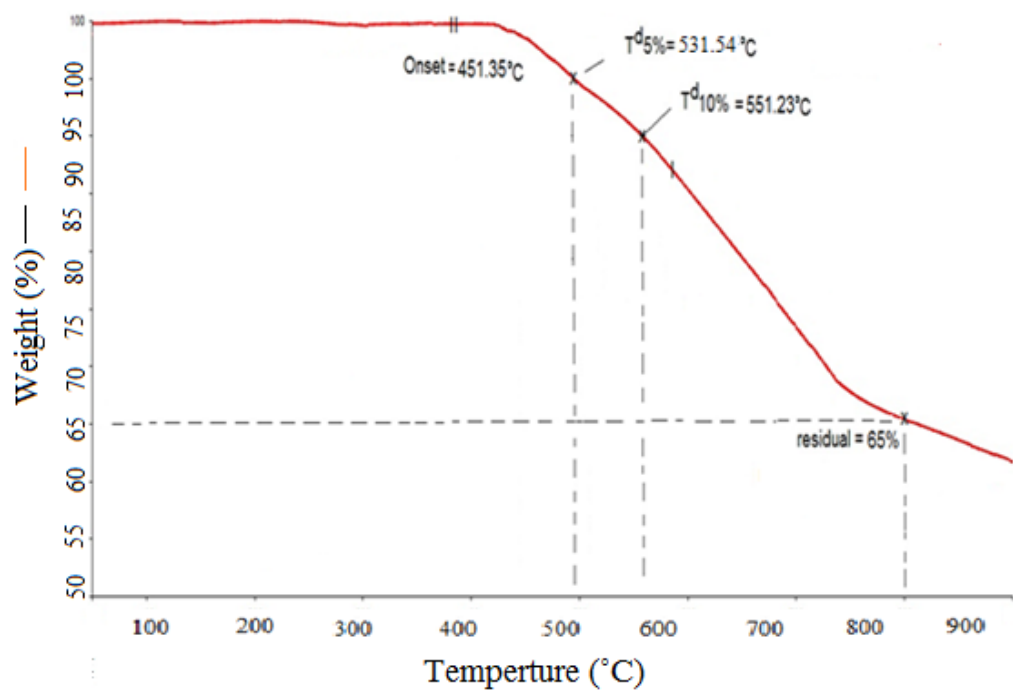
**Figure 6:** TGA thermogram for **Pd2**



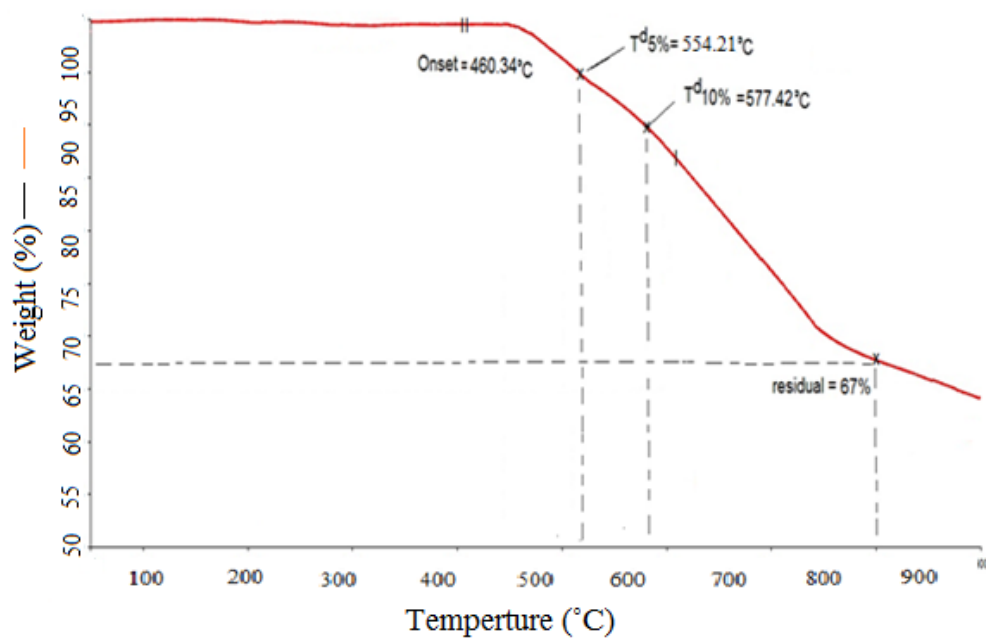
**Figure 7:** TGA thermogram for **Pe1**



**Figure 8:** TGA thermogram for **Pe2**



**Figure 9:** TGA thermogram for **Pf1**



**Figure 10:** TGA thermogram for **Pf2**